Investigation on the multiscale multiphysics based approach to modelling and analysis of precision machining of metal matrix composites (MMCs) and its application perspectives

A thesis submitted in partial fulfilment of the requirements of Brunel University London for the degree of Doctor of Philosophy

By

Zhichao Niu

September 2018

College of Engineering, Design and Physical Sciences
Brunel University London

Abstract

Over the last two decades or so, metal matrix composites (MMCs) have been drawing the attention of the industry due to their potentials in fulfilling demands for high performance industrial materials, products and advanced engineering applications. On the other hand, the high precision machining is becoming one of the most effective methods for enabling these difficult-to-machine composites to be applied particularly in precision engineering. Therefore, in-depth scientific understanding of MMC precision machining is essential and much needed so as to fulfil the gap between fundamental issues in precision machining of MMCs and their industrial scale applications. This thesis focuses on development of a multiscale multiphysics based approach to investigating the machinability of particulate MMCs and the machining process optimisation. In order to investigate the surface generation in relation to the process variables, this PhD study covers the key fundamental issues including chip formation process, dynamic cutting force, cutting temperature partition and tool wear by means of combining modelling, simulation and experimental study.

The chip formation mechanisms and the minimum chip thickness in precision machining of SiC_p/Al and B_4C_p/Al MMCs by using PCD tools are investigated through a holistic approach. Minimum chip thickness (MCT) value is firstly identified based on the modified mathematical model. The certain threshold of the uncut chip thickness, i.e. chips starting to form at this chip thickness point, is then established. The chip formation process including the matrix material breakage, particles fracture, debonding, sliding or removal and their interfacial interactions are further simulated using finite element analysis (FEA). The minimum chip thickness and chip formation simulations are evaluated and validated via well-designed experimental trials on a diamond turning machine. The chips and surface profiles formed under varied process variables in periodic material removals are inspected and measured in order to obtain a better understanding on MMC chip formation mechanisms.

The improved dynamic cutting force model is developed based on the micro cutting mechanics involving the size effect, undeformed chip thickness effects and the influence of cutting parameters in the micro scale. Cutting process variables, particle form, size and volume fraction at different scales are taken into account in the modelling. The

cutting force multiscale modelling is proposed to have a better understanding on the MMCs cutting mechanics and to predict the cutting force accurately. The cutting forces are modelled and analysed in three cutting regimes: elastic recovery zone, ploughing zone and shearing zone. A novel instantaneous chip thickness algorithm including real chip thickness and real tool trajectory is developed by taking account of the tool runout. Well-designed cutting trials are carried out under varied process variables to evaluate and validate the force model. In order to obtain the actual cutting forces accurately, transfer function technique is employed to compensate the measured cutting forces. The cutting force model is further applied to correlate the cutting tool wear and the prediction of the machined surface generation.

Multiphysics coupled thermal-mechanical-tribological model and FE analysis are developed to investigate the cutting stress, cutting temperature, tool wear and their intrinsic relationships in MMCs precision machining process. Heat generation, heat transfer and cutting temperature partition in workpiece, chips and cutting tool are simulated. A modified tool wear rate model is proposed, tool wear characteristics, wear mechanisms and dominate tool wear are further investigated against the real machining process. Cutting tool wear is monitored and assessed offline after machining experiments.

The experimental study on the machined surface generation is presented covering cutting force, tool wear, tool life, surface roughness and machining efficiency. Process optimisation is explored by considering the variation of cutting parameters, cutting tool conditions and workpiece materials in order to achieve the desired outcomes and machinability.

Acknowledgements

First and foremost, I would like to thank my supervisor Professor Kai Cheng. His precious advices, instructions, encouragement and invaluable support throughout my PhD study have led me go through the most difficult stages during the process. Without his help and support, the completion of this research study would not have been possible. His professional, passion and commitment have definitely influenced and motivated my life not only in engineering research.

Personal appreciation is given to my colleagues Dr Atanas Ivanov, Mr Paul Yates, Dr Feifei Jiao and Dr Chao Wang for their invaluable discussion, support and their assistance in machining trials in particular.

Special thanks also go to Professor G.H. Wu and his team at Harbin Institute of Technology and Prima Tooling Ltd in providing the MMC materials and PCD tools for machining trials, and interesting and helpful discussion on the MMC materials design and fabrication.

This thesis is also dedicated to my parents; their unconditional love, patience, encouragement and tremendous support have been a powerful source, inspiration and motivation for all I have achieved so far in my life.

Last, but by no means least, my love and heartful gratitude go to my wife. Her never-ending love, encouragement and support have been an endless source to ease and enhance the way I conducted this research.

Table of Contents

Nomenclature

Symbols:

a	Actual depth of cut	*(μm)*
a_{i1}	Chip contact length in the cutting direction	*(μm)*
a_p	Minimum chip thickness	*(μm)*
a_{p1}	Un-deformed chip thickness at matrix material	*(μm)*
a_{p2}	Un-deformed chip thickness at tool-particle interaction	*(μm)*
A	Initial yield strength	*(MPa)*
A_i	Tool-workpiece contact area	*(μm^2)*
A_p	Elastic recovery area	*(μm^2)*
A_{pa}	Elastic recovery area in axial diection	*(μm^2)*
A_{pc}	Elastic recovery area in radial diection	*(μm^2)*
A_{pt}	Elastic recovery area in tangential diection	*(μm^2)*
B	Hardening modulus	*(MPa)*
c	Actual feed rate	*(μm /rev)*
C	Strain rate sensitivity coefficient	
C_1	Specific heat capacity	*(J/K)*
C_p	Material heat capacity	*(J/K)*
C_{pc}	Heat capacities of chip surface	*(J/K)*
C_{pt}	Heat capacities of tool surface	*(J/K)*

d	Depth of cut	*(μm)*
D_1, D_2, D_3, D_4, D_5	Material constants for damage model	
e	Total energy per unit volume	*(J/m^3)*
e_{max}^{ck}	Material parameter	
e_{nn}^{ck}	Crack opening strain	
e_{MMC}	Tool-MMCs material friction coefficient	
e_1	Tool-matrix material friction coefficient	
e_2	Tool-particle friction coefficient	
E_c	heat energy conducted on chip	*(J)*
E_D	Energy per unit volume consumed for the particle debonding from the matrix material	*(J/m^3)*
E_P	Specific energy for plastic deformation in the primary shear zone	*(J/m^3)*
E_t	Heat energy conducted on cutting tool	*(J)*
E_S	Specific energy for plastic deformation in the secondary shear zone	*(J/m^3)*
f	Feed rate	*(μm /rev)*
f_1	Fraction of generated heat into top surface	
f_2	Fraction of generated heat into bottom surface	
F_a	Axial cutting force	*(N)*
F_C	Total cutting force	*(N)*
F_{CC}	Cutting force during MMCs micro cutting	*(N)*
F_{CD}	Debonding force of the reinforced particles	*(N)*

F_{CP}	Ploughing forces parallel to the cutting tool path	*(N)*
F_c	Radial cutting force	*(N)*
F_f	Total friction force	*(N)*
F_N	Normal loading force	*(N)*
F_{N1}	Normal force for each fractured particles	*(N)*
F_p	Two body rolling abrasive force	*(N)*
F_r	Three body rolling friction force	*(N)*
F_T	Total thrust force	*(N)*
F_t	Tangential cutting force	*(N)*
F_{TC}	Thrust forces during MMCs micro cutting	*(N)*
F_{TD}	Fracture force of the reinforced particles	*(N)*
F_{TP}	Ploughing forces perpendicular to the cutting tool path	*(N)*
g	Strain in the chip	
G	Shear modulus of the un-cracked material	*(GPa)*
G_c	Fraction of un-cracked shear modulus	*(GPa)*
G_f^I	Energy required for opening a unit area of crack	*(J/m^2)*
h	Uncut chip thickness	*(μm)*
H	Height of the particle ploughing zone	*(μm)*
H_t	Hardness of tool	
i	Oblique angle	*(°)*
k	Thermal conductivity of MMCs workpiece	*(W/m/C)*
k_{as}	Axial force coefficient	

k_{rs}	Radial force coefficient	
k_t	Shearing stress for tool material	*(MPa)*
k_{ts}	Tangential force coefficient	
k_{te}, k_{ce}, k_{ae}	Cutting force coefficients in the elastic recovery zone	
K	Tool teeth number	
K_{ac}	Corresponding cutting constant	
K_c	SiC particle fracture toughness	*(J/mm^3)*
K_{rc}	Corresponding cutting constant	
K_{tc}	Corresponding cutting constant	
K_0	Material recovery constant	
K_1	Thermal diffusivity of the workpiece material	*(W/m/C)*
l	Equivalent cutting edge length	*(μm)*
L_1, L_2	Dimensionless velocity parameter	
m	Thermal softening exponent	
n	Strain hardening exponent	
N	Numbers of tool teeth of the cutting tool	
N_p	Total number of the reinforced abrasive particles	
p	Pressure stress effective cutting stress	*(MPa)*
p'	Volume fraction of particle along the cutting edge	
P	Material parameter	
P_c	Total energy consumption	*(J)*
P_{deb}	Power consumption of particles debonding	*(J)*

P_{e1}	Peclet number in tool-workpiece sliding	
P_{e2}	Peclet number in chip formation	
P_{fns}	Power consumption for the formation of new surfaces	*(J)*
P_{mnc}	Power consumption for the minor cutting edge effect	*(J)*
P_{pd}	Plastic deformation power of MMC workpiece	*(J)*
P_{tc}	Power consumption at tool-chip interface	*(J)*
P_{tw}	Power consumption at tool-workpiece interface	*(J)*
q	Effective cutting stress	*(MPa)*
q_g	Heat flux density generated by the interface element	*(W/m^{-2})*
q_k	Heat flux generated due to conduction	*(W/m^{-2})*
q_r	Heat flux generated due to radiation	*(W/m^{-2})*
Q	Heat source	*(J)*
r_e	Edge radius	*(μm)*
r_f	Heat rate per unit area	
rg	Depth of groove	*(μm)*
r_n	Nose radius	*(μm)*
r_o	Cutting tool runout	*(μm)*
r^{pl}	Heat rate per unit volume	
r_s	Average radius of particle	*(μm)*
R_a	Surface roughness	*(nm)*
R_0	Nominal radius of cutting tool	*(μm)*
R'	Actual tool tip rotation radius	*(μm)*

$R_1 * q_1$	Heat per unit time per unit area left on the chip in the shear zone	*(J/mm^{2}s)*
$R_2 * q_2$	Heat per unit time per unit area left on the chip in the tool-chip interaction zone	*(J/mm^{2}s)*
$(1 - R_1) * q_1$	Heat per unit time per unit area left on the workpiece in the shear zone	*(J/mm^{2}s)*
$(1 - R_2) * q_2$	Heat per unit time per unit area left on the cutting tool in the tool-chip interaction zone	*(J/mm^{2}s)*
t_{ac}	Actual chip thickness virus rotation angle	*(μm)*
t_{cmin}	Minimum chip thickness	*(μm)*
t_{fric}	Friction force	*(N)*
T	Current cutting temperature	*(°C)*
T_m	Melting temperature	*(°C)*
T_0	Room temperature	*(°C)*
u_{n0}	Crack normal displacement at the failure point	*(μm)*
U	Total fracture energy of SiC particle	*(J)*
V	Cutting velocity	*(m/s)*
V_{trans}	Velocity of moving part	*(m/s)*
w	Initial interface crack width	*(μm)*
W	Total wear height	*(μm)*
Y_i	Surface roughness value in the i^{th} test	*(nm)*
Y_0	Young's modulus of tool-chip interface	*(GPa)*
Y_1	Young's modulus of MMCs	*(GPa)*

Y_2	Young's modulus of cutting tool	*(GPa)*
$\emptyset$	Shear angle	*(°)*
α	Rake angle	*(°)*
α_o	Initial runout angle of tool centre	*(°)*
β	Friction angle	*(°)*
$\dot{\gamma}$	Slip rate	
δ_n	Normal pressure	*(MPa)*
δ_p	Critical value of the relative penetration (MMCs/PCD)	
δ_y	Material initial yield stress	*(MPa)*
ε	Compressive stress	*(MPa)*
ε^{pl}	Effective plastic strain	
$\bar{\varepsilon}_f^{pl}$	Strain at material failure	
$\varepsilon_1, \varepsilon_2, \varepsilon_3$	Compressive stress of MMCs in tangential, radial and axial diection	*(MPa)*
$\dot{\varepsilon}$	Equivalent plastic strain rate	*(s^{-1})*
$\dot{\varepsilon}_0$	Reference strain rate	*(s^{-1})*
θ	Rotation angle of tool tip	*(°)*
θ_p	Apex angle	*(°)*
θ_1	Maximum rotation angle in elastic recovery zone	*(°)*
θ_2	Maximum rotation angle in ploughing zone	*(°)*
θ_3	Maximum rotation angle in shearing zone	*(°)*
λ	Initial interface crack length	*(μm)*

μ	Friction coefficient	
μ_s	Specific stress of SiC particles fracture	*(MPa)*
μ_3	Three body rolling friction coefficient	
v_1	Poison ratio of MMCs	
v_2	Poison ratio of cutting tool	
ω	Damage parameter	
ρ_1	Density of MMCs	*(kg/m^3)*
σ	Material flow stress	*(MPa)*
σ_{tu}^{I}	Mode I fracture energy	*(MPa)*
$\sigma_{y(tool)}$	Yield strength of tool material	*(MPa)*
τ_m	Shearing stress of matrix material	*(MPa)*
τ_c	Frictional stress	*(MPa)*
τ_s	Limit shear stress	*(MPa)*
φ	Approach angle	*(°)*
φ'	Actual approach angle	*(°)*
η_f	Fraction of the friction energy convert into heat	
η_m	Fraction of dissipated energy converted to heat	

Abbreviations:

AE	Acoustic emission
ALE	Arbitrary Lagrangian–Eulerian

ANOM	Analysis of means
ANOVA	Analysis of variance
BUE	Build-up-edge
CVD	Chemical vapor deposition
DAQ	Data acquisition
DOC	Depth of cut
EDS	Energy-dispersive X-ray Spectroscopy
FEA	Finite element analysis
FEM	Finite element modelling
FRF	Frequency response function
HSS	High speed steel
MD	Molecular dynamics
MMCs	Metal matrix composites
MRR	Material removal rate
PCBN	Polycrystalline Cubic Boron Nitride
PCD	Poly-Crystalline Diamond
PM	Powder metallurgy
PMMC	Particulate metal-matrix composites
PRMMC	Particle-reinforced metal matrix composite
PSD	Power spectral density
RMS	Root mean square
SCD	Single Crystal Diamond

S/N	Signal to noise ratio
SEM	Scanning electron microscope
TCMS	Tool condition monitoring system

Chapter 1 Introduction

1.1 Background of the research

In the last two decades or so, metal matrix composites (MMCs) have been gradually drawing the attention of the industry due to the MMCs have the potential to fulfil the industrial demands for high performance components, products and advanced engineering applications. Substantial progress in developing MMCs has been achieved as shown in Figure 1-1 [1]. The increasing demands for high performance components and products enable these advanced heterogeneous materials to be considered in numerous industrial fields especially for aerospace, optics, energy, automotive, medical, military defence and nuclear industries [2-5]. Conventional industrial materials such as plastics, metals and ceramics have their own strengths and weakness through horizontal comparison; however, MMCs are observed as the combination of conventional materials associating with their advantages to make better use of their virtues and also avoid their deficiencies as shown in Figure 1-2. Due to their attractive physical and mechanical properties such as light weight, specific high strength and stiffness, high wear and creep resistance, long fatigue life, high corrosion/oxidation resistance, low thermal expansion, excellent corrosion and heat resistance [6-8], MMCs have been increasingly developed and gradually replace the conventional homogeneous materials in various engineering areas [9] as shown in Figure 1-3.

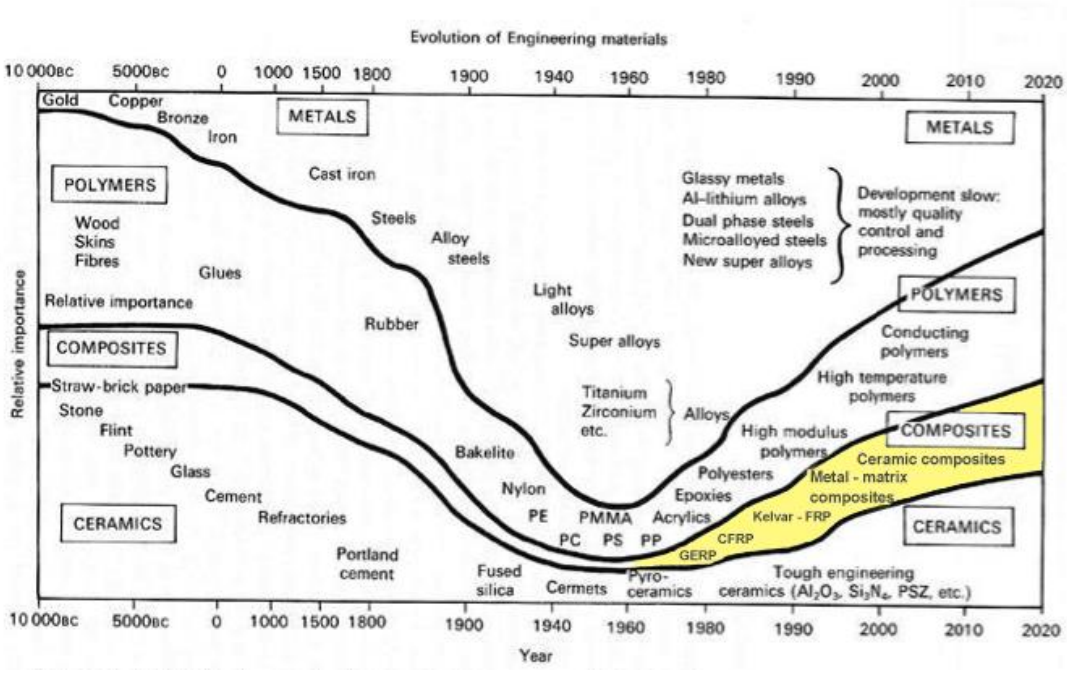

Figure 1-1 The relative development and importance of composites [1]

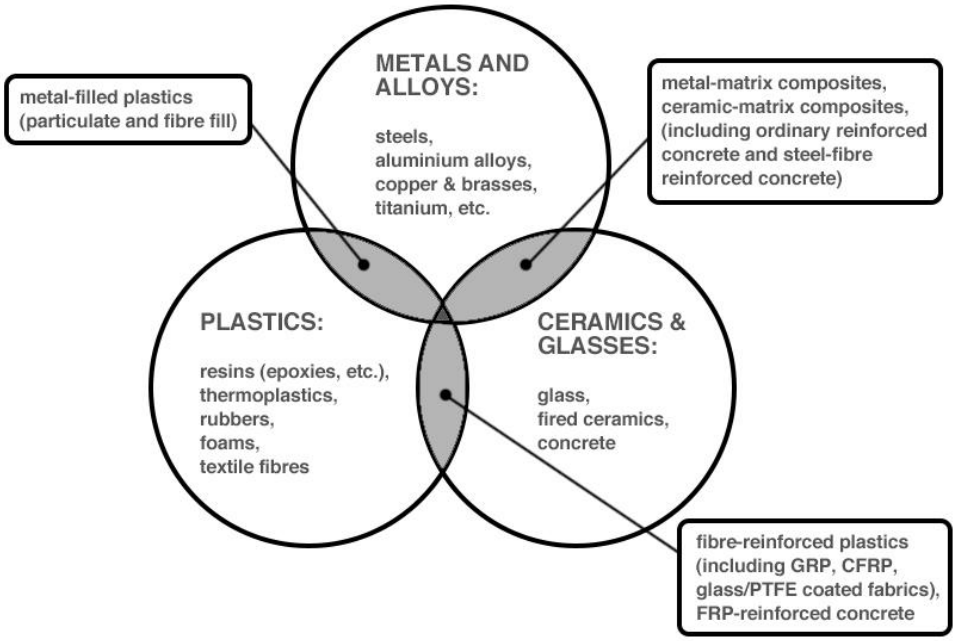

Figure 1-2 Relationship between conventional materials and composite materials

On the other hand, the MMCs miniaturised components under appropriate circumstances and micro featured surfaces with high accuracy and outstanding performance shown in Figure 1-4 have been witnessed in various areas. MMCs precision machining process is then substantially developed and highly required in varied engineering industries. Conventional metal cutting methods such as turning, milling, drilling and grinding have been widely applied to composite materials by using a variety of cutting tools under varied cutting conditions. However, the difficult-to-machine property of MMC accompanied with poor surface generation and extremely high wear of cutting tools is becoming the most critical issues [10-13]. These difficulties associate with high precision and efficient composites machining are urgently need to be solved [14]. Thus, high precision machining with high performance tooling system, as an enabling and effective technology, not only bridges the gap of industrial knowledge between macro-scale and nano-scale [15] but also increases the accuracy of machined parts down to micro-scale.

According to the aforementioned requirements, both outstanding properties and miniature size with high surface performance are required in MMCs industrial applications. MMCs, particularly for aluminium alloy matrix strengthened by micro or nano particles (i.e. SiC and B_4C), have been extensively investigated and utilised in

various applications. In order to achieve the industry-driven requirements on MMCs, the precision machining process has been investigated. Although MMCs machining is kinematically similar to the machining of conventional homogeneous materials, the cutting mechanisms particularly in MMCs precision machining is much more complicate. In addition, various factors affect the MMCs precision machining mechanisms that invalidate the knowledge and physics laws against conventional material machining [16-17]. Thus, it is critical to have a better understanding on the MMCs precision machining process, particularly for the fundamental cutting mechanisms, in order to increase the MMCs machinability.

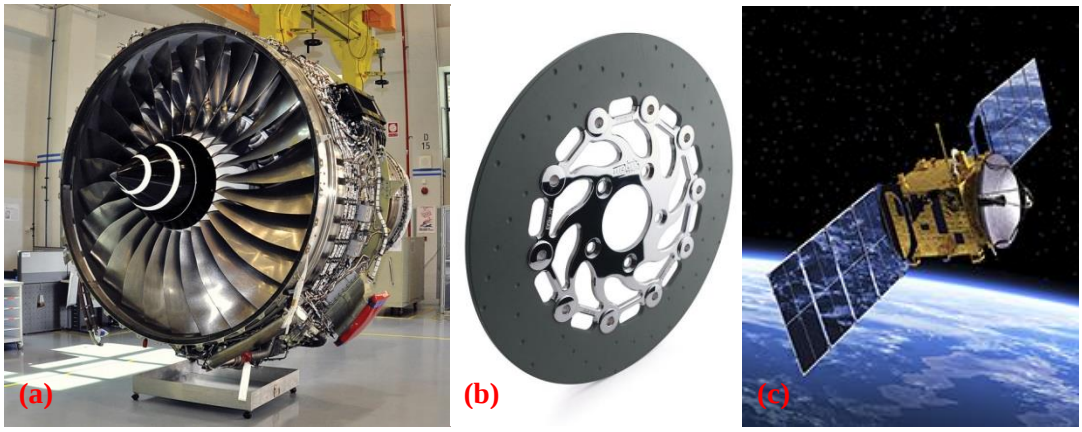

Figure 1-3 (a) Turbofan constructed using MMC materials providing a lightweight but still strong design with higher efficiency for whole aircraft [18] (b) Friction brakes for motorcycles, race cars and high-performance sports cars [19] (c) Satellite structures [20]

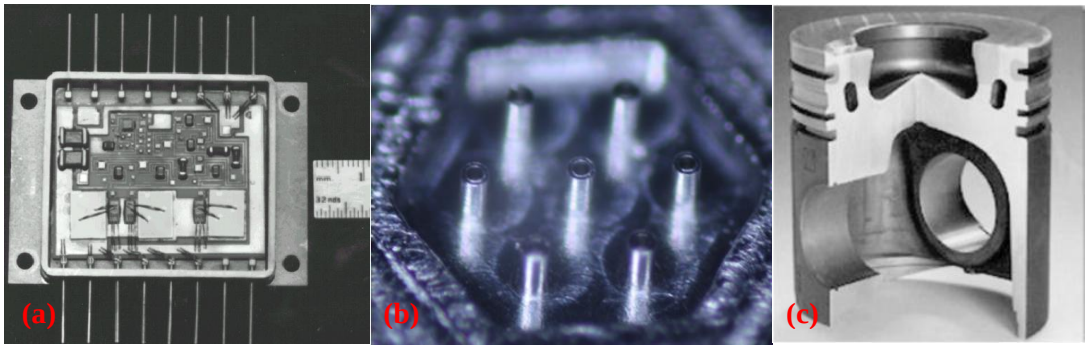

Figure 1-4 (a) SiC_p/Al electronic package for a remote power controller [21] (b) Micro machined electrospray atomizers [22] (c) Partial short fibre reinforced light metal diesel pistons [23]

1.2 Scientific and technological challenges in machining MMCs

MMCs are highly competitive compared with conventional materials for many engineering applications due to their outstanding performance. However, the typical inhomogeneity, anisotropy and low ductility of particulate MMCs lead to their hard-to-machine property and high costs in manufacturing [24]. The investigation on the macro and micro machining of conventional homogeneous materials and fibre composite materials has been massively done. In addition, the cutting mechanics, system dynamics, process dynamics, tool wear mechanism, machining performance and even machinability optimisation of these kinds of materials have been extensively understood. Differentiate from these, hard and brittle particles reinforced metal matrix composites machining process and their cutting mechanisms are currently intricate and less understood. In addition, the remarkably enhanced mechanical performance of particulate MMCs leads to a great challenge in precision machining. Rapid tool wear, higher energy requirement, and the associated poor machinability and surface integrity are observed as the potential drawbacks. These drawbacks are hindering the industrial scale applications of MMCs [25, 26]. Thus, the scientific understanding on the following aspects in MMCs precision machining is still limited.

(1) Cutting mechanisms in MMCs precision machining

Considering the inhomogeneous properties of MMCs and the micro scale cutting parameters, investigation and analysis on the fundamental cutting mechanics of MMCs is of great importance. Although the investigation on MMCs machining processes has been extensively developed [27], most research and development work are focused on an individual application case study. Furthermore, the cutting mechanics particular for the chip formation and surface generation are still less understood. In addition, few researches present the role that these reinforced particles play during chip formation and the way in which the particles are removed or fractured, which can be very useful data and information for the materials design and fabrication particularly towards having much improved machinability performance.

(2) Cutting force modelling

Cutting force, as the most efficient and effective signal, is able to interpret the chip formation, cutting dynamic, cutting temperature, tool wear and even surface generation

in MMCs precision machining process. The existing cutting force models are effectively utilized to analyse on homogeneous material in conventional cutting process. However, the process behaviours in MMCs precision machining cannot be sufficiently explained by using these theories or force models. Substantial development of MMCs cutting force models and also the better understanding on the cutting behaviours of particle reinforced heterogeneous materials has been obtained using analytical or empirical methods. These have been proposed by various researchers [27-30]. However, these numerical, simulation and experimental based models are mainly focused on the prediction of force magnitude on specific time points or consistent chip load conditions. In addition, the 3-dimensional milling processes, taking continued-changed chip formation, the real chip formation conditions and also their significant effects on the cutting force into account, are still less understood in these proposed models. In addition, there is also few understanding on explicit modelling of cutting forces for particles reinforced MMCs. Thus, a force model to illustrate the insight characteristics of force transforms and force amplitude by considering the size effects of cutting tool, un-deformed chip thickness effects, microstructure of target material and process variables comprehensively in MMCs precision machining process is a challenge need to be addressed.

(3) Cutting tool wear and cutting temperature partition

In MMCs precision machining, the cutting force magnitude is normally much smaller than that in conventional machining process due to the conservative small-scaled cutting parameters. However, the extensive tool wear can be significantly observed. This occurs due to the extremely high hardness and high abrasive property of reinforced particles and also the specific cutting force including cutting force on unit length, unit area or unit volume is still quite large. Thus, the machining process in term of tool wear mechanisms can be better understood by using specific cutting force rather than the absolute force value [31]. Abrasive tool wear, as the primary wear mechanism, is still significant when rubbing on the hard particles and seriously affect the machining form accuracy and machined surface quality. In addition, the temperature partition on the cutting tool is another factor that accelerates the wear speed. The poor cutting tool performance results in the burr formation and surface defects which have further effects on the surface roughness and surface functionality. In continuous cutting process, the maintenances of on-machine tool wear, cutting temperature and the utilization of high

performance cutting tools with long life are of great importance. The previous methods that analysing the tool wear according to the cutting force model or Johnson-Cook stress model with different algorithms are not reliable and accurate under this condition [32, 33]. Thus, a multiphysics coupled thermal-mechanical-tribological analysis is required to predict tool wear and cutting temperature effectively and accurately and further maintain the MMCs machining in a higher accuracy and consistency level.

(4) Machinability assessment of MMCs

The MMCs precision machining is observed as a holistic process. Due to the machining behaviour of MMCs is complicated, machinability which can be assessed on the basis of criteria such as material removal, surface finish and tool life is of great importance for industrial engineers [34]. The higher surface roughness value and also the deterioration and defects of the machined surface that significantly affect the machinability and functional performance of engineering components is becoming one of the major reasons that limiting the widespread application of MMCs in high precision industries. Considering the surface roughness is observed as a key factor in the evaluation of surface quality and machining accuracy, better surface generation with lower surface roughness is required. However, precision machining on particles reinforced MMCs is observed as a scientific challenge. Although various non-traditional processes of material removal from MMCs to produce parts even with intricate shape and profiles have been extensively introduced [35], conventional machining process is still indispensable during finish machining [36]. An improved approach for ultraprecision and micro machining towards high producible, predictable and productive is shown in Figure 1-5. This holistic approach indicates that machine tools, cutting tool properties, workpiece properties and machining process variables are the main factors that involved in the precision machining process and obviously influence the machining qualities. According to the industrial demands on machining efficiency, cost-effective, accuracy and consistency, the assessment of tool life, achievable surface finish, surface integrity and material removal rate, and also the machining process optimisation are then becoming of great economic importance for the improvement of material machinability and final products quality.

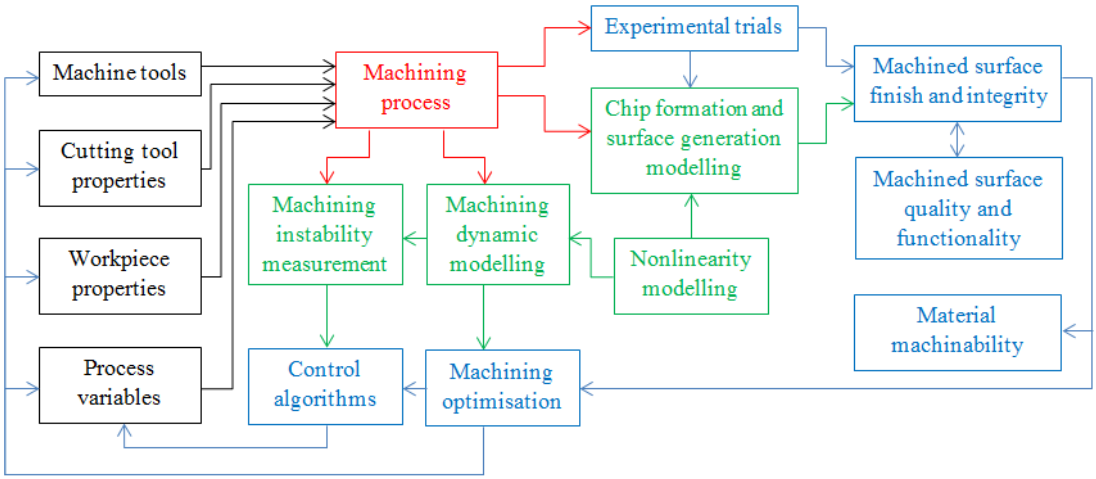

Figure 1-5 Improved machining approach towards ultraprecision manufacturing

1.3 Aim and objectives of the research

This research aims to investigate the fundamental micro cutting mechanics in MMCs precision machining and the associated tool wear and surface generation, so as to achieve the scientific understanding on MMCs machinability and the process optimisation. The distinct objectives of the research are:

- To develop a multiscale multiphysics based approach to precision machining of metal matrix composites (MMCs).
- To investigate the cutting mechanics in precision machining of metal matrix composites (MMCs) particularly for its chip formation mechanisms.
- To develop the improved dynamic cutting force model for MMCs machining process.
- To investigate on the cutting temperature partition, tool wear and tool performance through thermal-mechanical-tribological coupled analysis.
- To undertake machinability assessment and process optimisation in MMCs precision machining.

1.4 Scope of the dissertation

Figure 1-6 illustrates the scope of the dissertation. The chapters consisted in this thesis are further demonstrated in details as below.

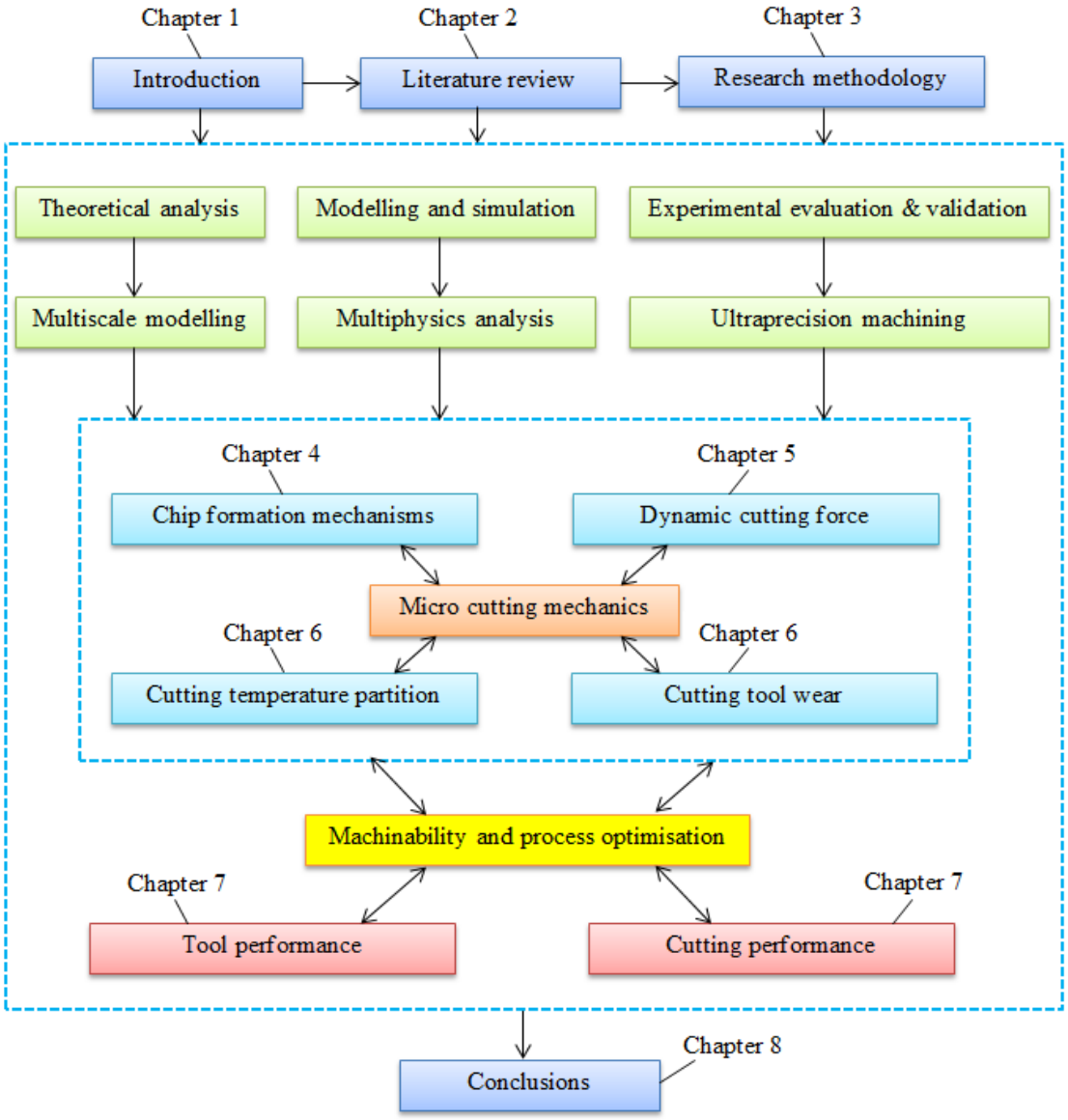

Figure 1-6 Thesis scope

Chapter 1 introduces the research background and briefly history of machining metal matrix composites (MMCs). The scientific and technological challenges are involved in this chapter. The scope of the full thesis is presented after the aim and objectives of this research.

Chapter 2 briefly introduces the state-of-art characterisation of MMCs machining. The fundamental cutting mechanics issues in current MMCs machining community are reviewed. The detailed chip formation, cutting force, cutting temperature, tool wear, surface generation and process optimisation are further conducted respectively.

Chapter 3 illustrates the development of a multiscale multiphysics based integrated approach to modelling and analysis the MMCs precision machining process. Research methodology, associate software package, experimental facilities utilized in this research and experimental set-up are further elaborated.

Chapter 4 investigates the characterisation of MMCs in precision machining process and its manifestation of cutting mechanics. Theoretical analysis is conducted to identify the minimum chip thickness of particulate MMCs in precision machining. Multiscale multiphysics phenomena and their implications are performed through Abaqus/Explicit based finite element analysis in order to study the MMCs chip formation process including the matrix material breakage, particles fracture/debonding/dislocation and their interfacial reaction in details. Theoretical and simulation results are evaluated and validated through well-designed experimental trials conducted on high precision machine using PCD tools.

Chapter 5 proposes a new modified dynamic cutting force model in MMCs precision machining. The innovated multiscale based force model illustrates the full 3-deminational cutting force flows. The cutting forces are modelled and analysed in three cutting regimes: elastic recovery zone, ploughing zone and shearing zone. A novel instantaneous chip thickness algorithm including real chip thickness and real tool trajectory is developed by taking account of the tool runout. Experimental trials are carried out to evaluate and validate the dynamic cutting force model.

Chapter 6 studies the cutting temperature and cutting tool wear by means of thermal-mechanical-tribological coupled FE analysis and experimental evaluation respectively. The cutting temperature partition in MMCs precision machining is simulated under varied cutting conditions. Tool wear mechanisms are investigated through the experimental work. The potential parameters that affect the cutting tool wear are identified and tool wear rate is predicted in application of tool wear monitoring.

Chapter 7 introduces the process optimisation by focusing on the cutting parameters, tool conditions and workpiece material microstructures, and their effects on the cutting force, tool wear, tool life, surface quality, material removal rate and form accuracy and further the machinability improvement of particulate MMCs.

Chapter 8 makes concluding remarks for this research work and draws the recommendations for the future research work.

Chapter 2 Literature review

Metal matrix composite materials are designed in light of the material requirements for high precision engineering and proposed as the alternative in various engineering applications. However, the potential drawbacks of MMCs precision machining significantly hinder its widespread applications. The scientific and technical challenges mentioned in Chapter 1 are urgently need to be solved in order to obtain the industrial demands on machining efficiency, cost-effective, reliable, accuracy and consistency. This chapter surveys the research background and the previous research achievements in MMCs machining particularly for the MMCs material removal characterisation and the state of the art machining technology. In addition, the knowledge gaps for the previous investigations are identified subsequently.

Precision machining of particle reinforced MMCs is different from conventional machining of homogeneous materials in various aspects. Thus, the fundamental understanding on the cutting mechanics of MMCs precision machining is crucial. MMCs properties, size effect, chip formation mechanisms, cutting force model, cutting temperature generation, tool wear, surface generation, machinability assessment and process optimisation, as the crucial aspects in MMCs machining process, are investigated respectively as below.

2.1 Particle reinforced metal matrix composites

2.1.1 Fabrication

Conventional and developed fabrication methods for mass production of high performance composites have been previously reported and reviewed in many research studies. Solid-phase processes and liquid-phase processes shown in Figure 2-1 are commonly used for MMCs fabrication in industrial level [37, 38]. Powder metallurgy (PM) processing, which is blending of powder followed by isostatic pressing, spray deposition techniques and diffusion bonding, is the well-established method used in solid-phase processes [40]. Melt stir casting, melt infiltration, spray casting, and in situ reactive processing are mainly used as liquid-phase processes [40]. The main fabrication techniques and categories for composites including fabrication processing, application, cost and key features are illustrated in Table 2-1.

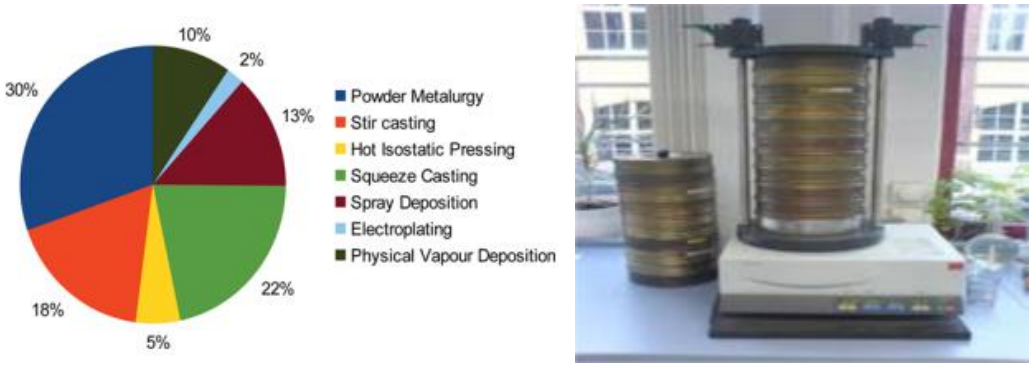

Figure 2-1 Fabrication routes of MMCs [39, 40]

Table 2-1 Comparison of MMCs fabrication techniques [41]

Route	Cost	Application	Comments
Diffusion bonding	High	Used to make sheets, blades, vane shafts, structural components	Handles foils or sheets of matrix and filaments of reinforcing element
Powder metallurgy	Medium	Mainly used to produce small objects (especially round), bolts, pistons, valves, high-strength and heat-resistant materials	Both matrix and reinforcements used in powder form; best for particulate reinforcement; since no melting is involved, no reaction zone develops, showing high-strength composite
Liquid–metal infiltration	Low/medium	Used to produce structural shapes such as rods, tubes, beams with maximum properties in a uniaxial direction	Filaments of reinforcement used
Squeeze casting	Medium	Widely used in automotive industry for producing different components such as pistons, connecting rods, rocker arms, cylinder heads; suitable for making complex objects	Generally applicable to any type of reinforcement and may be used for large scale manufacturing
Spray casting	Medium	Used to produce friction materials, electrical brushes and contacts, cutting and grinding tools	Particulate reinforcement used; full-density materials can be produced
Compocasting/rheocasting	Low	Widely used in automotive, aerospace, industrial equipment and sporting goods industries; used to manufacture bearing materials	Suitable for discontinuous fibres, especially particulate reinforcement

PM, as a promising and versatile method, is seen as the best suitable technique for the fabrication of these particle reinforced MMCs [42, 43]. The detailed schematic diagram of processing steps for the MMCs workpiece fabrication is shown in Figure 2-2. Spray deposition technique followed by diffusion bonding is applied to ensure that each individual reinforcement is coated along with the matrix material afterwards. This fabrication process can be carried out at much lower temperature around 550-650 degree, as compared to the conventional sintering which is normally 750-975 degree, resulting in material with lower densities [46]. The MMCs fabricated by PM method have more homogeneous microstructure along with favourable mechanical and structural properties compared to other fabrication techniques [47]. This is due to the constituents of MMCs are mixed into solid-state diffusion and the desired shape has been formed as the composite. In addition, there is no other by-product or unwanted layer formed between reinforcement and matrix material by using the PM technique [48]. Normally, 95–98% of the reinforcements are even distributed in the matrix

material [42, 43]. For a given set of constituents, the fundamental link between properties and cost is determined by the fabrication method [49].

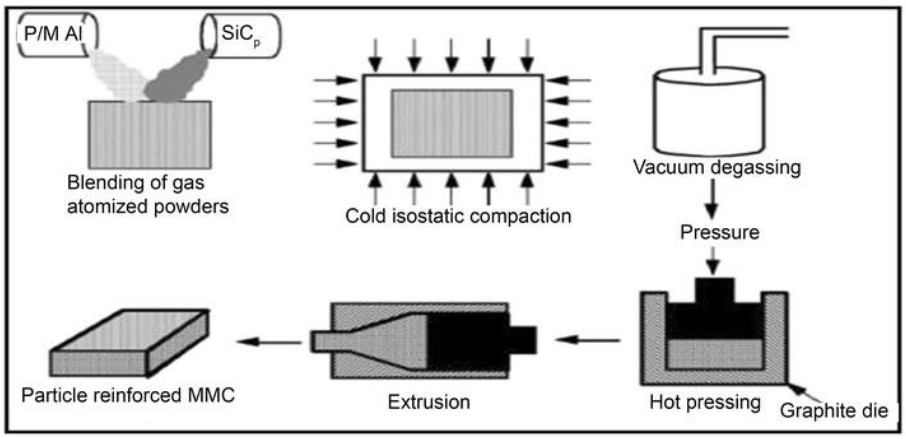

Figure 2-2 Schematic of typical powder metallurgy composites processing [44, 45]

2.1.2 Mechanical properties and applications

Due to the outstanding physical and mechanical properties, particle reinforced MMCs have already replaced the conventional homogenous materials in some industry area and also have the potential to replace the light weight metallic materials such as aluminium, titanium and their alloys [50]. The features of the MMCs microstructure are influenced by the interaction between matrix material and reinforcements, which normally include their type, size, distribution, microstructural defects and interfacial characteristics. Thus, the mechanical properties of MMCs are significantly affected by these factors [51].

In term of the MMCs composition, it has been noted that there is an increasing trend to use aluminium alloy based matrix material due to its ductility and low density [52]. In addition, oxides, carbides and nitrides, which have excellent properties like specific strength and stiffness at both high and ambient temperatures, are normally used as the reinforced materials in metal matrix composites [53, 54]. Thus, SiC/Al and B_4C/Al MMCs are usually performed as the new functional material with excellent properties in high precision areas. The particle size of reinforcement is another factor that detrimental to the mechanical properties of MMCs. Reinforced particles with smaller size provides better mechanical properties and thermal stability, while reinforcements with large size and higher volume fraction provide better wear resistance [48]. The MMCs properties and its industrial applications are extensively shown in Figure 2-3 and Table 2-2.

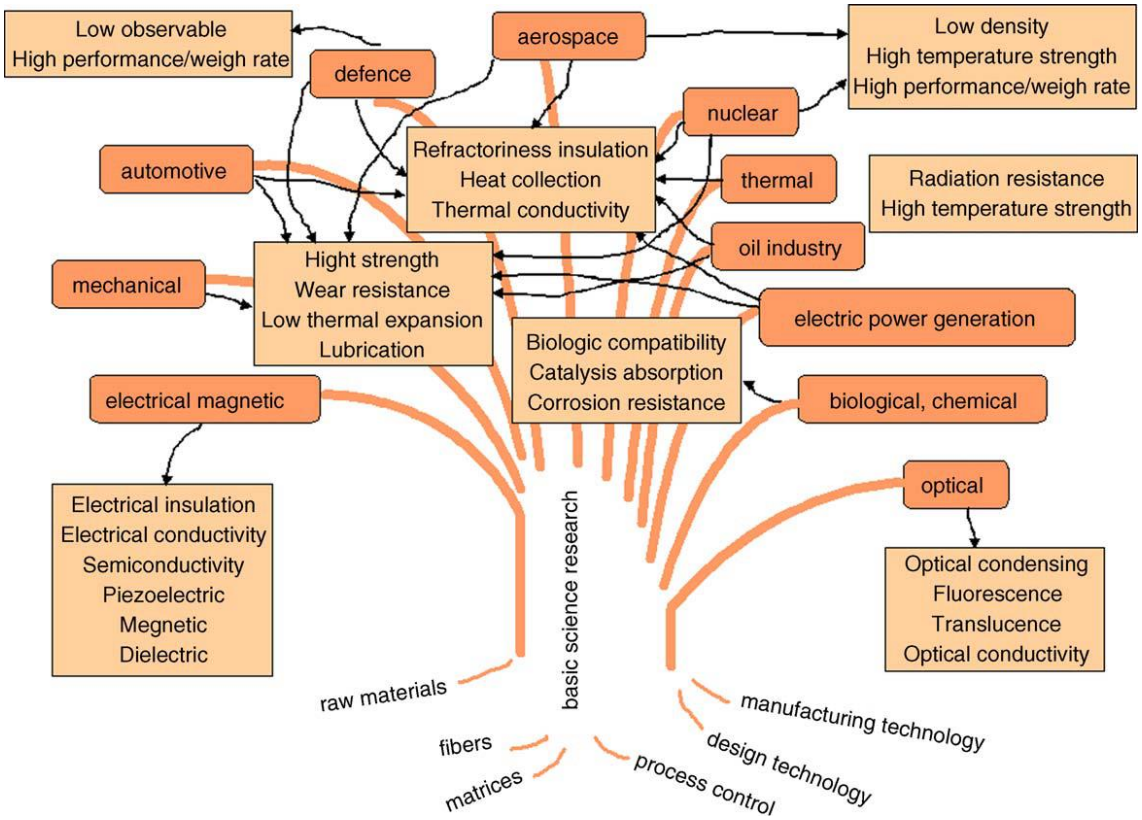

Figure 2-3 Applications of MMCs in engineering industries [55]

Table 2-2 Current and future industrial applications of advanced MMCs [55-57]

Mechanical engineering	Aerospace	Automotive	Defense industry
Cutting tools and dies	Fuel system and valve	Heat engines	Tank power trains
Abrasives	Power units	Catalytic converters	Submarine shaft seals
Precise instruments parts	Low weight components	Dri vetrain components	Improved armors
Molten metal filter	Fuel cells	Turbines	Propulsion system
Turbine engine components	Thermal protection systems	Fixed boundary recuperators	Ground support vehicles
Low weight components for rolary equipment	Turbine engine components	Fuel injection components	Military weapon system
Wearing parts	Combustors	Turbocharger rotors	Military aircraft (airframe and engine)
Bearings	Bearings	Low heat rejection diesels	Wear-resistant precision bearings
Seals	Seals	Waterpump seals	–
Solid lubricants	Structures	–	–
Biological, Chemical processing engineering	Electrical, Magnetic Engineering	Nuclear industry	–
Artificial teeth, bones and joints	Memory elements	Nuclear fuel	–
Catalysts and igniters	Resistance heating elements	Nuclear fuel cladding	–
Hearts valves	Varistor sensor	Control materials	–
Heat exchanger	Integrated circuit substrate	Moderating materials	–
Reformers	Multilayer capacitors	Reactor mining	–
Recuperators	Advanced multilayer integrated packages	–	–
Refractories	–	–	–
Nozzles	–	–	–
Oil industry	Electric power generation	Optical Engineering	Thermal Engineering
Bearings	Bearings	Laser diode	Electrode materials
Flow control valves	Ceramic gas turbines	Optical communication cable	Heat sink for electronic parts
Pumps	High temperature components	Heat resistant translucent porcelain	High-temperature industrial furnace lining
Refinery heater	Fuel cells; (solid oxide)	Light emitting; diode	–
Blast sleeves	Filters	–	–

2.2 Characterisation of machining metal matrix composites and chip formation mechanisms

From the theory of metal cutting, it is well known that the study of chip formation is the most effective method to understand the machining characteristics of a material. However, numerous researches have revealed that MMCs machining is significantly more difficult than those of conventional homogeneous material due to the joint of action of adhesion and abrasion resulting from the reinforcing elements [58-62]. Meanwhile, the machining characterisation particularly for the chip formation mechanisms in MMCs precision machining are quite unique [63]. Thus, the underlying chip formation mechanisms in MMCs precision machining is investigated fundamentally in this section.

2.2.1 Size effect

In the applicability of micro machining, the well-known size effect has been extensively discovered [64-68]. The size effect is recognized as the decreases in un-deformed chip thickness results in the non-linear increase of specific cutting forces especially for extremely small depth of cut down to regime of the minimum chip thickness. A variety of explanations on the size effect have been proposed in several aspects. It is initially ascribed to the relative increase of friction energy or to the reduced probability to find stress reducing defects in the shear zone [69]. The hardening effects due to strain gradients that result in the variation of material strength with specimen volume have extensively drawn the attention on the size effect aspect [70]. The change of heat distribution in the workpiece for smaller dimensions, especially for higher cutting velocities [71], is another factor that affects the size effect [72]. Strain rate hardening, as another critical factor, results in the increase of the yield stress when the system size decreases. This leads to the increase of the specific cutting force [73]. The effective rake angle, which is affected by the ratio of the uncut chip thickness to the effective cutting tool edge radius, is another reason of size effect investigated by Denkena et al [74]. In recent research, size effect is also found that influenced by the cutting parameters in micro machining [75].

The size effect also plays an important role in precision machining of particle reinforced MMCs. This performs the similar phenomenon to the size effect in conventional

homogeneous material machining due to the chip thickness is in the same order as the cutting tool edge radius and also the grain size of workpiece material [75]. Thus, the size effect that attributed to the above mentioned cutting tool edge radius effect, material microstructure effect including dislocation density and availability, material strengthening effect due to strain, strain rate, strain gradient, and subsurface plastic deformation and material separation effect [75] can be observed as the most significant factor influencing the cutting performance [76]. The speculation on size effect has already gained wide attentions in the following research studies.

For the size effect in MMCs machining process, Liu et al [76] proposed that the ratio of particle size to the uncut chip thickness, and the volume fraction of reinforcement have significant effects on the cutting performance of MMCs. In their study, the experimental based investigation on the specific cutting energy trends for machining pure Mg and 10 Vol.% Mg-MMCs has been done respectively. The experimental results indicate that the specific cutting energy trends, due to size effect in MMCs machining, are in the same order as those in machining of pure Mg. However, the size effect has slightly difference as shown in Figure 2-4 due to the present of reinforced particles.

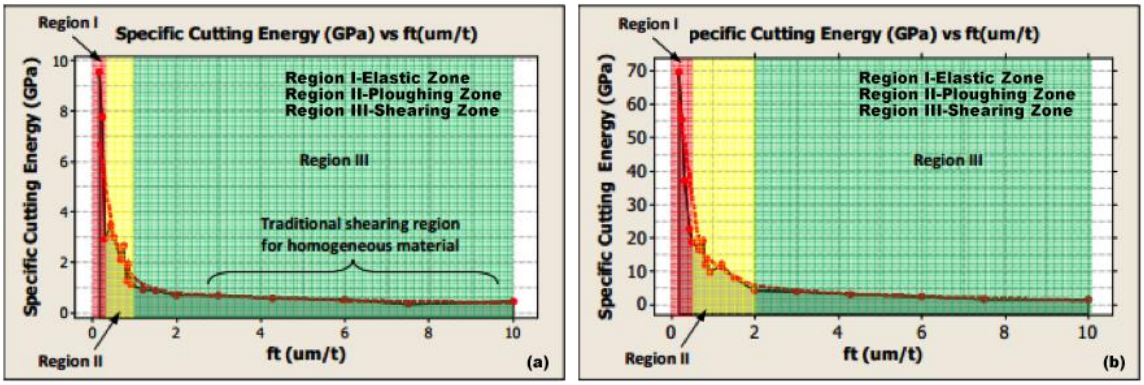

Figure 2-4 (a) Specific cutting energy vs. nominal feed/tooth for Pure Mg (b) Specific cutting energy vs. nominal feed/ tooth for 10 Vol.% Mg-MMCs [76]

Teng et al [77] carried out the experiments on micro machining of MMCs and the size effect was found and characterised by studying the specific cutting energy, cutting force and surface morphology in their research. With the ratio of feed per tooth to the cutting edge radius increases, the specific cutting energy decreases dramatically and transit to a stable value afterwards. In addition, the cutting force is relatively large when machining with a small feed per tooth. Moreover, more defects on the slot edges and machined surfaces can be found when the feed per tooth is relative small.

2.2.2 Minimum chip thickness effect

Due to the existence of unneglectable cutting tool edge radius and the reinforced particles, chips will not be formed at a large negative angle when machining with an extremely small depth of cut; only when the uncut chip thickness reaches a certain critical value, chips start to produce. This minimum chip thickness effects can be illustrated schematically in Figure 2-5. As the minimum chip thickness plays an important role in precision machining, theoretical analysis, simulations and experimental methods have been adopted to determine the minimum chip thickness in large numbers of researches [78-81].

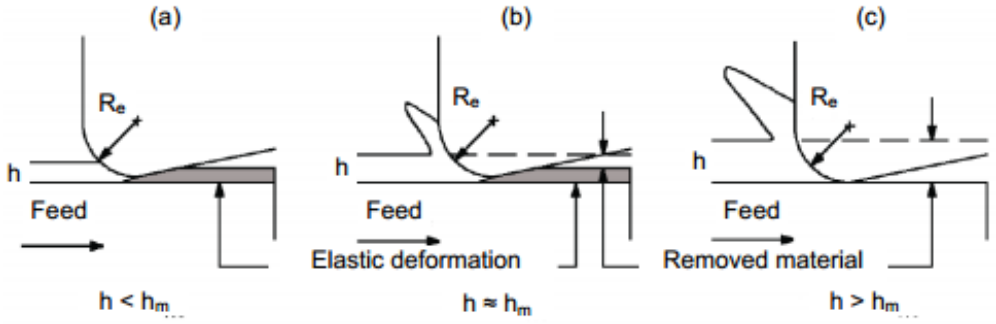

Figure 2-5 Minimum chip thickness in orthogonal cutting [82]

In MMCs precision machining, the chip formation model has been developed by Liu et al [76]. In this study, it can be observed that when the machining process takes place at an extremely small DOC, composite materials including matrix material and particles experience pure elastic deformation and then recover to their original position. With the continue increase of uncut chip thickness, the elastic-plastic deformation occurs on the matrix material when the DOC value beyond the elastic recovery threshold. In this situation, particles will experience fracture or displacement rather than recover to the original position. Only when the DOC is larger than the minimum chip thickness threshold, chips start to form. Matrix material will not experience the elastic recovery process any more, accompanies with the particles either removed with chips or fracture and displacement in the separation zones. The value of minimum chip thickness is also determined by carrying out the investigation on size effect according to the specific cutting energy and resultant surface morphology [77]. In the research from Teng et al, the stable value of transition for the specific cutting energy approaching to is expected as the minimum chip thickness value. In addition, at a certain value of uncut chip thickness, the workpiece material at the same position is cut more than once, which

results in overlapping tool mark; over this value, this machining phenomenon disappear. Thus, this uncut chip thickness value is observed as the minimum chip thickness.

2.2.3 Chip formation and morphology

The chip formation process has intrinsic relationship with size effect and minimum chip thickness effect. According to these effects, it can be observed that workpiece material undergoes pure elastic deformation when the DOC is extremely small; then plastical deformation will occur when increasing the DOC; only if the DOC value is larger than the minimum chip thickness, chips start to be removed. However, material deformation and material removal mechanisms in precision machining of particle reinforced MMCs are different from that of conventional monolithic metals even in micro scale due to the existence of reinforcements [14, 83]. The chip formation cannot be explicitly predicted by only using a threshold value in micro machining of MMCs due to the complex physics [22]. On the other hand, even minor change on chip formation in MMCs machining will significantly affect the tool life, machined surface finish and form accuracy [84]. Hence, the in-depth understanding on the chip formation mechanism is necessary for efficient chip control, further used to improve the machinability of composites and also enhance their applicability [85, 86]. In this part, the investigation on chip formation and chip morphology, which is observed as the result of specific chip formation mechanisms presenting the MMCs machining process [87], is concluded.

Experimental based chip formation analysis has already done by large numbers of researchers [88-92]. In order to have a better understanding on the machining characteristics of Al/SiCp composite material, Monaghan [88] studied the fundamental aspects of chip formation and chip breaking during orthogonal machining. In his study, the chip formation is considered as the combined fracture/rupture/crumbling process with higher shear plane angle. This is further investigated by Joshi et al [89], which demonstrates that the chips showed a systematic breaking pattern depending upon the volume of reinforcement. It is found that chip curl is depended on the tool rake angle; initial radius of formed chip increases when the volume of reinforcement decreases especially at lower rake angles. On the other hand, the chip breaking can be observed that strongly related to the mechanical properties by a chip breaking criterion. This is helpful to develop the tool geometries. He further developed a microstructural analysis on the chip formation, which found that outer surfaces of chips produced showed a

significant variation ranging from prominent saw-tooth profile to light waviness. In addition, the profile becomes prominent when the volume of reinforcement increases as shown in Figure 2-6. However, when increasing the cutting speed, the trend reverses. The chip formation mechanism in the machining process shows that initiation of gross fracture occur at the chip free surface toward the cutting edge and the remaining portion of material on the shear plane are removed by flow-type deformation as shown in Figure 2-7.

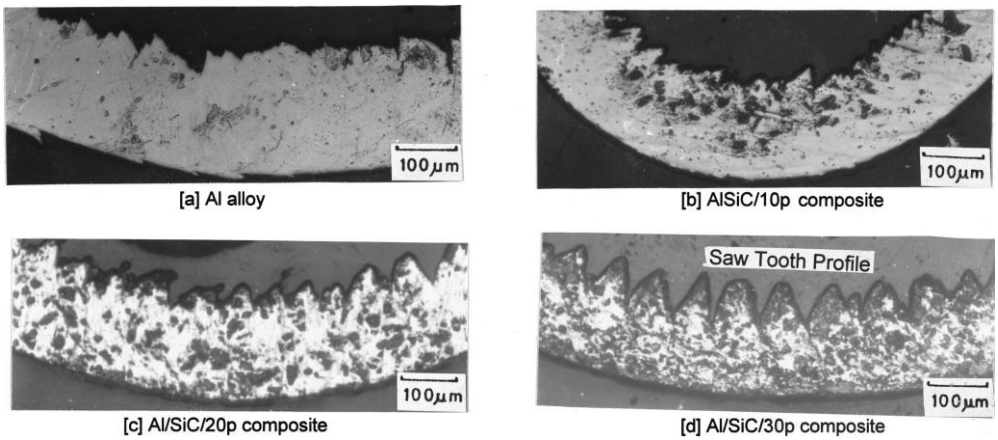

Figure 2-6 Chip formation at different volume of reinforcement [89]

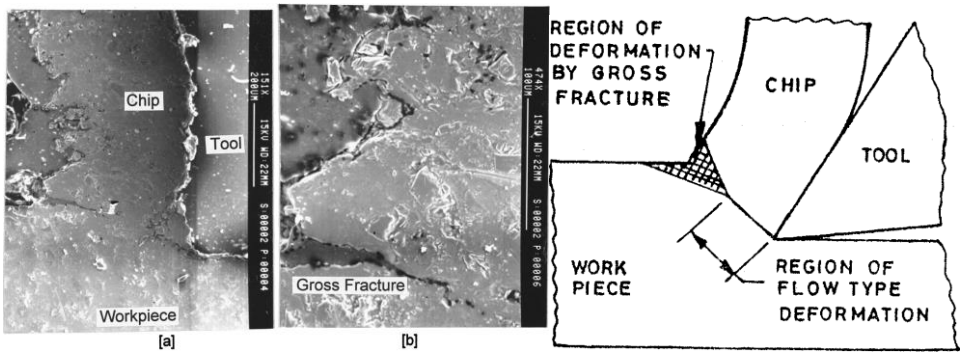

Figure 2-7 Chip formation mechanism in the machining process of MMCs [90]

A quick-stop study on the aluminium matrix composites is developed by Karthikeyan et al [91]. The experimental results revealed that continuous chips are formed when machining MMCs with lower volume fraction of reinforcements. In addition, discontinuous chips are formed when machining MMCs with larger volume fraction of reinforcements. The cracks on the workpiece occur at the free surface and extend towards the tool tip. The shear band spacing across the chip decreases when increasing the particle volume fraction, feed rate and depth of cut. In addition, the spacing also increases when the cutting speed increased. Moreover, chip thickness ratio and shear

angle will also decrease when increasing the cutting time cutting speed and depth of cut, or reduce the feed rate and volume fraction of reinforced particle due to the chip disposability decreases.

Gallaba and Skladb [92] investigated the chip formation mechanism by machining Al/20%SiC particulate metal-matrix composites (PMMC). The experimental results indicate that the matrix material deforms and the reinforced particles are aligned along the maximum shear bands. Increase of the cutting speed leads to ductile tearing of chips. In term of the reinforced particles, some of them are pulled-out while others are fractured. In addition, voids and cracks are observed around the particles due to the matrix material plastic deformation. Moreover, the voids surrounding the particles join up and cause chip segmentation when the feed rate and depth of cut increase.

The chip formation is further investigated experimentally by considering the effects of reinforced particles in MMCs machining. From Pramanik's research, chip breakability is found improved due to the existence of particles. As a result, short chips are formed under almost all conditions. In addition, chips with different shapes are found under various conditions. This is due to the chips formation is strongly related to the material properties and cutting parameters such as speed and feed, etc. [14]. Dabade and Joshi [93] achieved the similar results by studying the chip formation mechanism during machining of Al/SiC_p composites. In their research, needle type and segmented chips are formed at lower cutting speed; whereas semi-continuous, continuous, scrambled ribbon and tubular helix chips can be observed at higher cutting speed. In addition, when increasing the feed rate, both the length of chip and the number of chip curl increase. Moreover, the chip formation mechanism is significantly affected by the size and volume fraction of reinforcement. In case of finer reinforcement, the chip segments are longer and gross fracture only occurs at outer surface of the formed chips. Meantime, secondary crack formation is evident at inner surface due to its higher ductility as shown in Figure 2-8. However, in case of coarser reinforcement, the complete gross fracture of chip formation results in smaller chip segments. In addition, the coarser reinforcement particles act as a chip breaker that produce both segmented and small curled chips and finally improve the machined surface roughness.

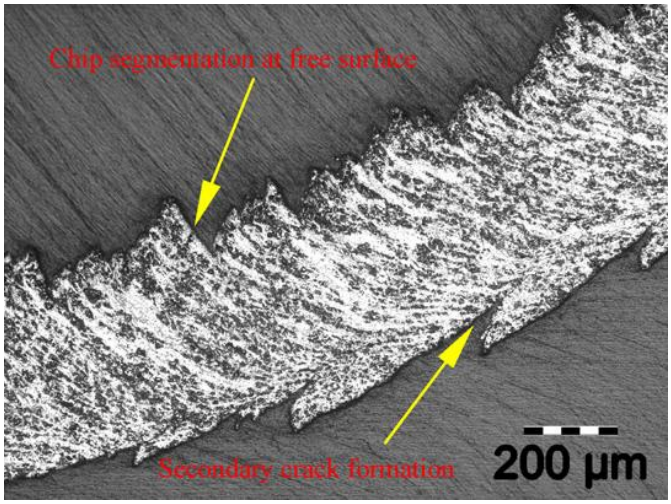

Figure 2-8 Chip formation mechanisms during machining of Al/SiCp composites [93]

Based on the researches mentioned above, it can be observed that little effort has been given to characterising the chip formation mechanism and chip morphology through experimental abased analysis in MMCs precision machining. Previous researches indicate that finite element analysis (FEA) is applied to better illustrate the material removal mechanism including matrix material removal and particle fracture or de-bonding. Thus, FEA is observed as the principal technique for modelling and predicting the chip formation with reasonable accuracy [94-99].

In the chip formation modelling for particulate heterogeneous materials, Monaghan and Brazil [94] developed a complex micromechanical process for effectively modelling the machining of particle-reinforced metal matrix composite (PRMMC) using FEA sub-modelling. The flowing chips are formed in this model. In addition, particles are partly debonded and subsequently rotated and ploughed on the machined surface. Another FE model, which applies a shear failure model by comparing effective plastic strain with the damage plastic strain value, is developed to simulate the machining of aluminium/aluminium oxide particulate composite [95]. Tool/particle contact mechanisms along interface is investigated in this research and the simulation results shown in Figure 2-9 indicate that the debonded or partly debonded hard particles due to the failure of interface are sliding and scratching on the tool rake face. The hard particle is then pushed inside the chip after a certain moving distance.

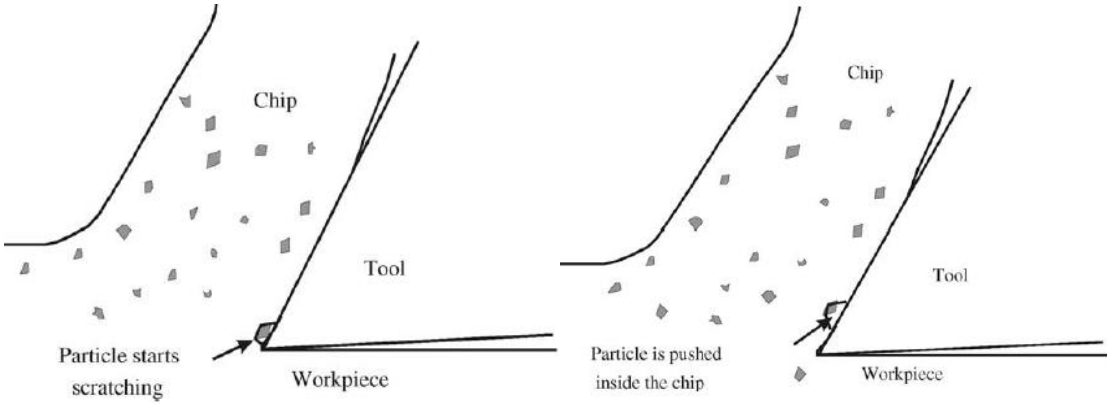

Figure 2-9 Machining of aluminium/aluminium oxide particulate composite [95]

A modelling strategy by integrating the microstructure-level material model and the failure model is developed and implemented by Dikshit to investigate machining of polycarbonate carbon nanotube composites. A modified version of the Gearing and Anand failure model for polycarbonate is used by taking the competition between ductile and brittle failure into account. In addition, the carbon nanotubes are modelled by using a strain-to-failure criterion [85, 86]. The simulated and experimental results of chip formations are shown in Figure 2-10.

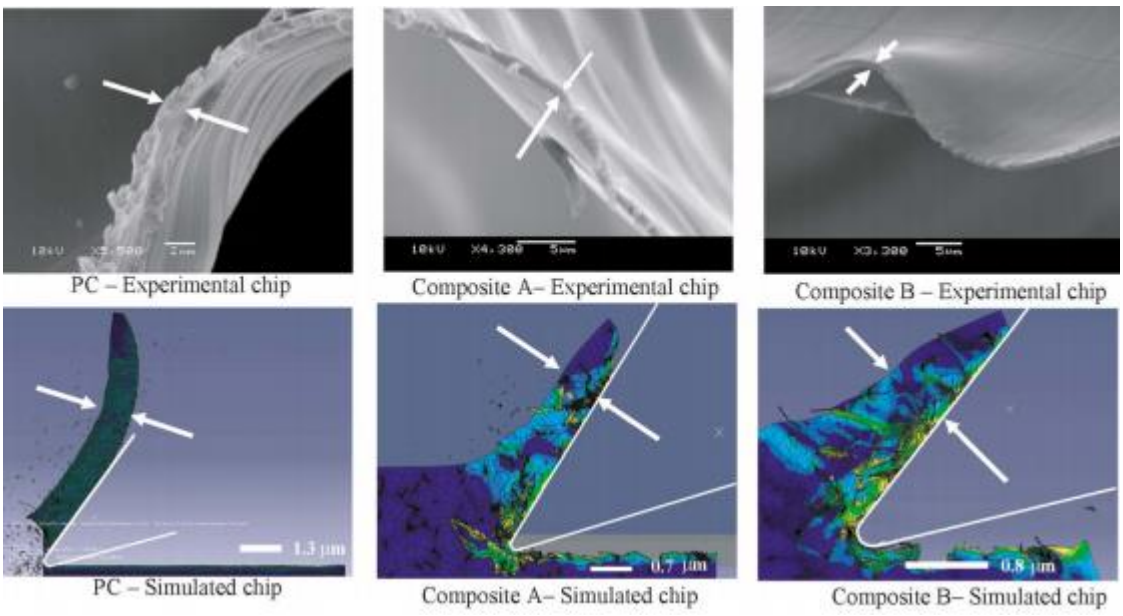

Figure 2-10 Simulated and experimental chip formations in machining of polycarbonate carbon nanotube composites [85, 86]

Pramanik and Zhang investigated the behaviour of tool–particle interaction during orthogonal cutting metal matrix composites [96]. The simulation results reveale that particles in the lower part of the cutting edge are debonded and leaving a cavity on the

machined surface. These particles further take part in ploughing of the machined workpiece surface. The particles in the upper part of the cutting edge are partially debonded and moves up with chips sliding over the rake face.

Zhou et al developed a thermal-displacement coupled FE model for the simulation of SiC_p/Al composites orthogonal cutting. The simulation results show when the cutting tool faces the upper part of the particle, the tool will plough over the hard particle; when the tool faces the middle part of the particle, cracking in the middle of the reinforcement will occur and further plough through it; when the tool encounters the lower part of the SiC particle, the continue approaching promoting the failure of bonding interface of reinforcement and matrix, as a result, particles are pulled out [97].

Chip formation in MMCs machining is also studied by Fathipour et al through FEM [98]. In this study, saw-tooth shapes are common features of the chip formation in MMC machining. Distance among saw-tooth and size of these saw-tooth formed on chips are increased by increasing the cutting speed. While only the size of saw-teeth increases by increasing feed rate. Chip shape obtained from simulation is shown in Figure 2-11.

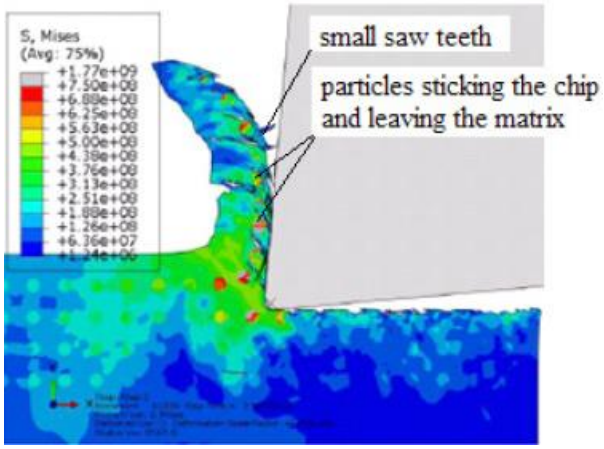

Figure 2-11 Chip shape obtained from simulation in MMCs machining [98]

In order to explore the influence of the SiC particles on chip formation mechanism, the simulation of machining aluminium and SiCp/Al composites with different composition are conducted under the same cutting conditions. As for the chip morphology, the simulation results indicate that continuous chips are formed in machining aluminium, while discontinuous chips are formed for MMCs reinforced by both rounded SiC particles and polygonal SiC particles. In addition, some particles even totally deboned

from the matrix material as shown in Figure 2-12 when the volume fraction of the SiC particle is high.

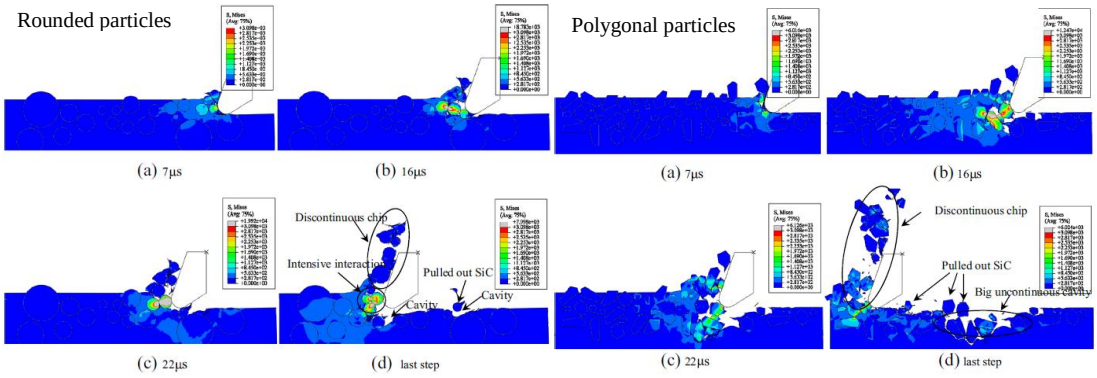

Figure 2-12 Chip formation in the simulation of machining aluminium and SiC_p/Al composites [99]

2.2.4 Modelling of MMCs machining

A tremendous amount of studies have been arisen to have better understanding on the cutting mechanics associated with MMCs machining process. Empirical and analytical methods have been extensively applied in studying the machining process. However, finite element modelling (FEM), molecular dynamics (MD) studies and multi-scale modelling are more powerful that allowed researchers to study MMCs machining process through sophisticated numerical techniques. FEM, to some extent, is preferred for macro-scale machining, where continuum mechanics principles are applicable. On the other hand, MD technique is suitable for nano-metric simulation, where capture atomic interactions are applicable. Thus, in order to bridge the gap between these two scales, multiscale methods have been proposed [100]. The review and comparison of modelling techniques in MMCs precision machining are provided in Table 2-3.

Table 2-3 Review and comparison of modelling techniques in precision machining of metal matrix composites

No.	Constitutive materials modelling	Software/ Model type	MMCs	Output variables	REF.
1	Norton–Hoff model	FORGE2/ ANSYS/ 2D	SiC PRMMC	Chip formation, Interfacial debonding, tool wear/ Matrix flow, tool wear and residual stresses	94, 101

2	Johnson–Cook model	ABAQUS/ 2D	60 μm, 56%, Al/SiC	Cutting forces and stress distribution and tool-particle interaction	97
3	Cowper–Symonds model	ANSYS/LS-DYNA/2D	18 μm, 20%, Al/SiC	Stress distribution and particle debonding	96
4	Johnson–Cook model	ABAQUS/ 2D	20 μm, 5,15,20%, Al/SiC	Chip formations and machining forces	98
5	Johnson–Cook model	ABAQUS/ 2D	10 μm, 65%, Al/SiC	Defect formation mechanisms	99
6	Johnson–Cook model	ABAQUS/ 2D	5 μm, 45%, Al/SiC	Particle behaviour and surface formation	103
7	Equivalent Homogeneous Material (EHM) model	Third Wave Systems AdvantEdge/ ABAQUS/ 2D/3D	28 μm, 20%, Al/ SiC	Cutting forces, stress distribution and subsurface damage	102
8	Johnson–Cook model	ABAQUS/ 2D (ALE)	Al/Al_2O_3	Temperature and stress distribution	95
9	Johnson–Cook model	ABAQUS/ 2D (ALE)	Al/SiC	Tool-reinforcement particle interaction, reinforcement particle debonding, cutting forces, chip morphology, stresses and temperature distributions	104
10	Johnson–Cook model	ABAQUS/ 2D (ALE)	15 μm, 10%, Al/Al_2O_3	Cutting force, interaction between tool and particles, particle debonding and fracture	105
11	Johnson–Cook model	ABAQUS/ 2D (ALE)	23 μm, 20%, Al/Al_2O_3	Effect of cutting speed on the tool–particle interactions as well as the stress and temperature	106
12	Tvergaard-Needleman damage model	ABAQUS/ 2D	7 μm, 20%, Al/SiC	Matrix damage, particle cracking and interface debonding	107

2.3 Cutting force

2.3.1 Cutting force models in machining MMCs

Due to the abrasive nature of reinforced particles that bring up the rapid tool wear, poor surface quality and high machining cost [108], MMCs precision machining is considerable difficult and machining mechanism is observed as complex phenomenon. As the surface quality and machining cost can be improved via machining optimisation process, cutting force modelling that close relate to the machining quality and efficiency is becoming critical [22]. Thus, cutting forces generation, which highly depends on the microstructure of composite material including matrix material, reinforcement properties and their interfacial reaction [109], plays a significant role. It is expected to reflect most of micro machining phenomenon collectively including size effect, chip formation, cutting temperature and tool wear status, and also has potential to optimise the machining conditions and cutting tool conditions. A number of researchers have focused on the investigation of MMCs micro cutting mechanisms, and therefore the dynamic cutting force models based on theoretical assumptions and experimental observations have been developed or improved. The extensive cutting force models for MMCs precision machining have been summarised as follows.

(1) Cutting force model based on the energy consumption

The analytical force model is firstly developed by Kannan et al. [110]. The cutting forces are estimated based on the energy consumption in primary, secondary shear zone, and reinforcement particle displacement and fracture. According to this model, the total energy per unit volume (e) of metal removed can be expressed as:

$$e = E_P + E_S + E_D \tag{2.1}$$

where, E_P is the specific energy for plastic deformation in the primary shear zone, E_S is the specific energy for plastic deformation in the secondary shear zone and E_D is the energy per unit volume consumed for the particle debonding from the matrix material.

In this force model, cutting force is calculated by multiplying the width of cut and under deformed chip thickness. However, the energy consumed in the secondary deformation zone is assumed as one third of that in the primary shear zone and this is purely for monometallic material rather than MMCs. In addition, only the force in the cutting

direction is calculated and energy due to ploughing has not been considered in this model.

Considering these problems, Ghandehariun et al. [111] provided a more accurate estimation of the cutting forces by modelling cutting force based on partition of energy. They focus on the total power consumption P_c in the MMC cutting system and calculate the cutting force through total energy consumption with the following equation:

$$P_c = P_{pd} + P_{tc} + P_{tw} + P_{fns} + P_{mnc} + P_{deb} \tag{2.2}$$

where, P_{pd} is the plastic deformation power of MMC workpiece, P_{tc} and P_{tw} are the power consumption at tool-chip interface and tool-workpiece interface respectively. P_{fns} and P_{mnc} are the power consumption for the formation of new surfaces and minor cutting edge effect respectively. P_{deb} is the power consumption of particles debonding in MMCs cutting process.

Thus, the cutting force can be written as:

$$F_c = \frac{P_c}{V} \tag{2.3}$$

where, V is the cutting velocity.

(2) Cutting force model based on the total force

Most of these models are developed from the conventional milling force model which is formulated from the tangential, radial and axial cutting forces proposed by Altintas [112] and can be given by:

$$\begin{aligned} Ft(\emptyset) &= K_{tc} a h(\emptyset) + K_{te} a \\ Fr(\emptyset) &= K_{rc} a h(\emptyset) + K_{re} a \\ Fa(\emptyset) &= K_{ac} a h(\emptyset) + K_{ae}\, a \end{aligned} \tag{2.4}$$

where, a is cutting depth, $h(\emptyset)$ is the chip thickness at rotating angle of $\emptyset$. The chip thickness variation h can be approximated as:

$$h = c * sin\,(\emptyset) \tag{2.5}$$

The corresponding cutting constants K_{tc}, K_{rc} and K_{ac} are given by:

$$K_{tc} = \frac{\tau s}{sin\emptyset n} \frac{\cos(\beta n - \alpha n) + tanitan\eta sin\beta n}{\sqrt{cos^2(\emptyset n + \beta n - \alpha n) + tan^2\eta sin^2\beta n}}$$

$$K_{rc} = \frac{\tau s}{sin\emptyset ncosi} \frac{\sin(\beta n - \alpha n)}{\sqrt{cos^2(\emptyset n + \beta n - \alpha n) + tan^2\eta sin^2\beta n}} \quad (2.6)$$

$$K_{ac} = \frac{\tau s}{sin\emptyset n} \frac{\cos(\beta n - \alpha n)\, tani - tan\eta sin\beta n}{\sqrt{cos^2(\emptyset n + \beta n - \alpha n) + tan^2\eta sin^2\beta n}}$$

where, $\emptyset n$ is the shear angle, τs is the shear yield stress and i is oblique angle. Altintas also proposed a further understanding on the cutting mechanics particular for the development of cutting force model by incorporating the effect of tool edge radius in the micro reinforcement oriented micro cutting process onto the conventional force model. This model is widely applied in homogeneous material machining process. This conventional model is then developed to predict the cutting force in composite material micro machining. Due to the complex machining mechanism of MMCs, the cutting force hence depends on the matrix material, reinforced particles and their interface [113]. The cutting process mechanisms and process modelling particular for dynamic cutting force modelling are reviewed by Liu et al. [114]. It has been presented that process models have been developed to predict cutting force at the micro-milling scale in the last few decades. The geometric chip formation mechanism is studied and mechanistic model of micro-milling forces and energy-based analytical force model are proposed respectively to better predict the particle reinforced MMCs. As for calibration of cutting force coefficients, nonlinear exponential function and constant cutting force coefficients are the two main methods that used to express the instantaneous force coefficients. Additionally, FE models, which are developed with accurately calibrated material properties, can also be used to acquire cutting coefficients. Based on these previous researches, Liu et al. [114] further developed a multiscale method to predict the cutting force more accurately by considering the cutting force coefficients. The cutting force model and the relevant cutting force coefficients are shown in equation (2.7). However, the reinforced particles were seen as the rigid bodies in this experimental based force model and the specific cutting energy from the experimental results is seen as linear to the nominal uncut chip thickness.

$$dF_t = k_{ts} * t_c * dz$$

$$dF_c = k_{rs} * t_c * dz \quad (2.7)$$

$$dF_a = k_{as} * t_c * dz$$

where, k_{ts} , k_{rs} and k_{as} are tangential, radial and axial force coefficients in the MMCs shearing zone. These coefficients are linear to uncut chip thickness t_c and can be calculated by optimising the measured cutting force data as shown in equation (2.8) as below:

$$k_{ts} = k_{ts1} * t_c + k_{ts2}$$

$$k_{rs} = k_{rs1} * t_c + k_{rs2} \quad (2.8)$$

$$k_{as} = k_{as1} * t_c + k_{as2}$$

where, k_{ts1} , k_{ts2} , k_{rs1} , k_{rs2} , k_{as1} , k_{as2} are the defined constants which have linear relationship with k_{ts} , k_{rs} and k_{as}.

Considering the complicated cutting mechanics of MMCs, theoretical methods are then introduced by various researchers in order to achieve a general MMCs cutting force model. The cutting force models are developed by analysing shearing of matrix material, breakage of reinforced particles and matrix-particle interface together. Several models have been built for the estimation of cutting force in MMCs micro turning process. These cutting force models are originated from the fundamental theory and then developed and modified through comprehensive analysis.

Pramanik et al. [115] proposed an analytical model to predict the cutting force and the thrust force based on the fundamental cutting theory and the conventional force model. Their models consider the shearing of the MMCs to form chips, ploughing of the matrix material under the rounded tool edge and particles fracture, de-location or particles debonding from the MMCs together. Thus, the total force is considered as the sum of chip formulation force, ploughing force, and particle fracture force. The force prediction on matrix ploughing deformation and particle fracture are formulated with the aid of the slip-line field theory of plasticity and the Griffith theory of fracture respectively. The resultant cutting force F_C and thrust force F_T in micro cutting process can be written as below:

$$F_C = F_{CC} + F_{CP} + F_{CD}$$
$$F_T = F_{TC} + F_{TP} + F_{TD} \quad (2.9)$$

where, F_{CC} and F_{TC} are the cutting and thrust forces generated during the MMCs micro cutting process respectively. F_{CP} and F_{TP} are the ploughing forces parallel and perpendicular to the cutting tool path respectively. The forces generated by the debonding and fracture of the reinforced particles are expressed as F_{CD} and F_{TD} respectively. However, the tool-chip friction force result from reinforced particles has not been considered. Even Dabade et al. [116] considered chip-tool interface friction to predict cutting forces in three directions during oblique cutting; they did not consider the effect of particle debonding and ploughing force. Sikder and Kishawy [117] modified the force model by considering the frictional force along the chip tool interface, the force due to particle debonding and ploughing forces. These are then added to the total generated cutting forces based on the model from Pramanik.

Cutting forces are also obtained through finite element simulation of the steady phase of cutting process. In the numerical modelling, cutting forces are predicted associated with the interactions between cutting tool and reinforced particles [98, 99, 103-105]. Most of the simulation results indicate that cutting forces perform fluctuations due to the existence of reinforced particles without analysing the tool-particle interaction. Only Ghandehariun et al demonstrated the relationship between force magnitude and tool-matrix-particle interaction. However, this force model can only be used to predict cutting force under theoretical condition by ignoring the process errors.

In order to predict cutting force accurately, process models have been developed at micro machining scale. A new algorithm to present the instantaneous chip thickness by incorporating the effects of elastic recovery, ploughing and minimum chip thickness is proposed by Liu et al. [114]. Afterwards, by taking tool run-out into consideration, Niu et al proposed comprehensive instantaneous chip thickness model and dynamic cutting force model that focus on the homogeneous material [118]. Vogler et al. [119, 120] proposed a mechanistic model for heterogeneous materials micro end milling process. This model explicitly accounts for different phases and the predicted frequency in cutting force signal is higher due to the multiple phases in material model. In addition, the frequency component of the variation is highly related to the spacing of the secondary phase and the magnitude is affected by the size of the secondary phase

particles. However, this model did not analyse the particle fracture process and also the situation of particle debonding.

On the other hand, the process errors such as tool alignment error and tool geometry error result in the system vibration. Thus, a more sophisticated dynamics model considering these errors is essential to mitigate un-balance induced vibration [22]. In addition, tool vibration and tool deflection that affecting the system dynamics is another challenge. However, the researches on above mentioned aspects are currently less understood. Therefore, the microstructure effects on cutting dynamics in particulate MMCs machining is crucial and need to be further studied. Cutting force models with new capability that considering these above mentioned factors in interpreting the phenomenon encountered MMCs precision machining process is still essential.

2.4 Cutting temperature

Cutting temperature in micro machining of MMCs is of critical importance due to it has significant influence on the cutting performance including force magnitude, tool-workpiece-chips friction, tool wear, surface generation and surface integrity. Thus, the heat generated in machining process cannot be ignored. Theoretical method is normally inadequate in predicting the temperatures due to the complex microstructure of MMCs [22]. Thus, a number of researches on modelling of heat transfer mechanisms during machining MMCs have been conducted by introducing finite element models [121-124]. This is observed as an attractive alternative numerical method [100].

The simulation results from Zhu and Kishawy [95] indicate that three heat sources are found in the second deformation zone as shown in Figure 2-13: the first one is the plastic deformation in the chip contacting with tool rake face; the second one is the heat generated by the tool-chip friction; the last one is the heat generated along the tool rake face due to chip sliding. In addition, the effects of cutting conditions on the resultant cutting temperature are similar to those in conventional metal cutting when the volume fraction of particles is low. This is validated by Umer et al. [104]. In term of their simulation, higher temperature is obtained corresponding to the region around matrix-particle interface with maximum deformation.

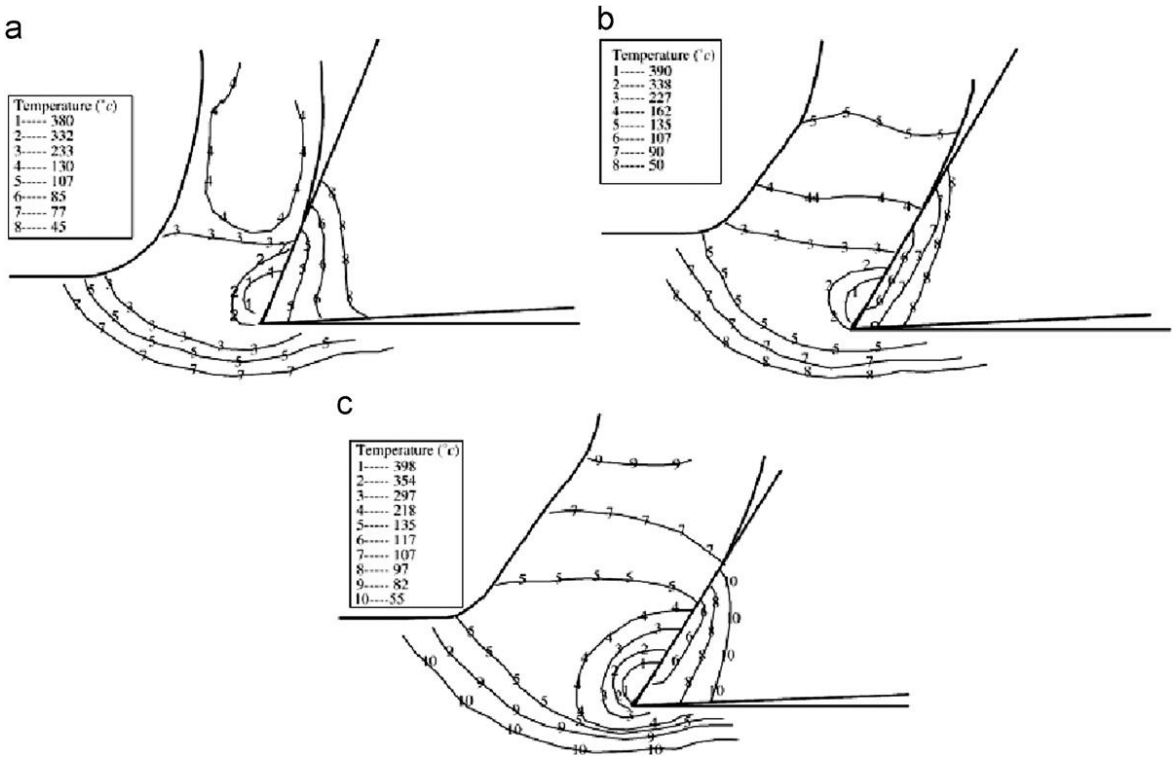

Figure 2-13 Three heat sources in the second deformation zone [95]

Aurich et al. [125] found that the heat generation significantly affect the machinability of composite materials. In addition, thermal load and the thermal expansion of the workpiece are influenced by the cutting conditions and the reinforcement phase. In order to decrease the thermal load of the workpiece, high cutting speed, feed rate and moderate depth of cut are required. From the experimental results, the Al based MMC workpieces are subjected to greater thermal loads than the non-reinforced alloy.

To sum up, the investigation on cutting temperature is limited and heat partition on tool, workpiece and chips are less understood in MMCs precision machining process. Thus, the investigation on cutting temperature, heat partition and their effects on machining process are urgently required.

2.5 Tool wear and underlying mechanisms

Identifying the cutting tool wear mechanisms associated with precision machining process is important for predicting the cutting force, cutting temperature and surface generation, and also optimising the process performance. In MMCs precision machining, matrix material conditions, reinforcement conditions including type, size and fraction, tool material and its geometry, and also cutting parameters are observed as the main factors that contribute to the characteristics of tool wear. In turn, the existent

tool wear makes the MMCs precision machining process even more complicated and unpredictable, and further affect the cutting performance. Therefore, to identify the proper wear mechanisms for a particular machining situation is extremely imperative.

2.5.1 Cutting tool types

According to the recent researches, machining MMCs materials remains a challenging task due to the highly abrasive nature of the reinforcements coupled with the high temperatures generated even in micro machining process. The excessive tool wear and high temperature will be detrimental to the tool life and further result in bad surface quality and form accuracy. These make the selection of optimal cutting tools become vital to optimise cutting parameters and ensure machining quality.

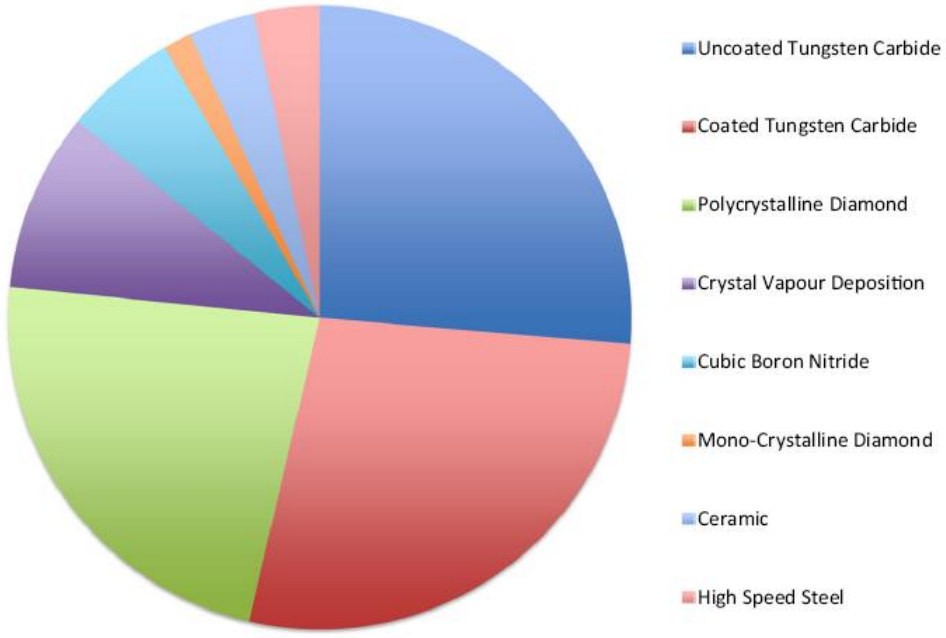

Figure 2-14 Distribution of tools used in MMCs machining [126]

Figure 2-14 shows the distribution of different tools used in MMCs machining process according to the previous experimental tests surveyed. From the previous research, carbide tools are extensively used as the alternative in short run or rough machining operations since the tool tip is much cheaper [127-129]. However, the relatively rapid tool wear make it ineffective and unsuitable in MMCs machining [130-132]. High speed steel (HSS) is also found unsuitable for MMCs application [133-135] as the hardness of reinforced particles in MMCs are typically much higher than HSS tools [136]. Due to the brittle nature and not cost-effective, ceramic tools are found unsuitable for MMCs [133-135, 137]. Diamond tools are also used in MMCs machining due to the superior

hardness and thermal conductivity properties. A lot of researches on investigating and comparing the machinability aspect of MMCs using diamond tools including Single Crystal Diamond (SCD), Chemical Vapor Deposition Diamond (CVD) and Poly-Crystalline Diamond (PCD) tools have been done. A comparative study on machining ductile regime using PCD and SCD tools was done by Hung et al. [138]. This research shows that more fractured SiC particles on the workpiece surface are formed by using PCD tool than SCD tool. Although both these two tools exhibited characteristic abrasive wear patterns, excessive wear is found on the SCD tool particularly when machining the SiC_p reinforced MMCs. Weinert and Biermann [139] advocated PCD, CVD and Polycrystalline Cubic Boron Nitride (PCBN) tools in machining MMCs owing to their hardness, low tool wear rates, thermal and fracture properties. However, PCBN tools are found susceptible to intergranular fracture and amount of material adhering to the tool is significantly higher [140]. CBN and PCBN tools suffered from significantly larger built-up edge and resultant a shorter tool life accompanies with tool tip chipping has been identified [141-143]. While, PCD tools exhibit better performance than PCBN tools in MMCs machining due to their higher abrasion, lower adhesion and higher fracture resistance [140]. In addition, significant lack of performance including surface roughness and tool life in MMCs machining using CVD tools comparing to PCD tools is found by some researchers [123, 144, 145]. Davim [147] found that catastrophic levels of flank wear on CVD tools were developed ten times faster than PCD tools. Thus, CVD tools become a far less desirable option for MMCs machining.

As a synthetic diamond tool material, PCD is manufactured by sintering micron sized diamond grains with a cobalt binder to form hard, nearly chemically inert and abrasion resistant surface. According to the comparison of MMCs and cutting tool materials hardness shown in Table 2-4 and Table 2-5, PCD is observed as the best performance and has been recommended as the most suitable tool material for machining MMCs. A lot of researchers found that PCD tools, owing to higher hardness and thermal conductivity than other tools, have the ability to help heat flow away from the cutting zone [136,140,148-151]. From their research, excellent chemical affinity of the MMC with the PCD is also pointed out. In addition, PCD tools with larger grains have better performance than those with smaller grains before the edge chipping occur [152]. From the tool life test of different cutting tools at varied cutting speed shown in Figure 2-15, PCD tool with longer tool life is observed as the most suitable tool in MMCs machining.

Table 2-4 Relative Vickers Hardness value of MMCs

Matrix material and reinforcements in MMCs (HV)		
Al2024 [153]	SiC [154]	B_4C [154]
130	2,400-3,500	3,000-3,700

Table 2-5 Relative Vickers Hardness value of cutting tools

Cutting tools (HV)				
PCD [154]	SCD [155]	CBN [155]	CVD [155]	WC [154]
5,000-8,000	6,000-10,200	4,100-4,900	5,000-10,000	1,600-1,800

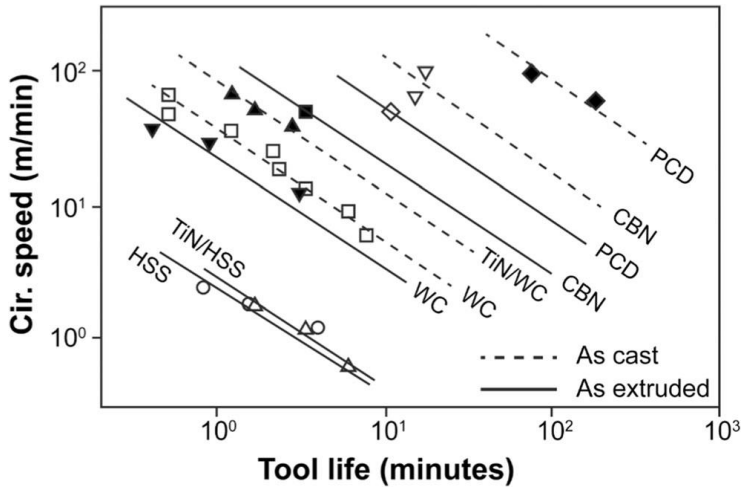

Figure 2-15 Tool life vs Cutting speed [156]

2.5.2 Tool wear mechanisms

From the above review, PCD tools are observed as the most suitable tools in MMCs machining. In term of tool wear in metal cutting, once a certain level of land width reaches, the flank wear has a negative influence on dimensional accuracy and surface finish of machined part. It further affects the machining process stability. Thus, flank wear is usually taken as the tool life criterion [157]. High flank wear due to higher cutting forces and built-up-edge (BUE) in MMCs machining is found in many researches [158]. According to these researches, it can be seen that the flank wear as the major tool wear is explained by various wear mechanisms. Typical tool wear patterns and prominent wear mechanisms of PCD tools are shown in details as below.

(1) Abrasion wear

Abrasion tool wear is found to be the most dominant wear mechanism in machining hard particle reinforced MMCs [148, 159, 160]. Abrasion wear with parallel grooves generated in the direction of the chip flow is found as the primary wear mechanism for PCD tools when machining Al/SiC MMCs [148]. This tool wear is also identified and validated on various anisotropic and non-homogeneous composites as a result of embedded particles dislodged from workpiece and dug into the tool surface [147, 161-163]. On the other hand, abrasion wear is considered to be associated with micro mechanical damage rather than micro-cutting due to the hardness of PCD is higher than the reinforced SiC particles [145, 164].

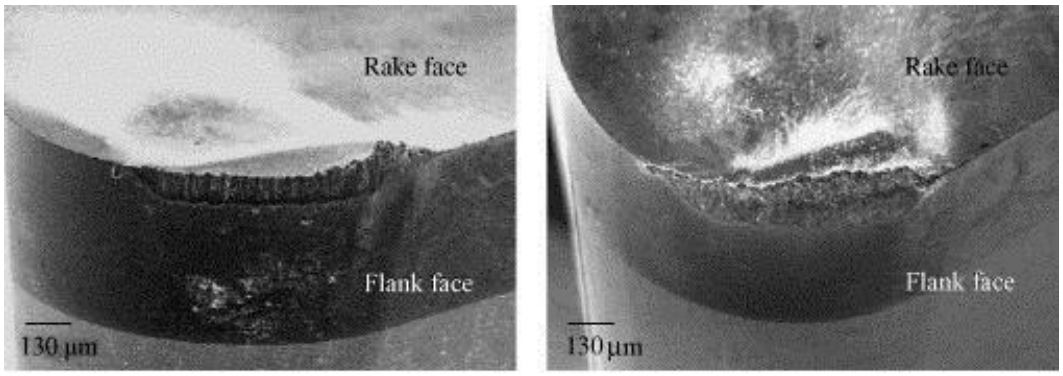

(a) at 50 m/min for a distance of 1760 m (b) at 400 m/min for a distance of 880 m

Figure 2-16 SEM of the used PCD tools without coolant (before etching) [140]

(2) Adhesion wear

Adhesion wear is observed as another tool wear in MMCs machining [140, 145]. The worn flank face of cutting tool contributes to the adhesion of workpiece material on the cutting tool insert and BUE easily formed at lower cutting speed [145]. The research from El-Gallab and Sklab [148] indicates that the BUE is able to protect the cutting tool from abrasion wear. However, the unstable BUE easily induces the tool edge chipping and further affects the surface finish adversely [148,165].

(3) Edge chipping

Edge chipping and grooving are found on the edge and flank face of cutting tool by various researchers [140, 166]. This is due to the impact of reinforced hard particles on the cutting tool surface. In addition, the wear degree increases with the increase of cutting speed [167].

(4) Notch wear

Normally, a series of undulating ridges, which has the similar size with cutting feed rate, formed on the machined surface in MMCs precision machining. These ridges result in the notch wear and micro-cracking on the flank face of cutting tools particular in wet cutting [140]. This is due to the coolant reduces the cutting temperature, increases the hardness of workpiece and further impacts on the cutting tools. However, the coolant effects only work at lower cutting speed. The notch wear is not significant at higher cutting speed due to the coolant is unable to absorb heat efficiently and the hardness of thermally softened workpiece decreases at higher cutting temperature [130].

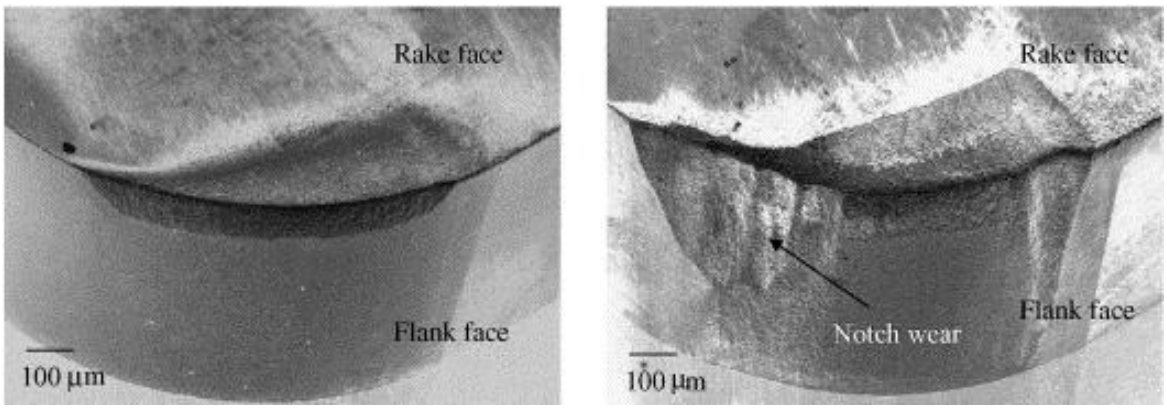

Figure 2-17 SEM of the used PCD tools with/without coolant [140]

(5) Crater wear and micro-cracking due to fatigue

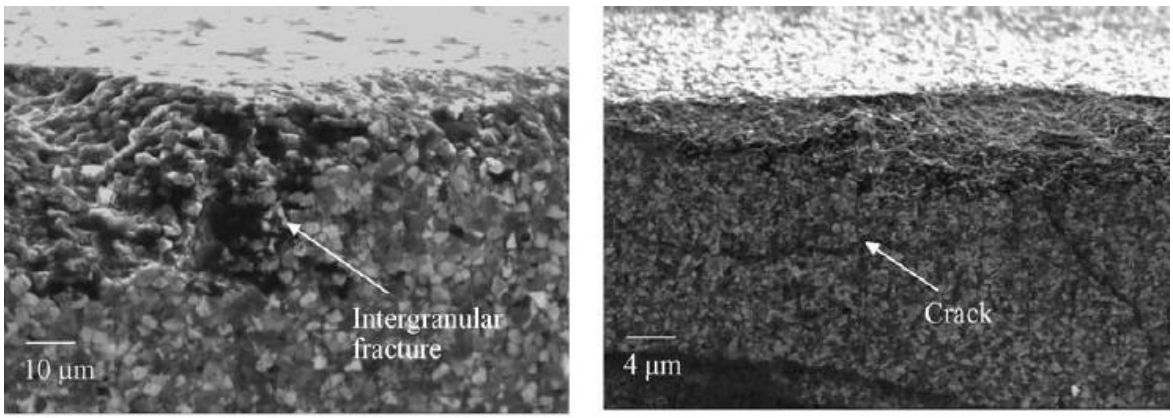

(a) Intergranular fracture formed on the tool edge (b) Crack formed on the flank face

Figure 2-18 Notch wear and micro-cracking on the flank face of cutting tools [140]

Crater wear is also found in MMCs machining. However, this is not concerned to be the major wear mechanism when machining Al/SiC metal matrix composites [168, 169].

Micro-cracking due to fatigue is another tool wear observed in MMCs machining [164, 170]. This occurs due to the lower hardness of reinforced particles against PCD [164].

2.5.3 Tool wear monitoring

Previous researches on tool wear monitoring indicate that a variety of process parameters in the machining environment can be used to predict the cutting tool state [171]. Acoustic emission, static or dynamic cutting forces, vibration signature, cutting tool temperature and miscellaneous methods including stress and strain analysis, spindle motor current/torque/power, ultrasonic and optical measurements, workpiece surface finish quality, and also workpiece dimensions are observed as the typical tool wear monitoring methods that can be correlated to wear state in different application scenarios [171-173]. The tool condition monitoring process can be illustrated in Figure 2-19 as below.

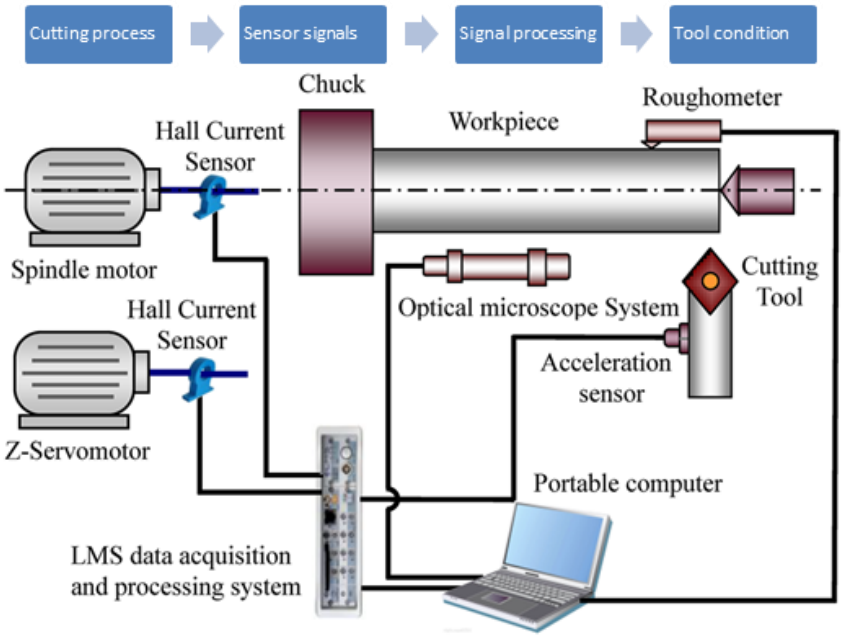

Figure 2-19 Tool condition monitoring process [174]

In term of these above mentioned methods, acoustic emission (AE) and force signals are regarded as the most commonly used and most effective parameters in monitoring tool wear science they provide collectively most data. In order to develop a real-time tool condition monitoring system (TCMS), Choi et al [175] fused AE and cutting forces in their tool wear experiments. In their method, a fast block-averaging algorithm for features and patterns indicative of tool fracture is introduced by analysing the signals,

and the results show that large burst of AE occurs at the time of tool breakage. A similar statistical signal-processing algorithm is introduced by Jemielniak and Otman [176] in order to identify the root mean square (RMS), skew and kurtosis of the AE signal in the detection of catastrophic tool failure. The RMS value is found dramatically increased when the tool fractured. This method is sensitive to the cutting tool edge chipping [177]. Force signal based TCMSs that typically operate independently of absolute force levels are also applied for tool wear prediction. The relationships between tool wear and associated cutting forces or its power spectra have been extensively investigated by various researchers [178-180]. It can be found in Figure 2-20 that relative changes of acoustic emission signals indicate the wears or fractures of cutting tools is another effective method for tool wear monitoring [181-183].

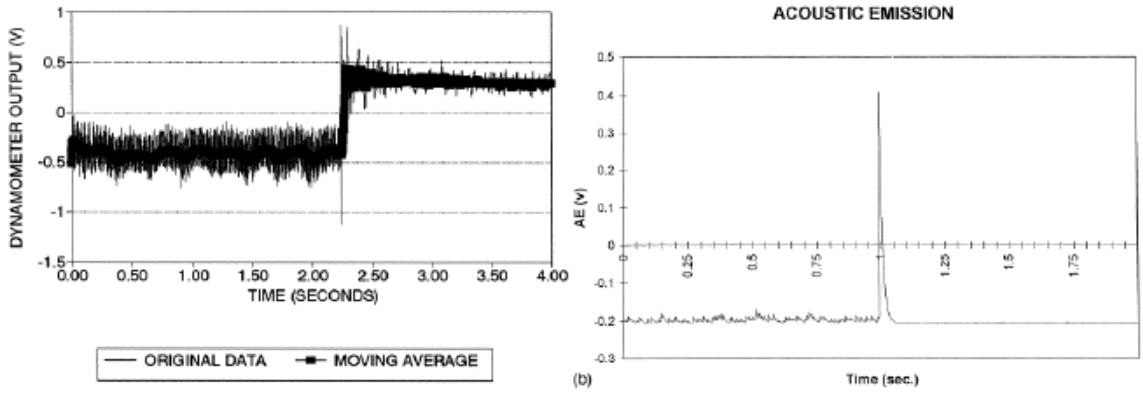

Figure 2-20 Cutting force and acoustic emission when tool is broken [181]

Other TCMSs including cutting edge temperature [184-187], vibration signatures [188-190], and miscellaneous sensors and methods [191-193] are also increasingly investigated and applied to monitor tool wear. In addition, sensor fusion of several signals rather than single type of signal [194] and also the intelligent analysis on process signals [33, 195-197] are employed to estimate the tool wear.

In spite of the current investigation on tool wear monitoring, however, the accurately represent of tool wear status can only be successfully accomplished under specific and limited conditions and the method is deemed unsuitable in some situations. Integrated investigation and new algorithm are still need to be developed in order to improve the TCMS comprehensively.

2.6 Surface generation and machining process optimisation

In high precision engineering industries, machined parts with high quality including lower surface roughness, higher form accuracy and higher functional performance are required. Optimal cutting parameters, cutting tools and workpiece microstructure are then adopted in order to improve the material removal rate, minimise tool wear, extend tool life and further enhance the machining efficiency and cost effective.

2.6.1 Surface generation

The surface quality is a characteristic that significantly affect the reliability and functional performance of finish product. Surface roughness, dimensional accuracy and sub surface damage caused by MMCs machining operation are the main factors that influence the machining quality and surface generation. In addition, surface roughness, defined as a combination of the micro feature of machined surface with surface texture, is extensive applied to evaluate the characterisation of machined surface. The surface generation especially for the surface roughness in MMCs machining is difficult to predict via analytical method. Thus, simulation and experimental based studies on the surface generation of MMCs are extensively done.

In term of simulation based studies on surface generation, the tool-particle interaction is extensively analysed. In most cases, particles are simulated as rigid, and only debonded from the matrix material and leave big pits and cavities on the machined surface as shown in Figure 2-21 and Figure 2-22 [96-99, 104]. However, this is not reliable in real cutting and only few studies simulate the fracture of reinforced particles. Ghandehariun et al. [105, 106] simulated the tool-particle interaction which found that crack progressively occurred in the particles. With the continue moving of cutting tool, particles are fractured or fully debonding from the machined surface. Some of the fractured particles are remain on the machined surface, some are stress free debonded, while some are still bonded on the top surface and embedded into the chip afterwards. In addition, the crack evolution around the matrix-particle interface leads to the fracture of matrix material, which further increases the surface roughness as shown in Figure 2-23. Liu et al. also develop a simulation of machining 45% SiC_p/Al MMCs by considering the tool-particle interaction. However, only the cavity depth is considered to perform the machined surface quality [103]. The particle fracture model is also conducted in the simulation of machining SiC/Al MMCs with high volume fraction [99].

In this simulation, round particles are fracture and leave a cleavage on the machined surface, while polygonal particles are perfectly cut through and a relative smoother surface generated afterwards.

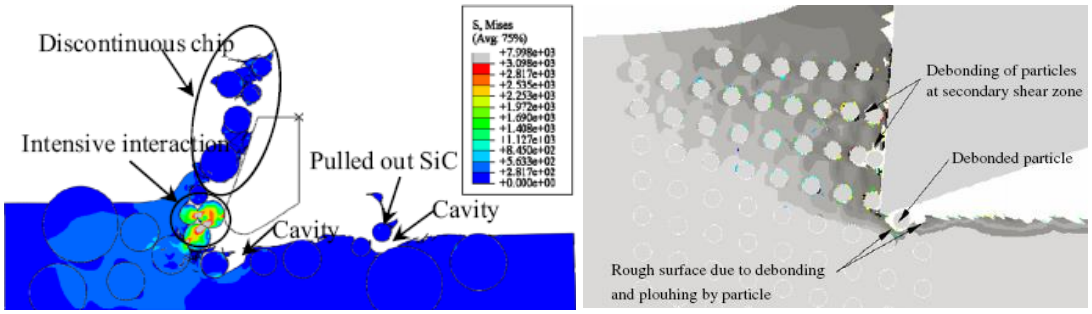

Figure 2-21 Rigid particles debonding process [96, 99]

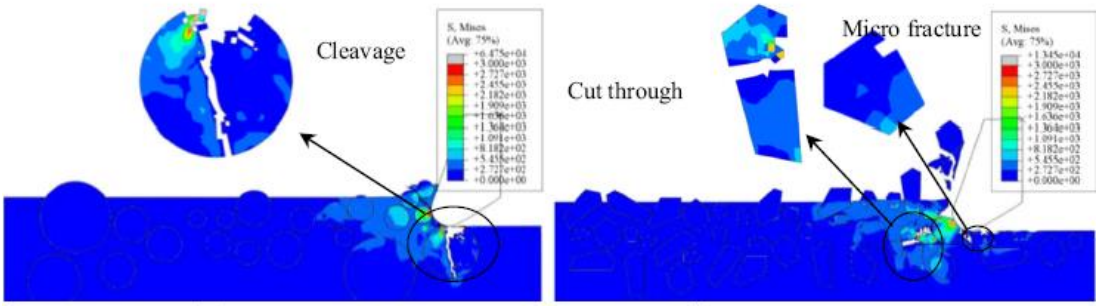

Figure 2-22 Particle fracture in machining high volume fraction SiC/Al MMCs [99]

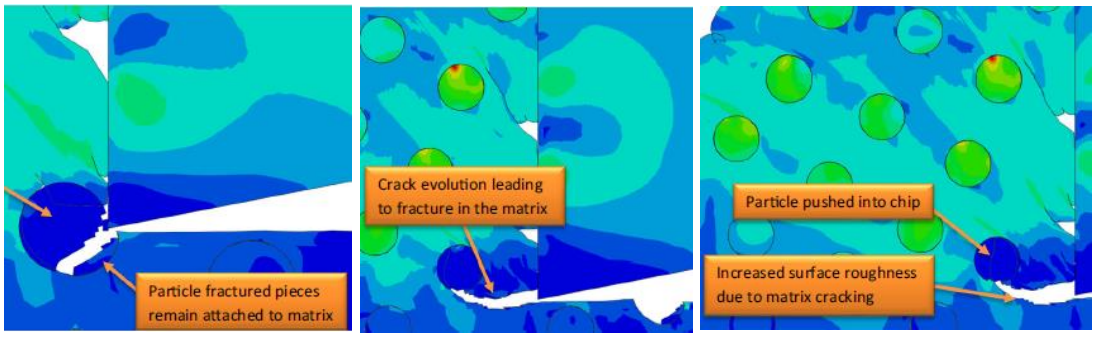

Figure 2-23 Tool-particle interaction and surface generation [105, 106]

In term of experimental based studies on surface generation, a vast number of surface defects are found on the machined surface in various researches. These defects normally include cavities and pits with different sizes formed due to particle pulled out, voids around matrix particle bonding area and cracks at particle fracture. Due to SiC and matrix have good stick in the workpiece, only tiny surface cracks and very small pit holes on the machined workpiece shown in Figure 2-24 are found by Muthukrishnan and Davim when machining Al/SiC/20p MMCs [198]. They also found the transformed

aluminium particles during machining were embedded around the SiC particles and further formed a relative homogeneous composite [199, 200]. The similar results are reported by other researchers [92].

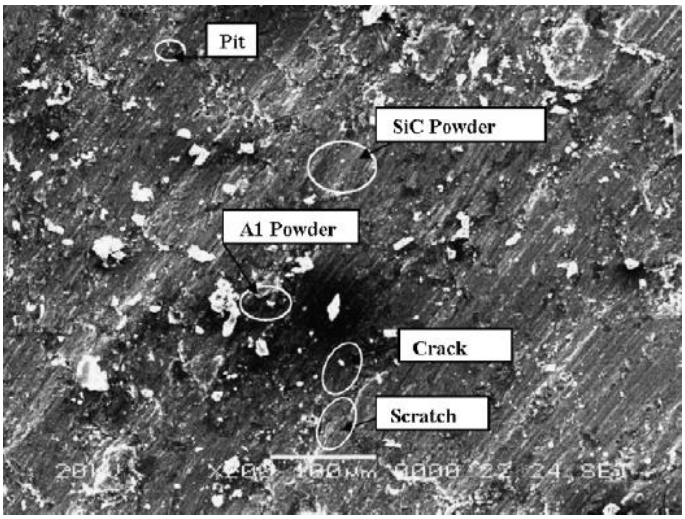

Figure 2-24 Typical texture of machined surface [201]

As for machining MMCs with high volume fraction of reinforced particles, the material removal process is more complicate and surface quality is supposed to be deteriorated greatly. When the volume fraction of particles is relatively large, the surface generation is extensively presented by analysing the complicated material removal mechanism. In the research of Bian et al. [201], 65% SiC_p/Al MMCs is machined by using PCD tool. Even the matrix material is removed plastically and leave a smooth machined surface, micro-fractures and cracks can still be found due to most of the reinforcements are partial ductile removal. On the other hand, big fracture and cleavage of particles occur and the fractured particles are further pulled out to form large pits as shown in Figure 2-25 and Figure 2-26.

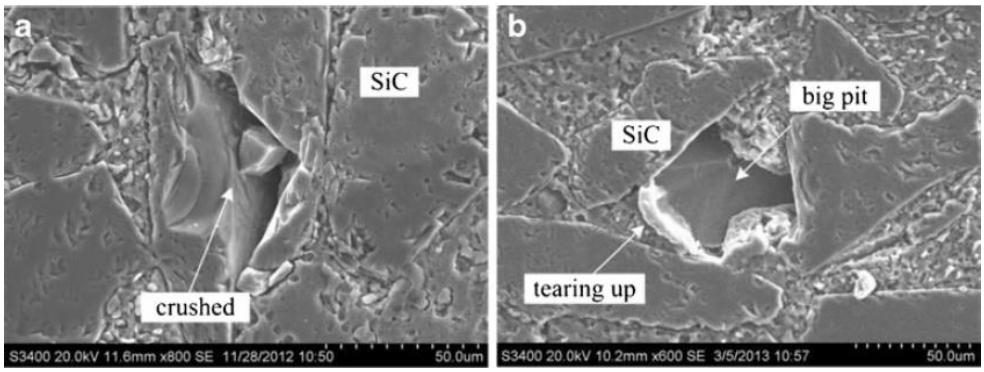

Figure 2-25 Surface generation in large volume fraction SiC_p/Al MMCs machining [201]

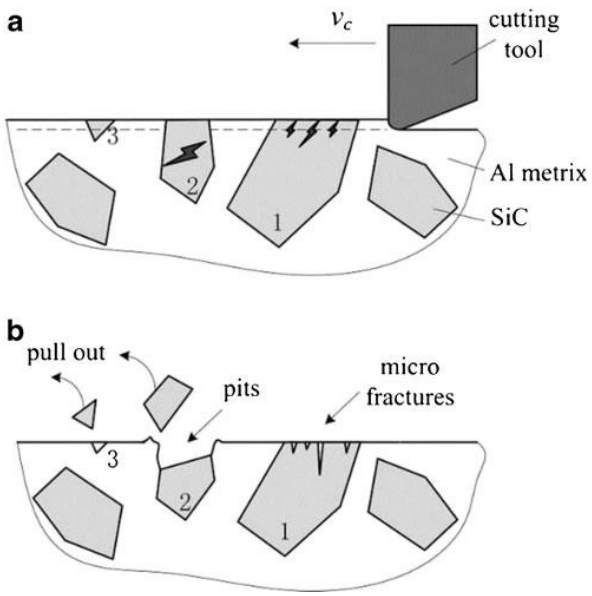

Figure 2-26 Material removal and surface generation in MMCs machining [201]

Wang et al validated his particle fracture model via micro milling experiments [99, 202]. The experimental results shown in Figure 2-27 perform a good surface profile and some typical defects occur on the machined surface. In cutting direction, part of particles are pressed into the matrix by the cutting tool and only leave deep and narrow crack on the top of machined surface. In addition, some cavities occur that attribute to the pull-out of particles. In feed direction, both big cavities and relative smooth surface can be observed due to the pull-out or cut through of reinforced particles.

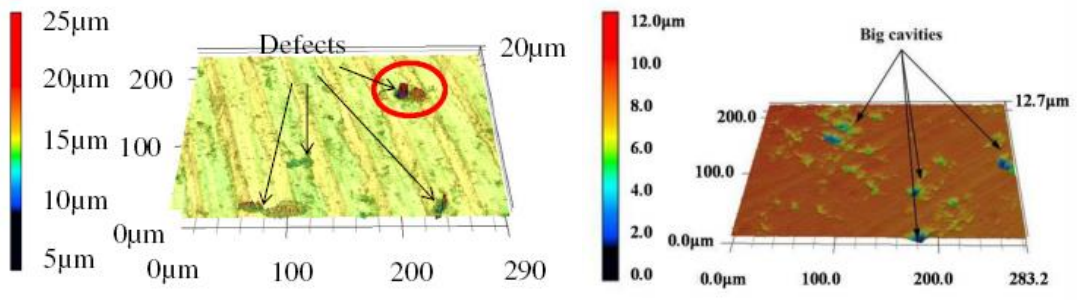

Figure 2-27 Surface morphology in MMCs micro milling [99, 202]

Substantial researches have been undertaken on optimising the machining processes such as tool wear and surface generation in machining of particulate MMCs.

2.6.2 Optimisation on process variables

Optimisation on the machining process parameters is one of the most important steps towards improving the efficiency and sustainability in MMCs machining process. This

is becoming increasingly critical in both machining and fabrication industries. A variety of studies investigate the effect of process parameters on the surface roughness of particulate MMCs by using PCD tools. The modelling techniques of ANOVA and ANN provide a systematic and effective methodology for predicting the main effects and interaction effects result from different influential combinations of machining parameters and also optimising these process parameters in order to achieve a higher accuracy of machined surface. These experimental results indicate that the feed rate has highest physical and statistical influence on the machined surface roughness, followed by DOC and cutting speed [198, 200, 203, 204]. Interaction between cutting speed and feed rate has primary contribution to surface roughness comparing to other interactions [204, 205]. In addition, relative higher feed rate and lower cutting speed that produce an acceptable surface finish is recommended by Tomac et al. [206] to reduce time and also increase material removal rate. However, most researchers found that surface roughness increases along with feed increases and cutting speed decreases [205, 207]. Thus, higher speed, lower feed and lower depth of cut are recommended in order to achieve better surface finish. Moreover, Bian et al. [201] found that the surface roughness Ra around 0.1 μm, by using small parameters in the range of a few micro-meters, can be obtained in precision milling of SiC_p/Al composites. Karabulut et al. [208] presented an experimental investigation on the surface roughness in micro milling of B_4C/Al MMCs. In this study, the best surface roughness can be observed at high milling speed and the lowest feed rate under dry cutting conditions when machining on Al6061 reinforced with 15 wt% B_4C. The application of coolant is found not necessarily reduce tool wear or improve the surface finish as the coolant can reduce the material transfer, while in turn lead to the abrasion increases [140]. In addition, Kannan and Kishawy [209] found that using coolant results in the loosely bonded particulates flushed away and leave a higher percentage of voids and pits that significantly deteriorate the surface quality.

On the other hand, the tool flank wear is directly related to cutting speed, feed and depth of cut owing to thermal softening behaviour, diffusion wear and higher kinetic energy of chip when abrading against the cutting tool [140, 161, 210]. Cutting speed is found as the most dominate parameter for flank wear followed by feed rate and depth of cut has the most insignificant effect on flank wear [211, 212]. At low cutting speed, the flank wear is high due to the generation of higher cutting forces and increased formation of BUE [212]. However, Karakas et al. [213] found that the wear rate reduces and cutting

tool has higher performance due to the BUE acts as thin film and temporarily protects the cutting tool from abrasive wear. In addition, when the cutting speed increases, increasing flank wear is found due to the higher effective kinetic energy by various researchers [148, 210, 214]. In term of depth of cut, it has limited effect on tool wear [213], while more significant as compared to the feed rate [131]. The increased depth of cut will result in the increase of flank wear attribute to the increase in contact area and abrasion on tool flank face [215, 216]. In term of feed rate, the tool wear decreases due to the shorter contact time between the cutting edge and the abrasive reinforced particles, and formation of BUE when the feed rate increases [130]. The thermal softening of composite material and tool material at higher feed rate also contributes to increase the tool life [161, 206]. Thus, various researchers propose that feed rate and depth of cut should be maximised for a given cutting speed in order to minimise the wear down of cutting tool due to the abrasion between tool and workpiece with abrading particles [210, 217]. Most authors have found that with the help of coolant, BUE is less likely to develop and lead to the increase of tool wear. However, BUE results in the poor surface finish and increase of cutting forces. As a result, the beneficial to use coolant is not fully understood and its effect is not clear [218].

2.6.3 Optimisation on cutting tools

The cutting tool geometry is another factor that intensely affects the tool wear mechanisms. Negative rake angle that results in the higher cutting forces will further increases flank wear of cutting tool. On the other hand, positive rake angle also increases flank wear irregularly and pitting occurs extensively on cutting tool. Thus, the smallest cutting tool wear and best surface quality only can be obtained by using tool with zero rake angle [219, 220]. In addition, higher cutting forces are found at smaller tool nose radius. This results in the greater chipping, crater and flank wear on the cutting tool [219,220]. Thus, cutting tool with smaller nose radius is only recommended for surface finishing process and better form accuracy can be achieved [220, 221].

2.6.4 Optimisation on workpiece material characteristics

The MMCs workpiece material characteristics are observed as a critical factor in determining its machinability. The present of hard abrasive particles in metal matrix composites leads to extremely high tool wear. For instance, these reinforced particles can be treating as abrasive grains between tool and workpiece during machining and

significantly affect the surface finish. Looney et al. [141] found that metal matrix composites with the large size and high volume fraction of reinforced particles have poor machinability. In addition, Li and Seah [222] investigate the machinability of MMCs with varied SiC reinforcements. From their study, the size of particles is found has more effects than the volume fraction on the tool wear. However, the tool wear is found accelerate when the volume fraction of reinforcement is higher than a critical value [222, 223]. Kanta et al. found that the increased particle size results in higher tool wear and hence shorter the tool life due to the particles are coarse and easy to break compare to the smaller ones [224]. Kannan et al. concluded that the flank wear of cutting tool increase with the increase of both volume fraction and average particle size [225]. This is due to the contact between tool and particle dramatically increases and higher abrasion on the cutting tool occurs when increasing the particle ratio. In addition, the well distributed particles in the matrix material will help to reduce the tool wear slightly and consequently improved the machinability of MMCs.

A lot of researches state that the increase of particle ratio both for volume fraction and particle size affects the surface roughness negatively [226-228]. Volume fraction of reinforcements is found proved detrimental to the tool life [222]; however, it has great influence on surface roughness [204]. Ozben et al. investigated the effects of particle volume fraction on the resultant surface roughness and higher surface roughness is obtained at higher fraction in this study [227]. Pendse and Joshi observed that volume of reinforcement has significant effects on the machined surface roughness only when the cutting tool nose radius is comparable to the size of reinforcement [229]. In addition, the reinforced particles will interfere with the machined surface roughness if the tool nose radius is equal or smaller than the particle size; otherwise, it has no effect [229]. This has been confirmed by Basheer et al. From their experimental study, it is found that when the particle size is comparable to the value of feed rate and tool nose radius, the particle size has largely influence on the machined surface roughness [230]. The particle size effect is also studied by Tosun and Muratoglu [231]. In their study, the increased particle size obstructs the plastic deformation of matrix material and stress gradients at the matrix-particles interface occur. This results in the surface defects and finally increases the surface roughness.

According to the above reviewed research work, it appears that the selection of optimal cutting parameters, cutting tool conditions and workpiece materials must therefore take

into account the primary factors which are the importance of surface finish, the BUE of cutting tool, the tool life and the material removal rate etc.

2.6.5 Machinability study of MMCs

With increasing demands for functional MMCs, machinability and precision machining of MMCs have become bottleneck issues and thus drawn extensive attention and research. The machined surface roughness, material removal rate, and the tool wear and tool life are essential in machinability assessment, especially for high precision engineering applications. The machinability assessment is heavily dependent on the machining accuracy, surface quality, production efficiency and costs. Precision machining on particle reinforced MMCs is observed as an even higher challenge both scientifically and technologically due to their complex micro-structure and hard-to-machine property. Although various non-traditional processes have been attempted on machining MMCs to even produce parts with intricate shape and profiles [35], the processes are normally inefficient and often limited. The conventional machining process is still indispensable during finish machining [36].

However, high tool wear, high surface roughness, deterioration and defects of the machined surface significantly affect the functional performance of engineering components. This is becoming one of the major reasons limiting the widespread application of MMCs. In addition, only few researches focus on precision machining of particulate MMCs, thus, its machinability is less understood as being progressed so far. A systematic research approach is required to investigate the machinability of particle reinforced MMCs in precision machining process. The effects of cutting process variables, particularly for the cutting parameters including cutting speed, depth of cut and feed rate, on the tool wear, machined surface roughness, surface morphology and surface texture need to be adjusted in order to achieve better surface quality.

2.7 Summery

In this chapter, the state-of-the-art research work on precision machining of metal matrix composites is critically reviewed and the following research gaps being identified:

1. Precision machining of particulate MMCs is observed as a complicate process; however, this is currently less understood and need to be investigated thoroughly.

2. The characterisation of MMCs precision machining and its underlying cutting mechanics especially for chip formation mechanisms have not been fully understood.
3. The current cutting force models are mainly focused on the prediction of force magnitude on specific time points or consistent chip load conditions, while still not considered the 3-dimensional milling processes with continued-changed chip formation, the real chip formation conditions and also their significant effects on the cutting force. In addition, there is also limited understanding on explicit modelling of cutting forces for particles reinforced MMCs.
4. Only few research focus on the close monitoring on the cutting temperature partition and resultant tool wear in order to enhance the machining accuracy, machined surface quality and process stability. As for the industrial-driven application of hard-to-machine MMCs, deterministic representation on tool wear status and maintain the MMCs machining in a higher accuracy and consistency level is still absent.
5. According to the industrial demands on machining efficiency, cost-effective, accuracy and consistency, the MMCs machinability assessment and process optimisation need to be further investigated.

Chapter 3 A multiscale multiphysics based approach to modelling and analysis of MMCs precision machining

3.1 Research methodology framework

In the previous chapter, the literature review presents the current understanding on the precision machining of particulate metal matrix composite materials, which is different from machining of homogeneous materials in various aspects. The existence of multiscales on cutting edge radius, material microstructure, particle size and the process parameters in MMCs precision machining reveals that the cutting mechanics are much more complicated. Therefore, an innovative multiscale multiphysics based approach is investigated to modelling and analysis in precision machining of MMCs.

The critical aspect of industrial-scale challenges in MMCs precision machining is the machinability. Multiscale multiphysics based integrated approach to investigate the MMCs precision machining process and its machinability assessment are shown in Figure 3-1. Chip formation mechanisms, cutting force, cutting temperature, tool wear and surface generation are observed as the five crucial issues that affect the machining process and resultant machinability of MMCs. The intrinsic relationship between these closely linked or mutually coupled issues and factors are also contained as shown in this figure. The workpiece properties, cutting tool conditions, machining conditions and other initial conditions observed as the indirect factors for MMCs machinability that affect the tool-workpiece interaction, and further influence the cutting mechanics and cutting dynamics. The multiscale approach shown in Figure 3-1 is applied to have better understanding and accurate prediction on the chip formation mechanisms, cutting force, cutting temperature and tool wear. These outputs are the direct contributory factors for the MMCs machinability in term of machining quality, material removal rate and tool life. In order to improve the MMCs machinability from industrial aspects, process optimisation is introduced and rapidly developed. This is of great importance to optimise the influence brought by the process input and help to enhance the performance of final products. Therefore, this research work contribute to an integrated investigation on the particle reinforced MMCs precision machining process in order to identify the issues that less understood, obtain the scientific understanding on the MMCs cutting mechanics, optimise the critical process variables, improve the

machinability of MMCs and broad its industrial application in various engineering aspects.

3.2 Multiscale modelling

In MMCs precision machining, cutting tool conditions, workpiece material microstructure and cutting parameters are the key process variables that significantly affect the cutting mechanics and also the resultant cutting performance as shown in Figure 3-1. Since the cutting performance in MMCs precision machining is influenced by these factors in three different scale levels, a multiscale modelling and analysis on the cutting mechanics is of great importance. Figure 3-2 schematically illustrated the interrelationship among micro, meso and macro scales. In micro scale level, the material microstructure including particle size, particle volume fraction and their distribution in matrix material, and strengthening mechanisms of particle-matrix interface strongly influence the material properties, cutting mechanics and dynamics. In meso scale level, the tool-workpiece interaction and MMCs chip formation mechanisms are extremely different from those in conventional material machining process due to the material microstructure effect, tool edge radius effect, minimum chip thickness effect and most dominate size effect etc. Due to the size of cutting tool edge radius and reinforced particles cannot be ignored, the MMCs chip formation are significantly influenced by the tool edge radius, tool nose radius, particle form, average particle size and particle volume fraction. In macro scale level, the chip formation oriented dynamic cutting force, cutting temperature and cutting vibration including process kinematics and tool deflection affect the cutting mechanics and dynamics as well. In addition, these have critical and direct effects on the quality of machined parts in terms of form accuracy and surface integrity. As shown in Figure 3-1, these three scales are fully coupled together and have instinct relationship to determine the machining process and also the machinability of MMCs.

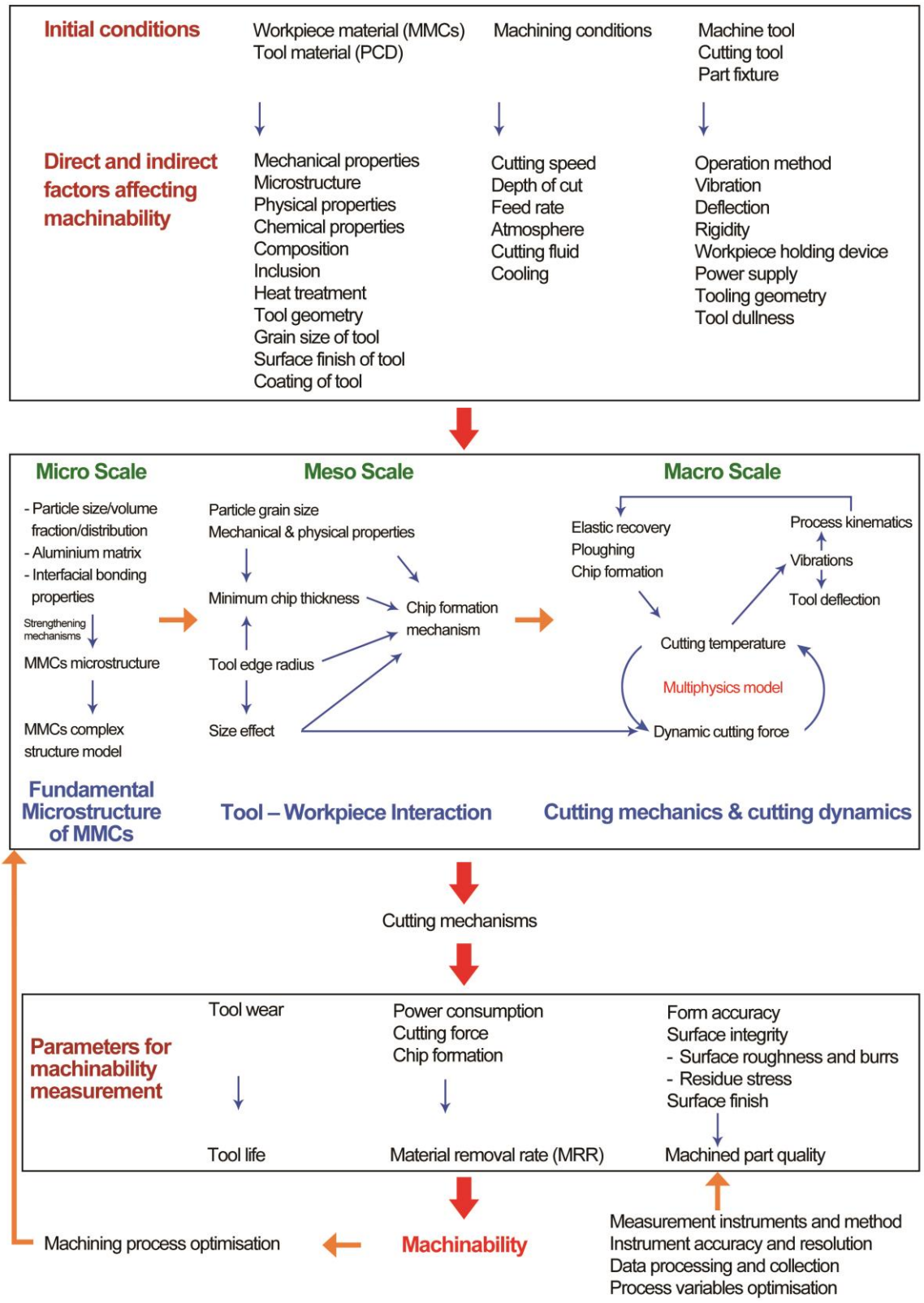

Figure 3-1 Research methodology

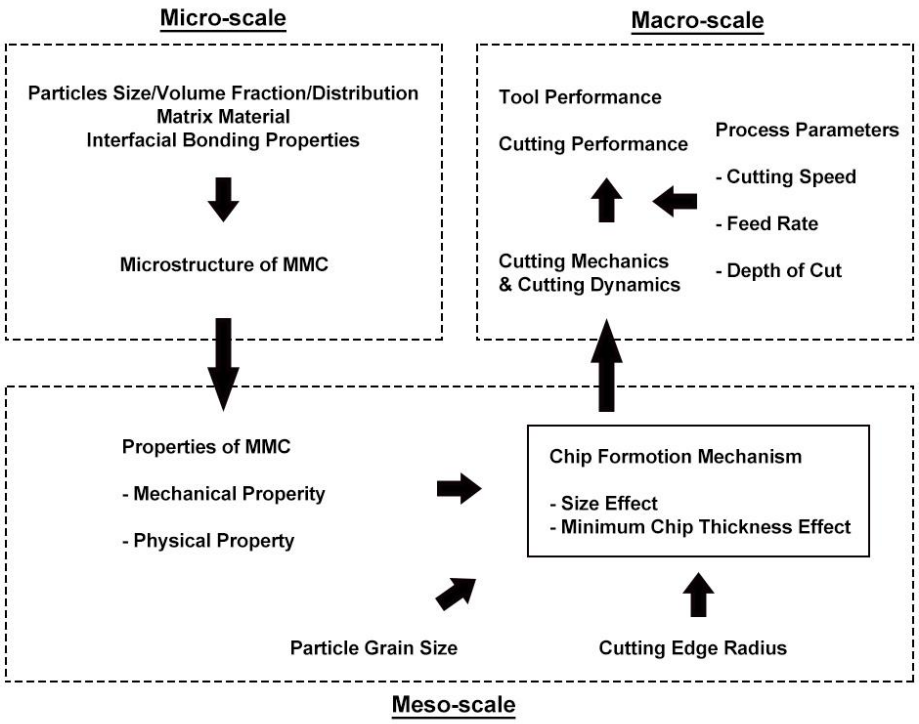

Figure 3-2 Interrelationship among micro, meso and macro scales

3.3 Multiphysics modelling and analysis

Chip formation, cutting force, cutting temperature and tool-chip-workpiece interfacial friction are the most dominate variables that present and evaluate the interrelationship between the process inputs, including cutting tool conditions, target material microstructures and cutting parameters, and outputs which are the resultant tool performance and cutting performance. In MMCs precision machining, the cutting physics closely linked together. During chip formation process, cutting force and chip/tool/workpiece friction normally occur. Consequently, the heat generation presented by cutting temperature occurs due to the plastic deformation of matrix material, the particle fracture and too-workpiece/chip-tool interfacial friction during the chip removal process. The increased cutting temperature has significant effects on the cutting force, tool wear and machined surface performance. In addition, the extensive tool wear reacts on the initial cutting conditions, and cutting force and chip formation change dramatically accompanied with unstable surface generation. Later on, the increased cutting force results in the increase of heat generation on the contact zones. In addition, the resultant form accuracy, material removal rate and surface roughness, in turn, affect these contributory factors and physics. Therefore, the vicious circle prompts

to develop a comprehensive approach to modelling and analysis on the tool performance and cutting performance. Thus, a thermo-mechanical-triboligical coupled multiphysics modelling and analysis approach is applied. In addition, a process optimisation approach is essential to optimise the cutting inputs and improve the MMCs machinability assessment. Figure 3-3 illustrates the multiscale multiphysics based integrated approach to modelling and analysis the MMCs precision machining process and its optimisation.

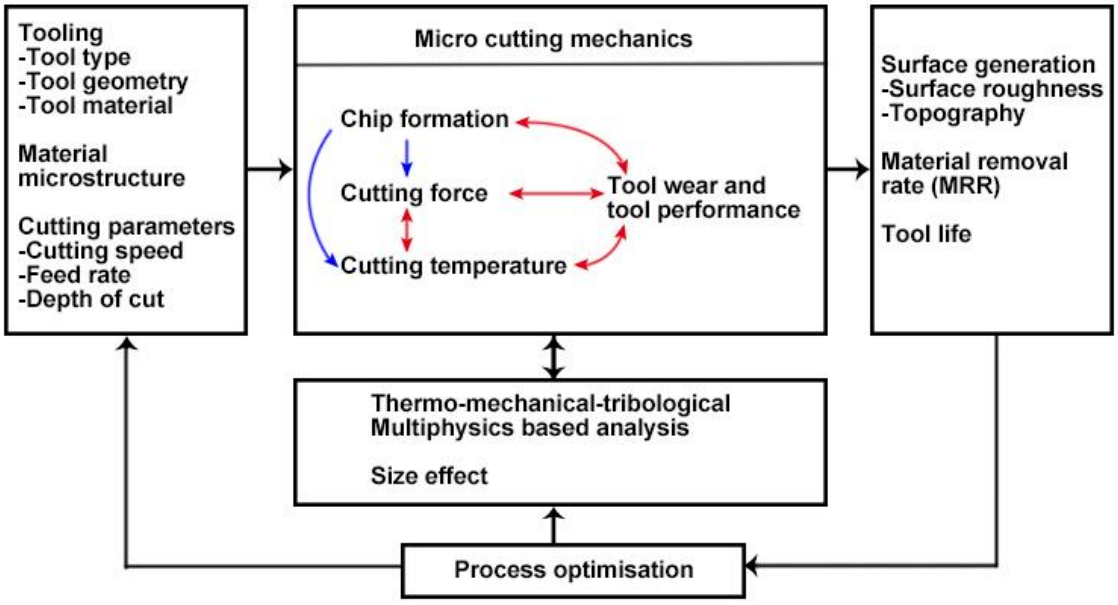

Figure 3-3 Multiphysics based analysis on machining process and its optimisation

3.4 Modelling and simulation tools

The numerical models and their evaluation and validation approach are conducted with appropriate modelling and simulation software packages. Abaqus CAE and COMSOL Multiphysics are performed as the effective tools for the simulation and analysis. FE analysis is conducted on Abaqus/Explicit for chip formation simulations including matrix material breakage and particles fracture and their interfacial reaction. Cutting stress, cutting force and temperature partition are also achieved in this simulation process. The cutting stress from Abaqus is then transit to COMSOL Multiphysics for further analysing on tool wear magnitude based on the modified tool wear rate model.

3.5 Experimental evaluation and machinability assessment

3.5.1 Experimental facilities

The MMCs precision machining processes are conducted with the high precision machine tools, high quality cutting tools and high accuracy measurement instruments. Meanwhile, various high precision devices are used in the data collection system in order to analyse the cutting process accurately. This part introduces the essential experimental equipment used in the MMCs precision machining.

3.5.1.1 High precision machine tools and cutting tools

(1) KERN milling machine

MMCs micro milling experiments are conducted on a high precision 5-axis KERN HSPC 2825 milling machine with ±1 μm positioning accuracy which is controlled by Heidenhain TNC426 control system. The machine spindle is derived by a Step_Tec ceramic bearing with a maximum rotation speed of 35,000 rpm. Cutting tools are clamped to the spindle via high precision collets. A controlled cooling system, which adjusts the temperature within ±0.5^{o}C, is applied to ensure the thermal stability during machining. Cutting tool dynamic length and radius are measured by on-machine Blum-Laser Tool Setting System. The tool setting system provides a high accuracy within 0.1 μm by measuring with visible red light laser.

(2) MOORE precision turning machine

The micro turning trials are performed on a Nanotech 250UPL precision turning machine which is controlled by a Delta Tau PowerPMAC motion controller. The high precision turning machine is equipped with an air spindle, which is driven by a frameless, brushless DC motor with total liquid cooling for long term thermal stability. The motion accuracy is less than 12.5 nm throughout the spindle speed range of maximum 10,000 rpm. The centre mounted thrust plate equipped on the spindle is engineered for both heavy loads and high throughput applications. Two high stiffness and low profile "box-way" style oil hydrostatic slides are driven by brushless DC linear motor. This enables the machine to achieve 1 nm linear motion accuracy.

(3) PCD cutting tools

PCD tools, which is widely applied and suitable for MMCs machining, are used in these MMCs precision machining experimental trials. These PCD tools are performed in micro cutting experiments in order to investigate the MMCs cutting mechanics, tool

wear and surface integrity and also to have better understanding on the precision machining process. The fine grade PCD inserts are used for micro turning trials on MOORE precision turning machine and the straight flute PCD end mills are used for conducting micro milling trials on KERN milling machine respectively.

3.5.1.2 Cutting force and machine dynamics measurement

Measurement on the signals formed during micro cutting is considered to be useful for understanding and interpreting the in-depth cutting process. System frequency, cutting tool variation and cutting force are widely investigated through signal recording and analysis. In this research, a series of signal recording systems are employed and illustrates in details as below.

(1) Kistler dynamometer system

Cutting force signal as a critical signal for interpreting the cutting process particular for cutting mechanics in-depth is investigated in this study. The three orthogonal cutting force signals are collected through an employed multicomponent dynamometer. In this study, a Kistler dynamometer 9256C2 with extremely low threshold is used for measuring small force less than 0.002 N. The measuring range of three axis is from -250 N to 250 N. The small temperature error, high sensitivity and natural fraction enable the dynamometer to use for cutting force measurements in ultra-precise machining. Collecting the input signals, the dynamometer is then connected to a Kistler multichannel charge amplifier 5080A. With a wide measure range, the measurement error is less than ±0.3% on full range when the temperature range is from 0 to 50. A liquid crystal display shows all channel settings. The amplifier is connected to charge modules type 5067 for voltage signal output. The output voltage range is ±10V, the frequency bandwidth is up to 200 kHz and the group time delay is around 2 μs. The output data are collected through NI9234 DAQ card and recorded in PC. The post-process data analysis is conducted in Matlab or Labview.

(2) Impact hammer system

Due to the nonlinear property of cutting process, the natural frequency, dynamic frequency response of tooling system and workpiece system and also transfer function of cutting force should be identified. An impact hammer 9722A500 is performed in this study. Dynamic quartz sensor elements contained within instrumented hammer are

applied to deliver a measurable force impulse to excite target parts. The range of output voltage is ±5 V, the force range is 0 to 100 lbf and the sensitivity is 50 mV/lbf. In order to generate a wider effective frequency range that suitable for the high speed cutting process, a steel impact tip 9902A with less deform and shorter duration is used in this study. A Thurlby series of laboratory bench power supply, which is connected with the impact hammer through Kistler 5108A piezotron coupler, is used to supply the power. Output signals are collected by NI9234 DAQ card.

(3) Capacitive sensor system

A non-contact capacitive sensor MicroSense 5810 is used for modal analysis and in-process measurement in micro milling of MMCs. The cutting tool runout, tool vibration and tool natural frequency are adopted through the non-contact capacitive displacement measurements and sensing. In addition, it also performed as a functional tachometer for ultra-high RPM mechanism analysis. The capacitive sensor has a high resolution at jumper selectable high bandwidths. In this study, the working bandwidth is 20 kHz and the output measurement range is full scale ±100 μm. The input signal is collected through a probe and analog output signal is achieved by DAQ card which connected to the PC.

(4) Accelerometer sensor system

A PCB Piezotronics 352C33 accelerometer is used for system natural frequency analysis. The accelerometer sensor has a measurement range of ±490 m/s^2 and a sensitivity of 10.2 $mV/(m/s^2)$. The power is supplied by a PCB Piezotronics 482A04 ICP Transducer Amplifier Power Supply. Output signals are collected by NI9234 DAQ card connecting with PC.

(5) NI DAQ 9234

NI DAQ 9234, which is a four-channel dynamic signal acquisition module for making high accuracy measurements from Integrated Electronic Piezoelectric (IEPE) sensors, is used in precision machining experiment. With the high resolution of 24-bit and signal sampling rate up to 51.2 kHz per channel, NI DAQ 9234 provides an extremely high accurate real-time data collection.

3.5.1.3 Metrology measurement instruments

(1) ZYGO New View 5000 white light interferometer

The NewView 5000 white light interferometer is used to characterize and quantify the surface performance including surface roughness, step heights, critical dimensions and other topographical features with excellent precision and accuracy. The frequency domain analysis and proprietary scanning technique guarantees a vertical resolution down to 0.1 nm. The image zoom (0.4x to 2x) and objective turret (20x) are equipped in order to achieve a large magnification range. A closed-loop piezoelectric actuator driven scanner, employing low-noise capacitive sensors, ensures the surface measurement accurate and repeatable. Data and images are then collected and analysed through the build-in MetroPro software.

(2) JCM-6000 benchtop scanning electron microscope (SEM)

Morphological measurement is conducted on JCM-6000 benchtop scanning electron microscope (SEM). SEM with high resolution (60,000x) down to nano-scale and an accelerating voltage range up to 15 kV is mainly used on the measurement of workpiece micro structure, surface texture and cutting tool structure and wear in this research. The SEM offers both an Everhart Thornley type secondary electron (SE) detector as well as high sensitivity solid state backscattered electron BSE detector. A full-featured Energy-dispersive X-ray Spectroscopy (EDS) with SDD technology is optionally available for elemental analysis.

(3) TESA V 200 microscope

Large geometries, feature dimensions and surface profile of cutting tools and workpiece are measured by powerful TESA V 200 microscope. The maximum measuring volume is 200*100*150 mm and a display resolution of 0.001 mm. The opto-electronic measuring system with incremental glass scales has a resolution up to 0.05 µm. The TESA machine is operated by TESAVISTA 2.0 software.

(4) ALICONA InfiniteFocus

Large area surface profile and surface roughness such as cutting tool surface are measured by Alicona InfiniteFocus optical form measurement system for quality assurance. This system provides the functionalities of an optical profiler and a 3D micro

coordinate measurement. The actual surface roughness and texture can be accurately generated by coupling the roughness and the real surface topography images in each section together respectively. The Focus-Variation based traceable measurement system has almost unlimited range of measurable surfaces, high resolution, high accuracy and high repeatability. The vertical resolution is up to 10 nm.

3.5.2 Experimental trails

The ultraprecision machining processes are affected by various factors such as size effect, cutting tool geometries, material compositions, chip formation, minimum chip thickness, cutting parameters and also cutting conditions. The finite element analysis and the cutting trials for both micro turning and micro milling addressing different phenomenon are applied. The simulation process and experimental trials are introduced in details in the following chapters.

3.5.2.1 Cutting trials on the precision turning machine

In order to have a better understanding on the cutting characterisation and cutting mechanics particularly for minimum chip thickness and chip formation mechanisms in MMCs precision machining, cutting trials are conducted on precision turning machine. PCD inserts and natural diamond inserts with both zero rake angles are performed in these cutting trials. Both PCD tool and diamond tool contain small edge radius which are around 3.5 μm and 100 nm respectively. With the high precision performance of turning machine, the movement of cutting tools is performed on nanometer level. The micro cutting experimental trials are conducted to evaluate and validate the modified minimum chip thickness model and FE based chip formation analysis. Cutting forces are recorded and machined surface roughness is measured under varied cutting parameters including cutting speed, feed rate and depth of cut. All the cutting trials are performed with dry cutting condition, only air blow are provided during the machining process. In addition, the surface in each cutting trial is pre-machined in order to achieve the same datum surface and avoid the error during machining and measurement processes. The experimental set-up for micro turning trials is shown in Figure 3-4.

3.5.2.2 Cutting trials on the micro milling machine

To evaluate and validate the dynamic cutting force model, and further investigate tool wear and machined surface generation in MMCs micro milling process, cutting trials

are performed on KERN milling machine. 10 mm diameter double straight flutes PCD end mills with 2 µm edge radius and 0.2 mm nose radius are applied in these micro milling trials. Three different MMCs workpiece, which are 5 µm 45% SiC/Al, 90 µm 60% SiC and 5 µm 50% B_4C/Al, are performed in the micro milling experiments under varied cutting parameters. The cutting system modal analysis is conducted before machining process. Cutting force signals are collected to verify the modified force model. Surface roughness, tool wear rate and chip formation are further measured and analysed using high precision measurement instruments. Figure 3-5 below shows the experimental set-up on the micro milling machine in details.

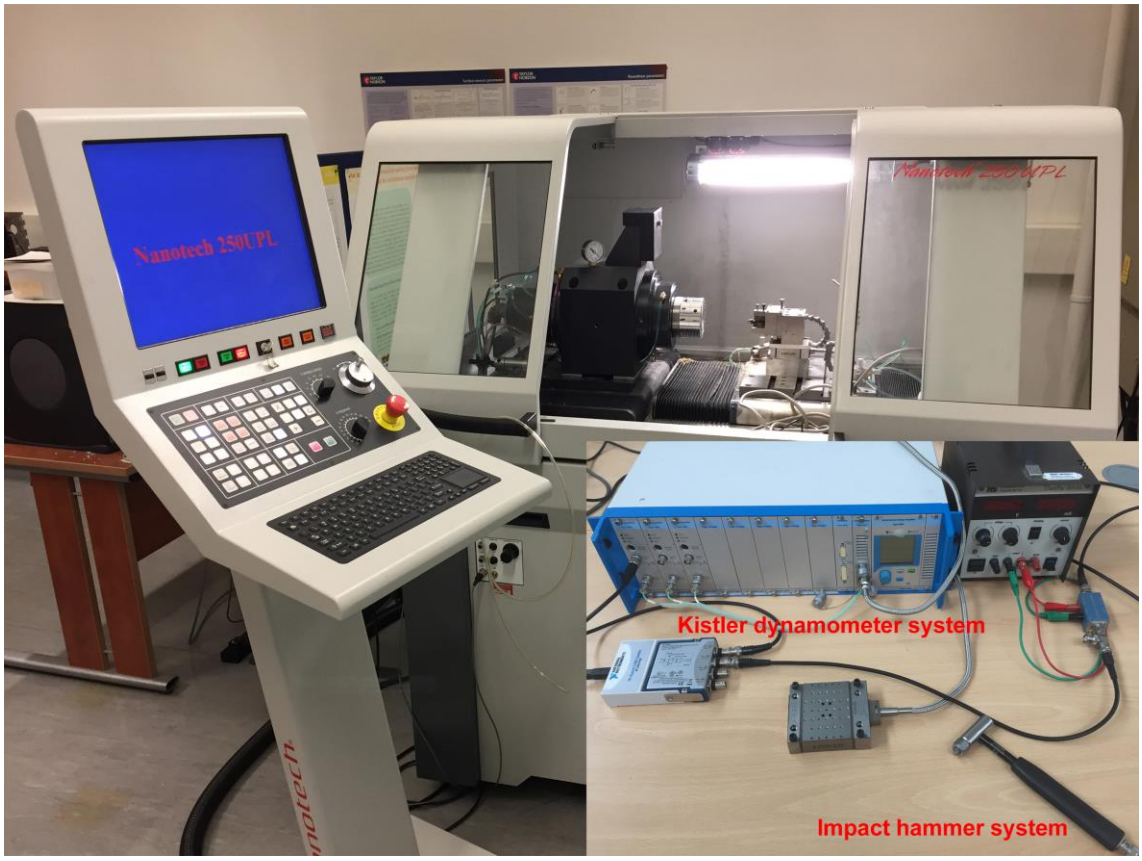

Figure 3-4 Precision turning experimental set-up

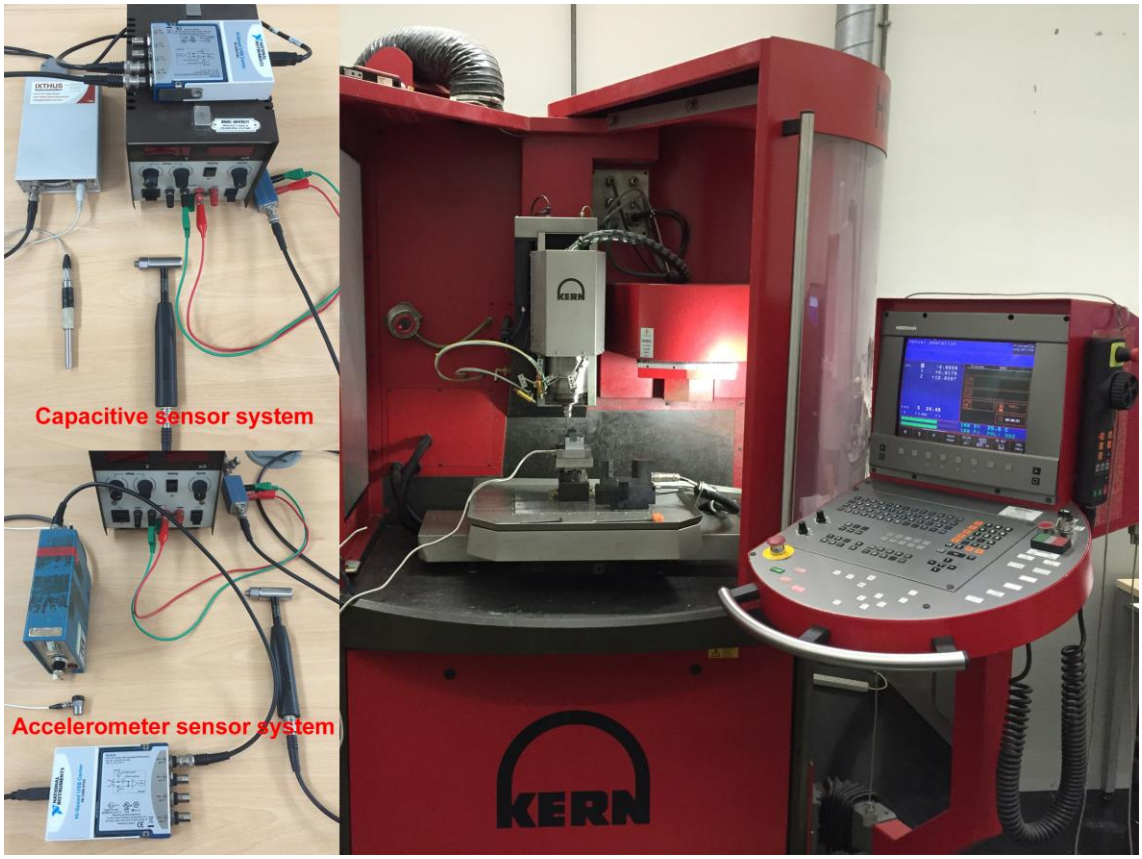

Figure 3-5 Micro milling experimental set-up

3.6 Conclusions

In this chapter, the formulation of research methodology is presented particularly focusing on multiscale multiphysics based approach to modelling and analysis in MMCs precision machining and the corresponding experimental study. The methodology is fully adopted and applied to the research presented in the following chapters.

Chapter 4 Analysis of precision machining metal matrix composites (MMCs) and cutting mechanics

4.1 Introduction

Scientific understanding and analysis on the material deformation behaviour, the chip formation mechanisms and the MMCs machinability are extremely crucial for achieving higher surface integrity, extended tool life, and further minimizing machining cost and extending the MMCs into high-volume industrial scale applications. As the microstructure and material properties of metal matrix composites are quite unique, the chip formation in precision machining of particles reinforced MMCs is then extremely different from those of homogeneous materials in conventional machining or even in micro machining process. This becomes a critical issue that has been identified and investigated by various researchers [84-92]. However, from the metal cutting point of view, the researches on the cutting mechanics particular for the chip formation process and related areas in MMCs precision machining are extremely limited. Thus, further studies and analyses are necessary to have in-depth understanding on the uniqueness of chip formation mechanisms in MMCs machining process. In addition, the role that these reinforced particles play during chip formation and the way in which the particles are removed or fractured are also absent, which can be very useful data and information for the materials design and fabrication particularly towards having much improved machinability performance.

In this chapter, a fundamental study on the chip formation mechanism as well as the minimum chip thickness in MMCs precision machining are investigated through a holistic theoretical analysis, multiphysics simulation and experimental trials based integrated approach. First of all, minimum chip thickness (MCT) value is identified theoretically based on the basic MCT model in abrasive machining process. The certain threshold of uncut chip thickness, that chips starts to form at this chip thickness point, is then adopted. The MMCs chip formation including the matrix material breakage, particles fracture and their interfacial debonding, sliding or removal is further simulated using comprehensive FE analysis approach. Minimum chip thickness and chip formation simulations are evaluated and validated via well-designed precision turning trials on diamond turning machine. The chips and surface profiles formed under varied

cutting conditions in periodical material removal are inspected and measured in order to have a further understanding on the MMCs cutting mechanics.

4.2 Theoretical analysis of minimum chip thickness (MCT) in MMCs precision machining

Due to the significantly effect on the chip formation, the well-known size effect and minimum chip thickness effect for homogeneous materials can be extensively understood in a MMCs precision machining process. However, the minimum chip thickness of MMCs is largely different from those of homogeneous material. Due to unneglectable cutting edge radius and the existence of micro particles, the chip formation is complicated. Particle size, tool edge radius and cutting parameters as the most prominent factors that affect the MMCs chip formation need to be further considered. The conventional un-deformed chip thickness involved in this MMCs precision machining process has a further consequence: the minimum chip thickness model shifts from the homogeneous material shearing process to a combination of matrix material breakage and reinforcements fracture. As a result, the actual prediction of MMCs' minimum chip thickness is much complicated. The chip formation mechanisms at the matrix breakage region and particle fracture region are also different. Due to the normal distribution of particles in MMCs, the cutting edge plough and shear both on the matrix material and the reinforcements when the tool approaches on the workpiece surface. The one involving concentrated shear is then divided into two separated shearing process. Thus, the minimum chip thickness in precision machining of MMCs can be illustrated by introducing the combination of these two aspects including the matrix material thickness in chip formation a_{p1} and particle fracture thickness in chip formation a_{p2}. The intrinsic relationship is $a_p = a_{p1} + a_{p2}$ and detailed MCT models are shown as below.

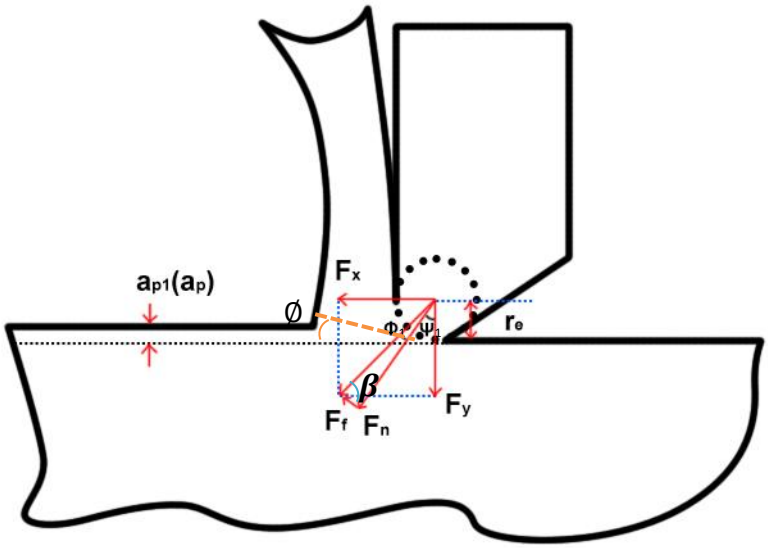

Figure 4-1 Matrix material thickness in chip formation process

For the matrix material breakage, the chip formation model is shown in Figure 4-1. The relationship between cutting edge radius r_e and un-deformed chip thickness a_{p1} at the matrix material chip formation point is [113]:

$$a_{p1} = r_e - r_e * \cos\psi_1 = r_e * (1 - \cos\psi_1) \tag{4.1}$$

where,

$$\psi_1 = \frac{\pi}{4} - \phi_1 = \frac{\pi}{4} - \tan^{-1}(\frac{F_f}{F_n}) \tag{4.2}$$

$e_1 = \frac{F_f}{F_n}$ is the friction coefficient between PCD tool and matrix material in precision machining process. F_f is the friction force and F_n is the normal force. ϕ_1 is the angle between cutting force and normal force and ψ_1 is the angle between normal force and the cutting force in y direction. Thus, the minimum cutting depth with chip formation for the matrix material part is:

$$a_{p1} = r_e * \left(1 - \cos\left(\frac{\pi}{4} - \tan^{-1} e_1\right)\right) \tag{4.3}$$

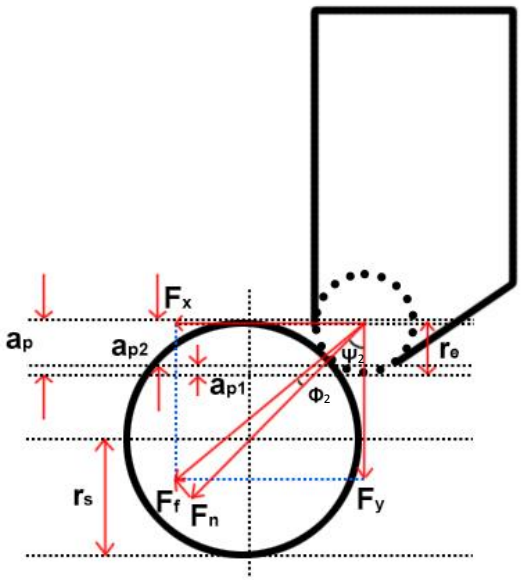

Figure 4-2 Particle fracture thickness in chip formation process

For the reinforced particles fracture, the chip formation can be illustrated in Figure 4-2 and the relationship between particle radius r_s and un-deformed chip thickness a_{p2} at the tool-particle interaction point can be expressed as:

$$a_{p2} = r_s - r_s * \cos\psi_2 = r_s * (1 - \cos\psi_2) \tag{4.4}$$

where,

$$\psi_2 = \frac{\pi}{4} - \phi_2 = \frac{\pi}{4} - \tan^{-1}(\frac{F_f}{F_n}) \tag{4.5}$$

$e_2 = \frac{F_f}{F_n}$ is the friction coefficient between PCD tool and reinforced particle material in micro milling process. ϕ_2 is the angle between cutting force and normal force and ψ_2 is the angle between normal force and the cutting force in y direction. Thus, the minimum cutting depth with chip formation for the particle fracture part is:

$$a_{p2} = r_s * \left(1 - \cos\left(\frac{\pi}{4} - \tan^{-1} e_2\right)\right) \tag{4.6}$$

Therefore, the combined minimum cutting depth with chip formation can be expressed as minimum chip thickness in MMCs precision machining process as shown below.

$$a_p = a_{p1} + a_{p2}$$
$$a_p = r_e * \left(1 - \cos\left(\frac{\pi}{4} - \tan^{-1} e_1\right)\right) + r_s * \left(1 - \cos\left(\frac{\pi}{4} - \tan^{-1} e_2\right)\right) \tag{4.7}$$

Due to the chip formation process contains the combination of matrix material breakage and particle breakage, the friction coefficient for the MMCs micro milling process is observed as the friction coefficient between the tool material and MMCs workpiece material. Thus, the minimum chip thickness can be further expressed as below.

$$a_p = (r_e + r_s) * \left(1 - \cos\left(\frac{\pi}{4} - \tan^{-1} e_{MMC}\right)\right) \quad (4.8)$$

According to the properties of cutting tools and workpiece material, and also the interaction and contact properties between the tool surface and workpiece utilized in this research, the constant friction coefficient e_{MMC} is assumed as 0.35 [99] in this MMCs precision machining process. Thus, based on the minimum chip thickness equation, the minimum chip thickness for MMCs with 5 μm particle size can be then predicted as 0.594 μm. Due to the negative rake angle and the prominent particles size, chips may not be produced when the uncut chip thickness is smaller than the MCT of matrix material. In addition, only matrix materials are removed and remained particles still rubbed on the flank face of cutting tool, which leaves a poor machined surface when DOC is larger than MCT of matrix material while still smaller than the MCT of MMCs material. Only when the DOC reaches a certain threshold, matrix material and reinforced particles can be cut through and MMCs chips start to form continued. This is similar to the minimum chip thickness effect in micro milling homogeneous materials while distinguishes the heterogeneous material micro milling process from the homogeneous material micro milling process.

From the predicted results, it can be observed that the minimum chip thickness for MMCs is closely relative to the tool edge radius and particle size. However, the actual MCT is much smaller than the cutting edge radius in this precision machining process. The modified minimum chip thickness model is further evaluated and validated via well-designed cutting trials in the following parts.

4.3 Finite element analysis of chip formation in MMCs precision machining

The MMCs chip formation mechanisms is commonly divided into three aspects which are matrix materials plastically deform, matrix-particle interfacial reaction and brittle particles fracture. The simulation approach is developed to investigate the effects of

cutting parameters, particular for cutting speed and depth of cut, on material removal, chip formation and the consequent scientific understanding of the machining mechanics in MMCs precision machining. The findings are also essential for developing the machining process optimisation strategy.

4.3.1 FE simulation setup

The FE analysis on MMCs chip formation mechanisms are carried out in Abaqus/Explicit 6.14. The schematic of this 2D orthogonal micro cutting model is illustrated in Figure 4-3. In term of the MMCs workpiece, B_4C particles with a volume fraction of 50% are evenly distributed in Al 2024 matrix. The average particle size of B_4C is 5 μm in diameter. According to the PM fabrication method, mechanical bonding is found and applied on the interface between matrix material and particle. Thus, particles are only simulated by tied together with the matrix material which enables their initial displacements at the interface area are both equal to zero rather than constructing an artificial layer in interface when modelling interface properties. The interfacial de-bonding can be achieved through matrix material failure [232]. The MMCs cutting behaviour is significantly affected by the cutting parameters and the location of particles relative to the position of cutting tool. Thus, models are conducted under various cutting parameters and particle positions relative to the cutting tool. Poly-Crystalline Diamond (PCD) tools, which offer higher tool life due to their high hardness and thermal conductivity, are normally used in MMCs machining [140, 233]. In order to ensure the consistent with the following experimental trials, a PCD tool with the rake angle and the relief angle defined as -5^o and 5^o respectively is applied in this model. The PCD tool can be configured as a rigid body in the whole cutting process due to its extremely high strength, while heat transfer on the cutting tool is still active. The edge radius of cutting tool tip is defined as 3.5 μm. Free mesh with quadrilateral continuum elements CPE4RT units and triangle elements CPE3T units are used to model the MMCs workpiece and PCD tool respectively. The material removal process is simulated under a fully coupled dynamic, temp-disp, explicit multiphysics condition. FE simulation and analysis below are conducted through a thermal-mechanical-tribological coupled integrated approach. In this model, left and bottom sides of the workpiece are constrained on the movement in each direction and rotation, while the cutting tool moves towards the workpiece with a defined velocity. A reference point is defined on the cutting tool in order to control the boundary conditions and achieve the simulation

results. The simulations are carried out under various cutting speed and depth of cut. The cutting speed of 157.0 m/min, 125.7 m/min, 94.2 m/min and DOC of 1 μm, 2.5 μm, 4 μm are selected and performed in the simulation processes and further used in the machining trials.

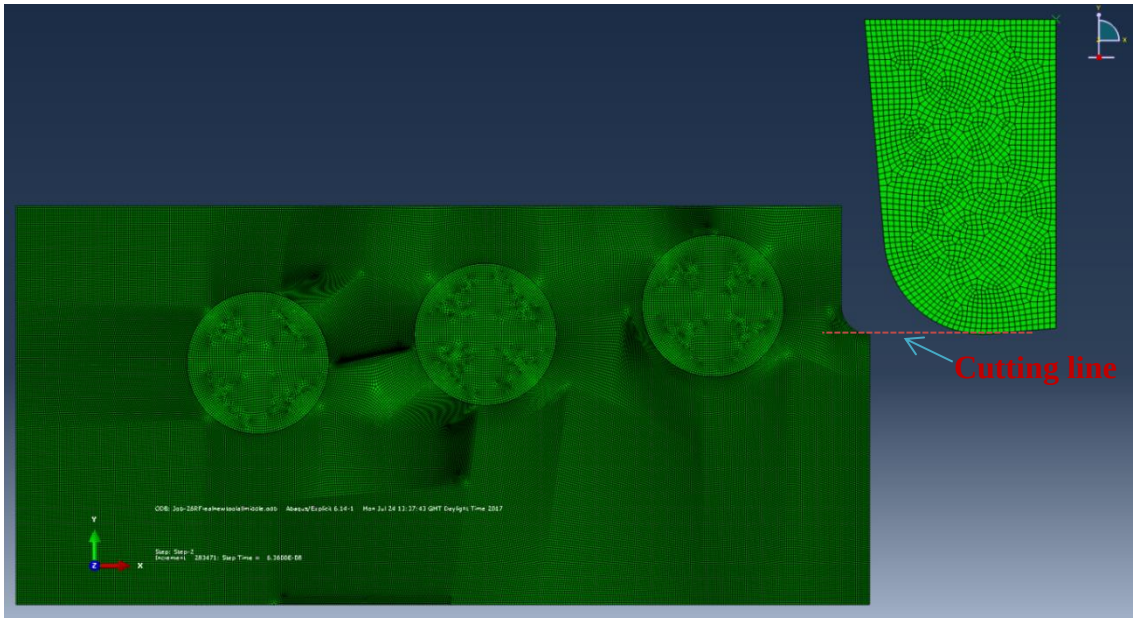

Figure 4-3 Finite element model for MMCs precision machining

4.3.1.1 Material constitutive model, damage initiation and evolution

(1) Matrix material: As the Al 2024 matrix is a typical elastic-plastic material, Johnson-Cook model is applied. This matrix material is modelled by introducing a thermal-elastic-plastic constitutive equation until material failure. The material flow stress σ can be represented by the following equation [234]:

$$\sigma = [A + B(\varepsilon^{pl})^n]\left(1 + C ln\frac{\dot{\varepsilon}}{\dot{\varepsilon}_0}\right)\left[1 - \left(\frac{T - T_0}{T_m - T_0}\right)^m\right] \quad (4.9)$$

ε^{pl}: effective plastic strain;

$\dot{\varepsilon}$: equivalent plastic strain rate;

$\dot{\varepsilon}_0$: reference strain rate;

T, T_0 and T_m are the current cutting temperature, room temperature and melting temperature of material respectively. A, B, C, n and m are the material model parameters measured at or below the transition temperature, which illustrate as follows.

A: initial yield strength of the material at room temperature;

B: isotropic strengthening parameter during the strains;

C: strain rate sensitivity;

n: strain hardening exponent;

m: thermal softening exponent;

The physical properties of matrix material, particles and PCD tool used in this simulation, and material constants are shown in Table 4-1 and Table 4-2 respectively.

Table 4-1 Properties of workpiece and cutting tools [97, 235]

Material	Matrix: Al 2024	Particles: B_4C	Tool: PCD
Thermal conductivity (W/(mK))	190	42	2100
Density (g/cm^3)	2.77	2.52	4.25
Elasticity modulus (GPa)	73	460	1147
Poisson's ratio, ν	0.33	0.19	0.07
Specific heat (J/(kgK))	875	945	525

Table 4-2 Material constants for Johnson-Cook plasticity model [102]

Material	**A**	**B**	**C**	**n**	**m**	**T_m**	**T_0**
Al 2024	369MPa	684MPa	8.3e-3	0.73	1.7	502ºC	20ºC

In MMCs shearing progress, the matrix material experiences progressive damage and failure. This performs the similar failure progress to the conventional homogeneous material that respects the typical stress-strain behaviour as shown in Figure 4-2. Under the condition of high shear stress and large strain rate, matrix material starts to elastically deform, plastically deform associating with strain hardening and thermal softening, damage starts and damage evolution, further fracture with accumulate damage and finally fails.

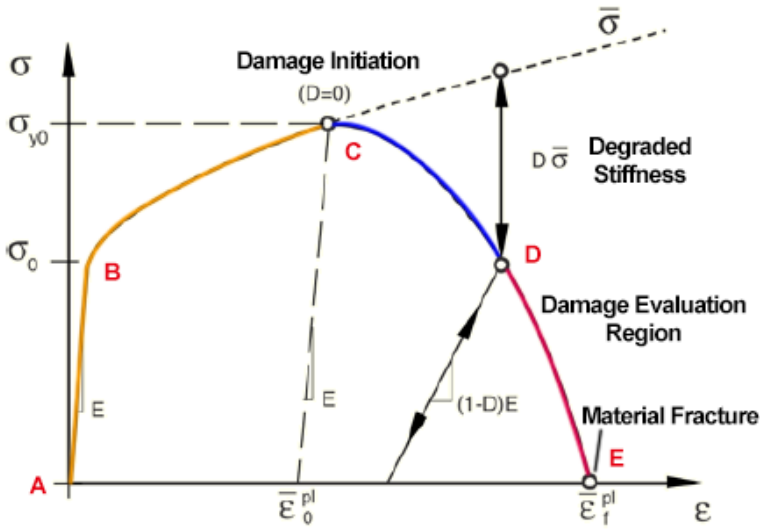

Figure 4-4 Typical stress-strain behaviour with progressive damage degradation

Johnson-Cook dynamic failure model, which is recommended as the critical technique for modelling the cutting progressive damage and the material failure, is applied in this simulation. The damage of matrix material is expressed by equation [234]:

$$\bar{\varepsilon}_f^{pl} = \left[D_1 + D_2 exp\left(D_3 \frac{p}{q}\right)\right]\left[1 + D_4 \ln\left(\frac{\dot{\varepsilon}}{\dot{\varepsilon}_0}\right)\right]\left(1 + D_5 \frac{T - T_0}{T_m - T_0}\right) \qquad (4.10)$$

where $\bar{\varepsilon}_f^{pl}$ is the equivalent strain as a function of temperature, strain rate, equivalent stress and pressure at material failure, $D_1 \sim D_5$ are the material constants for damage model, $\frac{p}{q}$ is a dimensionless pressure-deviatoric stress ratio, where, p is the pressure stress and q is the Mises stress which represents the effective cutting stress, $\frac{\dot{\varepsilon}}{\dot{\varepsilon}_0}$ is the nondimensional plastic strain rate. Table 4-3 below shows the material constants for this damage model.

Table 4-3 Material constants for Johnson-Cook damage model [102]

Material	D_1	D_2	D_3	D_4	D_5
Al 2024	0.112	0.123	1.5	0.007	0

A linear evolution of damage variable is assumed for the progressive damage and fracture model. Based on the value of the equivalent plastic strain at element integration points, the damage parameter ω can be defined as

$$\omega = \sum \left(\frac{\Delta \bar{\varepsilon}^{pl}}{\bar{\varepsilon}_f^{pl}} \right) \tag{4.11}$$

where, $\Delta \bar{\varepsilon}^{pl}$ is the change of equivalent plastic strain in each integration cycle. Thus, the material stiffness will be fully degraded and material failure occurs when the damage parameter ω exceeds 1. As long as the damage occurs, material behaviour is no longer accurate by using the stress-strain curve. Thus, a stress-displacement response law is introduced in Hillerborg's fracture energy proposal in order to follow the strain-softening branch of stress-strain curve as shown in Figure 4-4 and this better illustrates the material progressive damage.

(2) Reinforced particles: Due to the brittle properties of B_4C, particles are observed as perfectly elastic material until failure. A brittle cracking model is used to present the fracture of particles. In this model, the crack normal displacement at the failure point can be determined as:

$$u_{n0} = \frac{2G_f^I}{\sigma_{tu}^I} \tag{4.12}$$

where, G_f^I is expressed as energy required for opening a unit area of crack, σ_{tu}^I is defined as a tabular function of the associated Mode I fracture energy. In addition, the post-cracking shear modulus G_c in brittle shear model is defined as a fraction of uncracked shear modulus as shown in equation (4.13).

$$G_c = \left(1 - \frac{e_{nn}^{ck}}{e_{max}^{ck}}\right)^P G \tag{4.13}$$

where, G is shear modulus of the un-cracked material; e_{nn}^{ck} is crack opening strain; e_{max}^{ck} and P are material parameters [236]. Material parameters for brittle cracking model are shown in Table 4-4.

Table 4-4 Material parameters for brittle cracking model [235]

Material	σ_{tu}^I(MPa)	p	G_f^I(J/m^2)	e_{max}^{ck}
B_4C	155	1	50	0.001

4.3.1.2 Tool-workpiece interaction

The interaction between cutting tool and workpiece is of importance to realize the material removal mechanism in MMCs precision machining process. The accurate set-up of tool-workpiece interaction and friction is critical as they significantly affect the cutting force, heat generation and tool wear rate. In addition, the power consumption for material removing and resultant surface quality are also determined by their interaction. To simulate the interaction between tool and matrix material/particles, a kinematic surface-to-surface contact pair model is employed in ABAQUS. In order to adopt the friction more accurately, a modified stick-slip friction law proposed by [237] based on Coulomb friction law is introduced by considering the normal stress and shear stress distribution on tool rake face. The cutting tool edge region is assumed as the sticking region and the sliding region takes place beyond the sticking region on the rake face [237]. The friction model in this simulation can be described by the following equation.

$$t_{fric} = \min(\mu\delta_n, \tau_s) \tag{4.14}$$

where, μ is the friction coefficient that defined as a function of contact pressure; δ_n is the normal pressure on the chip and cutting tool interface; τ_s is the limit shear stress which can be calculated from the equation $\tau_s = \delta_y/\sqrt{3}$. δ_y is the material initial yield stress. In this MMCs precision machining process, the contact pairs which are controlled by the Coulomb friction law [238] are given a constant friction coefficient of 0.35 [99].

4.3.1.3 Heat generation and heat transfer

In MMCs precision machining, a thermal module is applied and integrated with mechanical module due to most energy consumption in chip formation progress including the chip generation and chip sliding on tool surface are finally convert to the thermal energy. The dissipated energy generated by material plastic deformation and tool-workpiece friction is mostly performed as heat source afterwards. The heat generation and heat transfer on the tool/workpiece contact area result in the material soften, tool wear occurrence and tool failure. In addition, the cutting stress and cutting force change significantly under varied heat. Thus, a comprehensive heat generation and heat transfer model is introduced.

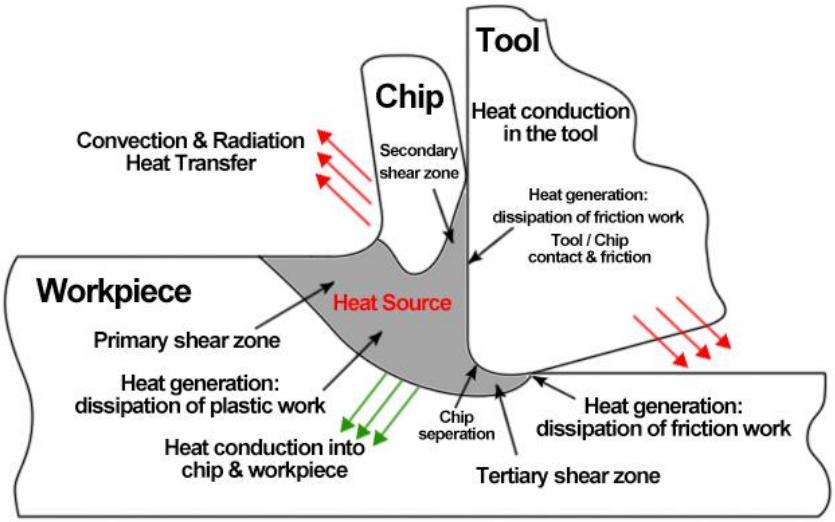

Figure 4-5 Heat generation and heat transfer [31]

Figure 4-5 demonstrates the schematic heat generation and heat transfer in MMCs micro-cutting by extending the same assumption in the conventional homogeneous material micro cutting. The generated heat in cutting zone is partly transfer to the chips and taken away along with the chips. Another part of heat is conducted to the remained workpiece. The rest part is transferred to the cutting tool which easily results in tool soften and wear.

In MMCs micro machining, heat transfer in the solid considering the translation motion is defined as follows [27]:

$$\rho C_p \frac{\partial T}{\partial t} - \nabla * (k \nabla T) = Q - \rho C_p \mathrm{V}_{trans} \nabla T \tag{4.15}$$

where, ρ is density, C_p is heat capacity, k is thermal conductivity, Q is heat source and V_{trans} is the velocity of moving part.

The heat flux densities q_1 and q_2 going out the surfaces on tool/chip slide and tool workpiece slide respectively are given by:

$$\begin{aligned} q_1 &= q_k + q_r - f_1 q_g \\ q_2 &= -q_k - q_r - f_2 q_g \end{aligned} \tag{4.16}$$

where, q_g is the heat flux density generated by the interface element due to frictional heat generation; q_k is the heat flux generated due to conduction; q_r is the heat flux

generated due to radiation; f_1, f_2 are the fraction of generated heat into these two interface respectively.

The thermal contact depicts the correlation for the conductance h at the two surface contact interfaces. By involving the heat transfer coefficient at the interface h, heat flux over the surfaces is defined as follows:

$$\begin{aligned} -n_d(-k_d\nabla T_d) &= -h(T_u - T_d) + rQ_{fric} \\ -n_u(-k_u\nabla T_u) &= -h(T_d - T_u) + (1-r)Q_{fric} \end{aligned} \tag{4.17}$$

where, u and d describe the upside and downside slit, which are tool/chip interface and tool/workpiece interface respectively in this model. In the heat generation and heat transfer model, the PCD tool used in the cutting process can be configured as a rigid body due to its extremely high strength, while, the heat transfer is still active. Thus, the heat flow on the cutting tool can be generated in the simulation process.

4.3.2 Simulation results, analysis and discussion

4.3.2.1 Chip formation mechanisms

The chip formation process including matrix material breakage, reinforced particles fracture and their interfacial reaction in MMCs precision machining is complex. The fracture orientations, which determine the chip formation properties and the resultant surface quality, are varied under different cutting conditions. Thus, an in-depth understanding of chip formation mechanisms is of great importance in order to achieve better surface roughness and surface performance. The interaction between cutting tool tip and workpiece are involved in the simulations. Three cutting scenarios, which are defined as particle centre is located higher than the cutting line, particle centre is located on the cutting line and particle centre is located lower than the cutting line, are investigated respectively.

For the scenario of the particle centre is located higher than the cutting line, the cutting tool firstly approaches into the matrix material. Plastic and elastic deformation on the matrix material occurs and it can be observed that chips generated along the cutting line. With the continued approach of the cutting tool, dramatically increased stress results in a high strain on the matrix/particle interface.

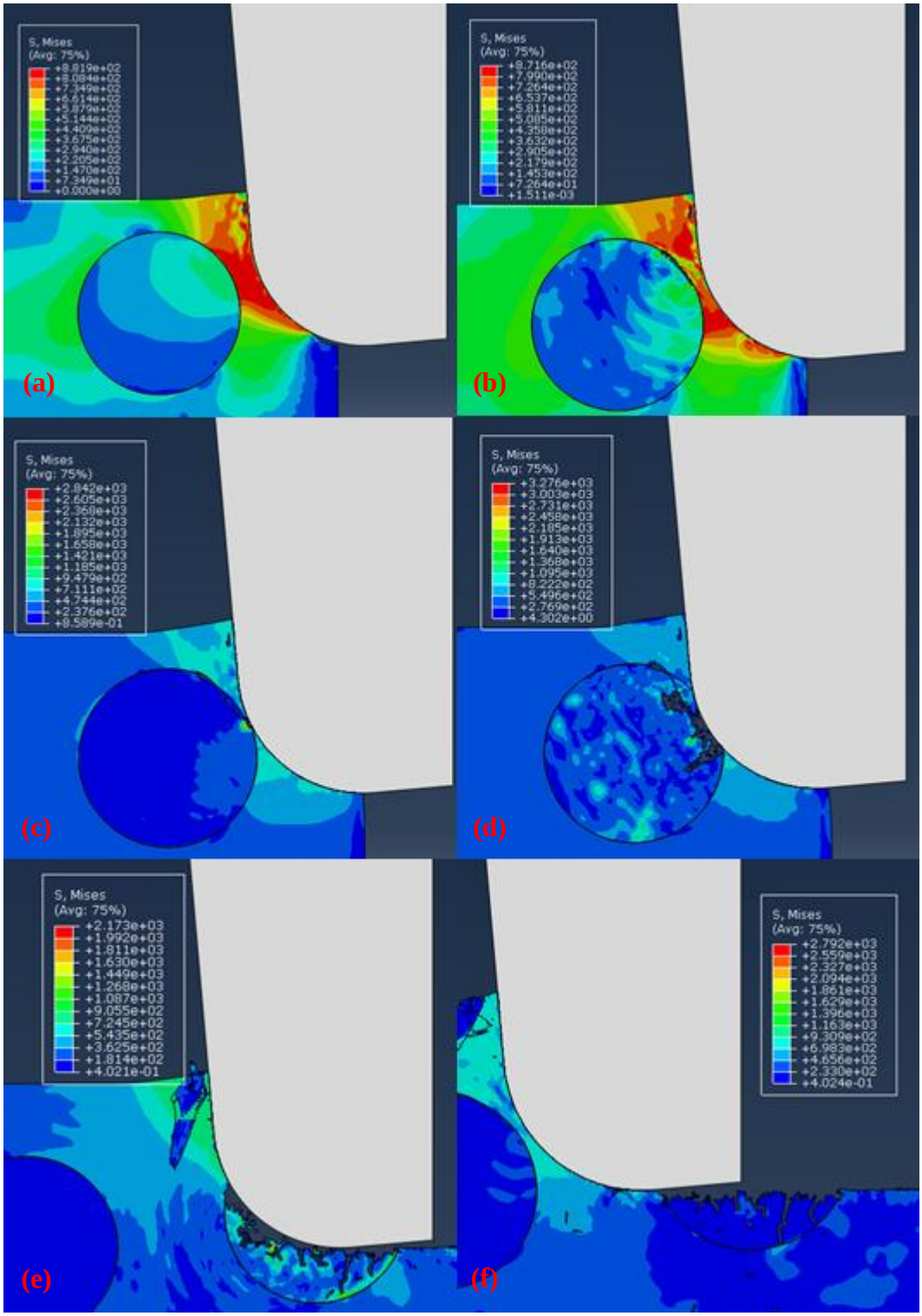

Figure 4-6 Scenario of the particle centre is located higher than the cutting line

When the cutting force exceeds the bonding force, bonding failure occurs on the interfacial boundary. Meanwhile, some small voids are formed along the separation direction of matrix/particle pairs due to the stress concentration at the interface. The crack propagation is enhanced through the coalescence of these voids that can be

observed in Figure 4-6(b). Matrix material breakage significantly occurs and chips formed on the shearing plane with the further approach of cutting tool. When the tool attaches on the reinforced particle, the high stress leads to the fracture of brittle particle and a groove leaves on the particle at first. With the continue fracture of particle, cracks are generated towards both upper and lower directions of un-machined particle area shown in Figure 4-6(d). As the tool keeps moving forward, more cracks are found and dis-continued chips of matrix material can be observed in Figure 4-6(e). The cavities, particularly on the particle/matrix interfacial area, can be found after the tool cuts through the whole surface. In addition, more cracks occur at the approach in side of fractured particles. This occurs due to the suddenly increased stress on the interface results in the crack propagation enhanced dramatically.

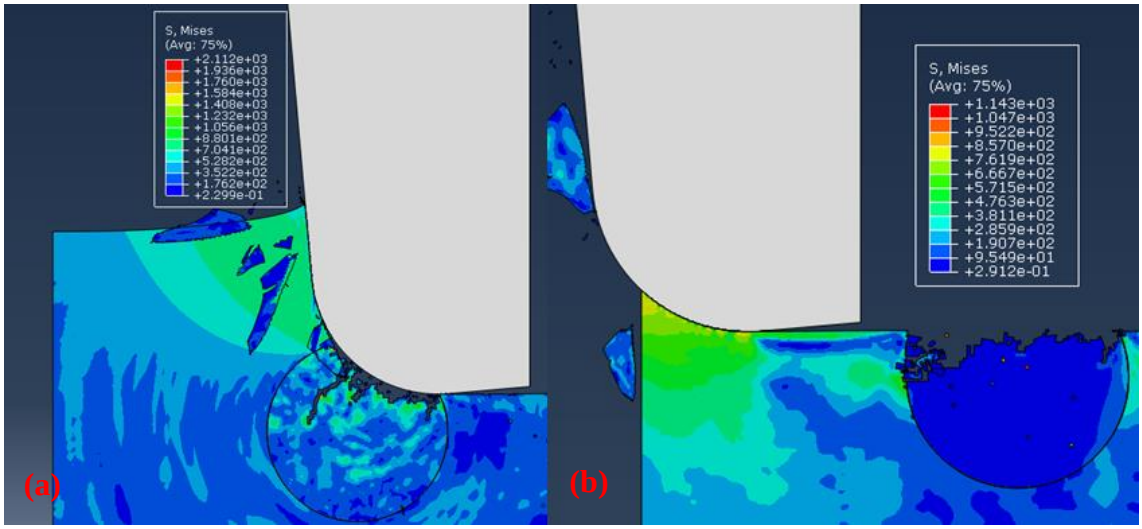

Figure 4-7 Scenario of the particle centre is located lower than the cutting line

For the scenario of the particle centre is located lower than the cutting line, the matrix material breakage is similar as the particle centre is located higher than the cutting line. Interfacial de-bonding and matrix breakage occur significantly. While the fracture properties of particle have slightly differences. When the tool attaches on the particle, the high stress leads to the fracture of brittle material and further approach of cutting tool results in almost all of the cracks generated towards lower direction of un-machined particle area as shown in Figure 4-7(a). As the tool keeps moving forward, more cracks are found as well. The cavities, particularly on the particle/matrix interfacial area also can be found after the tool cuts through the whole surface. While, more cracks can be observed at the tool approach out area of fractured particle. This can be attributed to the

particle has been fractured before the tool approach out and these fractured elements go along with the formed matrix material chips afterwards.

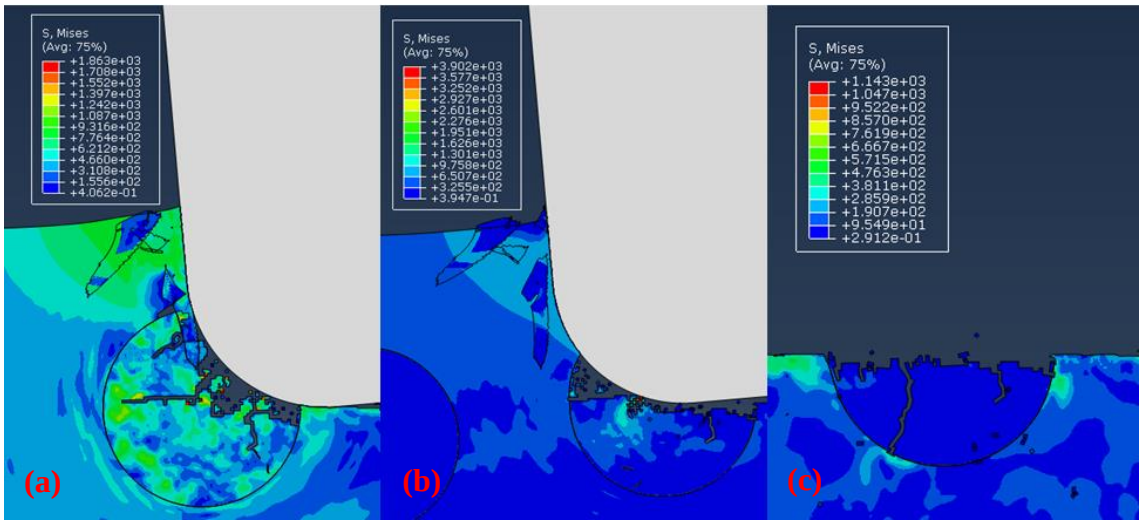

Figure 4-8 Scenario of the particle centre is located on the cutting line

For the scenario of the particle centre is located on the cutting line, the matrix material breakage is still similar as those in the other two scenarios. The particle fracture properties are interesting that the high stress leads to the fracture of brittle material when first attach and with further approach of cutting tool, the cracks generated towards the cutting direction of un-machined particle area as shown in Figure 4-8(a). This indicates that the particles break along the cutting line with fewer cracks formed along the tool path and finally leaves a much smoother surface when cutting on the cutting line.

Due to the extremely high shear stress, the primary chip-forming mechanism involves the initiation of cracks from the outer free surface of the chips. The normal distribution of reinforced particles and their high volume fraction result in the dis-continued chip formation. The average chip lengths shown in these three scenarios are similar which are around 5 μm. The particles with brittle properties are performed by small segments that link to each other. These segments are separated during the cutting process and brittle chips are observed as small segments in the end. Some of these segments may fill the cracks during the machining and make the resultant surface smoother, while most of them are removed along with the chips. Thus, the chip formation in MMCs precision machining can be seen as powder form chips according to the properties of matrix material breakage and particle fracture as shown in the integrated simulation results.

4.3.2.2 Machined surface performance

Along with the interaction of tool/matrix and tool/particle pairs, surface generated gradually. Material fracture and surface defects occur along the feed direction and cutting direction. Thus, cutting speed, depth of cut and feed rate are considered as the critical factors that influence the machined surface quality in the simulations.

(1) Influence of cutting speed: From Figure 4-9, it can be observed machined surface quality increases when the cutting speed is higher. According to the Johnson-Cook damage model, it is known that the strain at material damage is a function of dimensionless pressure-deviatoric stress ratio, non-dimensional plastic strain rate and cutting temperature. While considering the constants for the damage model showed in Table 4-3, the material failure strain is strongly depend on the stress ratio and has extremely low dependence on strain rate and temperature. Thus, the damage strain decreases with the increase of Mises stress. In addition, matrix material is easier to be removed and plastic deformation of the machined surface is reduced which leads to a smooth surface generation. Figure 4-10 shows the cutting stress on the MMCs cutting region vs time point at varied cutting speed. Figure 4-11 further shows the stress value on matrix material and reinforced particles. According to the stress curve, it can be found that machined surface roughness is smaller and surface quality is higher when machining with a higher cutting speed. Moreover, the larger strain rate results in the larger yield strength and failure stress, which means the material on the remained surface is more difficult to be removed. Thus, the stress acts on the matrix material increases when the cutting speed increases. As a result, the stresses that transfer to the bonding interface and uncut particles are larger as well. For the brittle particles, the stress does not state significant difference at varied cutting speed. This indicates that particles are fractured with similar cracks generated. However, when machining with higher cutting speed, the cracks have less time to transfer or further process into larger cavities due to the reduced tool-particle interaction time. Conversely, the particles deformation failure strain is larger which leads to more time for cracks growing when machining with a low cutting speed. The generated cracks extend and further link together into big cavities. Thus, machined surface quality is higher under higher cutting speed condition.

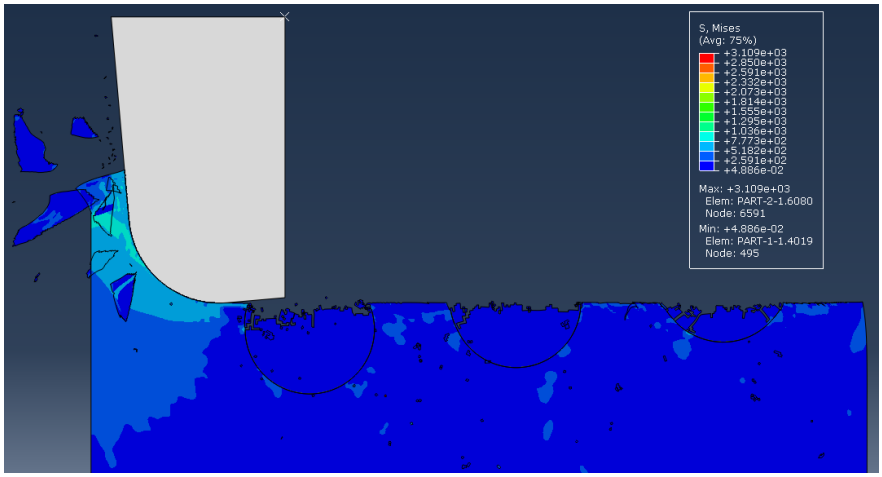

(a) Cutting speed: 157.0m/min

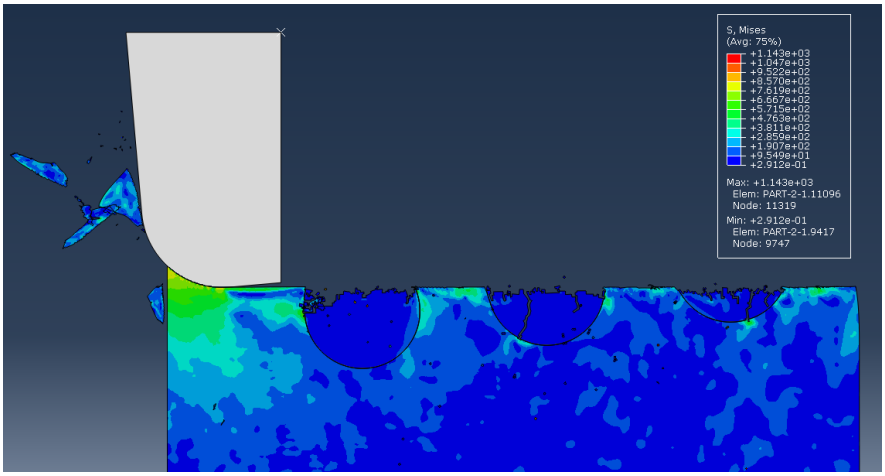

(b) Cutting speed: 125.7m/min

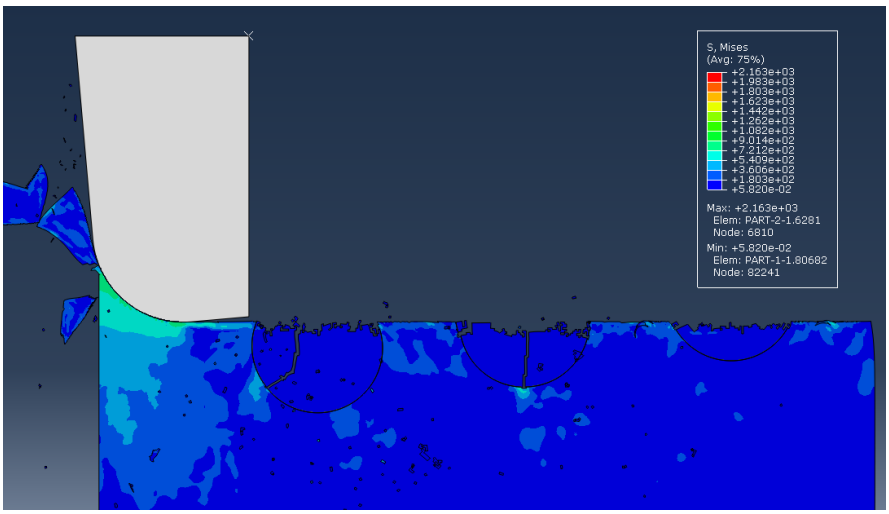

(c) Cutting speed: 94.2m/min

Figure 4-9 Surface performances at varied cutting speed

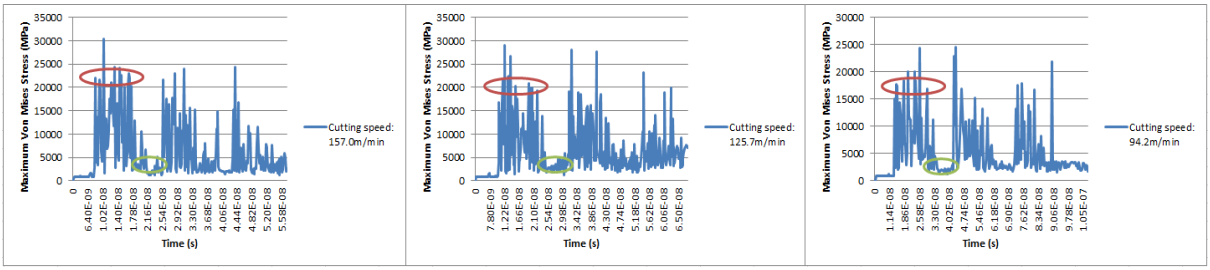

Figure 4-10 Cutting stress on the cutting region vs time point of the cutting region at varied cutting speed (Green: Matrix material breakage; Red: Particle fracture)

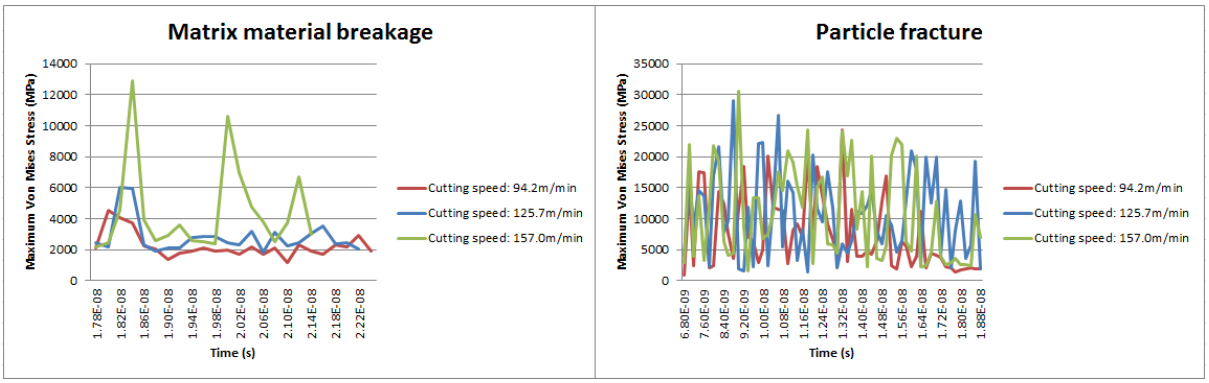

Figure 4-11 Influence of cutting speed on cutting stress

(2) Influence of depth of cut: Due to the uniform distribution of particles, the particles locations on each cutting line are almost the same. Thus, the interaction and the attach area between tool and particles can be seen as the same on each cutting line. In addition, the estimated minimum chip thickness is 0.525 μm in this case [118]. Thus, chips can be formed under these selected depths of cut. The influence of depth of cut on the machined surface performance in this simulation is shown in Figure 4-12. From the simulation results, it can be observed that surface roughness is not significantly affected by the DOC. Only slightly increase on surface roughness occurs when machining with larger DOC. Thus, the DOC is not dominating to the surface performance, while a better surface quality can be obtained by reducing the DOC in MMCs precision machining.

As a result, cutting speed and DOC are dominate on chip formation, material removal and surface roughness in multiphysics based integrated approach to modelling and simulation in MMCs precision machining processes. Considering the most prominent factors, matrix material breakage, particles fracture and surface generation are varied under different cutting conditions. The simulation results indicate that surface roughness can be reduced and surface quality can be enhanced under smaller depth of cut and a

higher cutting speed in MMCs micro turning process. These are further evaluated and validated through well-designed experiments shown as below.

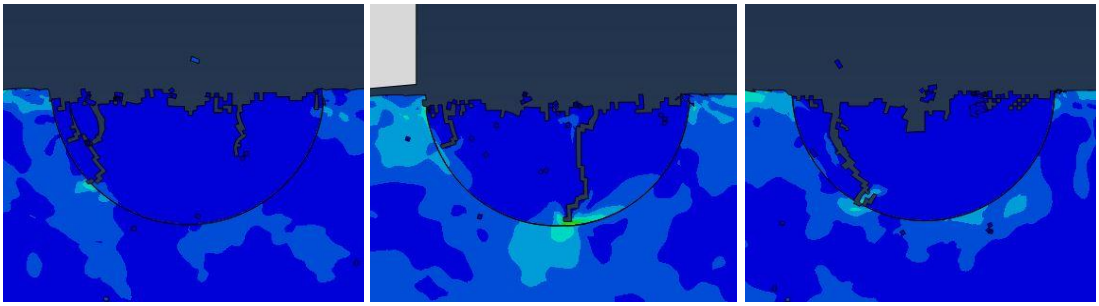

(a) DOC: 1 μm (b) DOC: 2.5 μm (c) DOC: 4 μm

Figure 4-12 Influence of depth of cut on surface performance

4.4 Experimental validation of chip formation mechanisms in MMCs precision machining

The validation of predicted chip formation mechanisms including MMCs minimum chip thickness, matrix material breakage, particles fracture and their interfacial reaction in MMCs precision machining are conducted on ultra-precision turning machine. The well-designed experimental trials are performed under the cutting parameters and experimental conditions that are set the same as those applied in the theoretical analysis and simulations. The measurement on the machined surface profile and surface roughness can be achieved accurately under the help of high precision measurement instrument. The verified results can be further utilized on the accurate prediction of chip formation and dynamic cutting force in precision machining of particulate MMCs.

4.4.1 Design of experiments

4.4.1.1 Experimental set-up

A series of machining trials for evaluating and validating the simulation results are carried out on MOORE Nanotech 250 UPL ultra-precision turning machine. The schematic of PCD inserts is shown in Figure 4-13 (a) and these tools with detailed parameters are performed in the experiments. The PCD tool with a cutting edge radius of 3.4279 μm and a nose radius of 1.200 mm is measured by Scanning Electronic Microscope (SEM). The rake angle and clearance angle for the inserts are both 0^o, while the whole tooling system shown in Figure 4-13 (b) has a 5^o negative rake angle and 5^o

clearance angle due to the geometry of tool holder. Experiments are performed on the basal plane of cylindrical Al2024/50B_4C_p workpiece with a diameter of 50 mm under various cutting conditions. The average grain size of particle is 5 µm and volume fraction is 50%. The cylinder workpiece is chunked on the spindle and tooling system is mounted on the work-plate slide. The entire experimental set-up is shown in Figure 4-13 (b).

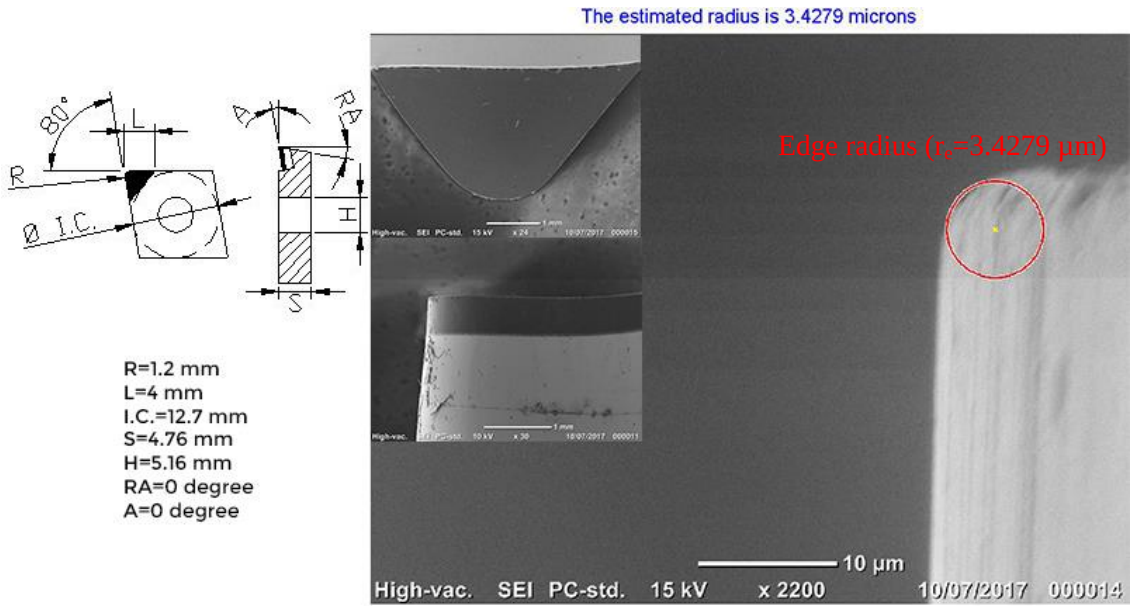

(a) Cutting tool conditions

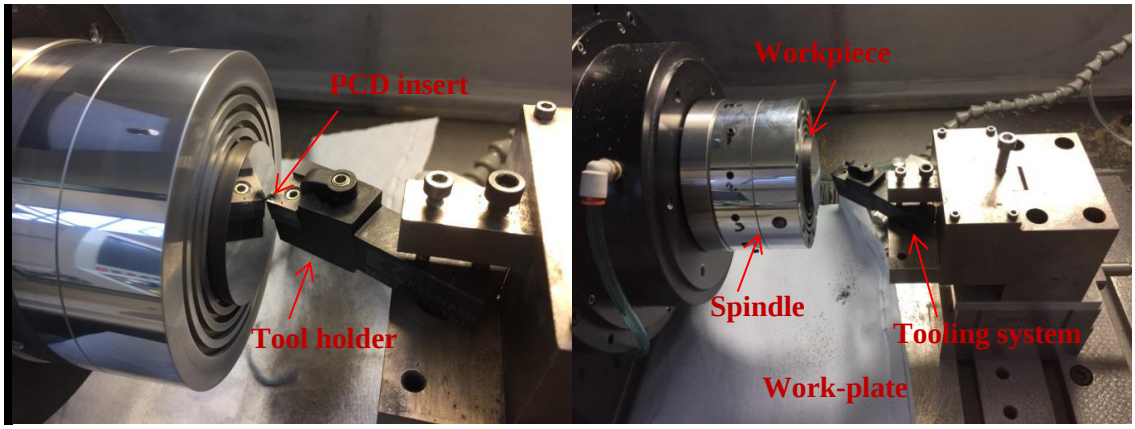

(b) Experimental set-up

Figure 4-13 Experimental set-up for precision machining of MMCs

4.4.1.2 Experimental procedures

For the minimum chip thickness experimental validation, machining trials are conducted on the pre-machined workpiece in order to find the datum surface and also control the surface performance. Due to the extremely large value of cutting tool nose radius compared to the depth of cut, the cutting edge adopted can be observed as a straight line. Thus, the tool wear during the minimum chip thickness experiments is negligible and can be ignored in the cutting trails. The cutting parameters are shown in Table 4-5. Varied depths of cut are adopted in order to determine the actual minimum chip thickness. Different cutting speeds are also carried out in order to determine their effects on the MCT. The machined surfaces with grooves in different sizes are measured on Zygo white light interferometer to determine the machined surface profile and chip formation conditions.

Table 4-5 Cutting parameters in minimum chip thickness cutting trials

Tool material	PCD turning insert		
Workpiece material	B_4C/Al MMCs		
Cutting speed	2.5 m/s	2 m/s	1.5 m/s
Depth of cut	0.20/0.30/0.40/0.50/0.60/0.70/0.80 μm		

For the validation of chip formation mechanisms, the adopted cutting parameters in the experimental approach are configured same as those utilized in the simulations. These varied cutting parameters shown in Table 4-6 are performed to determine the effects of process variables on the machined surface roughness. The full factorial experimental trials are conducted under various cutting parameters. The experimental results are assumed to compare with the simulation results. All the experimental trails are conducted under dry cutting condition, only air below is applied. The machined surface roughness, surface profile and topographical features are measured by ZYGO New View 5000 white light interferometer with excellent precision and accuracy.

Table 4-6 Cutting parameters used in micro turning experiments

Spindle speed (RPM)	1,000/800/600
Cutting speed (m/min)	157.0/125.7/94.2
Depth of cut (μm)	1/2.5/4
Feed rate (μm/rev)	10/20/30

4.4.2 Results, analysis and discussion

4.4.2.1 Minimum chip thickness determination in MMCs precision machining

The metrology measurement results on the machined surfaces at various depth of cut are shown in Appendix 5. Due to the initial pre-machined surface of MMCs workpiece is coarse and the surface roughness is still relatively much higher than machined homogeneous material, the actual depth of cut is then defined as the difference between peak point and valley point at the machined surface range. Thus, the PV values around cutting area in the surface roughness figures are determined as the realistic depth of cut. Each groove depth value is the average value from 5 measurements along the cutting path. Table 4-7 shows the average value of actual depth of machined grooves at varied DOC value that below or above the predicted MCT. It can be observed that the PV value is much smaller than the DOC in machining process when the DOC is smaller than 0.6 μm; However, when the actual DOC is equal to 0.6 μm or larger than 0.6 μm, the measured PV value is similar to the DOC value. This indicates that when DOC reaches 0.6 μm, the MMCs material including the matrix material and reinforced particles starts to be removed. Thus, the minimum chip thickness for precision machining of this particle reinforced MMCs is around 0.6 μm, which shows a good agreement with the theoretical prediction results. This modified MCT model can be used to determine actual MCT in MMCs precision machining process.

Table 4-7 Average value of actual depth of machined grooves and specific cutting force

Depth of cut (μm)	0.2	0.3	0.4	0.5	0.6	0.7	0.8
Actual depth of cut (μm)	0.167	0.272	0.279	0.331	0.590	0.688	0.796

Figure 4-14 and Table 4-8 illustrate the specific cutting energy against varied DOC obtained from experiments in MMCs precision machining. In order to achieve the accurate specific cutting force curve, DOC of 1 μm, 2 μm and 4 μm are further applied and specific cutting force values are measured in the experiment. According to this non-linear curve of specific cutting force at unit area, the dominate size effect that leads to a transitional regimes associated with intermittent shearing and ploughing can be observed. Under the condition of DOC smaller than 0.4 μm, the value of specific cutting energy is higher while decrease dramatically along the increase of DOC. This attributes

to the workpiece material undergo the elastic deformation and material will fully recover to its original position. The specific cutting energy will further experience a slightly decrease with the continue increase of DOC up to 0.6 µm. In this area, material undergoes plastic deformation, while keep ploughing without chip formation. Only when the feed rate excesses the critical minimum chip thickness value which is estimated as 0.6 µm, the specific cutting energy transits to a stable value which means MMCs material experiences plastically deformation represents by shearing and chip formation starts.

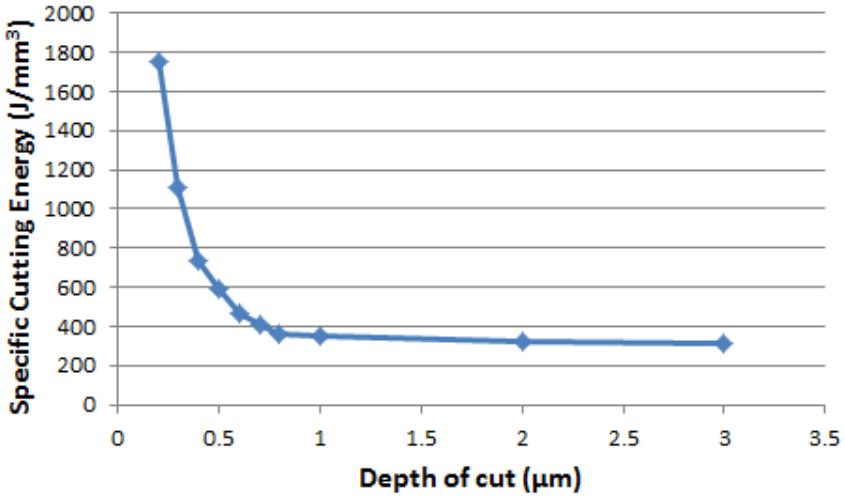

Figure 4-14 Specific cutting force at varied DOC

Table 4-8 Specific cutting energy at varied DOC

DOC (µm)	0.2	0.3	0.4	0.5	0.6
Specific cutting energy (J/mm^3)	1750	1110	733	589	464
DOC (µm)	0.7	0.8	1.0	2.0	4.0
Specific cutting energy (J/mm^3)	407	359	351	325	312

The MCT can be estimated via the above experimental analysis. On the other hand, the MCT for matrix material has been identified via simulation [118]. The perfectly matched results indicate that minimum chip thickness is equal to 14-17 % of cutting tool edge radius. In this case, the minimum chip thickness for Aluminium matrix is around 0.525 µm. The estimated MCT for MMCs material is 0.594 µm as shown in section, thus, the elastic recovery zone for particles can be observed as 0.069 µm.

Influence of cutting speed on MCT: Figures in Appendix 5 and Table 4-9 show the measurement depth of machined groove under the cutting speed of 157.0m/min, 125.7 m/min and 94.2 m/min respectively. The measurement results indicates that the real cutting depth is around 0.27-0.29 μm at 3 different cutting speeds when the DOC is 0.4 μm; the real cutting depth is around 0.59-0.60 μm at 3 different cutting speeds when the DOC is 0.6 μm. This indicates that the MMCs material is not totally removed and only matrix material sheared when the DOC is 0.4 μm. While the matrix and particle are removed together along the shearing line when the DOC excessed the MCT and the measured actual depth of groove value is close to the DOC. The verified MCT value at varied cutting speed is almost the same, which can be concluded that the effects of cutting speed on the MCT is negligible and can be ignored. The experimental results are clearly in alignment with the simulation results and significantly illustrate the relationship between MCT and cutting speed.

Table 4-9 MCT value at varied cutting speed

Depth of cut (μm)	0.4			0.6		
Cutting speed (m/min)	157.0	125.7	94.2	157.0	125.7	94.2
Actual depth of cut (μm)	0.272	0.289	0.285	0.590	0.594	0.592

4.4.2.2 Chip formation and morphology in MMCs precision machining

(1) Chip formation in multiphysics based simulation

Stagnation region of chip formation in precision machining of particulate MMCs by using PCD tool is shown in Figure 4-15. The stagnation point in this simulation can be defined as the point that divided the material displacement distribution in Y direction into positive value and negative value. Stagnation region is observed as a specific region that determines the material deformation orientation, real depth of cut and actual uncut chip thickness.

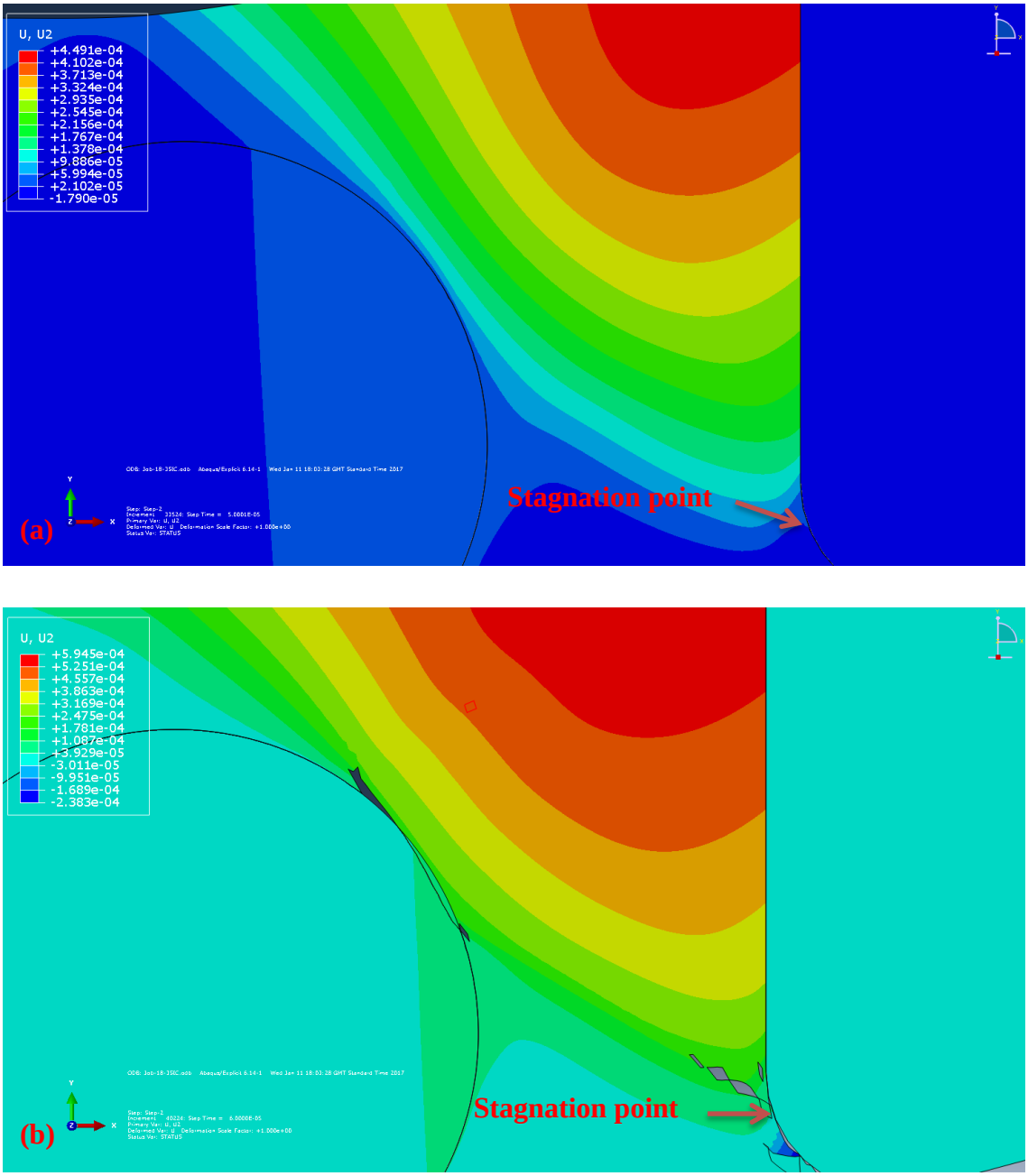

Figure 4-15 Stagnation region of chip formation in precision machining of MMCs

During the chip formation process, material separates at the stagnation point and splits upwards and downwards respectively. The material region with positive displacement value will move upwards, splits from the workpiece and further form the chips; whereas the material region with negative displacement value will move downwards, experience the flow along the cutting edge close to tool flank face and finally form the machined surface. The chip formation in the simulation is shown in Figure 4-16. It can be observed that the MMCs chips are formed with around 5 μm in length. Light waviness, saw-tooth profile and even large cracks can be seen on the outer surface of chips. Some

extremely small particle segments are also generated. These are evaluate and validated via precision machining experimental work as below.

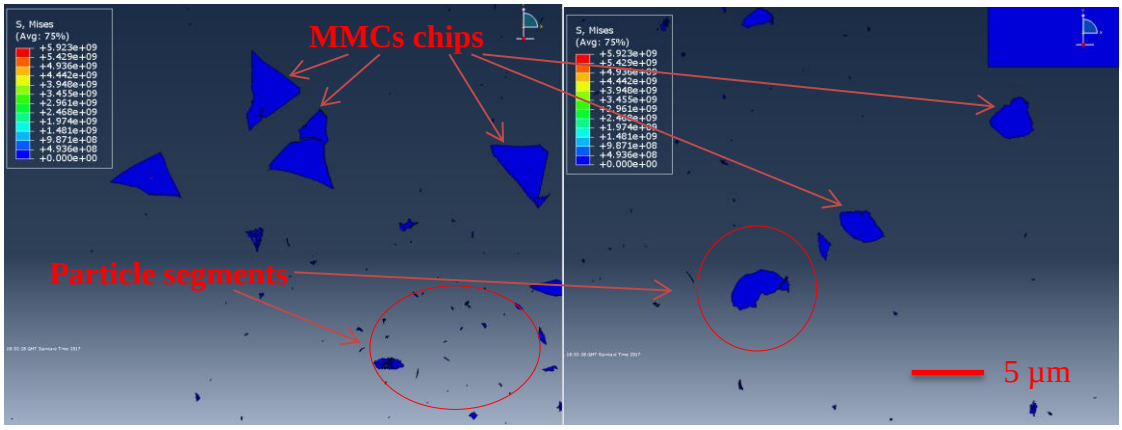

Figure 4-16 Chip formation and chip morphology in simulation

(2) Experimental results of chip formation and chip morphology

In precision turning experiments, the chips produced are collected and measured by TESA as shown in Figure 4-17. Short curled chips can be identified in each cutting cycle, which means the chips are formed discontinued. This occurs due to the chip formation of MMCs is considered as the combined fracture/rupture/crumbling process. In addition, the coarser reinforced particles are further acted as a chip breaker, which produces both segmented and small curled chips. On the other hand, initiation of gross fracture occurs at the material free surface and chip inner surface toward the cutting edge direction and the remaining portion of material on the shear plane are removed by flow-type deformation which formed small segmented chips as well. From the microstructural analysis on the SEM images, the inner surface of chip performs ribbon form topography due to the material shearing in chip formation process; while the outer surface of chip exhibits a relative smooth morphology with small texture along the cutting direction due to the rake face texture of PCD tool and tool-chip interfacial friction. In addition, a significant variation ranging from prominent saw-tooth profile to light waviness is commonly featured on the chip outer surface with the orientation vertical to the cutting direction. This attributes to the existence of reinforced particles which are located along the cutting line.

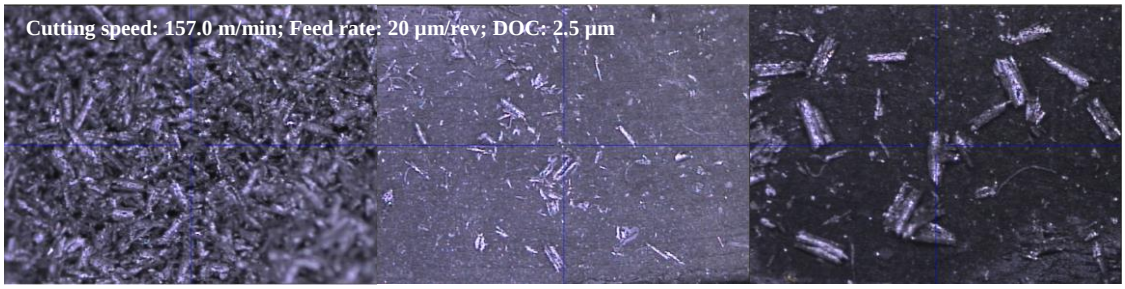

Figure 4-17 Chip formation characteristics in MMCs precision machining

For the machining process under varied cutting speed, the overall chip length is also observed varied as shown in Figure 4-18. Needle type chips with small segments are formed at lower cutting speed, whereas semi-continuous, scrambled ribbon and tubular helix chips are formed accompanied with the relative rougher outer surface at higher cutting speed. In addition, ductile tearing of chips occurs with the increase of cutting speed. However, no distinct variation on chip thickness performs under varied cutting speed. When machining with varied feed rate, the chip width is varied. In addition, chip thickness is varied under different depth of cut. However, only segmented chips with small chip length can be observed at higher feed rate and larger depth of cut. This is due to the matrix material plastic deformation results in the voids and cracks, and these voids and cracks surrounding the reinforced particles join up which further leads to the chip segmentation when increasing the feed rate and depth of cut. The real chip thickness is slightly larger than the feed rate due to the material deformation leads to the chips become shorter and chip thickness are therefore increased consequently. In micro milling experiments, chips perform a systematic breaking pattern depending upon the volume fraction of reinforcement.

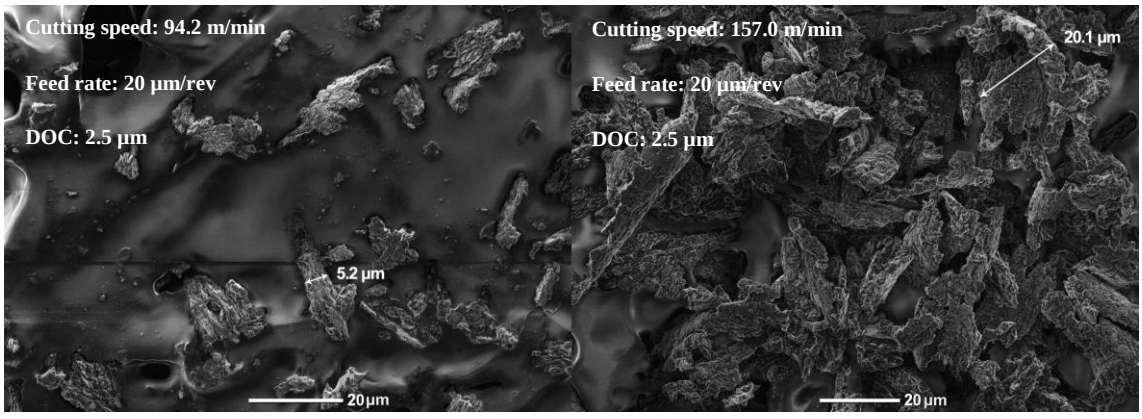

(a) Chip formation under varied cutting speed

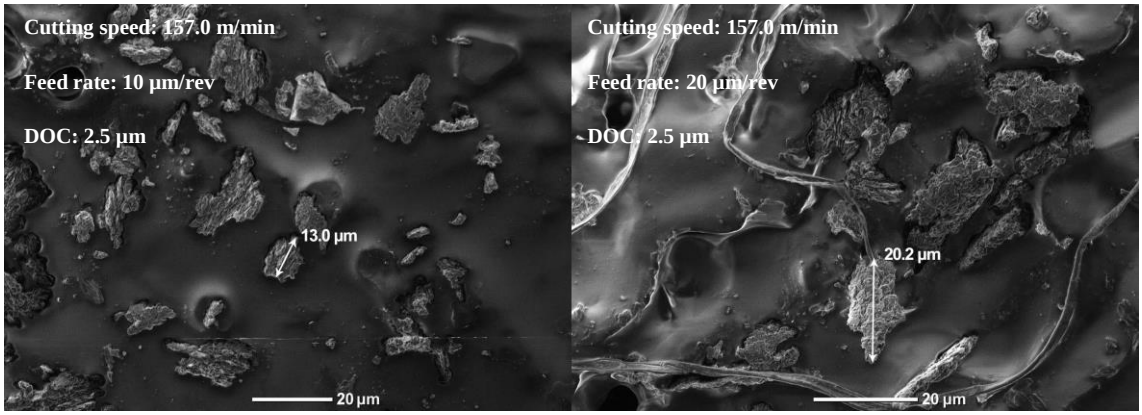

(b) Chip formation under varied feed rate

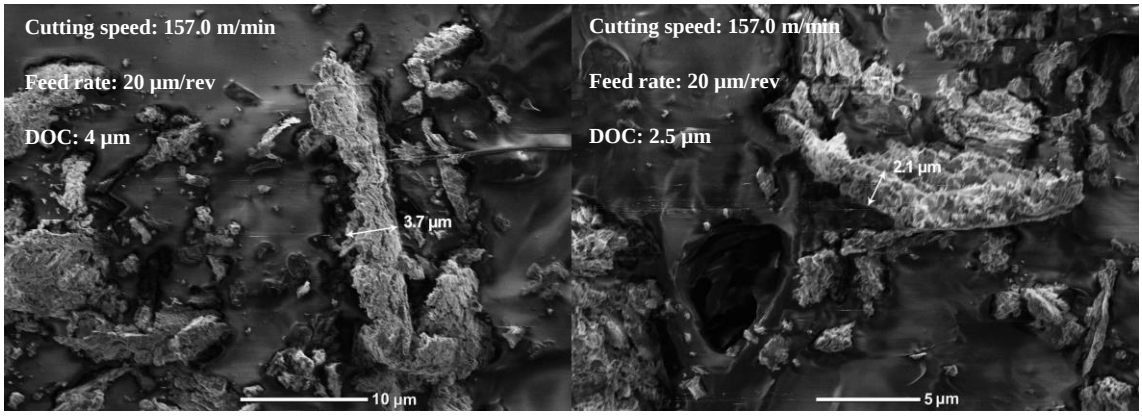

(c) Chip formation under varied depth of cut

Figure 4-18 MMCs chip formation under varied cutting parameters

4.4.2.3 Machined surface

Table 4-11 illustrates the orthogonal array of cutting parameters in the experiments and resultant surface roughness at varied cutting conditions. 3D arithmetic mean roughness is applied for the surface roughness measurement in order to better illustrate the performance of machined surfaces. From Table 4-10, it can be clearly observed that surface roughness values decrease with the decrease of feed rate when the actual feed rate is larger than minimum chip thickness. In addition, the surface roughness has a significant increase when cutting with larger cutting speed. Moreover, the best surface can be achieved when the depth of cut is same as or close to the radius of reinforced particles. The effects of these cutting parameters on surface integrity are illustrated in details in the following parts.

Table 4-10 Orthogonal array of cutting parameters and resultant surface roughness

Experimental number	Cutting speed (m/min)	Feed rate (μm/rev)	Depth of cut (μm)	Surface roughness (nm)
1	157.0	30	4	132
2	157.0	30	2.5	102
3	157.0	30	1	105
4	157.0	20	4	126
5	157.0	20	2.5	99
6	157.0	20	1	90
7	157.0	10	4	90
8	157.0	10	2.5	71
9	157.0	10	1	86
10	125.7	30	4	136
11	125.7	30	2.5	134
12	125.7	30	1	106
13	125.7	20	4	135
14	125.7	20	2.5	109
15	125.7	20	1	113
16	125.7	10	4	97
17	125.7	10	2.5	90
18	125.7	10	1	99
19	94.2	30	4	148
20	94.2	30	2.5	135
21	94.2	30	1	136
22	94.2	20	4	132
23	94.2	20	2.5	117
24	94.2	20	1	136
25	94.2	10	4	113
26	94.2	10	2.5	99
27	94.2	10	1	129

Figure 4-19 and Figure 4-20 illustrate the resultant surface roughness at varied depth of cut. When DOC is larger than MCT, the machined surface roughness slightly decreases until DOC reaches to the value that similar to the particle radius. This is due to the pre-machining process that significantly affects the micro structure of MMCs. The fracture of particles gradually change from the scenario of particles centre are located below the cutting line to the scenario of particles centre are located on the cutting line. With continue steady increase of DOC, the surface roughness increase significantly. With the further increases of DOC, the force, stress friction and temperature increase. Then the deposition of workpiece material results in higher surface roughness. In addition, when cutting with larger DOC, the stress generated on the matrix material may exceed the bonding stress. As a result, particles are much easier de-bonding and pulled out. The higher strain at un-cut area means the particles are preferred removing together with the matrix material instead of being cut through. These result in the large amounts of pits and cracks on the remained surface. Thus, the best surface quality can be achieved when the depth of cut is close to the radius of reinforced particles. This states a good agreement with the simulation results in the scenario of the particle centre is located on the cutting line.

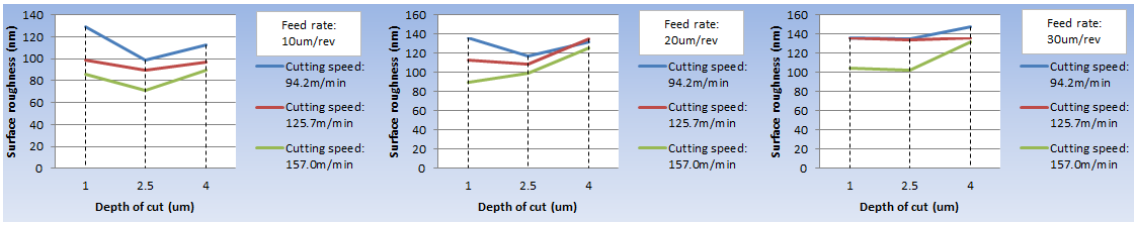

Figure 4-19 Surface roughness vs Depth of cut

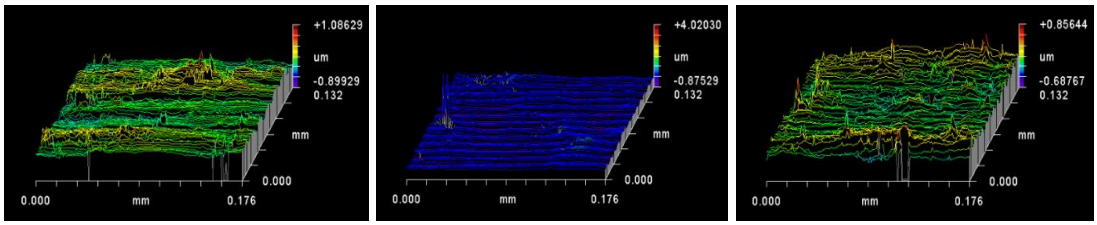

(a) DOC: 1 µm (b) DOC: 2.5 µm (c) DOC: 4 µm

Figure 4-20 Surface roughness at varied DOC (Cutting speed: 125.7 m/min, Feed rate: 10 µm/rev)

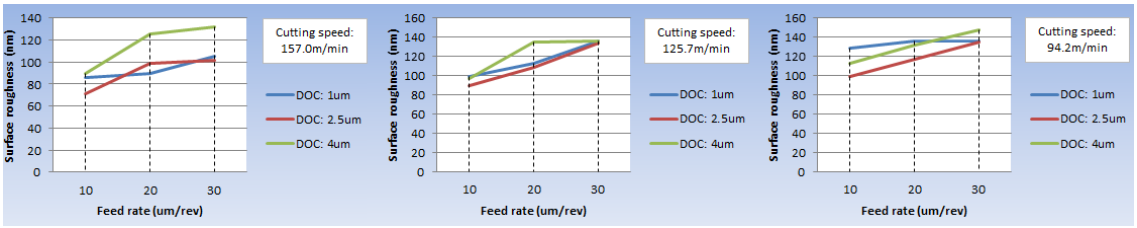

Figure 4-21 Surface roughness vs Feed rate

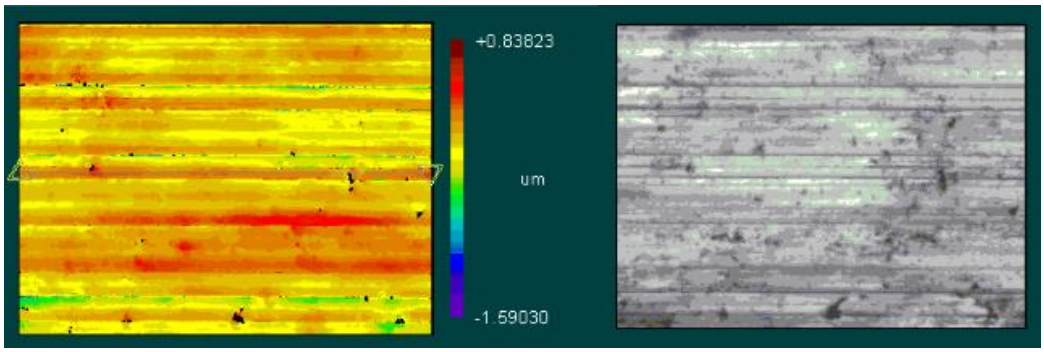

(a) Feed rate: 10 µm/rev

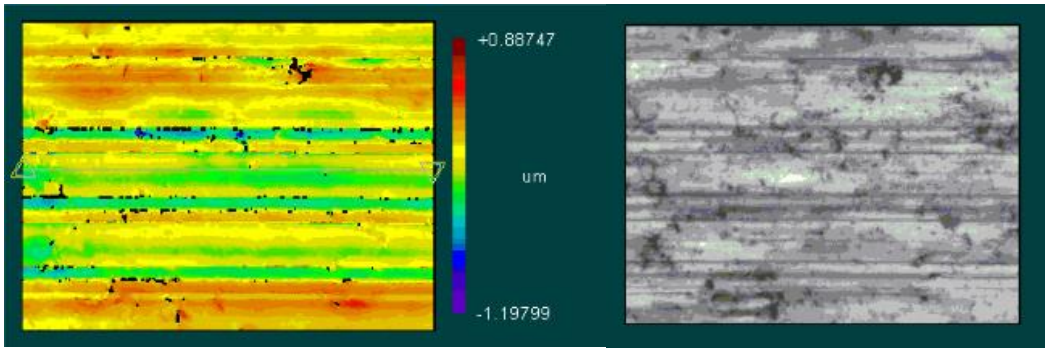

(b) Feed rate: 20 µm/rev

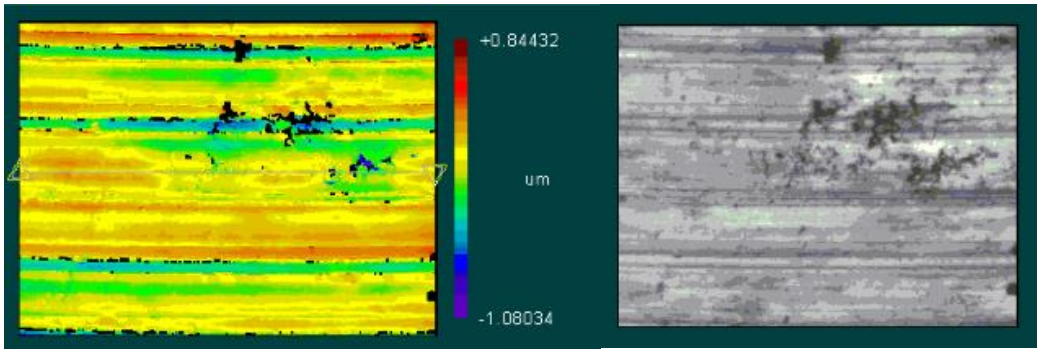

(c) Feed rate: 30 µm/rev

Figure 4-22 Surface roughness at varied feed rate (Cutting speed: 94.2 m/min, DOC: 4 µm)

The machined surface roughness and surface texture at varied feed rate are shown in Figure 4-21 and Figure 4-22 respectively. It can be observed that the surface roughness increase with the increase of feed rate and tool marks are becoming much more significant. The peaks on the remained surfaces are higher when cutting with larger feed rate and surface roughness is then become larger. This is perfectly matched with the simulation results.

The surface roughness and surface profiles along the tool paths and tool marks are also demonstrated in Figure 4-23. From the surface profile figures, it can be seen that larger cracks and defects area occur when cutting with a smaller cutting speed. The large cavity area is significant, this can be attributed to the particles are pulled out or even badly fracture on the matrix material which leads to various particles are removed together and leave a large cavity. While, the larger cracks and defects will be replaced by small ones when increase the cutting speed. In addition, large cavities will be replaced by few cracks due to the brittle fracture occurs on particles rather than matrix material breakage or particles pulled out. The machined surface becomes smoother and surface quality is higher when cutting with a larger cutting speed. Figure 4-24 shows that less cracks and cavities are generated along the cutting direction when machining with higher cutting speed. The detailed surface profile illustrates the surface roughness decreases with the increase of cutting speed. This can be assumed that particle fracture condition is dominated to the surface roughness and the particles are performed as perfectly cut through rather than pull out and leave smaller cracks or cavities at higher cutting speed. This is highly agreed with the simulation results in MMCs precision machining.

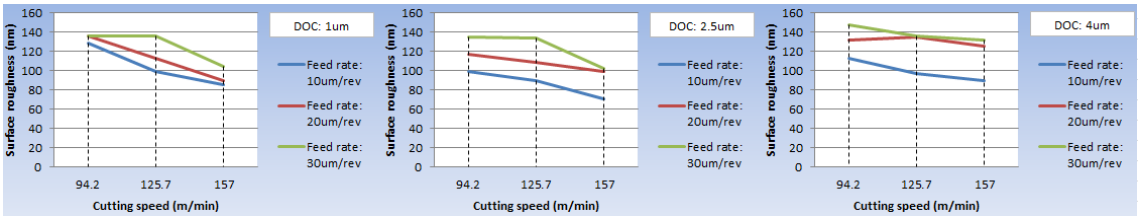

Figure 4-23 Surface roughness vs Cutting speed

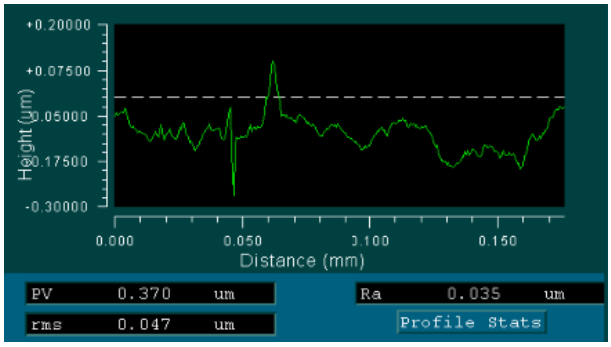

(a) Cutting speed: 157.0 m/min

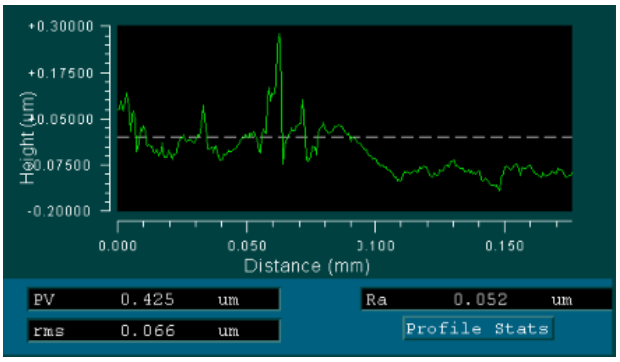

(b) Cutting speed: 125.7 m/min

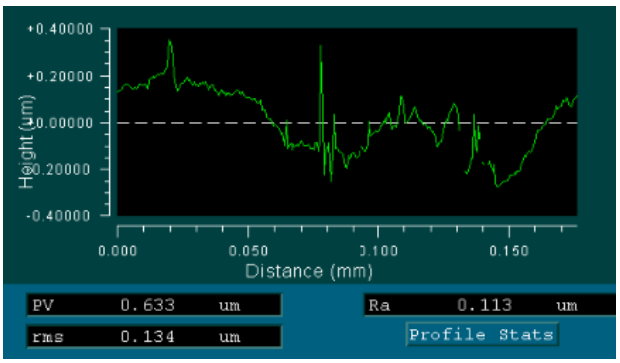

(c) Cutting speed: 94.2m/min

Figure 4-24 Surface roughness at varied cutting speed (Feed rate: 10 µm/rev, DOC: 1 µm)

Tool marks and surface waviness can be significantly observed on the machined surface as shown in the measurement results. This can be attributed to the existence of the micro hard particles. With the cutting tool shearing through the soft aluminium matrix and engaged on the hard particles, the suddenly increased stress and force result in the tool variation at the bonding interface. This increases the waviness and leave tool marks

on the remained surface. These surface waviness and tool marks finally result in the increase of surface roughness. During cutting on hard particles, the alternative stress change leads to the cutting tool variation. Cutting tool keeps rubbing on the machined surface and leaves more pits and cracks on the particles. After the tool cutting through the hard particles and engaged back into the soft aluminium matrix, stress and force on the cutting tool are suddenly released. The stress of this high stiffness machining system suddenly relax and leads to the waviness of cutting tool which leaves significant tool marks and surface waviness, and reduces the surface quality. Thus, the surface roughness and surface defects at the bonding area along the cutting line are larger than any other areas. In addition, due to the high volume fraction of reinforced particles, the stress changes alternatively in high frequency. The resultant fluctuation of the cutting force increases the vibration in the cutting system also reduces the surface quality and the machining form accuracy. The dislocation and cracking of particles and also the interface de-bonding will damage the subsurface of MMCs which results in the reduction of the surface integrity. Therefore, the selection of optimal process variables is of great importance to obtain better surface quality in MMCs precision machining, which is consistent with the research results in precision machining of other difficult-to-machine engineering materials [17].

4.5 Concluding remarks

This chapter presents the characterisation of machining metal matrix composites on various aspects. Theoretical analysis, simulations and experiments are carried out to investigate the minimum chip thickness and chip formation mechanisms of MMCs via an integrated approach. The research achievements are concluded substantially as below.

From the theoretical results and experimental results, it can be observed that the MCT can be accurately predicted using the mathematical equation by considering the tool edge radius and particle radius. This minimum chip thickness model demonstrates that the chip can be formed even when the tool radius is larger than the depth of cut. While, due to the existence of particles, the chip formation mechanism is much more complex and the minimum chip thickness in MMCs machining is highly relevant to the edge radius, particle size and the tool-workpiece interaction. In addition, the effect of cutting speed on the MCT is negligible for MCT prediction.

For the MMCs chip formation mechanisms, a simulation-experiment based approach to is presented, which aims to develop the scientific understanding of the process mechanics and the consequent process optimisation strategy, and furthermore the new protocol for the MMC material design and fabrication with much improved material machinability. The detailed conclusions can be drawn as follows:

1. Chip formation mechanics include the matrix breakage and particle fracture/de-bonding/dislocation in precision machining of particle reinforced MMCs is strongly depending on the location of particles against the position of cutting tool tip. Plastic and elastic deformations at the matrix material occur and chips are generated along the cutting line accompanied with the matrix/particle interfacial boundary de-bonding/defects in these three scenarios.
2. In the scenario of the particle centre located below the cutting line, small cracks are formed on the machined particles. Almost all of the cracks are generated towards lower direction of the un-machined particle area when cutting through the particles. Cavities, particularly at the particle/matrix interfacial area, can be observed, while more cracks can be observed at the tool approaching out area.
3. In the scenario of the particle centre located on the cutting line, cracks are generated towards cutting direction of the un-machined particles. This indicates that the particles break along the cutting line with fewer cracks formed on the tool path and finally leaves a much smoother surface with few defects.
4. In the scenario of the particle centre located over the cutting line, small cracks are formed on the machined particles. Cracks are generated towards both upper and lower direction of the un-machined particle area during machining. The cavities, particularly at the particle/matrix interfacial area, can be found. In addition, more cracks occur at the approaching in side of fractured particles.
5. Simulation results reveal that cutting speed, feed rate and depth of cut are the critical factors affecting the material removal and resultant surface roughness. Smaller surface roughness and better surface quality can be achieved by precision machining with higher cutting speed, smaller feed rate and appropriate small depth of cut.
6. The well-designed machining trials for evaluating and validating the simulation results indicate that the optimal cutting parameters for precision machining of MMCs are found under the higher cutting speed, the DOC close to the reinforced

particle radius and the appropriate lower feed rate. These perform a good agreement with simulation results. The process optimisation and the associated optimisation strategy are of great importance to obtain a higher machinability of MMCs.

Chapter 5 Dynamic cutting force modelling in precision machining of MMCs

5.1 Introduction

In MMCs precision machining process, cutting force significantly reflects the cutting phenomenon including size effect, minimum chip thickness effect, chip formation, cutting temperature and tool wear etc. Thus, cutting force in MMCs machining is observed of great importance to analyse the cutting mechanics, machinability and its further optimisation. On the other hand, the scaled-down cutting parameters enlarge the errors generated by the machine tools, cutting tools and micro cutting process variables and significantly affect the machining performance including form accuracy, surface roughness and tool life. These errors normally generated due to the size effect, tool and workpiece deflection, dynamic runout, tool wear, cutting friction and chatter vibration. Considering these errors, dynamic cutting force is considered as the major factor in MMCs machining optimisation. Thus, in order to reduce the error, an improved dynamic cutting force model is critical to illustrate the tool-workpiece interaction and accurately predict the cutting force on the high precision level. The cutting force modelling and its application in interpreting the machining process have been extensively researched and developed based on theoretical assumptions and experimental observations [110-117]. With the better understanding on the cutting mechanisms of particle reinforced heterogeneous materials and also the improvement of MMCs cutting force models, substantial progress have been achieved in MMCs machining. There is however a lack in investigating the machining phenomenon for particle reinforced heterogeneous materials and explicit modelling the resultant cutting forces. The current force models are still not considered the 3-dimensional milling processes with continued-changed chip formation, the real chip formation conditions and also their significant effects on the dynamic cutting force comprehensively.

This chapter presents an improved dynamic cutting force model based on the basic micro cutting theories and the improved cutting dynamics, which includes the size effect of cutting tool geometries, un-deformed chip thickness effects and also the influence of micro cutting process variables under various cutting conditions. The multiscale based improved dynamic cutting force model is proposed in order to have a

better understanding on the MMCs cutting mechanics and predict the cutting force accurately. A novel instantaneous uncut chip thickness algorithm including actual chip thickness and real tool trajectory is developed by taking the tool runout into consideration. The behaviours of the particle reinforcements are modelled and analysed in three cutting regimes including elastic recovery zone, ploughing zone and shearing zone. Cutting process variables, material volume fraction and particle size are explicitly taken into account in this innovative force model. In order to compensate the dynamic distortion of the measured cutting force, the Kalman Filter is performed. Well-designed cutting trials are carried out at different cutting parameters in order to validate the force model. This proposed force model is further applied to analysis the MMCs micro cutting tool wear, energy consumption and surface generation aspects.

5.2 Dynamic cutting force modelling

A three dimensional force model is proposed to predict the actual cutting forces in particle reinforced metal matrix composites micro milling process. This analytical force model is developed and modified through multiscale analysis approach. The size effects and multiscale aspects including the tool edge radius, particle size and cutting parameters as the main factors are involved in this analytical approach. The critical variables such as tool geometry, volume fraction of particles, tool properties and workpiece material properties are also explicitly taken into account. The cutting process is divided into three continued process: elastic recovery, ploughing and shearing. These three cutting zones are illustrated in Figure 5-1 below.

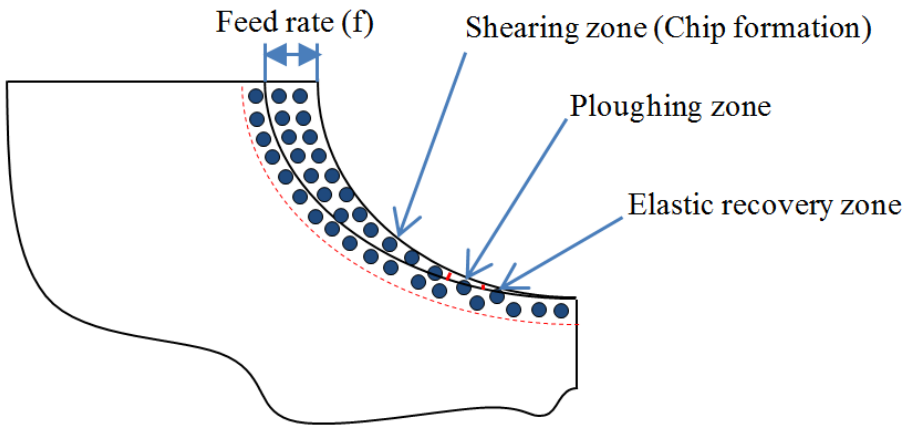

Figure 5-1 Three cutting zones in MMCs micro milling process

From the previous research and the force regions shown in Figure 5-1, it can be obtained that the cutting forces acting on the cutting tool are mainly dependent on the un-deformed chip thickness. In particulate MMCs micro milling process, the tangential force Ft, radial force Fc and axial force Fa are modified according to the actual chip formation and the associated process variables.

5.2.1 Cutting force in elastic recovery region

In the elastic recovery zone of micro milling process, the displacement of matrix material and the reinforced particles occurs when the tool contacts on the workpiece. The elastically deformed particles then recover to their original positions along with the matrix material. This elastic recovery process is shown in Figure 5-2.

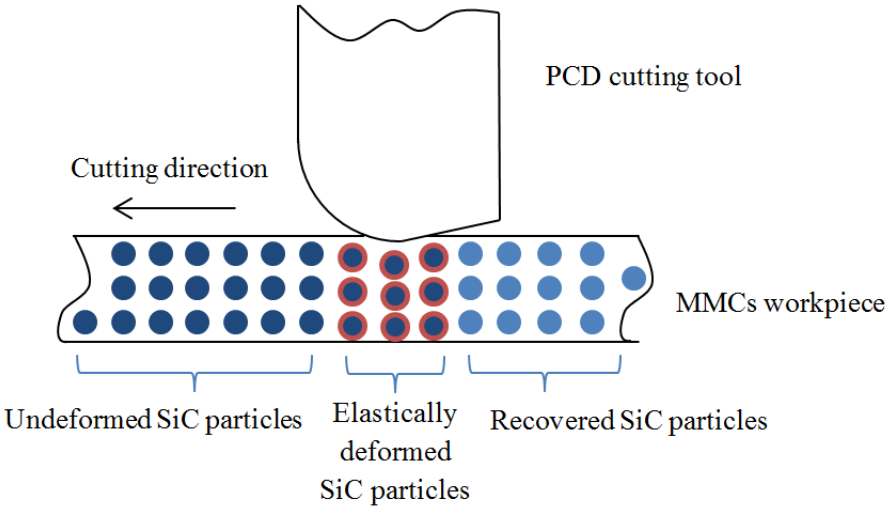

Figure 5-2 Particles displacement in elastic recovery zone

The tangential force, radial force and axial force in orthogonal cutting are formulated and shown as below:

$$dF_t = k_{te} * t_c * dz$$

$$dF_c = k_{ce} * t_c * dz \quad (5.1)$$

$$dF_a = k_{ae} * t_c * dz$$

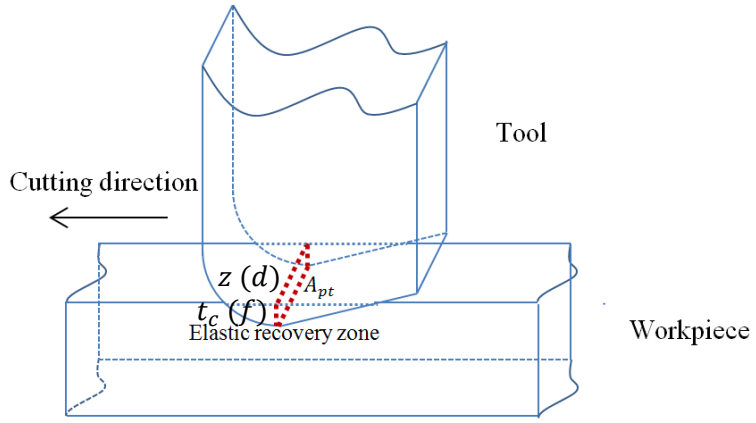

(a) Elastic recovery area A_{pt} in feed direction

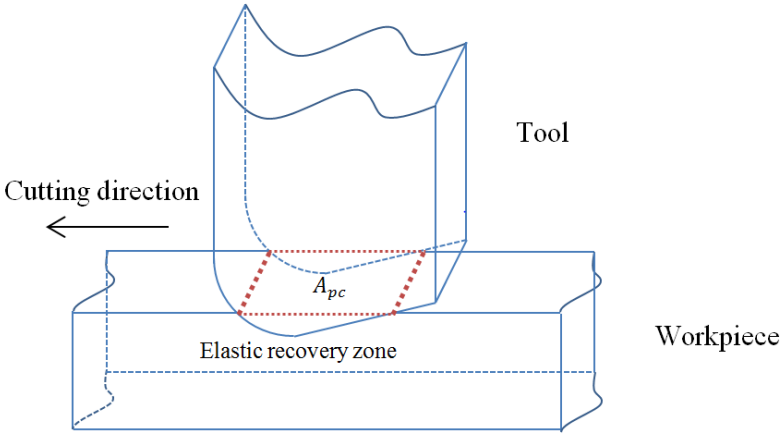

(b) Elastic recovery area A_{pc} in radial direction

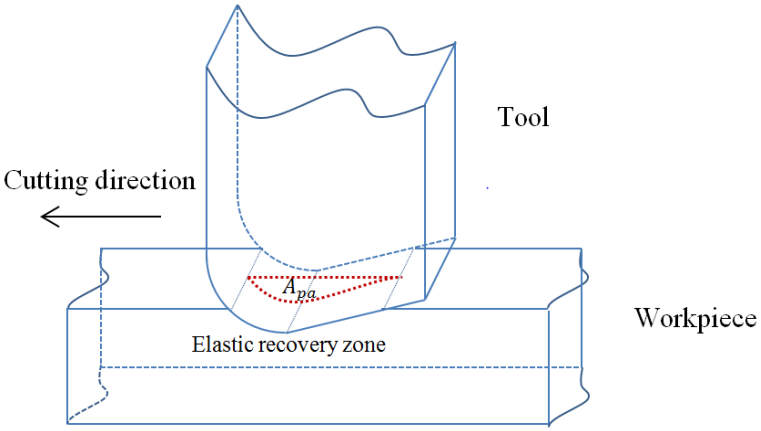

(c) Elastic recovery area A_{pa} in axial direction

Figure 5-3 Elastic recovery areas in three directions

where, t_c is the uncut chip thickness, z is the axial depth of cut as shown in Figure 5-3 (a) and k_{te}, k_{ce}, k_{ae} are the cutting force coefficients in the elastic recovery zone. Thus, in micro milling process, the cutting force in this region is relative to the actual feed rate and DOC. The different cutting forces can be formulated according to the elastic recovery area A_p in three directions as shown in Figure 5-3 and equation (5.2).

$$F_t = \varepsilon_1 * A_{pt}$$

$$F_c = \varepsilon_2 * A_{pc} \tag{5.2}$$

$$F_a = \varepsilon_3 * A_{pa}$$

Therefore, the modified cutting forces in elastic recovery zone can be expressed in the following equations:

$$F_t = \varepsilon * d * f * sin\theta \ (0 \le \theta \le \theta_1)$$

$$F_c = \varepsilon * d * 2 * \sqrt{{r_e}^2 - (r_e - f * sin\theta)^2} \ (0 \le \theta \le \theta_1)$$

$$F_a = \varepsilon * [{r_e}^2 * \sin^{-1}\left(\frac{\sqrt{{r_e}^2 - (r_e - f * sin\theta)^2}}{r_e}\right) - \sqrt{{r_e}^2 - (r_e - f * sin\theta)^2} * (r_e - f * sin\theta)] \ (0 \le \theta \le \theta_1) \tag{5.3}$$

where, ε is the compressive stress of MMCs in three directions respectively, d and f are the micro milling depth of cut and feed rate respectively, r_e is the cutting edge radius, θ is the rotation angle of tool tip and θ_1 is the maximum rotation angle in elastic recovery zone. Thus, the cutting force at the angle of θ_1 is observed as a threshold for material from elastic recovery to plastic deformation shown in Figure 5-5.

5.2.2 Cutting force in ploughing region

When the uncut chip thickness increases beyond the elastic recovery zone, the cutting tool will keep ploughing on the workpiece until the uncut chip thickness reach the minimum chip thickness. In this region, the ploughing force is dominated and elastic recovery still occurs on the remained surface of workpiece. Thus, in this ploughing process, both elastically and plastically deformation will occur in the meantime, while still no chip formation occurs in this region.

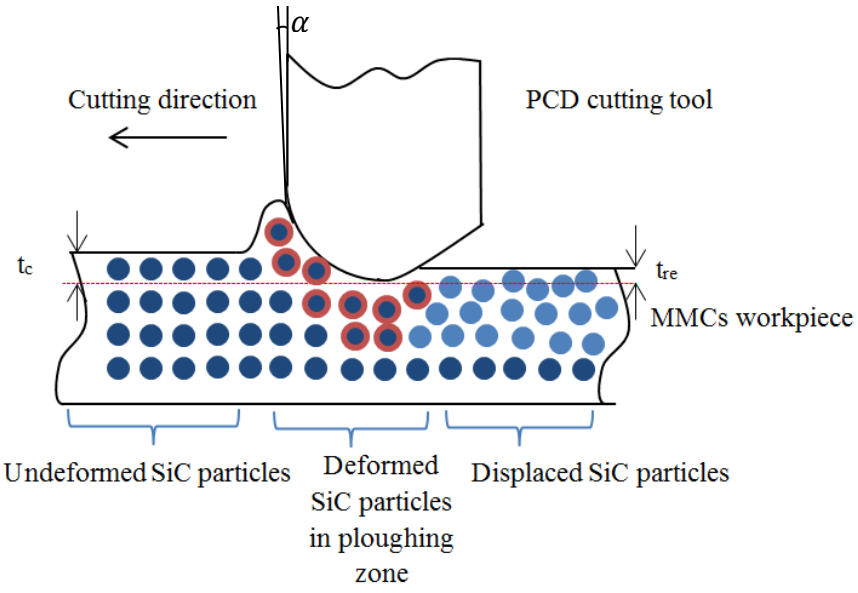

Figure 5-4 Particles displacement in ploughing zone

Due to the reinforced particles are rigid in ploughing process, only matrix material deformed elastically and plastically as shown in Figure 5-4. The particles only displaced in the ploughing zone. Thus, a slip line field model for a rigid wedge sliding on a half space in orthogonal cutting is suggested and then modified to estimate the tangential force, radial force and axial force on the lower boundary of the dead-metal zone in micro milling MMCs. The modified cutting force models determining the size effects and minimum chip thickness effects in ploughing zone can be expressed as:

$$F_t = \tau_m * l * t_{cmin} * sin\theta \ * \tan\left(\frac{\pi}{4}+\frac{\alpha}{2}\right) \ (\theta_1 < \theta \leq \theta_2)$$

$$F_c = \tau_m * l * t_{cmin} * sin\theta * \left(1+\frac{\pi}{2}\right) * \tan\left(\frac{\pi}{4}+\frac{\alpha}{2}\right) * \sin\vartheta \ (\theta_1 < \theta \leq \theta_2) \quad (5.4)$$

$$F_a = \tau_m * l * t_{cmin} * sin\theta * \left(1+\frac{\pi}{2}\right) * \tan\left(\frac{\pi}{4}+\frac{\alpha}{2}\right) * \cos\vartheta \ (\theta_1 < \theta \leq \theta_2)$$

where, τ_m is the shearing stress of matrix material, α is the rake angle of cutting tool and l is the active edge length representing the actual cutting width in ploughing process as shown in Figure 5-6, t_{cmin} is the minimum chip thickness of MMCs and θ_2 is the maximum rotation angle in ploughing zone. Thus, the cutting force at the angle of θ_2 is observed as a threshold for material minimum chip thickness. Figure 5-5 below shows the different cutting regions and their angular threshold occurs respectively.

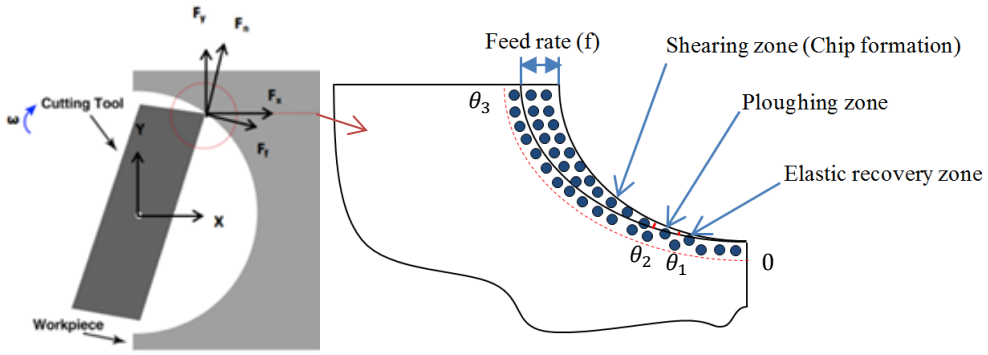

Figure 5-5 Cutting regions in chip formation process

Due to the existence of cutting tool nose radius, the encompassed straight and round sections on the cutting tool edge involved in micro milling cannot be ignored. The previous researches propose to replace the complex cutting edge by using an equivalent straight cutting edge as the engaged cutting edge in micro milling process. Thus, the active edge length l can be determined as below [30]:

$$l = r_n * (\varphi + \sin^{-1}\left(\frac{f}{2 * r_n}\right)) + (\frac{d - r_n * (1 - \cos\varphi)}{\sin\varphi}) \tag{5.5}$$

where, r_n is the nose radius of cutting tool, φ is the approach angle between tool and workpiece as shown in Figure 5-6.

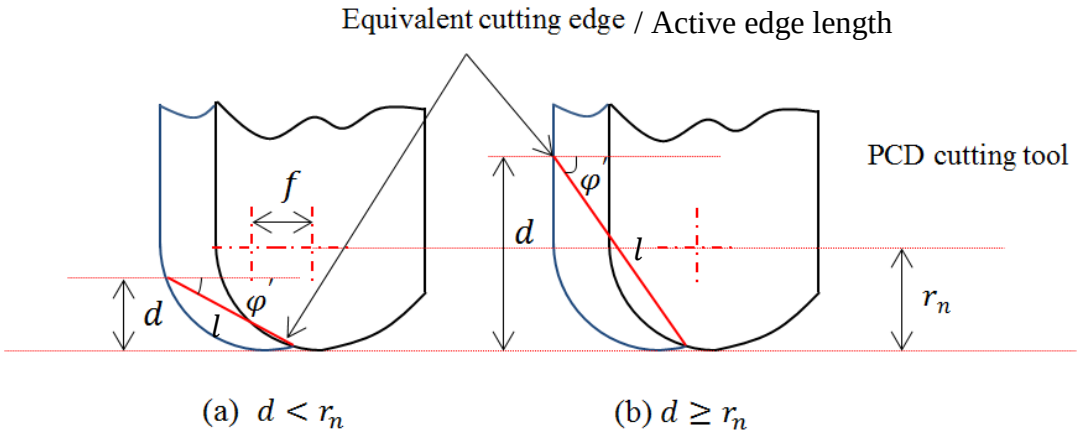

Figure 5-6 Equivalent cutting edges

5.2.3 Cutting force in shearing region

5.2.3.1 Shearing force in chip formation process

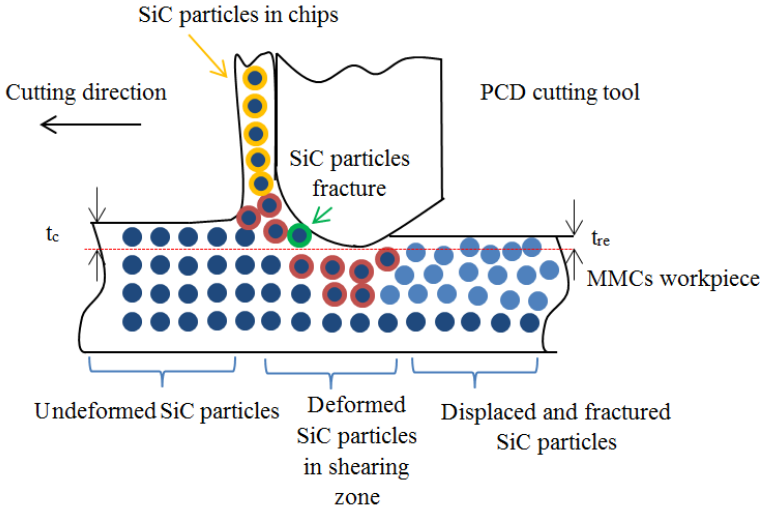

Figure 5-7 Particles displacement in shearing zone

From the previous research, it has been known that the chip formation mechanism in MMCs micro milling shown in Figure 5-7 has similarities to the homogeneous and monometallic materials although the formed chips properties are different in some aspects. The shearing force that result in the chip formation is modified from the previous analytical model and then developed according to the specific properties of particle reinforced MMCs. Thus, the tangential force Ft, radial force Fc and axial force Fa on the shearing plane can be determined and expressed respectively as below:

$$F_t = \tau s * a * c * sin\theta * \frac{\cos(\beta - \alpha)}{\sin \emptyset * \cos(\emptyset + \beta - \alpha)} (\theta_2 < \theta \leq \theta_3)$$

$$F_c = \tau s * a * c * sin\theta * \frac{sin(\beta - \alpha)}{sin \emptyset * cos(\emptyset + \beta - \alpha)} (\theta_2 < \theta \leq \theta_3) \quad (5.6)$$

$$F_a = 0 \ (\theta_2 < \theta \leq \theta_3)$$

where, a is the actual depth of cut, c is the actual feed rate in micro milling process. In addition, β is the milling friction angle and $\emptyset$ is the shear angle that has been shown in Figure 4-1. $t_{ac} = c * sin\theta$ is the instantaneous uncut chip thickness VERS immersion angle.

The friction that results from the formed chips sliding on the tool rake face cannot be ignored. The resultant friction energy that overcomes the chip-tool interaction is researched as the critical factor that effects on the friction angle β. Thus, the friction angle β can be investigated according to the previous theories of two-body rolling abrasion [240] and three-body rolling friction [222, 241] between the cutting tool and workpiece as below.

The friction angle β can be written as:

$$\beta = tan^{-1}(\frac{F_f}{F_N}) \tag{5.7}$$

where, the total friction force F_f is affect by the two body rolling abrasive force F_p and the three body rolling friction force F_r as shown below:

$$F_f = F_p + F_r \tag{5.8}$$

For the two-body rolling abrasion force F_p along the tool-chip interface can be expressed as:

$$F_p = N_p * A_i * 3 * \sigma_{y(tool)} * q \tag{5.9}$$

The total number N_p of the reinforced abrasive particles involved in the friction area between the tool edge and workpiece surface is

$$N_p = \frac{V_p * a * c}{\pi * {r_s}^2} \tag{5.10}$$

The tool-workpiece contact area A_i is

$$A_i = \frac{{r_s}^2}{2} * \left(\frac{\pi}{180} * \left(2 * \theta_p\right) - \sin\left(2 * \theta_p\right)\right) \tag{5.11}$$

where, the apex angle θ_p shown in Figure 5-8 can be illustrated as below.

$$\theta_p = \cos^{-1}(1 - \frac{\delta_p}{r_s}) \tag{5.12}$$

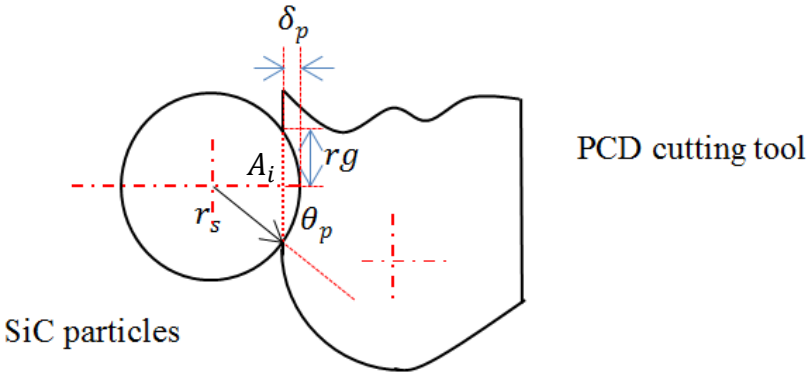

Figure 5-8 Abrasive particles and tool surface interaction

For the three-body rolling friction force F_r, the force can be calculated using equation:

$$F_r = \mu_3 * F_N \tag{5.13}$$

where, the friction coefficient μ_3 can be obtained from the following equation:

$$\mu_3 = \frac{k_t}{\pi * H_t} * \left(\frac{2 * r_s}{rg}\right)^2 * (1 - (1 - (\frac{rg}{2 * r_s})^2)^{1/2}) \tag{5.14}$$

where, rg is the depth of groove formed on the cutting tool surface due to the abrasive wear shown in Figure 5-8 and can be given by equation:

$$rg = \sqrt{{r_s}^2 - (r_s - \delta_p)^2} \tag{5.15}$$

The shearing stress k_t for the cutting tool material has relationship with the yield strength of tool material $\sigma_{y(tool)}$ and the hardness of the tool H_t that can be calculated with the following equation:

$$k_t = \frac{\sigma_{y(tool)}}{2} = \frac{H_t}{6} \tag{5.16}$$

The fraction of reinforced particles along the tool-chip interface contributes to the total normal loading force. The normal loading force F_N due to the particle fracture across the tool-workpiece contact area can be obtained with the following equation:

$$F_N = F_{N1} * N_p * q \tag{5.17}$$

where, F_{N1} is the normal force for each fractured particles along the tool edge. Due to the abrasive property of reinforced particles, the normal cutting force leads to the plastic deformation on the cutting tool surface when the particles are sliding on the tool surface. Thus, the normal cutting force on the single abrasive particle can be illustrated with the following equation [240]:

$$F_{N1} = 2.9 * \pi * r_e * \sigma_{y(tool)} * \delta_p \tag{5.18}$$

In this equation, δ_p is the critical value of the relative penetration between MMCs and PCD tool. This value can be achieved from the following equation:

$$\delta_p = (\frac{9 * \pi}{4})^2 * \left(\frac{\sigma_{y(tool)}}{Y_0}\right)^2 * r_e \tag{5.19}$$

where, Y_0 is the young's modulus of tool-chip interface that can be obtained according to the initial young's modulus of MMCs and PCD tool. Y_1 and Y_2 are the Young's modulus of MMC and cutting tool respectively. v_1 and v_2 are the poison ratio of MMC and cutting tool respectively. Thus, the combined tool-chip interface condition can be considered with the equation (5.20) given as below.

$$\frac{1}{Y_0} = \frac{(1 - v_1)^2}{Y_1} + \frac{(1 - v_2)^2}{Y_2} \tag{5.20}$$

Due to the nose radius effects, the developed equivalent cutting edge is applied in the micro milling process in order to replace the straight and round part of cutting edge by an equivalent straight cutting edge [242]. According to the equivalent cutting edge length, the actual depth of cut and actual feed rate, which represented by a and c, can be given as below. The chip formed and flows on the rake face of cutting tools and its direction is assumed to be perpendicular to the equivalent cutting edge. Thus, the equivalent actual depth of cut a and feed rate c can be predicted in this situation as shown in the following equations respectively.

$$a = \frac{d}{\sin \varphi'} \tag{5.21}$$

$$c = f * \sin \varphi' \tag{5.22}$$

The depth of cut is varied form small value that smaller than the nose radius to a large value that larger than the nose radius, which results in the difference of approach angle. Thus, the actual approach angle for the equivalent cutting edge is given in Figure 5-6 as below:

When the depth of cut is smaller than the tool nose radius,

$$\varphi' = \cot^{-1}\left(\frac{\sqrt{2 * r_n * d - d^2} + \frac{f}{2}}{d}\right),\ d < r_n \tag{5.23}$$

When the depth of cut is larger than the tool nose radius,

$$\varphi' = \cot^{-1}(\frac{r_n + f/2}{d}),\ d \geq r_n \tag{5.24}$$

5.2.3.2 Ploughing force in chip formation process

In shearing region, the chip formation process is accompanied with the combination of shearing and ploughing phenomenon. Thus, the ploughing force is a critical force signal that affects the cutting mechanics and eventually increases the resultant cutting force. In addition, the ploughing area in this ploughing zone is constant. Therefore, according to the slip line field model, the ploughing force in chip formation process can be given as below:

$$F_t = \tau_m * l * t_{cmin} * tan\left(\frac{\pi}{4} + \frac{\alpha}{2}\right)\ (\theta_2 < \theta \leq \theta_3)$$

$$F_c = \tau_m * l * t_{cmin} * \left(1 + \frac{\pi}{2}\right) * tan\left(\frac{\pi}{4} + \frac{\alpha}{2}\right) * sin\,\vartheta\ (\theta_2 < \theta \leq \theta_3) \tag{5.25}$$

$$F_a = \tau_m * l * t_{cmin} * \left(1 + \frac{\pi}{2}\right) * tan\left(\frac{\pi}{4} + \frac{\alpha}{2}\right) * cos\,\vartheta\ (\theta_2 < \theta \leq \theta_3)$$

5.2.3.3 Particle fracture and de-bonding force in chip formation process

With the continually engagement of cutting tool on the workpiece, the fracture of reinforced particles accompanied with the displacement occur when the tool cutting edge meets the particles. The remained parts of particle are then abrasion on the cutting tool during the ploughing or de-bonding from the matrix material, removed from the machined surface on workpiece and leave voids. Due to the uniform average radius and

fabrication oriented normal distribution of reinforced particles located in the workpiece material, the interaction between the cutting edge and the particles can be seen as shown in Figure 5-9. The particles fracture force is given as below:

$$F_t = \mu_{SiC} * \pi * {r_s}^2 * (l * p'/2 * r_s)\ (\theta_2 < \theta \leq \theta_3)$$

$$F_c = \mu_{SiC} * \pi * {r_s}^2 * (l * p'/2 * r_s)\ * tan\,\sigma * sin\vartheta\ (\theta_2 < \theta \leq \theta_3) \quad (5.26)$$

$$F_a = \mu_{SiC} * \pi * {r_s}^2 * (l * p'/2 * r_s)\ * tan\,\sigma * cos\,\vartheta\ (\theta_2 < \theta \leq \theta_3)$$

where, μ_{SiC} is the specific stress of SiC particle fracture, p' is the volume fraction of the particle involved in the workpiece along the cutting edge, r_s is the average radius of the particle, θ_3 is rotation angle that tool approach out the workpiece as shown in Figure 5-5 and σ is the angle between the resultant particle fracture force and the cutting direction. The angle σ is considered as the critical angle that demonstrates the direction of the resultant cutting force and the relationship between the tangential force and radial force. Thus, the angle σ is given as the equation [243] below:

$$\sigma = sin^{-1}(\frac{H}{2 * r_s + 2 * r_e}) \quad (5.27)$$

where, H is the height of the particle ploughing zone in the uncut chip of workpiece as shown in Figure 5-9. The equation and detailed illustration of H is given as below:

$$H = t_{ac},\ t_{ac} < t_{min}$$
$$H = r_e * (1 + sin\,\alpha),\ t_{ac} \geq t_{min} \quad (5.28)$$

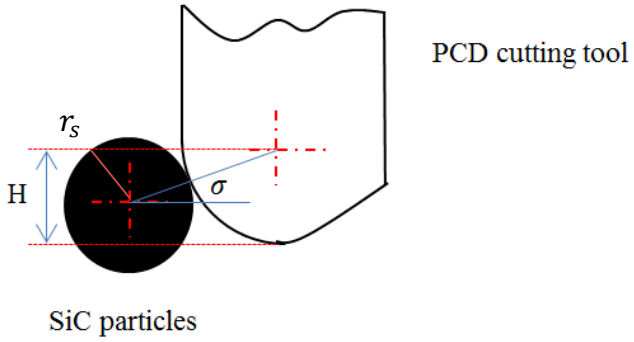

Figure 5-9 Height of the particle ploughing zone

The specific stress μ_{SiC} for the fracture of each reinforced SiC particle that represented by the fracture toughness K_c that can be found from the Griffith formula and expressed as below:

$$\mu_{SiC} = \frac{K_c}{\sqrt{2 * r_s}} \tag{5.29}$$

In addition, the total fracture energy of the particle U can be calculated following the equation [244] below:

$$U = \int \left(\frac{(1 - {v_1}^2)}{Y_1} \right) * \pi * {\mu_{SiC}}^2 * \lambda * w \tag{5.30}$$

where, v_1 is the poison ratio of MMCs, Y_1 is the Young's modulus of MMCs, λ is the initial interface crack length and w is the initial interface crack width.

The cutting force in shearing zone can be expressed as:

$$\begin{aligned}
F_t &= \tau s * a * c * sin\theta * \frac{\cos(\beta-\alpha)}{\sin\emptyset * \cos(\emptyset+\beta-\alpha)} + \tau_m * l * t_{cmin} * \tan\left(\frac{\pi}{4}+\frac{\alpha}{2}\right) + \mu_{SiC} * \pi * {r_s}^2 * \left(l * \frac{p'}{2 * r_s}\right) \\
F_c &= \tau s * a * c * sin\theta * \frac{\sin(\beta-\alpha)}{\sin\emptyset * \cos(\emptyset+\beta-\alpha)} + \tau_m * l * t_{cmin} * \left(1+\frac{\pi}{2}\right) * \tan\left(\frac{\pi}{4}+\frac{\alpha}{2}\right) * \sin\vartheta \\
&\quad + \mu_{SiC} * \pi * {r_s}^2 * (l * p'/2 * r_s) * \tan\sigma * sin\vartheta \\
F_a &= \tau_m * l * t_{cmin} * \left(1+\frac{\pi}{2}\right) * \tan\left(\frac{\pi}{4}+\frac{\alpha}{2}\right) * \cos\vartheta + \mu_{SiC} * \pi * {r_s}^2 * \left(l * \frac{p'}{2 * r_s}\right) * \tan\sigma * \cos\vartheta
\end{aligned} \tag{5.31}$$

Thus, the total cutting force in tangential, radial and axial directions can be expressed as:

$$F_t(total) = \begin{cases} \varepsilon * d * f * sin\theta, (0 \le \theta \le \theta_1) \\ \tau_m * l * f * sin\theta * \tan\left(\frac{\pi}{4}+\frac{\alpha}{2}\right), (\theta_1 < \theta \le \theta_2) \\ \tau s * a * c * sin\theta * \frac{\cos(\beta-\alpha)}{\sin\emptyset * \cos(\emptyset+\beta-\alpha)} + \tau_m * l * t_{cmin} * \tan\left(\frac{\pi}{4}+\frac{\alpha}{2}\right) \\ + \mu_{SiC} * \pi * {r_s}^2 * (l * p'/2 * r_s), \\ (\theta_2 < \theta \le \theta_3) \end{cases}$$

$$F_c(total) = \begin{cases} \varepsilon * d * 2 * \sqrt{{r_e}^2 - (r_e - f * sin\theta)^2}, (0 \le \theta \le \theta_1) \\ \tau_m * l * f * sin\theta * \left(1+\frac{\pi}{2}\right) * \tan\left(\frac{\pi}{4}+\frac{\alpha}{2}\right) * \sin\vartheta, (\theta_1 < \theta \le \theta_2) \\ \tau s * a * c * sin\theta * \frac{\sin(\beta-\alpha)}{\sin\emptyset * \cos(\emptyset+\beta-\alpha)} + \tau_m * l * t_{cmin} * \left(1+\frac{\pi}{2}\right) * \tan\left(\frac{\pi}{4}+\frac{\alpha}{2}\right) * \sin\vartheta \\ + \mu_{SiC} * \pi * {r_s}^2 * (l * p'/2 * r_s) * \tan\sigma * sin\vartheta, (\theta_2 < \theta \le \theta_3) \end{cases}$$

$$F_a(total)$$

$$= \begin{cases} \varepsilon * \left[{r_e}^2 * \sin^{-1}\left(\frac{\sqrt{{r_e}^2 - (r_e - f * sin\theta)^2}}{r_e} \right) - \sqrt{{r_e}^2 - (r_e - f * sin\theta)^2} * (r_e - f * sin\theta) \right], (0 \le \theta \le \theta_1) \\ \tau_m * l * f * sin\theta * \left(1 + \frac{\pi}{2}\right) * \tan\left(\frac{\pi}{4} + \frac{\alpha}{2}\right) * \cos\vartheta, (\theta_1 < \theta \le \theta_2) \\ \tau_m * l * t_{cmin} * \left(1 + \frac{\pi}{2}\right) * \tan\left(\frac{\pi}{4} + \frac{\alpha}{2}\right) * \cos\vartheta \\ + \mu_{SiC} * \pi * {r_s}^2 * \left(l * \frac{p'}{2 * r_s} \right) * \tan\sigma * \cos\vartheta, (\theta_2 < \theta \le \theta_3) \end{cases} \quad (5.32)$$

The total cutting force in X and Y directions, which are parallel and vertical to the cutting speed direction respectively at the initial machining starting point, are shown in Figure 5-5 and the cutting force in three directions can be expressed in the following equation:

$$F_x = F_t(total) * cos\theta + F_c(total) * sin\theta$$

$$F_y == -F_t(total) * sin\theta + F_c(total) * cos\theta; \quad (5.33)$$

$$F_z = F_a(total)$$

5.3 Dynamic cutting force simulation and analysis

A series of micro milling simulations of the MMCs precision machining are carried out at varied cutting parameters and process variables. Figure 5-10 shows the predicted instantaneous dynamic cutting force in a complete cutting circle. The continuous cutting force by utilizing by using two straight flute PCD end mills with a common diameter of 10 mm, a rake angle of 0^o, a feed rate of 10 μm/tooth, a radial depth of cut of 10 mm and a axial depth of cut of 0.25 mm when machining 42% volume fraction SiC/Al MMCs with 5 μm particle grain size is demonstrated. This force curves present the whole cutting process including the elastic recovery zone, ploughing zone and shearing zone. The cutting force variation indicates that the cutting force in X and Y direction dramatically reach to the maximum value when each tooth approach in the workpiece. The cutting forces reach to a negative value comparing to the original force value at the end of the cutting process of each tooth. These force variations significantly affect the resultant surface form accuracy and surface roughness of final parts. Figures below show the prediction of cutting forces when machining under varied cutting conditions.

Figure 5-11 shows the predicted value of cutting forces when the feed rate changes. It can be observed that the cutting forces increase with the feed rate increases after the feed rate reaches the minimum chip thickness. In addition, the only cutting force amplitude changes at different feed rate. Figure 5-12 shows the influence of radial depth of cut on the predicted cutting force value and Figure 5-13 shows the predicted cutting forces at different axial depth of cut. Gathering the influence of DOC in axial and radial directions, it can be seen that cutting force can be significantly reduced when selecting small axial DOC. The smaller force variation means less influence on the form accuracy on the machined parts. Thus, the simulation result indicates that choose appropriate cutting DOC can contribute to the reduction of form error especially in micro cutting process and also increase the surface performance including the surface roughness and form accuracy. Figure 5-14 and Figure 5-15 show the influence of particles on the predicted cutting forces in various conditions. In Figure 5-14, the only difference on the cutting force is the amplitude of particle fracture force value when machining MMCs with different particle size. In Figure 5-15, it worth mentioning that the amplitude of particle fracture force and the frequency of cutting force circle are different. It can be observed that the volume fraction of reinforced particles has significant effects on the cutting forces distribution and variation.

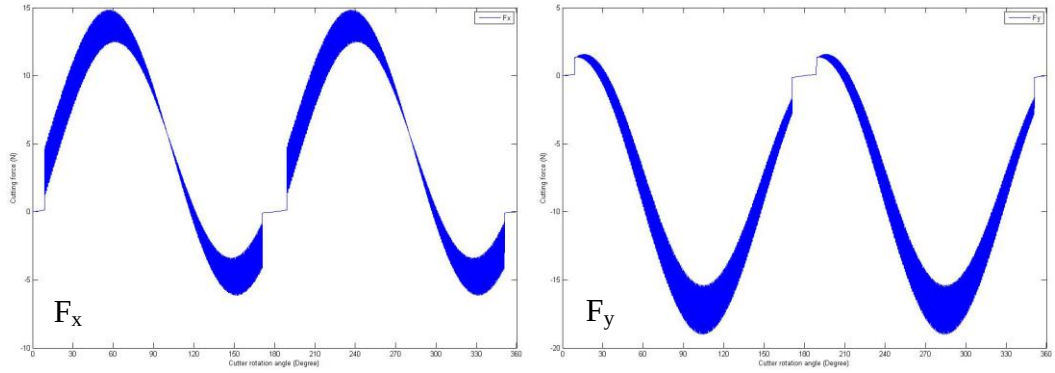

Figure 5-10 Predicted cutting forces for MMCs micro milling in X and Y directions respectively

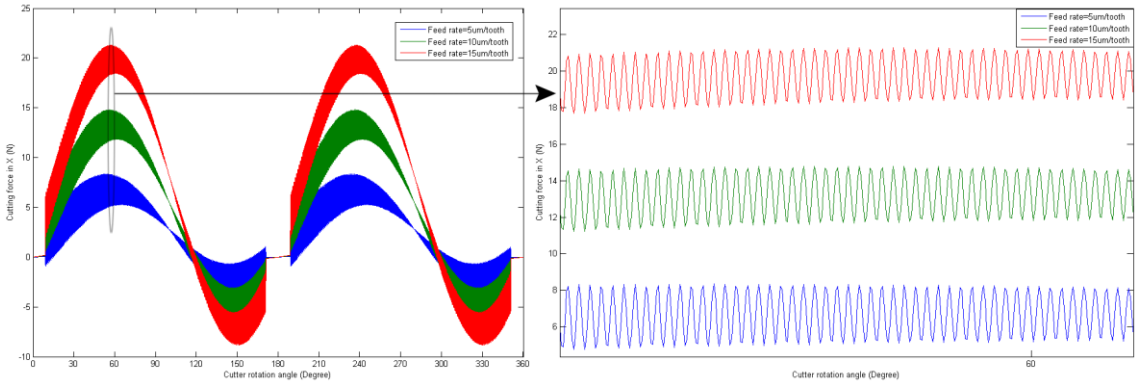

(a) Influence of feed rate on MMCs cutting force Fx

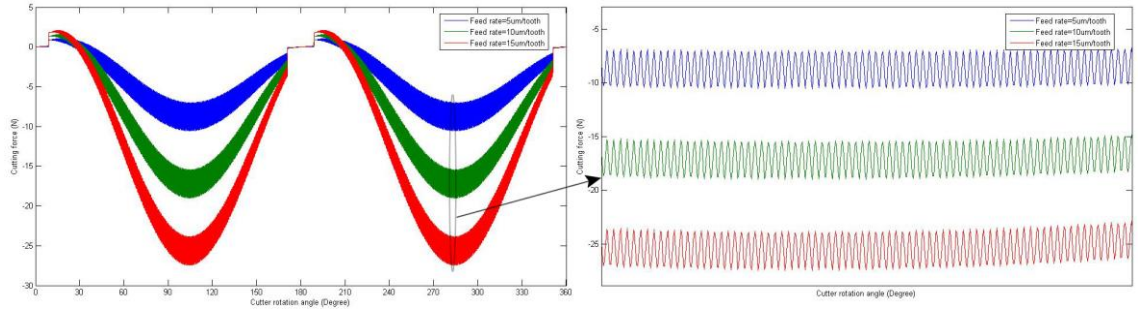

(b) Influence of feed rate on MMCs cutting force Fy

Figure 5-11 Influence of feed rate on MMCs cutting forces

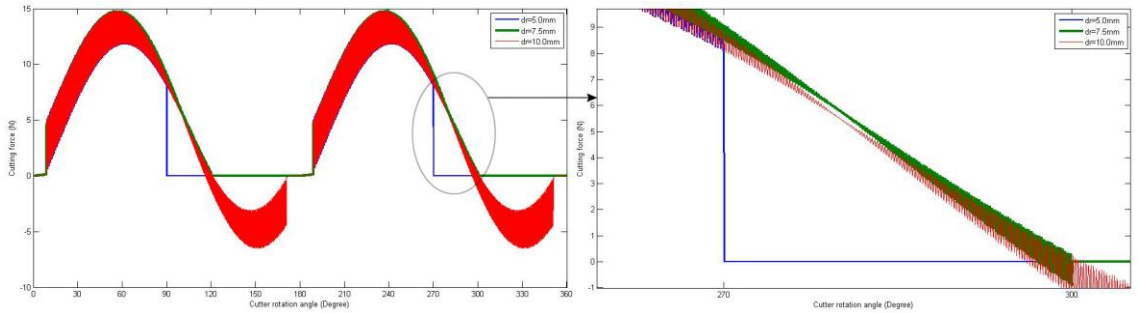

(a) Influence of radial depth of cut on MMCs cutting force Fx

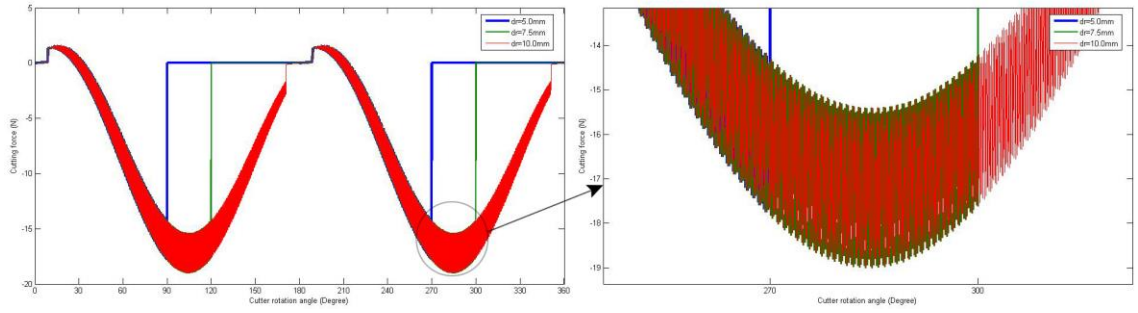

(b) Influence of radial depth of cut on MMCs cutting force Fy

Figure 5-12 Influence of radial depth of cut on MMCs cutting forces

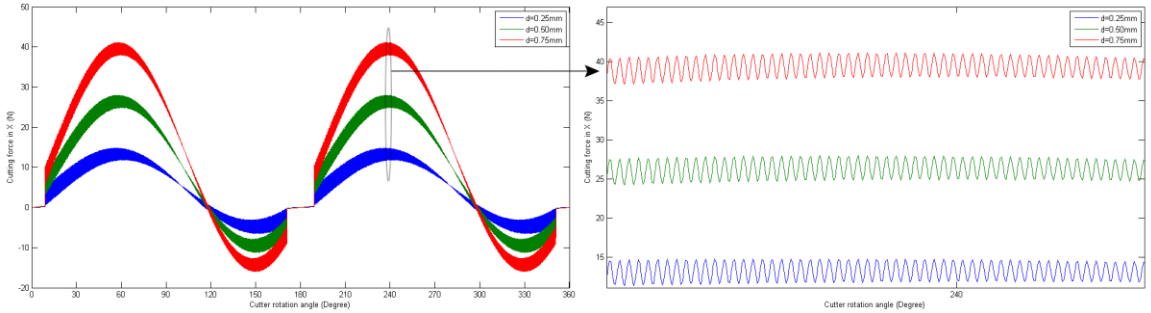

(a) Influence of axial depth of cut on MMCs cutting force Fx

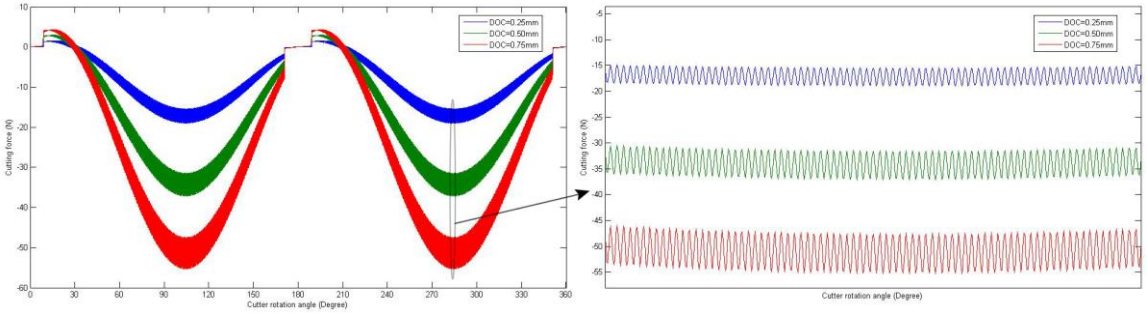

(b) Influence of axial depth of cut on MMCs cutting force Fy

Figure 5-13 Influence of axial depth of cut on MMCs cutting forces

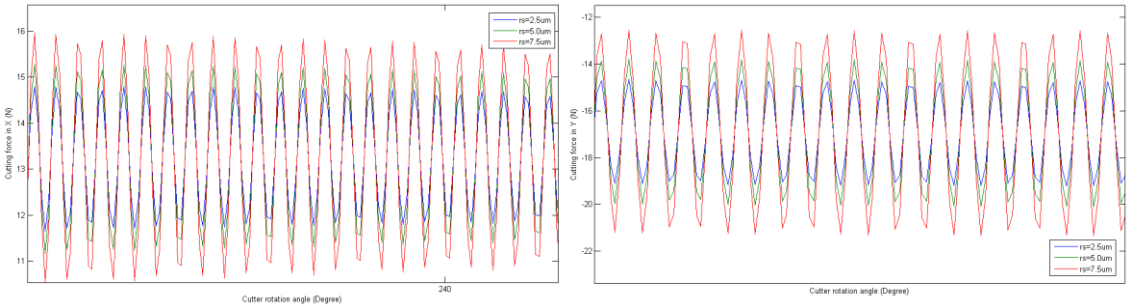

Figure 5-14 Influence of particle radius on MMCs cutting forces in X and Y directions respectively

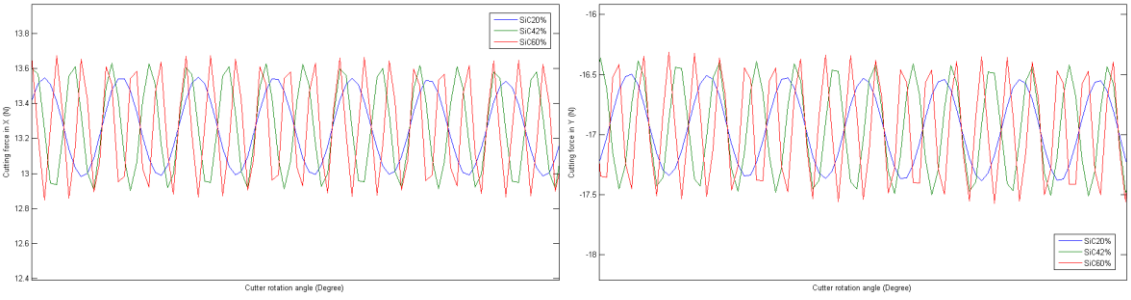

Figure 5-15 Influence of particle volume fraction on MMCs cutting forces in X and Y directions respectively

Thus, an innovative investigation on the dynamic cutting force model in micro milling particle reinforced MMCs has been presented in this part. The MMCs cutting force model is improved and modified closely from the previous homogeneous material machining force model. The theoretical model appropriately demonstrates the detailed MMCs milling force amplitude and variation including the matrix material shearing force and particle fracture force through analytical expression. Simulations of cutting force values under varied process variables are conducted and suitable for general MMCs micro milling process. The simulation results indicate that feed rate, radial depth of cut, axial depth of cut, and also the particle size and volume fraction have significantly effects on the predicted cutting forces. In addition, the accurate prediction on dynamic cutting force can be further used to improve the resultant surface form accuracy and also reduce the surface roughness and form error by choosing the optimal process variables and cutting parameters in MMCs precision machining process. The evaluation and validation of dynamic cutting force model is conducted via well-designed micro milling experiments in the following part.

5.4 Actual tool trajectory and analytical chip thickness model

Improved dynamic cutting force model in micro milling of MMCs has been demonstrated theoretically. However, the real tool position and tool tip trajectory need to be taken into consideration due to the runout of cutting tool cannot be ignored in micro cutting process [245]. As a result, the predicted chip thickness, which significantly affects the dynamic cutting forces, needs to be further modified by considering the tool runout. In order to accurately predict the dynamic cutting forces, new algorithm to determine the real chip thickness based on the real-time tool position and tool tip trajectory is proposed.

The conventional chip thickness model that presents the chip thickness at different rotation angle is given as below:

$$h(\theta) = f * sin\theta \tag{5.34}$$

where, $h(\theta)$ is the uncut chip thickness, f_t is the feed per tooth and θ is the position angle of tool tip from the beginning position of cutting as shown in Figure 5-5. Due to the existence of tool runout, which arising from the tooling dynamics, tool holder and manufacturing error, translation movement of the tool centre cannot be ignored in micro

milling. Thus, the actual position of cutting tool centre O' can be expressed in the following equation by considering the tool runout:

$$x = r_o * \sin(\omega * t + \alpha_o) + f * t/60$$
$$y = r_o * \cos(\omega * t + \alpha_o) \tag{5.35}$$

where, α_o is the initial runout angle of tool centre, r_o is the cutting tool runout at the rotation angle of $\omega * t$. The tool tip rotation radius and real trajectory of tool tip can be then obtained based on the cutting tool tip radius; however, the actual rotation radius of cutting tool tip is changing along with the rotation angle of cutting tool by considering the tool rotation in workpiece coordinate system. Thus, the change of tool geometry brought by the runout is critical and the actual tool tip rotation radius can be expressed by given the nominal tool radius and tool runout as below:

$$R' = \sqrt{{R_0}^2 + {r_o}^2 - 2 * R_0 * r_o * \cos(2 * \pi * \frac{K-1}{N} - \alpha_o)} \tag{5.36}$$

where, R_0 is the nominal radius of cutting tool, K is the tool teeth number and N is the numbers of tool teeth of the cutting tool. As a result, the real trajectory of tool tip represented by the tool tip position for this two flutes PCD end mill can be expressed as below.

$$x = R' * \sin\left(\omega * t + \tan^{-1}\frac{r_o * \sin\alpha_o}{R_0 + (-1)^{(K-1)}(r_o * \cos\alpha_o)}\right) + f * t/60$$
$$y = R' * \cos\left(\omega * t + \tan^{-1}\frac{r_o * \sin\alpha_o}{R_0 + (-1)^{(K-1)}(r_o * \cos\alpha_o)}\right) \tag{5.37}$$

In convention milling process, the nominal cutting tool rake angle is normally zero; however, the actual rake angle is different in micro milling by taking the tool runout into consideration. In term of real tool trajectory, the rake angle of cutting tool is always changing along with the tool rotation angle. In addition, when the angle between the first tooth and the kth tooth is smaller than α_o or larger than $\alpha_o + \pi$, the rake angles at these tooth are positive; when the angle between the first tooth and the kth tooth is larger than α_o while smaller than $\alpha_o + \pi$, the rake angles at these tooth are negative. Thus, the rake angle in each position according to the rotation angle can be calculated from the following equations.

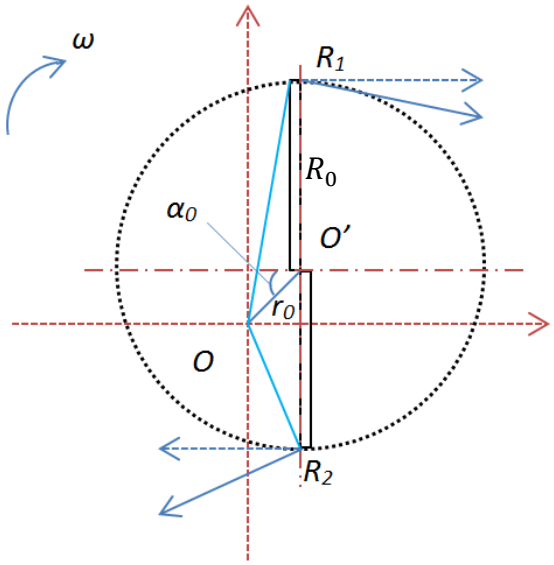

Figure 5-16 Cutting tool runout in MMCs micro milling

The angle between the first tooth and the kth tooth is smaller than α_o or larger than $\alpha_o + \pi$, the rake angle at the kth tooth will be:

$$\alpha_c = \cos^{-1}\left(\frac{R'^2 + {R_0}^2 - {r_o}^2}{2 * R' * R_0}\right) \tag{5.38}$$

The angle between the first tooth and the kth tooth is larger than α_o while smaller than $\alpha_o + \pi$, the rake angle at the kth tooth will be:

$$\alpha_c = -\cos^{-1}\left(\frac{R'^2 + {R_0}^2 - {r_o}^2}{2 * R' * R_0}\right) \tag{5.39}$$

Considering the real cutting condition that cutting tool keep approaching on the direction of cutting feed rate, the real tool trajectory is more complicated. In term of the actual chip thickness, the largest chip thickness is located at the rotation angle larger than 90 degree due to the continue feed of cutting tool. In addition, the point that tool approach in to the workpiece is located at the rotation angle smaller than 0 degree and tool approach out from the workpiece is located at the rotation angle larger than 180 degree. Thus, the chip formation particularly for the chip thickness at each position of tool tip in this research can be demonstrated in Figure 5-17 and the actual chip thickness can be expressed as below.

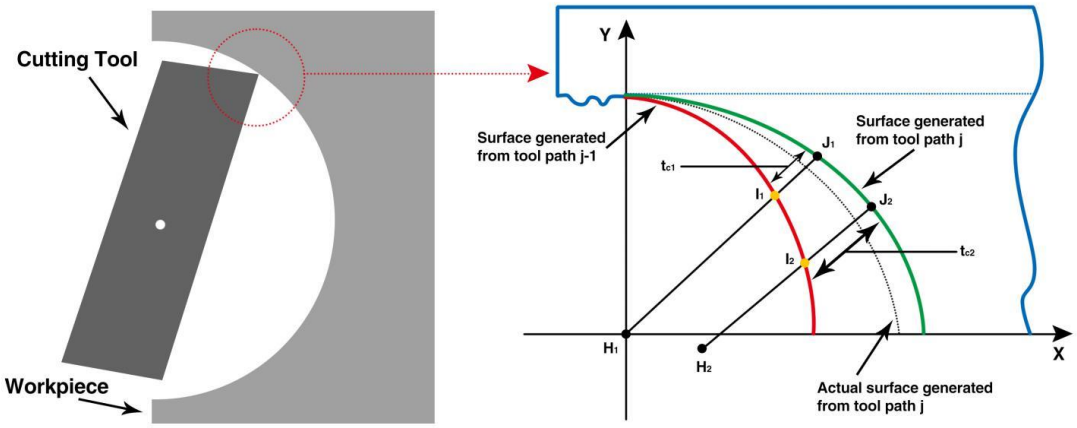

Figure 5-17 Real tool tip trajectory in micro milling

The instantaneous chip thickness t_c is given by:

$$t_c = HJ - HI \tag{5.40}$$

where, H is the tool centre at the j path of cutting tool, I is the edge coordinate at the j-1 path and J is the edge coordinate at the j path. Considering the tool run out, feed rate and also the material recovery, the actual chip thickness in the micro milling process at different rotation angle can be expressed as below:

$$\begin{aligned} x_{act} &= x_J - K_0 * \frac{t_c}{R'} * (x_J - x_H) \\ y_{act} &= y_J - K_0 * \frac{t_c}{R'} * (y_J - y_H) \end{aligned} \tag{5.41}$$

where, K_0 is the material recovery constant. $K_0 = 1$, when the chip thickness is smaller than the elastic recovery thickness; $K_0 = \varepsilon$, when the chip thickness is larger than elastic recovery zone while less than minimum chip thickness and ε is the elastic recovery rate; In these two situations, workpiece material only undergoes elastic and plastic deformation, while no material has been removed. The residual material will be cut during the next tool path. However, this process may be repeated several times without material removal and chips formation will be occurred only until the accumulated chip thickness is larger than the material minimum chip thickness. $K_0 = 0$, when the chip thickness is larger than minimum chip thickness. This means the actual chip thickness generated is equal to the predicted chip thickness. Thus, the actual chip

thickness is illustrated according to the actual cutting radius and can be expressed as below:

$$x_{act} = x_J - K_0 * \frac{t_c}{\sqrt{{R_0}^2 + {r_o}^2 - 2 * R_0 * r_o * \cos(2 * \pi * \frac{K-1}{N} - \alpha_o)}} * (x_J - x_H)$$
$$y_{act} = y_J - K_0 * \frac{t_c}{\sqrt{{R_0}^2 + {r_o}^2 - 2 * R_0 * r_o * \cos(2 * \pi * \frac{K-1}{N} - \alpha_o)}} * (y_J - y_H) \quad (5.42)$$

Therefore, the actual chip thickness is given by:

$$t_{act} = \sqrt{(x_{act(J)} - x_{act(I)})^2 + (y_{act(J)} - y_{act(I)})^2} \quad (5.43)$$

In real material removal and chip formation process, a threshold is defined as the chip formation starts. The algorithm stops when the absolute value becomes larger than the threshold. The chip formation procedures and actual chip thickness prediction are illustrated in Figure 5-18.

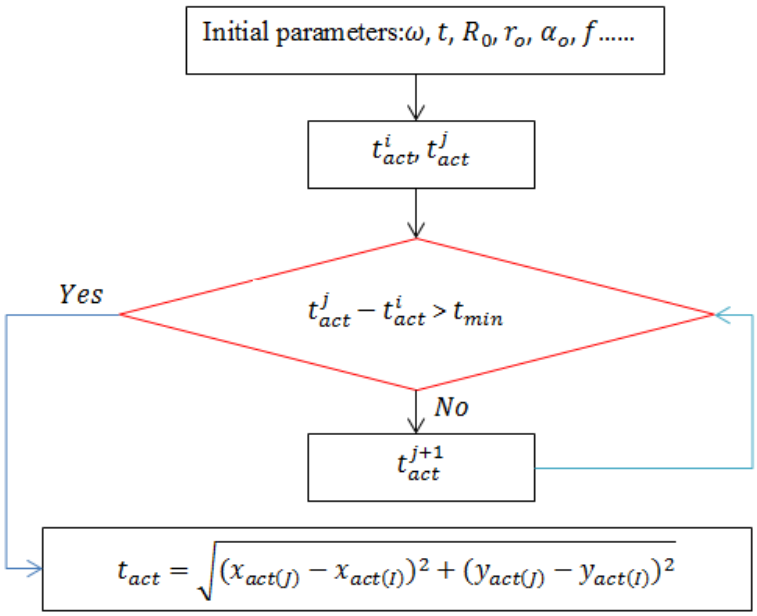

Figure 5-18 Chip formation procedures and actual chip thickness prediction

5.5 Experimental evaluation and validation

In the previous part, an improved theoretical dynamic cutting force model in metal micro milling particulate MMCs has been presented. By further considering the effects of cutting tool dynamic run-out, actual chip thickness and tool tip trajectory, the innovative expression on dynamic cutting force is evaluated and validated

comprehensively in this section. Well-designed cutting trials are carried out under different cutting parameters in order to verify the force model. In addition, run-out of cutting tool and spindle-workpiece vibrations are measured during the machining processes to ensure the accuracy of evaluation and validation.

5.5.1 Experimental set-up

Figure 5-19(a) illustrates the schematic of the micro milling experimental set-up. The experiments are conducted on a KERN HSPC 2825 micro milling machine featuring high accuracy, high precision and high dynamic performance. This enables the dynamic effects of the machine tool and cutting tool can be reduced to a minimum during the machining processes. Al2024/SiC/45p workpiece are performed in these experiments. Figure 5-19(b) shows the micro-structure of MMCs. The SiC particles with 5 μm grain size are evenly distributed in the matrix materials. Due to the high volume fraction of reinforced particles and their extremely high abrasive properties, polycrystalline diamond tools are performed better than other tools consistently and widely applied in MMCs machining. Two straight flutes PCD end mill with a diameter of 10 mm and a cutting edge radius around 1.7 μm as shown in Figure 5-19(c) are performed in the experimental work. In order to monitor the machine vibration and identify the dynamic response of tool and workpiece system, a MicroSense 5810 capacitance sensor and a PCB 352C33 piezotronics accelerometer are mounted on the spindle and workpiece respectively during micro milling processes.

5.5.2 Experimental procedures

Since the influence of radial depth of cut on surface integrity is found to be negligible [246], three mainly machining parameters including milling speed, feed rate and axial depth of cut are chosen as independent variables that significantly affect the machined surface roughness. In order to consider the interaction effect of these three factors, the L27 (3^3) full factorial experiments are conducted. The process parameters used for these experiments are shown in Table 5-1. In the micro milling experiments, only one of the machining parameters is varied while the others are holding constant in order to observe the effect and contribution of input parameter. Side milling with a constant radial depth of cut of 3 mm is performed in these cutting trials. In addition, cutting tool and machined surface are perpendicular. The experimental trials are conducted under dry cutting condition and only air below is applied. The machined surface roughness,

surface profile and topographical features are measured and adopted by using the ZYGO New View 5000 white light interferometer and a scanning electron microscope (SEM) with excellent precision and accuracy. Measurements of surface roughness are undertaken in feed direction and the average value of machined surface roughness at five different locations under each set of milling conditions is captured for further analysis in order to reduce the measurement uncertainty and assess repeatability.

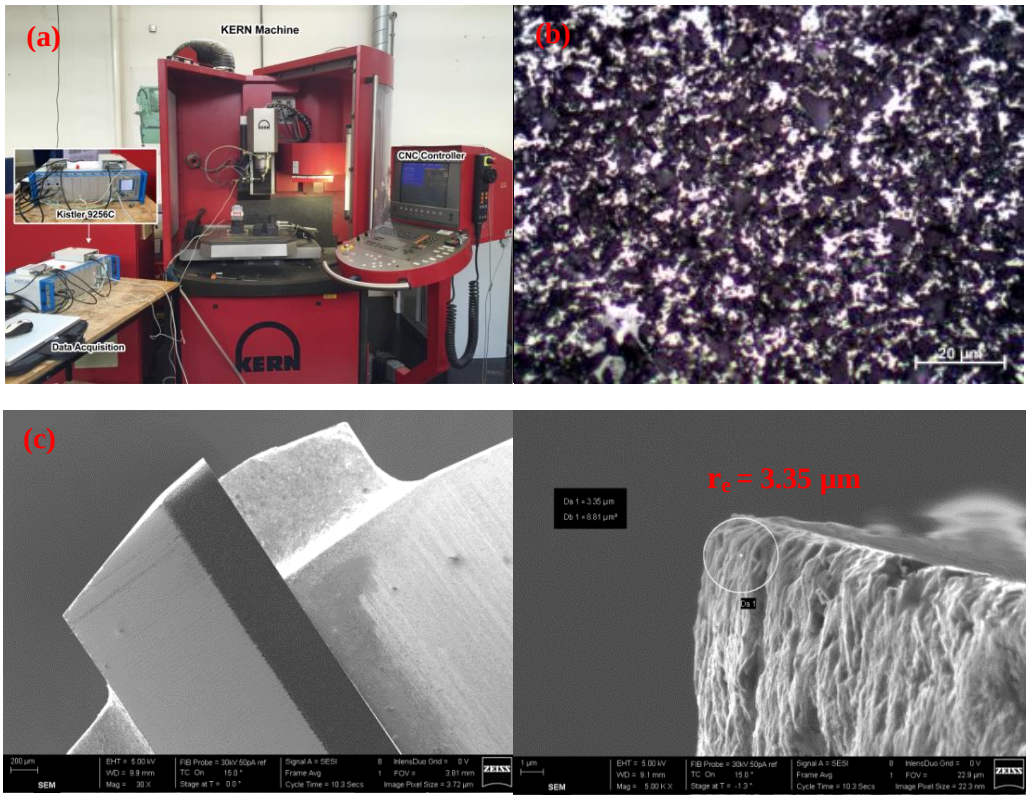

Figure 5-19 Experimental set-up for precision milling process

Table 5-1 Levels of independent process parameters

Process parameters	Levels		
	1	2	3
Spindle speed, s (rpm)	3,000	6,000	9,000
Cutting speed, v (m/min)	94.248	188.496	282.743
Feed rate, f (µm/rev)	5	10	20
Axial depth of cut, a_p (µm)	70	150	250
Workpiece material: Al/SiC/45p; Cutting condition: dry			

5.5.3 Model calibration

Cutting forces in the experiments are measured and collected by using the dynamometer at the highest sampling rate of 51.2 KHz. This high sampling rate is enable to accommodate most of the dynamic characteristic in MMCs micro cutting process. The workpiece, which is fixed on the dynamometer via a fixture, will significantly change the dynamic response of the dynamometer. In order to achieve the measured cutting force more accurate, the transfer function from workpiece to the dynamometer has been identified during the micro milling process. The transfer function that represents the dynamic force response indicates that the force signal response has different value at varied frequency. Thus, a hammer test at three directions is introduced and performed to obtain the altered transfer function from workpiece to dynamometer, and the collected cutting forces signals are compensated by applying an extended transfer function.

5.5.3.1 Natural frequency and machine vibration

The natural frequency and machine vibration for this MMCs micro milling system has been identified in each direction. Figure 5-20 below shows the experimental configuration. From the frequency response results shown in Figure 5-21, the frequency at which system vibration is close to zero is observed as the optimal one. The optimal parameters are selected to minimise the vibration of machining system itself. The measure of vibrations in each direction is used to compensate the measured real time cutting force.

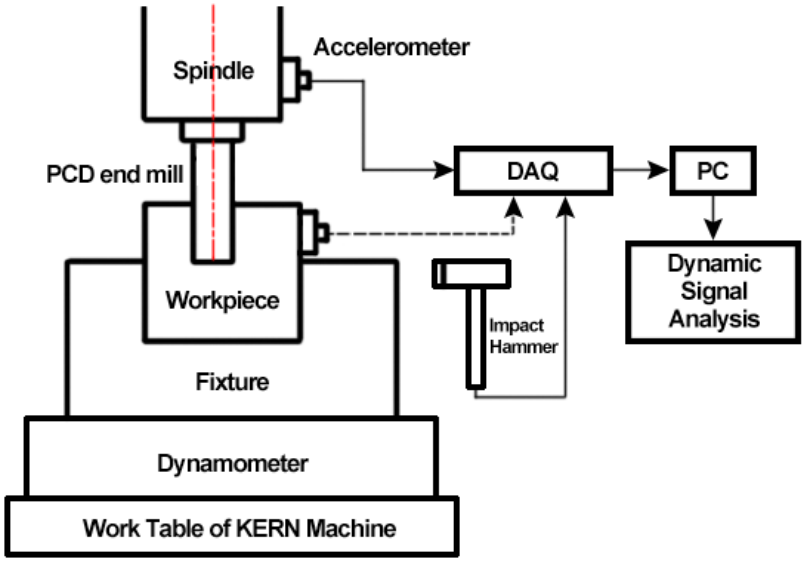

Figure 5-20 Experimental configurations

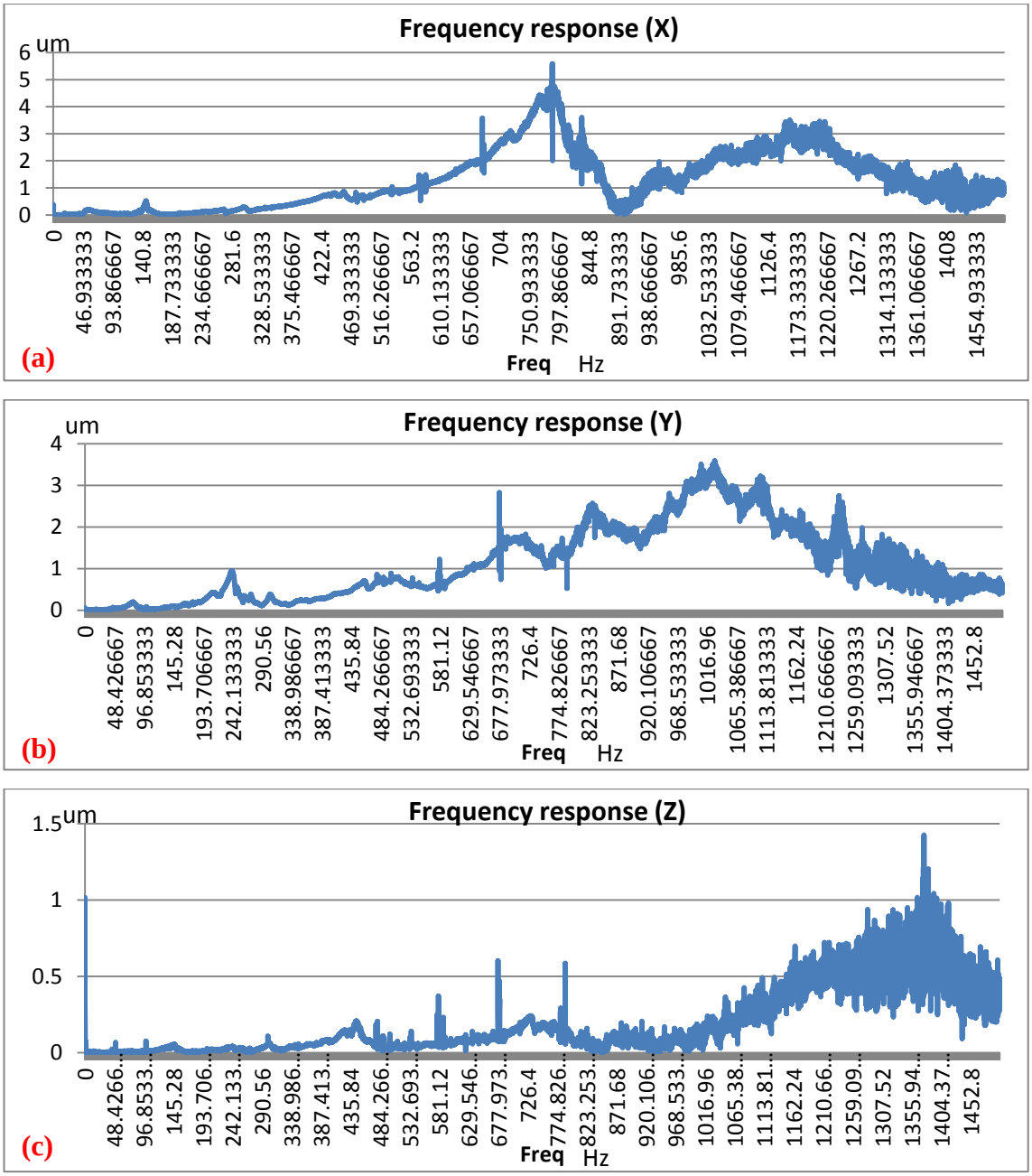

Figure 5-21 Natural frequency of machining system

5.5.3.2 Tool runout

The previous researches on the MMCs micro cutting forces indicate that the run-out of micro cutter is always unavoidable. The total net runout of cutting tool at different position is measured on the tool tip in order to calibrate the cutting force model. Tool manufacturing error, cutting tool dynamic error and alignment error are the main factors that affect the total tool runout value. The manufacturing error is measured by introducing the offline measurement with TESA-200 microscope and validated by using capacitive sensor MicroSense 5810 at extremely low spindle speed condition. The

cutting tool dynamic error is measured by using capacitive sensor at the spindle speed same to that used in experiments. In term of the alignment error, parallel tool offset error and tilt error are observed in the previous experimental research. Due to the depth of cut adopted is relative small in micro milling experimental trials, the effect of tilt error on the tool runout value is small. However, the parallel tool offset is significant. Thus, the alignment error is measured by using capacitive sensor during the MMCs micro milling process. The set-up for measurement of cutting tool runout is shown in Figure 3-5.

5.5.3.3 Machining system frequency response function

In order to determine the system dynamic characteristics in three cutting directions, the above mentioned hammer test is performed by using an impact hammer 9722A500 with hard steel head. The experimental configuration is illustrated in Figure 5-22. The pulse-form input signal with short duration time generated by impact hammer which contains wide range frequency and the response output signal on dynamometer are shown in Figure 5-23.

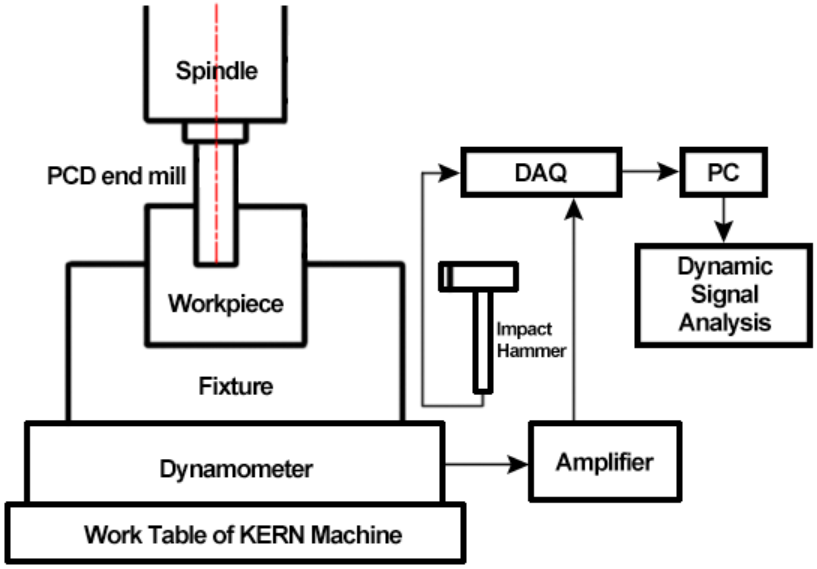

Figure 5-22 Experimental configurations

The curve fitted frequency response function (FRF) shown in Figure 5-24 performs spike at its natural frequency. This indicates that the measured signal is not the real force signal and has been amplified or diminished in this complicated measuring system. Thus, the compensation of measured force by introducing the transfer function is critical to achieve the actual cutting force value.

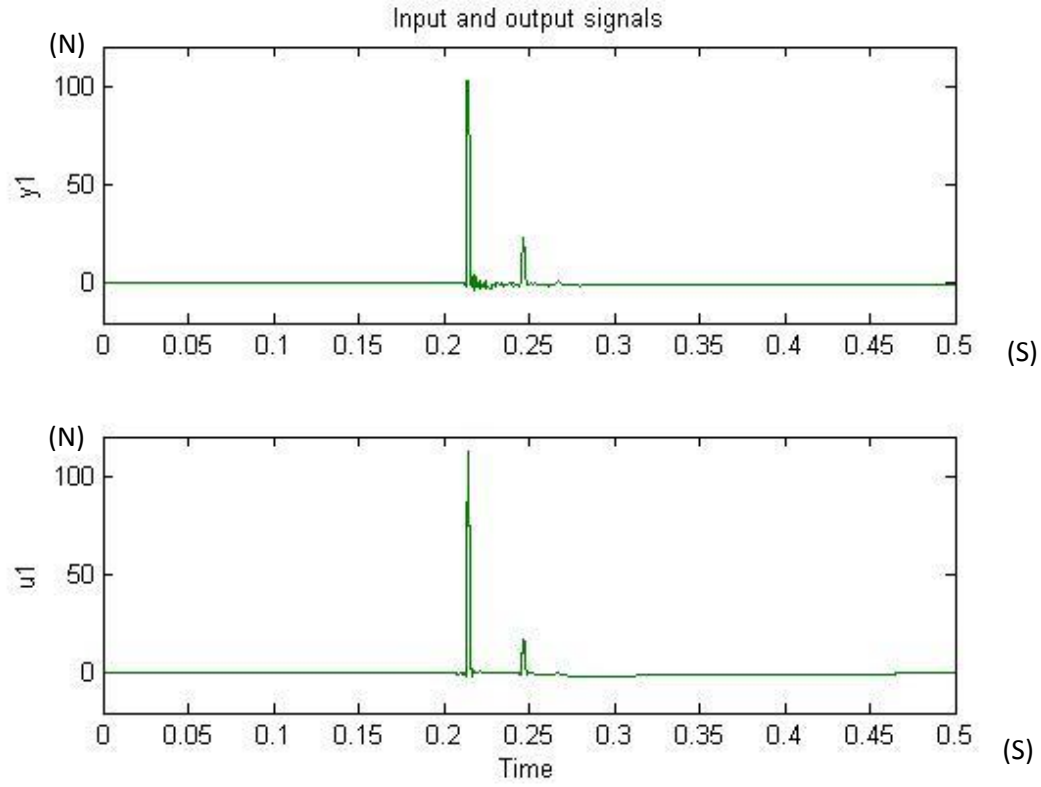

(a) System output and input signals in X axis

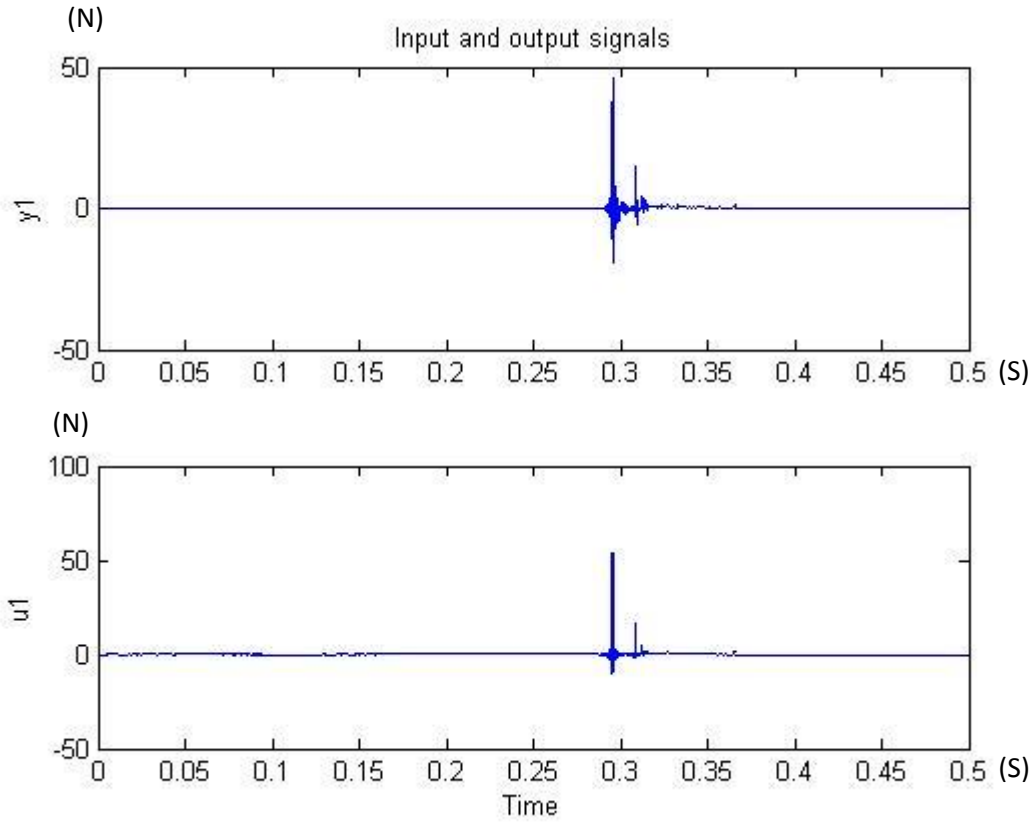

(b) System output and input signals in Y axis

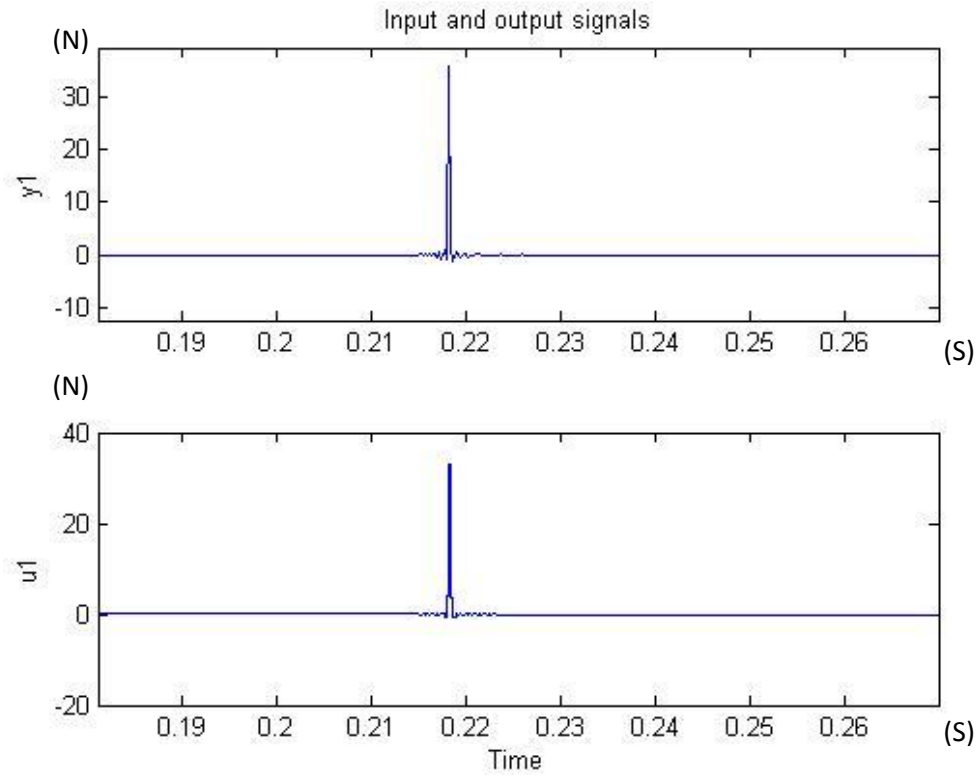

(c) System output and input signals in Z axis

Figure 5-23 System input and output signals in three directions

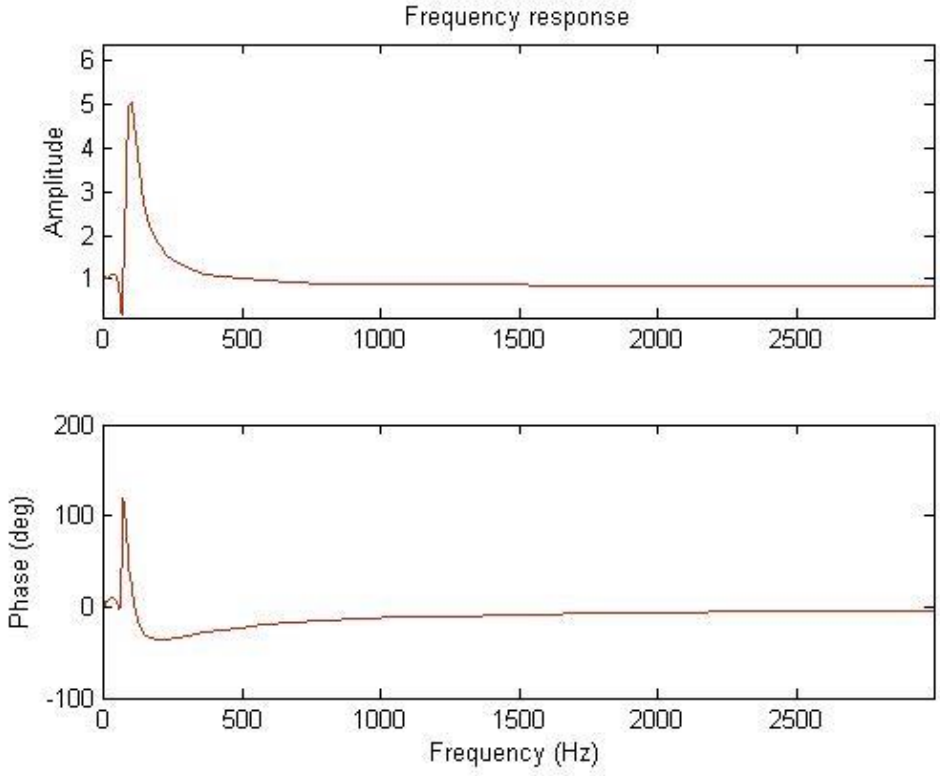

(a) System frequency response in X axis

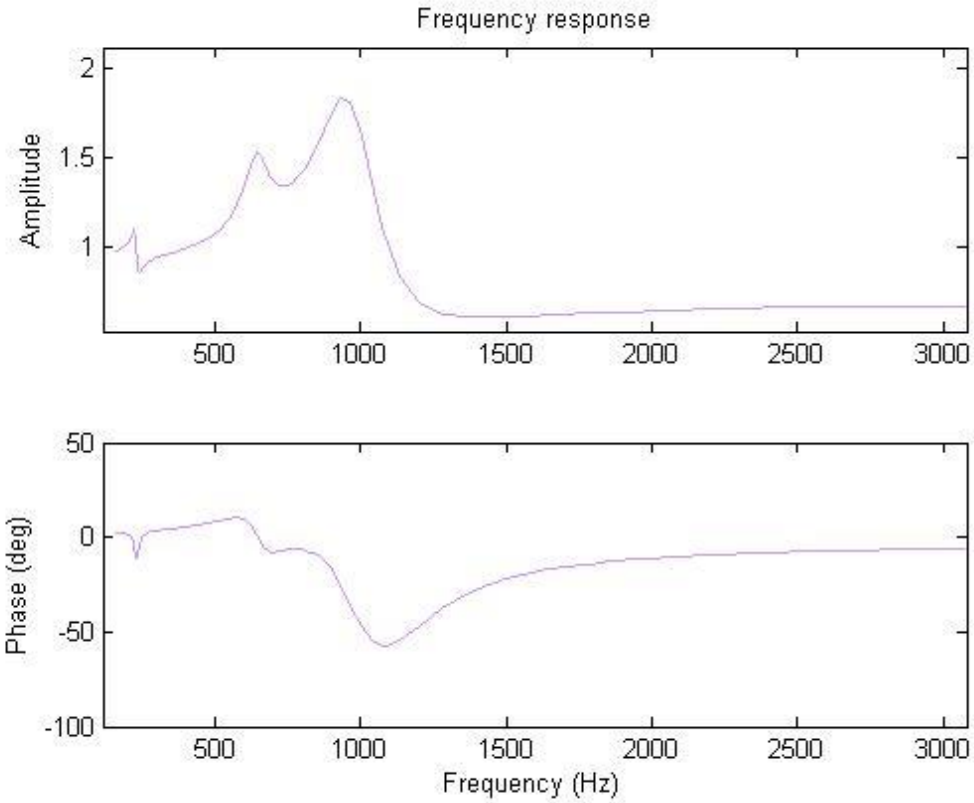

(b) System frequency response in Y axis

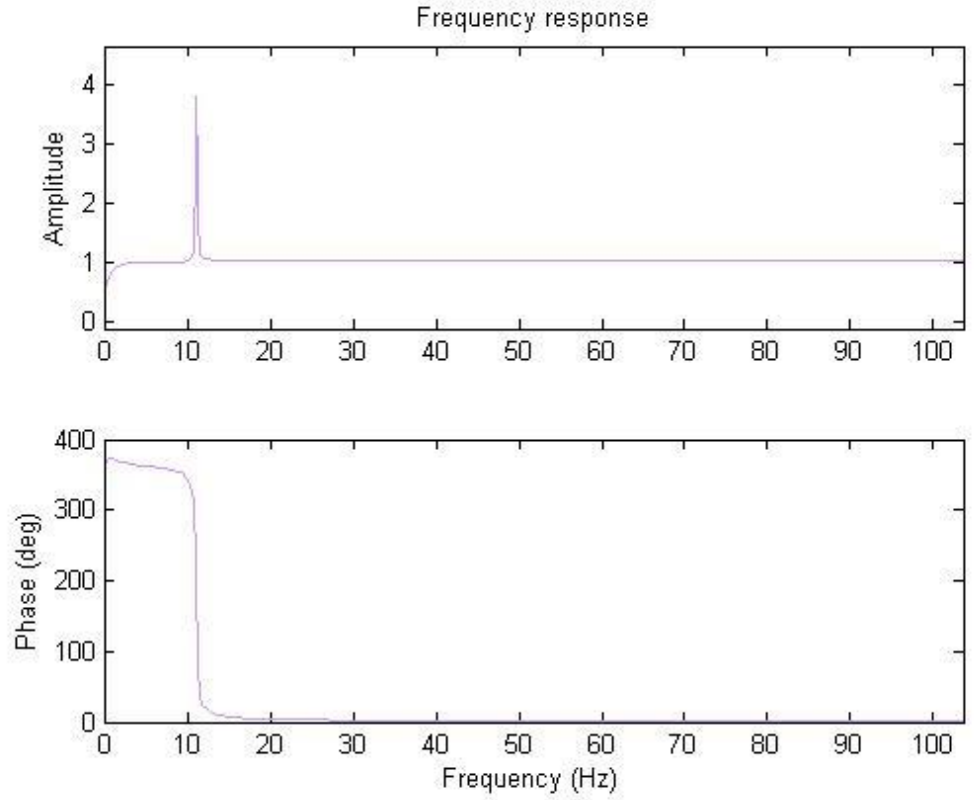

(c) System frequency response in Z axis

Figure 5-24 System frequency response in three directions

The transfer function from hammer to dynamometer stands for the actual force converts to the measured force. This is represented by a function of frequency H(s) in Laplace form which demonstrates the dynamic characteristics of this machining system. In order to achieve the actual forces from measured forces, a disturbance Kalman filter which acts as an inverse form transfer function $H^{-1}(s)$ is reconstructed shown as below.

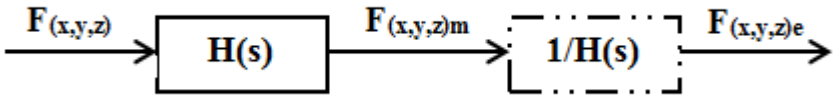

Figure 5-25 Schematic diagram of the cutting force measuring system

Thus, according to the machining system transfer function, the inverse form transfer function in x, y and z directions are estimated and given as below respectively.

The transfer function in x direction is derived as:

$$tfx = \frac{0.8522s^{10} + 1731s^9 + 7.267e^5s^8 + 3.165e^8s^7 + 9.3888e^{10}s^6 + 2.604e^{12}s^5 + 3.3e^{13}s^4 + 2.712e^{14}s^3 + 1.276e^{15}s^2 + 2.197e^{15}s - 9.399e^{14}}{s^{10} + 638.5s^9 + 6.999e^5s^8 + 1.974e^8s^7 + 9.16e^{10}s^6 + 2.447e^{12}s^5 + 3.822e^{13}s^4 + 2.867e^{14}s^3 + 1.791e^{15}s^2 + 3.159e^{15}s + 1.081e^{15}}$$

(5.44)

10 poles and 10 zeros are presented in this transfer function to demonstrate the complexity of dynamic characteristics. The transfer functions contains large scale coefficients in other directions are achieved in the similar methods shown as below.

The transfer function in y direction is derived as:

$$tfy = \frac{0.6948s^6 + 2604s^5 + 4.982e^7s^4 + 7.352e^{10}s^3 + 6.882e^{14}s^2 + 2.012e^{17}s + 1.214e^{21}}{s^6 + 2109s^5 + 5.728e^7s^4 + 5.693e^{10}s^3 + 7.373e^{14}s^2 + 1.682e^{17}s + 1.269e^{21}}$$

(5.45)

The parameterisation shows this continuous-time identified transfer function has 6 poles and 6 zeros.

The transfer function in z direction is derived as:

$$tfz = \frac{1.07s^4 + 2.136e^4s^3 + 3942s^2 + 1.024e^8s + 3.539e^8}{s^4 + 2.102e^4s^3 + 1.444e^5s^2 + 1.015e^8s + 5.782e^8} \quad (5.46)$$

The parameterisation shows this continuous-time identified transfer function has 4 poles and 4 zeros.

5.5.4 Model validation

Applying the frequency response function, the compensated cutting forces are more accurate to present the actual forces in MMCs precision machining process. The compensated cutting forces at varied cutting parameters are shown in figures below. The effectiveness of introduced functions is also shown in these figures by comparing the predicted and measured dynamic milling forces.

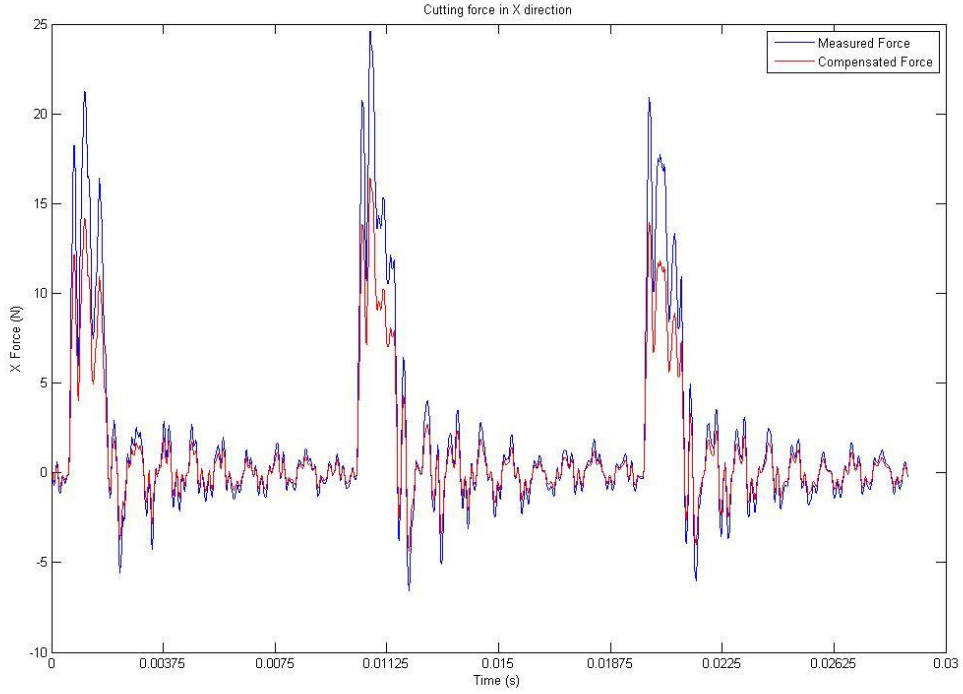

(a) feed rate: 10 µm/rev, depth of cut: 0.25 mm, cutting speed: 282.743 m/min

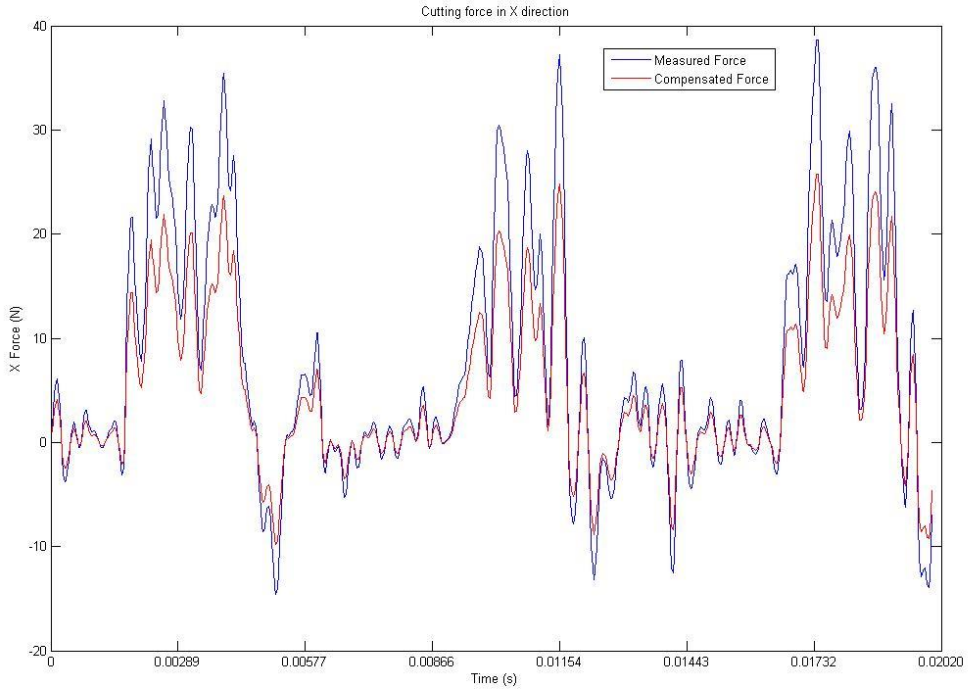

(b) feed rate: 20 μm/rev, depth of cut: 0.25 mm, cutting speed: 282.743 m/min

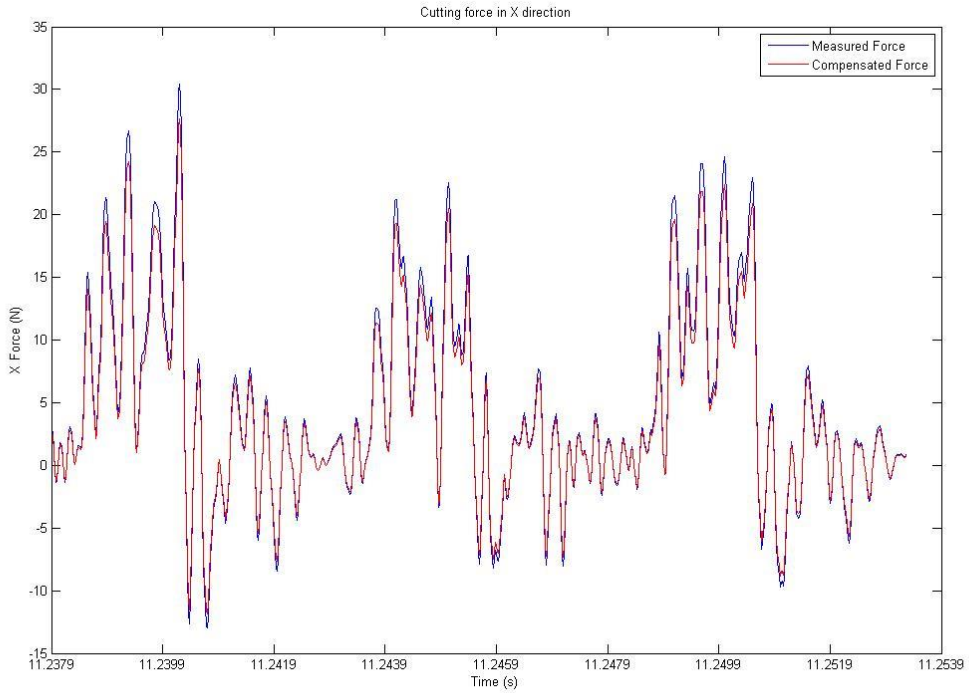

(c) feed rate: 20 μm/rev, depth of cut: 0.25 mm, cutting speed: 188.496 m/min

Figure 5-26 Measured and compensated forces in X axis

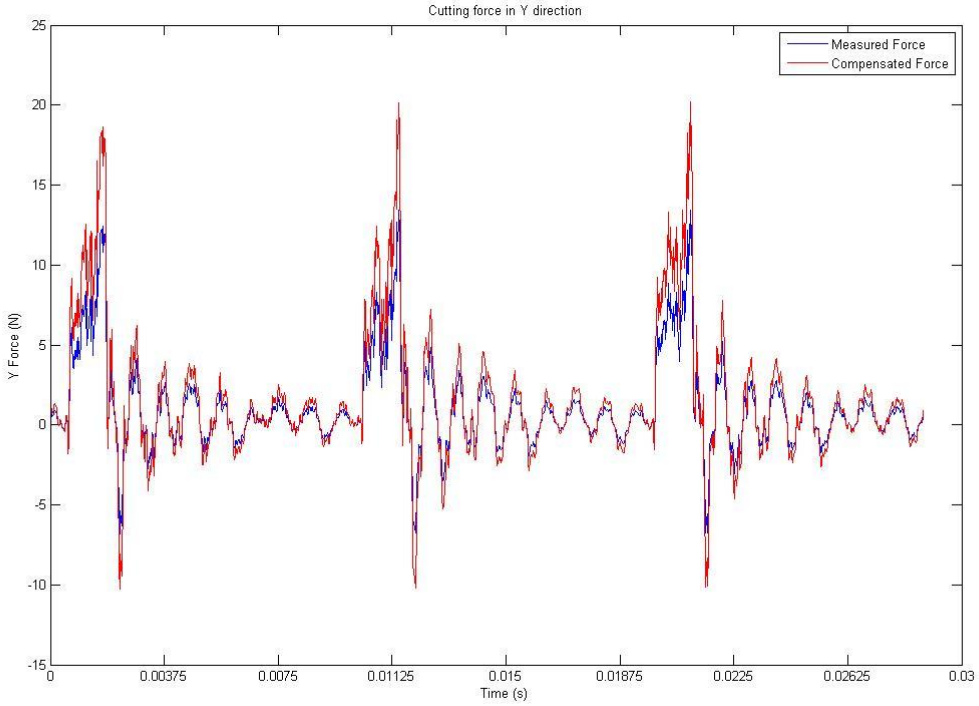

(a) feed rate: 10 µm/rev, depth of cut: 0.25 mm, cutting speed: 282.743 m/min

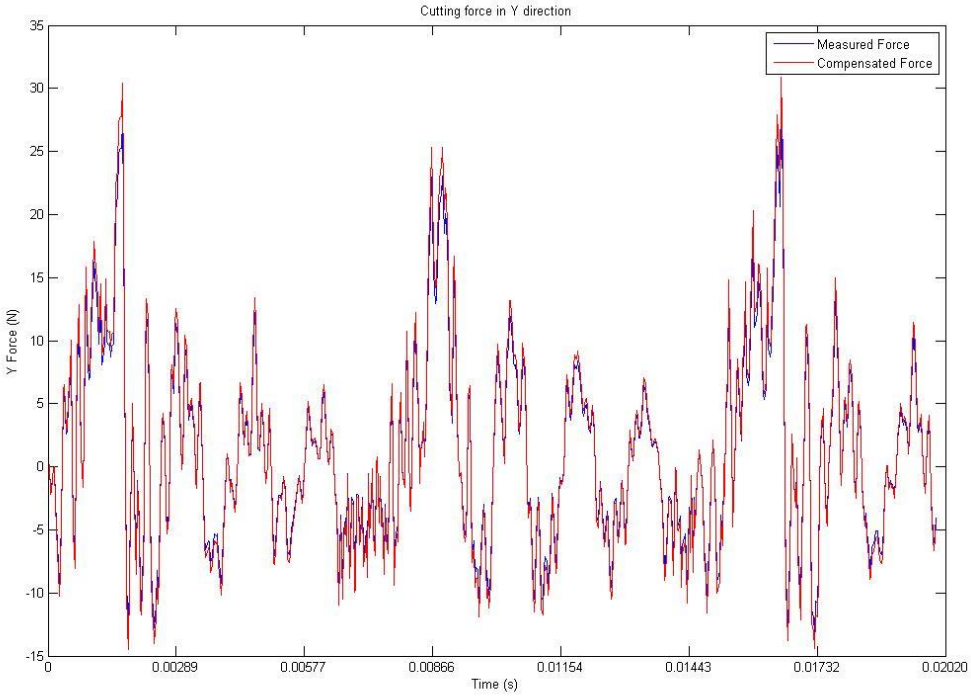

(b) feed rate: 20 µm/rev, depth of cut: 0.25 mm, cutting speed: 282.743 m/min

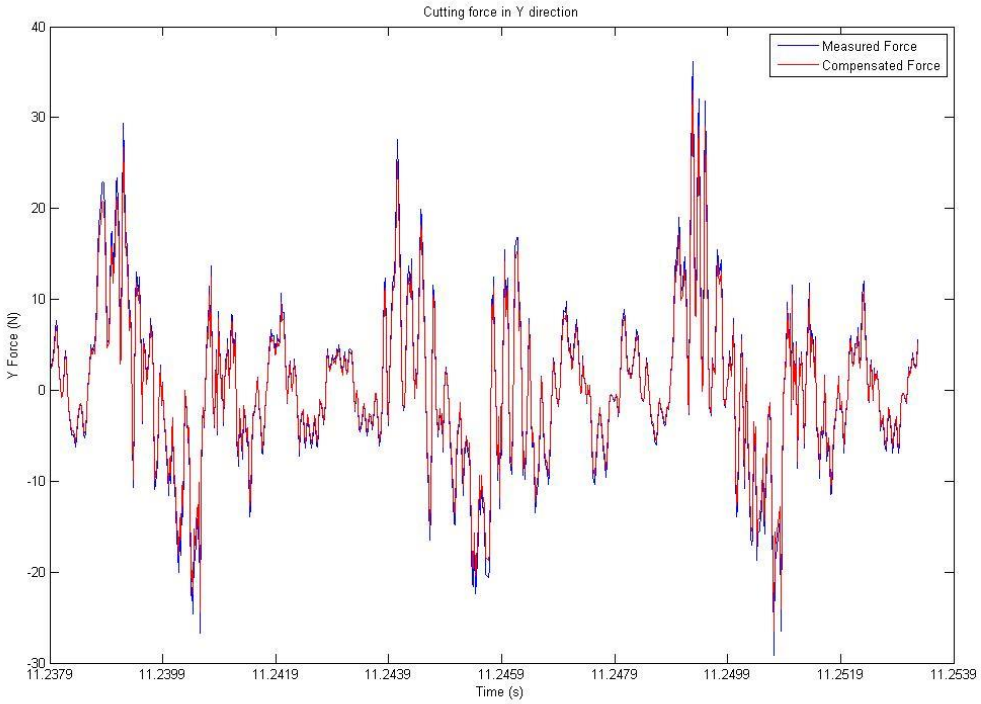

(c) feed rate: 20 µm/rev, depth of cut: 0.25 mm, cutting speed: 188.496 m/min

Figure 5-27 Measured and compensated forces in Y axis

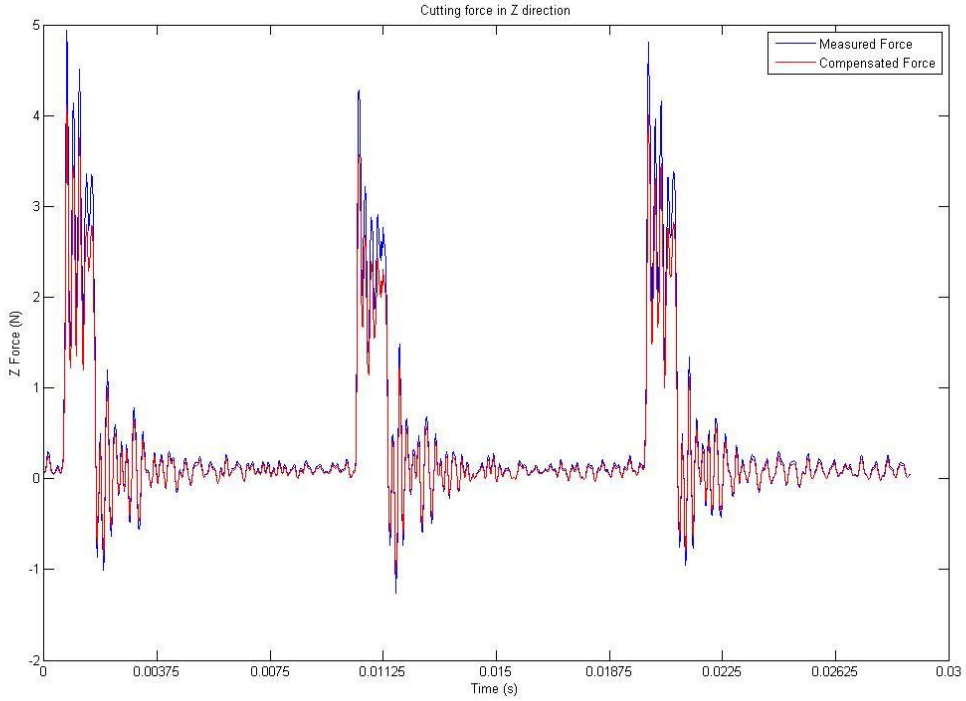

(a) feed rate: 10 µm/rev, depth of cut: 0.25 mm, cutting speed: 282.743 m/min

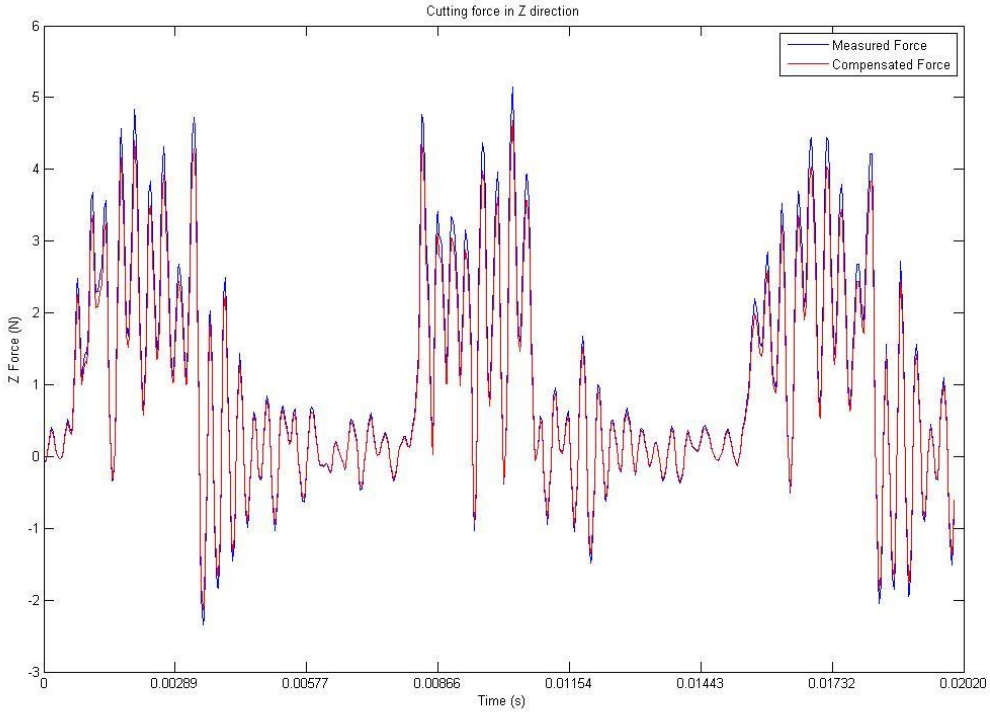

(b) feed rate: 20 μm/rev, depth of cut: 0.25 mm, cutting speed: 282.743 m/min

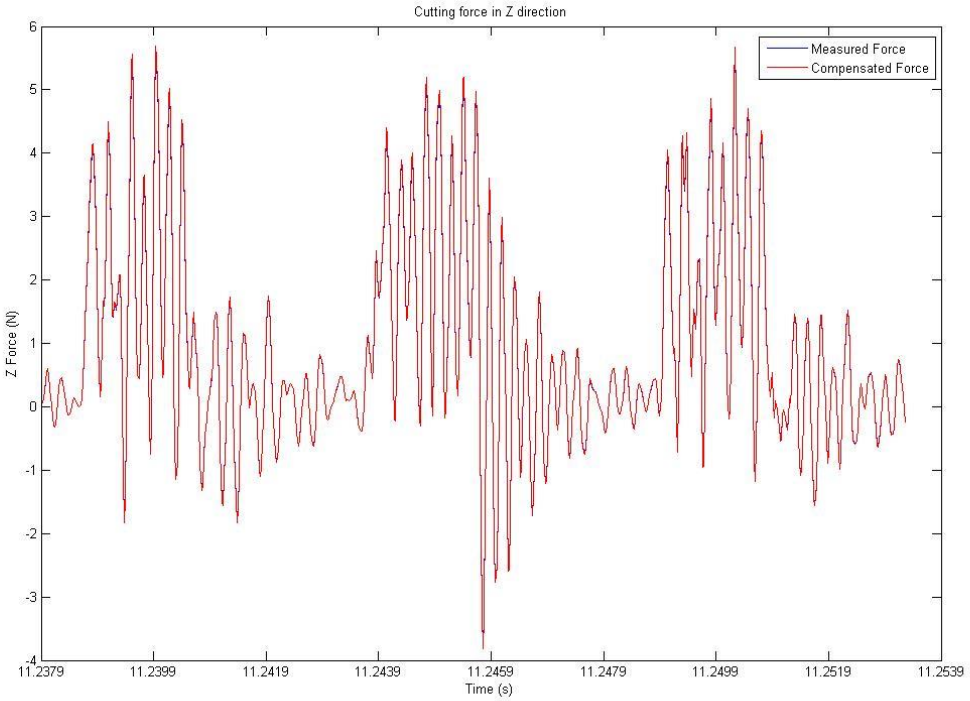

(c) feed rate: 20 μm/rev, depth of cut: 0.25 mm, cutting speed: 188.496 m/min

Figure 5-28 Measured and compensated forces in Z axis

From the distinct differences between measured force and compensated force shown in these figures, it can be observed that the cutting force magnitude at each time point reduced or increase after compensation. This indicates the value of measured cutting forces have been amplified or minified during the forces measuring process. In this research, all the measured cutting forces in the machining process including micro milling and precision turning are compensated according to this method and technique for accurate prediction and analysis. As the accuracy of compensated actual cutting force is strongly depended on the identified transfer function, the impact hammer and dynamometer should contain high accuracy and high sampling rate with high frequency response. On the other hand, the actual cutting forces at different cutting positions should be compensated by different transfer functions via multiple hammer tests.

The experiments are conducted under varied cutting parameters as shown in Table 5-1, the validation of dynamic cutting force model is carried out under these parameters by comparing the simulated cutting forces and compensated cutting forces. Power spectral density (PSD) represents the power present in the force signal as a function of frequency is also carried out. Figures below plot the predicted cutting force from simulation and measured cutting force from micro milling experiment at varied cutting conditions. These show a good agreement on cutting force vibration characteristics. This model is able to predict the magnitude and evolution of real cutting force.

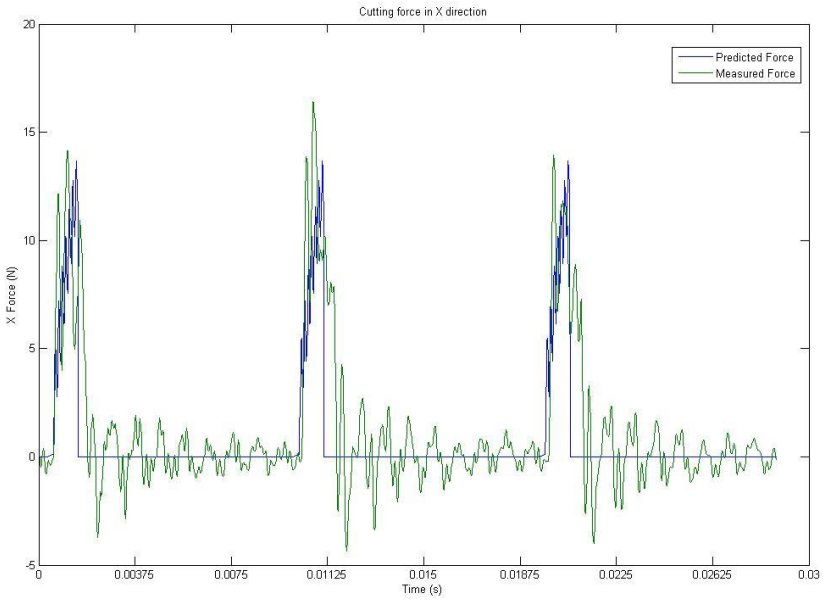

(a1) Predicted and measured cutting force in X direction

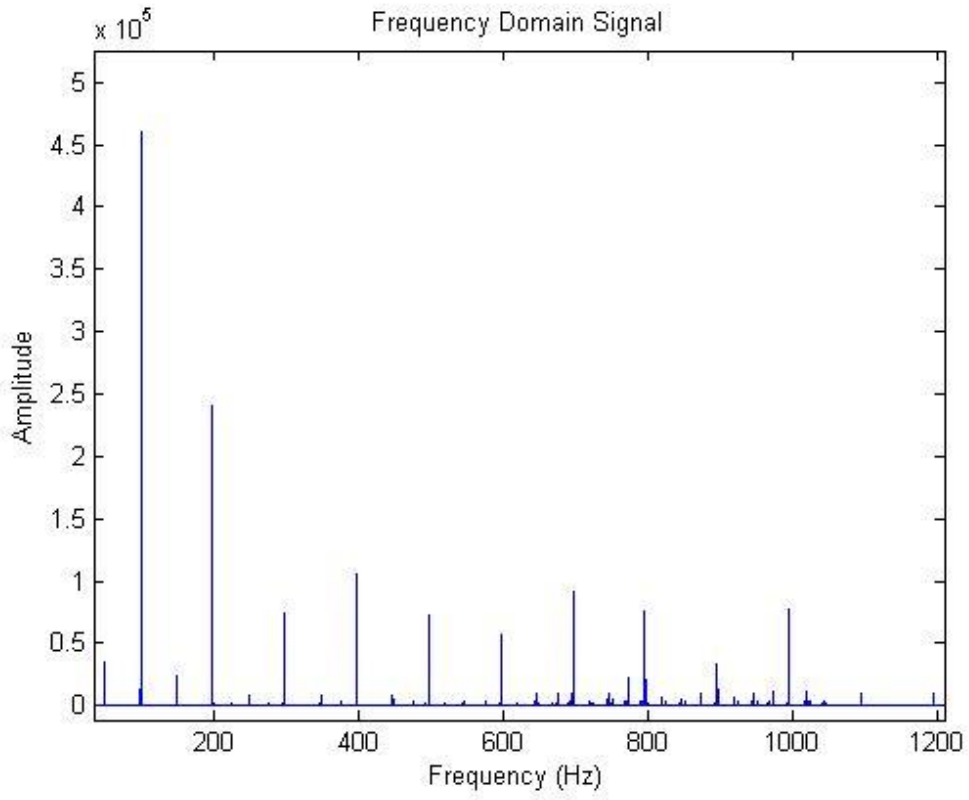

(a2) Power spectrum of Fx

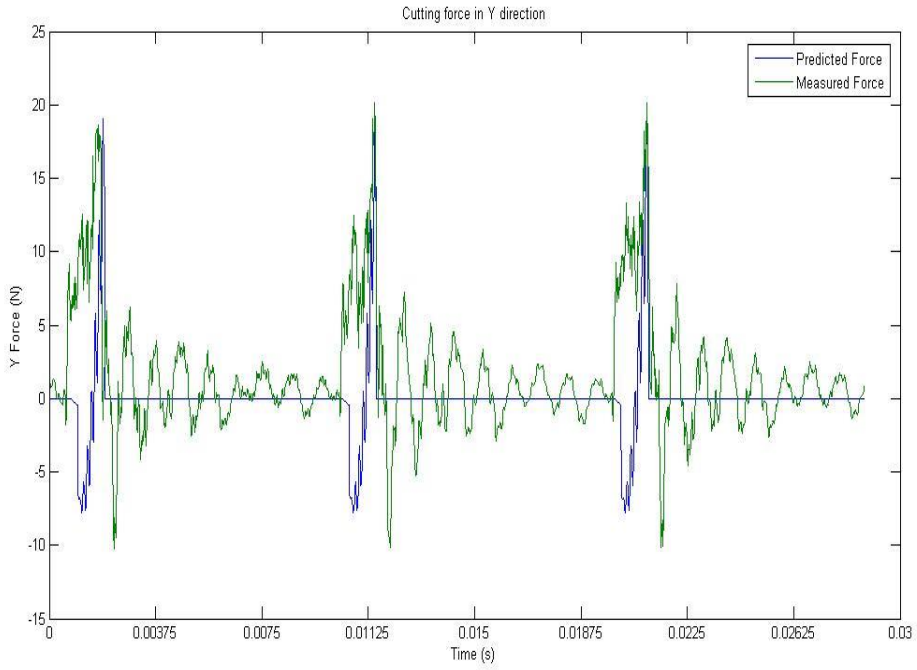

(b1) Predicted and measured cutting force in Y direction

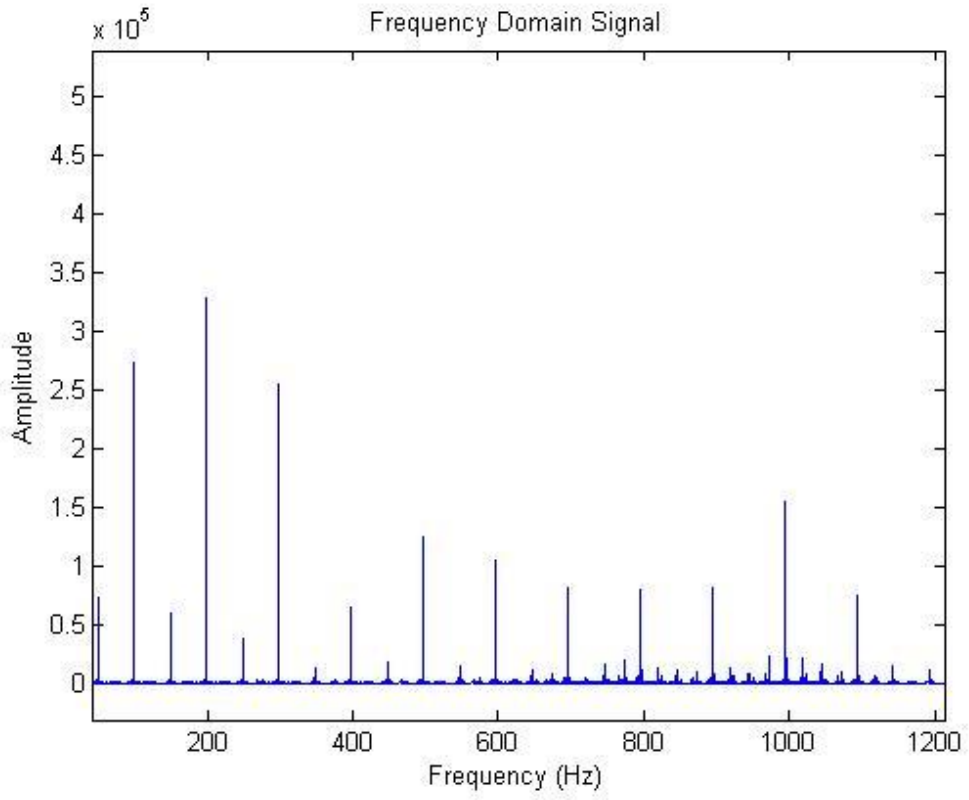

(b2) Power spectrum of Fy

Figure 5-29 Comparison between simulated and experimental forces in MMCs machining at feed rate: 10 μm/rev, depth of cut: 0.25 mm, cutting speed: 282.743 m/min

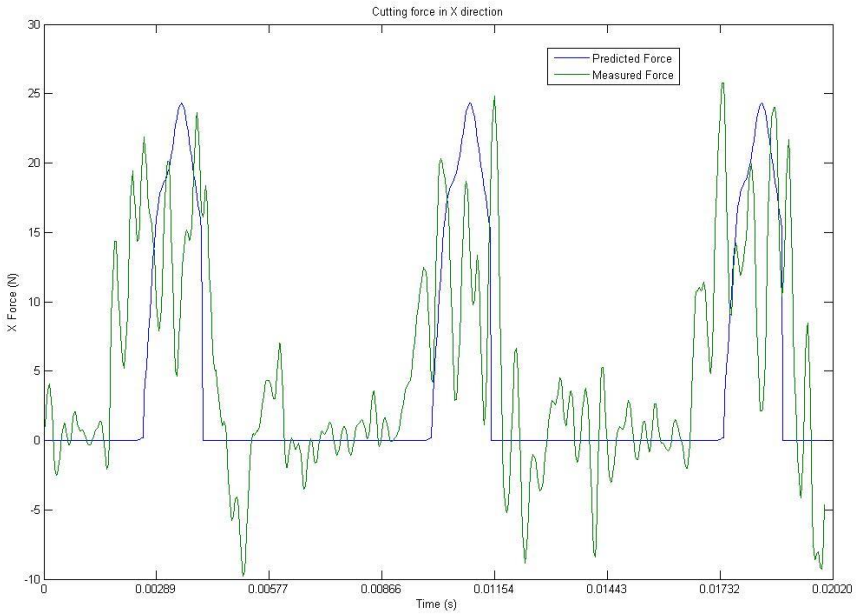

(a1) Predicted and measured cutting force in X direction

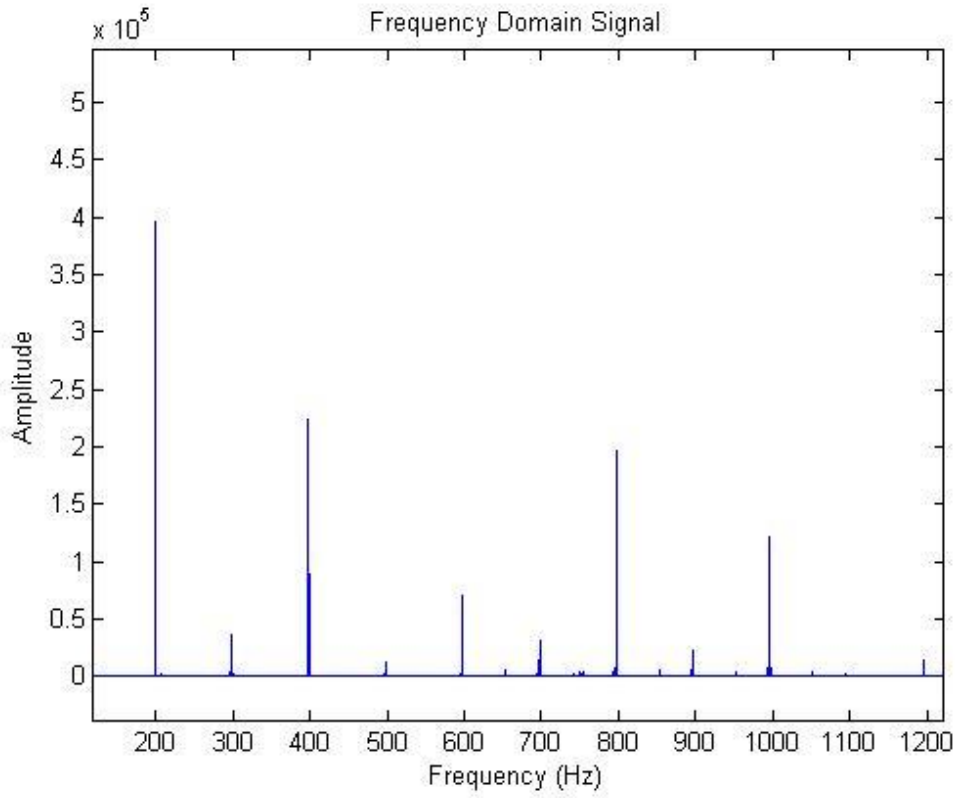

(a2) Power spectrum of Fx

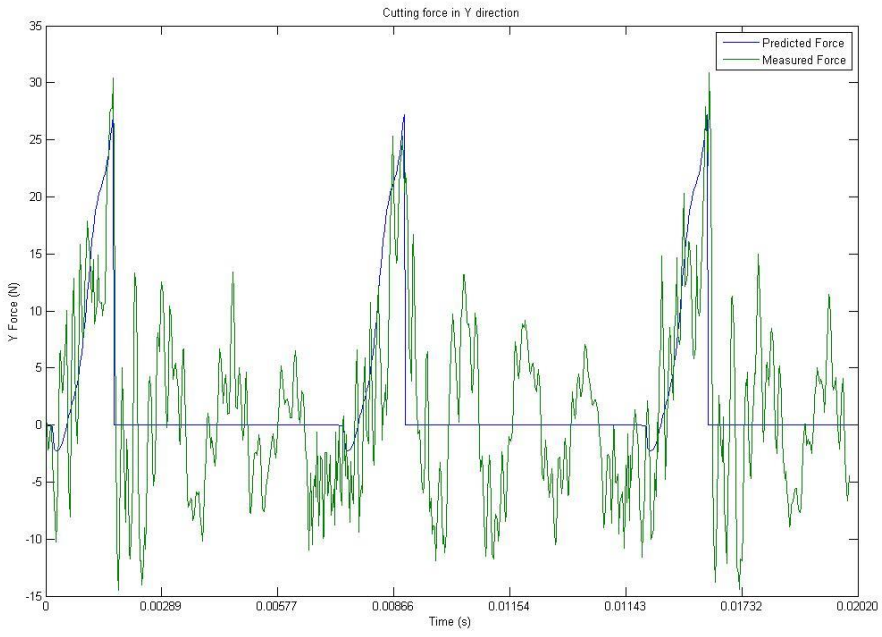

(b1) Predicted and measured cutting force in Y direction

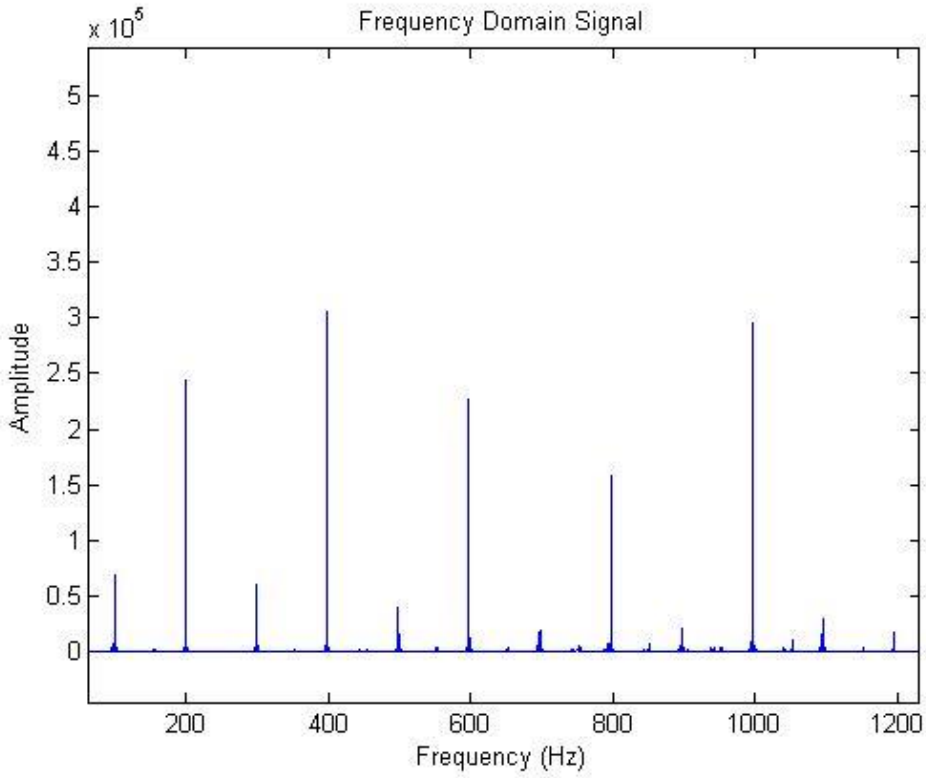

(b2) Power spectrum of Fy

Figure 5-30 Comparison between simulated and experimental forces in MMCs machining at feed rate: 20 μm/rev, depth of cut: 0.25 mm, cutting speed: 282.743 m/min

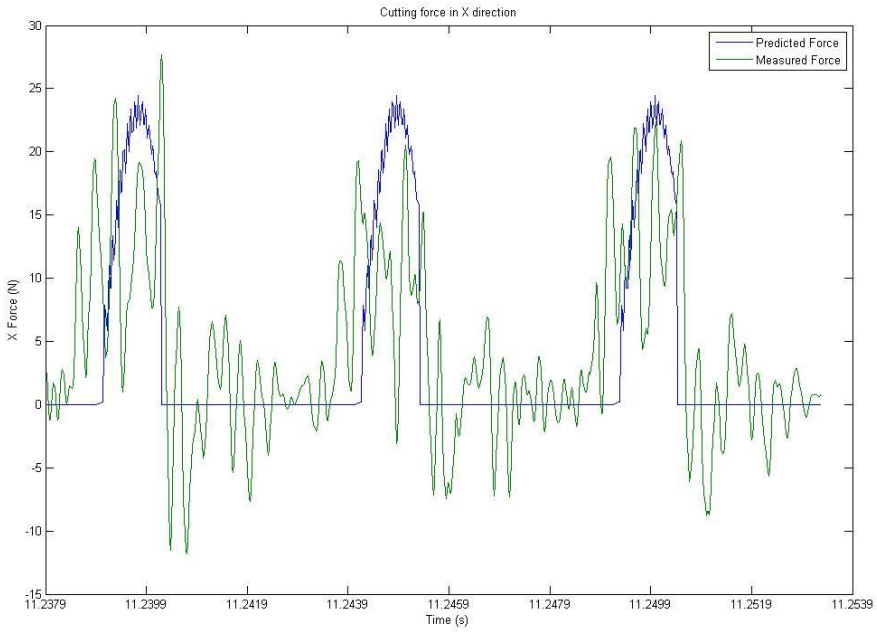

(a1) Predicted and measured cutting force in X direction

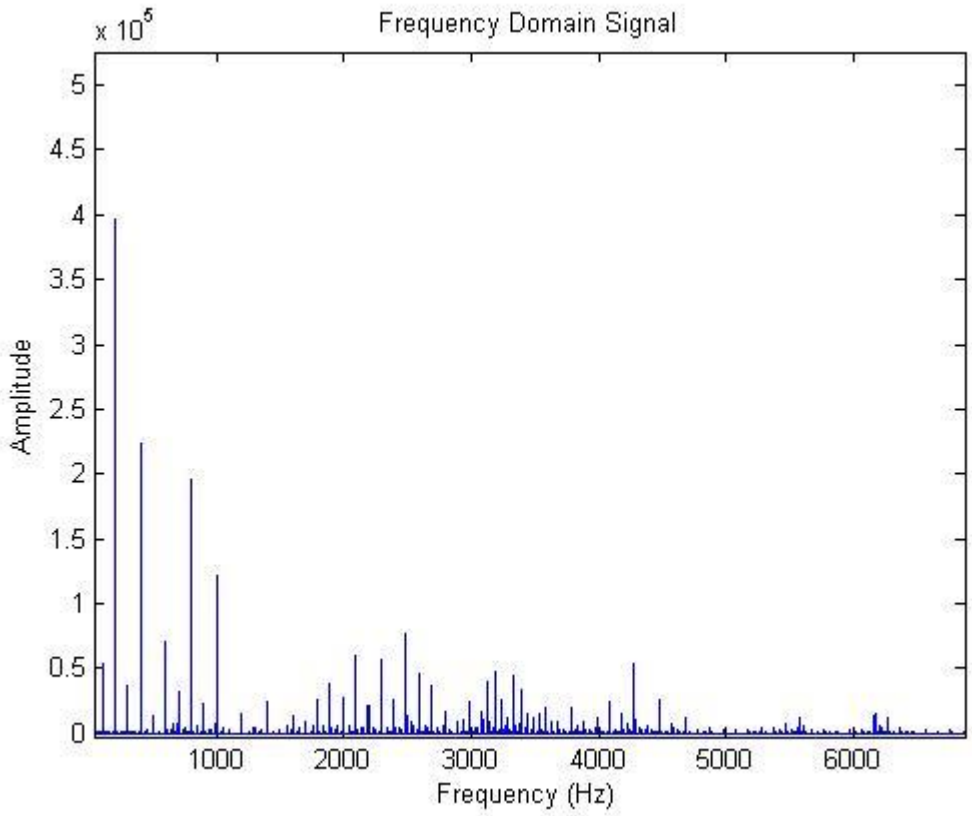

(a2) Power spectrum of Fx

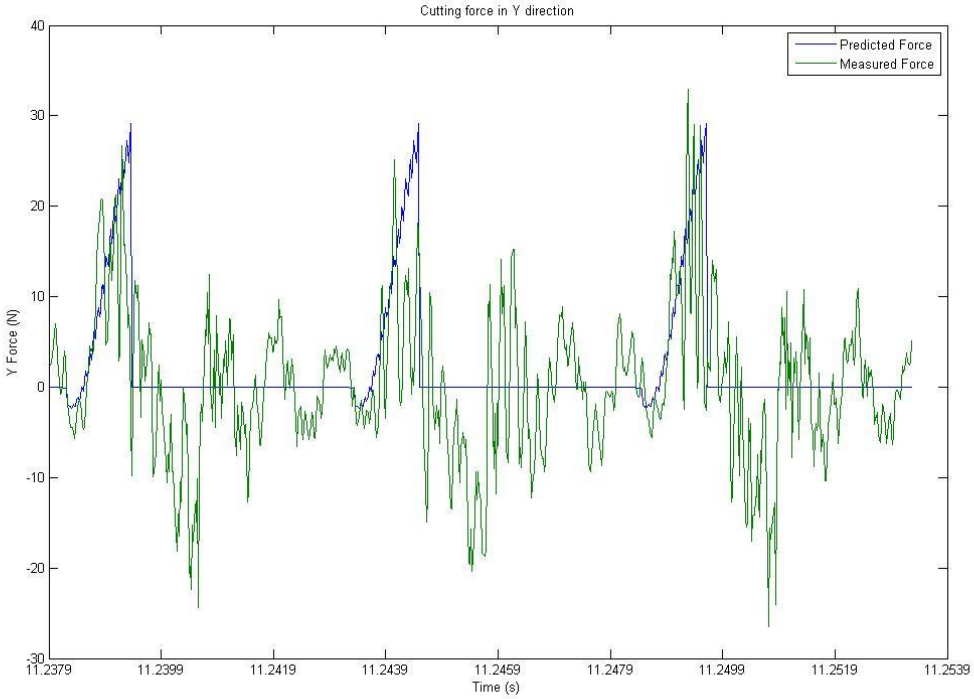

(b1) Predicted and measured cutting force in Y direction

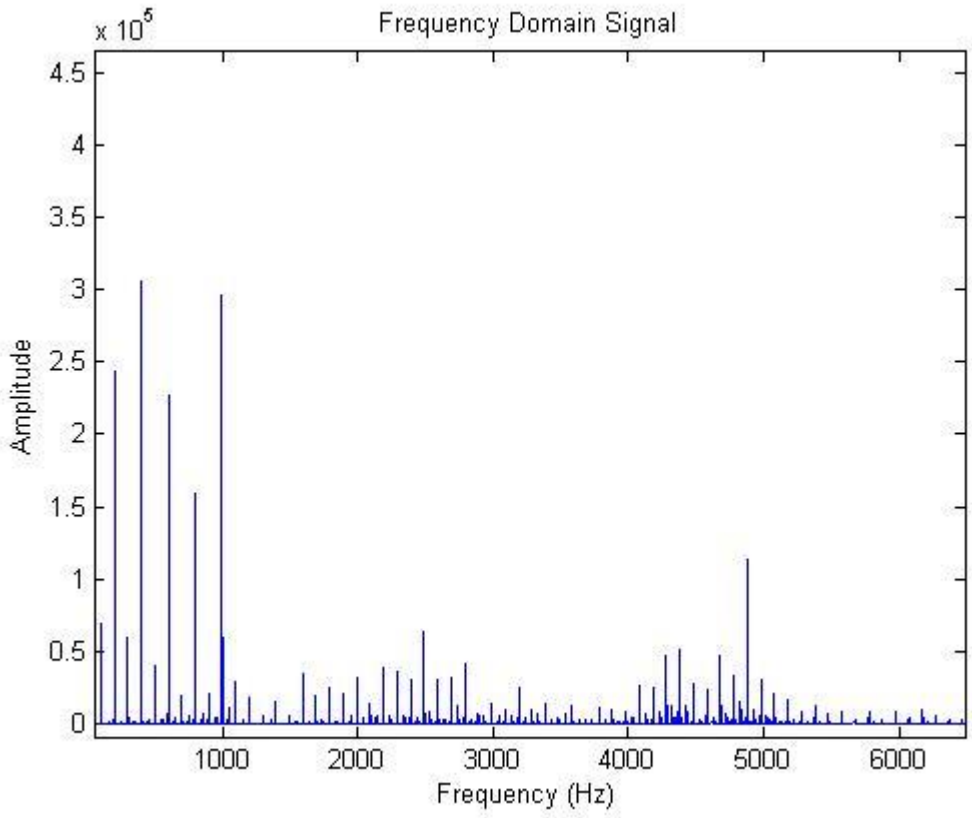

(b2) Power spectrum of Fy

Figure 5-31 Comparison between simulated and experimental forces in MMCs machining at feed rate: 20 μm/rev, depth of cut: 0.25 mm, cutting speed: 188.496 m/min

In general case, dominate cutting system vibration and force difference occur when the cutting force component experience the tooth passing frequency (TPF) and its harmonics. In turn, the vibration will result in the significant change of dynamic cutting forces. Thus, the amplitude of vibration and the influence of tool displacement on the dynamic cutting force can be minimised and undistinguished by considering the tool natural frequency and tool passing frequency. As a result, the predicted and measured forces after compensation perform consistency as shown in these cutting force figures. The milling force signals shown in Figure 5-29 to Figure 5-31 indicate that the predicted force value and force variation performs a reasonable agreement with the measured force value under varied cutting parameters in MMCs micro milling. Only slightly difference can be found on the force fluctuation in tool-material interacting process. The inconsistency and difference between simulated forces and measured forces at each time point can be attributed to the vibration of machining system in each direction that has been measured in section 5.5.3.1. However, it can be observed that the

measured force at uncut region is not zero and continue reduced force variation occurs. This is due to the unavoidable vibration between cutter and hard particles reinforced workpiece. Also, the attachment on the cutting tool may continue scratching the workpiece material and cause the further fluctuation of cutting force. In addition, the heterogeneous properties of MMCs workpiece and brittle character of reinforced particles may excite the vibrations between cutter and workpiece that result in the large force vibrations. Moreover, a significant difference between predicted and measured forces will be observed when a distinguished vibration or chatter is excited. While it is worth mentioning that there are some differences at various time points in cutting regions. This can be attributed to the unique size and unique distributions of reinforced particles. The differences on force magnitudes and force fluctuations are also influenced by the sampling frequency limitation and also the initial position and vibrations of cutting tools. Due to the large volume fraction of reinforced particles inside the matrix material, around 40 particles states between two signal time point. Thus, the slightly dislocation of particles may results in large force difference in real micro cutting process. These are the main reasons for severe vibration and further the distinguished inconsistency between the predicted forces and measured forces.

5.6 Concluding remarks

In this chapter, a theoretical analytical dynamic cutting force model generated in particle reinforced MMCs precision machining process is investigated and developed. This innovative dynamic cutting force model is presented by further considering the effects of unavoidable cutting tool run-out, actual chip thickness and tool tip trajectory. The expression on dynamic cutting force and its experimental evaluation and validation are aimed to further develop the scientific understanding on MMCs cutting mechanics and machinability. The detailed conclusions can be drawn as follows:

1. The MMCs dynamic cutting force model is improved and modified closely from the previous homogeneous material machining force model. The theoretical model appropriately demonstrates the detailed MMCs milling force variation including the matrix material shearing force and particle fracture force through analytical expression.
2. Cutting force values under varied process variables are conducted and suitable for general MMCs micro milling process. The simulation results indicate that feed

rate, radial depth of cut, axial depth of cut and also the particle size and volume fraction have significantly effects on the predicted cutting force variation.

3. Evaluation and validation of dynamic cutting force model is carried out through well-designed experimental trials. The measured forces are compensated via hammer-dynamometer test determined transfer function. The force model has a good agreement with the measured force value in MMCs micro milling process, when the system vibration is faint. The vibration is unavoidable and force component at TPF and machine natural frequency may increase the vibration of cutting system.
4. The accurate prediction on dynamic cutting force can be further used to improve the resultant surface form accuracy and also reduce the surface roughness and form error by choosing the optimal process variables and cutting parameters in MMCs precision machining.

Chapter 6 Thermal-mechanical-tribological multiphysics analysis on tool wear and tool performance

6.1 Cutting temperature partition in MMCs precision machining

6.1.1 Estimation of heat generation in MMCs precision machining process

The heat generated at the cutting zone and the resultant cutting temperature are of great importance in MMCs precision machining process due to their significant influence on the cutting force magnitude, machined surface properties, tool-workpiece friction, resultant tool wear and tool life, surface and sub-surface generation and energy consumption. The involved thermal-mechanical-tribological coupled interaction between cutting tool and target composite material significantly affect the cutting solid mechanics, heat transfer, material physical and mechanical properties etc. Although SiC/Al and B_4C/Al MMCs contain low sensitivity to the heat generated during the micro machining due to their specific high heat conductivity, the influence of heat generation and resultant cutting temperature on the mechanical aspects such as tool wear and cutting force are still significant. Therefore, it is essential to develop a scientific understanding on the heat generation, heat distribution and their associate influence particularly on cutting force and tool wear in MMCs precision machining.

The critical heat generation in MMCs precision machining can be observed as the heat generated and dissipated at five areas around tool-workpiece interface as depicted in Figure 6-1.

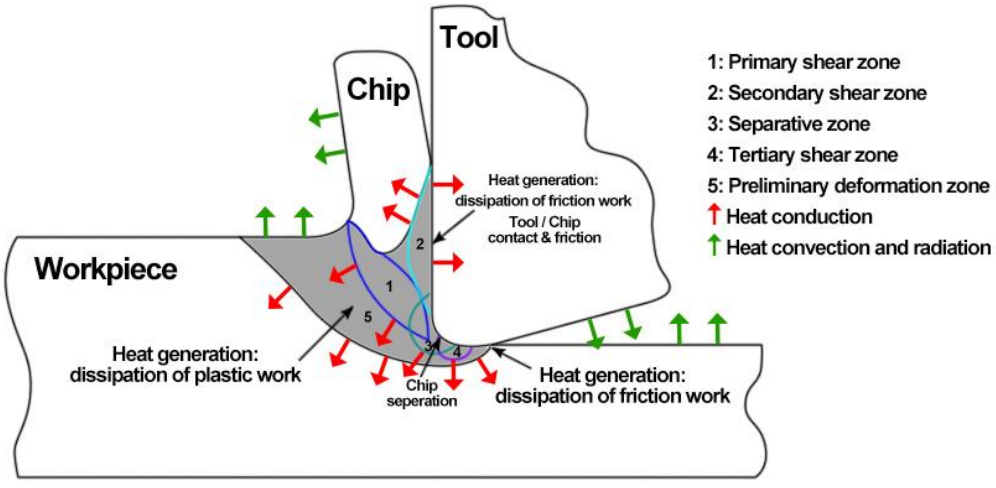

Figure 6-1 Heat generation in MMCs precision machining

The first heat source is the heat generated at the shear plane. The resultant heat in this zone will flow into the workpiece and chip. The second one is generated by the chip formation at the tool-chip contact surface. The converted heat source in this area will partly transfer to the tool-chip interaction point on the workpiece. The rest will transfer to chip and cutting tool respectively. The third one is the friction heat generated at the tertiary shear zone. In this area, the heat will partly transfer to the workpiece and tool body and the rest will transfer into the ambient environment. The fourth one is generated by friction between the tool and workpiece material at the material separate zone in sliding and chip formation direction respectively. One occurs at the tool-chip interface and the other one occurs at the tool-remain surface interface. The last heat source is the material deformation heat generated at the material deformation zone. The cutting energy results from the elastic and plastic deformation in this area will totally convert into heat source in the workpiece. Therefore, the resultant cutting temperature can be determined by the heat source which contains uniform heat flux distribution. It can be illustrated by introducing the temperature rise theory. The cutting energy consumption during the MMCs precision machining process can be obtained from the sum of $Q_{1\text{-}5}$, which is the cutting energy consumption in these five zones respectively as shown in Figure 6-1. While, the energy generated from tool and workpiece interaction will not completely convert to heat, thus, the actual cutting heat generation and resultant cutting temperature in each zone can be demonstrated as follows.

(1) Shear plane temperature in the primary shear zone

According to the analytical model from previous research by Shaw [247], the cutting temperature generated at the primary shear zone in micro machining process can be illustrated from the shear energy aspects. The conventional cutting temperature analytical method for the evaluation of the metal cutting is contributed by Trigger and Chao. Their theory determines the average chip temperature arise that influenced by the heat source at the shear plane. Thus, in MMCs precision machining process, the average cutting temperature of chip and workpiece on the shear plane can be modified and expressed as below:

$$\overline{T_{s-chip1}} = \frac{R_1 * q_1 * (t_c * d * \csc \emptyset)}{C_1 * \rho_1 * V * t_c * d} + T_0 \tag{6.1}$$

$$\overline{T_{s-workpiece1}} = 0.754 * \frac{(1 - R_1) * q_1 * \frac{(t_c * \csc \emptyset)}{2}}{k * \sqrt{L_1}} + T_0 \tag{6.2}$$

Thus, the cutting temperature can be written as:

$$\overline{T_{s-chip1}} = \frac{R_1 * q_1 * \csc \emptyset}{C_1 * \rho_1 * V} + T_0 = R_1 * q_1 * i_1 + T_0 \tag{6.3}$$

$$\overline{T_{s-workpiece1}} = 0.754 * \frac{(1 - R_1) * q_1 * \frac{(t_c * \csc \emptyset)}{2}}{k * \sqrt{L_1}} + T_0 = (1 - R_1) * q_1 * i_2 + T_0 \tag{6.4}$$

where,

$$i_1 = \frac{\csc \emptyset}{C_1 * \rho_1 * V} \tag{6.5}$$

$$i_2 = 0.754 * \frac{(t_c * \csc \emptyset)}{2 * k * \sqrt{L_1}} \tag{6.6}$$

where, k is the thermal conductivity of workpiece, $R_1 * q_1$ and $(1 - R_1) * q_1$ are the heat per unit time per unit area that left on the chip and workpiece in the shear zone respectively, t_c is the uncut chip thickness, T_0 is the initial temperature in the cutting zone, $C_1 * \rho_1$ is the volume specific heat at the mean temperature; where C_1 is the specific heat capacity and ρ_1 is the density. The heat flows from the shear zone per unit time per unit area q_1 can be expressed as below:

$$q_1 = \frac{F_s * V_s}{J * t_c * d * \csc \emptyset} \tag{6.7}$$

The cutting temperature on the chip and workpiece at the contact area should be equal, thus, the resultant cutting temperature can be expressed as:

$$\overline{T_{s-chip}} = \overline{T_{s-workpiece}} \tag{6.8}$$

$$R_1 = \frac{1}{1 + \frac{i_1}{i_2}} \tag{6.9}$$

The value of R_1 is modified and calculated from the following equations. According to the theory of Loewen and Shaw, the dimensionless velocity parameter L_1 is defined as follow in this precision machining process:

$$L_1 = \frac{V_s * (\frac{t_c * \csc \emptyset}{2})}{2 * K_1} = \frac{V * g * t_c}{4 * K_1} \tag{6.10}$$

Therefore, R_1 can be written as:

$$R_1 = \frac{1}{1 + 1.328 * \sqrt{\frac{K_1 * g}{V * t_c}}} \tag{6.11}$$

where, K_1 is the thermal diffusivity of the workpiece material and g is the strain in the chip. Therefore, the chip and workpiece temperature at the shear zone can be expressed as below:

$$\overline{T_{s-chip1}} = \frac{\frac{1}{1 + 1.328 * \sqrt{\frac{K_1 * g}{V * t_c}}} * \frac{F_s * V_s * V * \sin \emptyset}{J} * \csc \emptyset}{C_1 * \rho_1 * V} + T_0$$

$$\overline{T_{s-workpiece1}} = 0.754 * \frac{(1 - \frac{1}{1 + 1.328 * \sqrt{\frac{K_1 * g}{V * t_c}}}) * \frac{F_s * V_s * V * \sin \emptyset}{J} * \frac{(t_c * \csc \emptyset)}{2}}{k * \sqrt{L_1}} + T_0 \tag{6.12}$$

(2) Tool-chip interface temperature in the secondary shear zone

The friction between the contact surfaces of cutting tool and chip are observed as another heat source in MMCs precision machining. The resultant cutting temperature generated on the chip and tool surfaces in the secondary shear zone can be illustrated from the shear energy aspects as below:

$$\overline{T_{s-chip2}} = \frac{0.754 * R_2 * q_2 * \frac{a_{i1}}{2}}{k * \sqrt{L_2}} + T_0{}'$$
$$\overline{T_{s-tool1}} = \frac{(1 - R_2) * q_2 * a_{i1}}{k'} * \bar{A} + T_0{}'' \tag{6.13}$$

where, $R_2 * q_2$, $(1 - R_2) * q_2$ are the heat per unit time per unit area that left on the chip and cutting tool in the tool-chip interaction zone. $T_0{}'$ is the initial temperature in the tool-chip interaction surface, . $T_0{}' = \overline{T_{s-chip1}}$. $T_0{}''$ is the initial ambient temperature of the cutting tool, where in this MMCs micro milling process, $T_0{}'' = T_0$. k' is the thermal conductive of the cutting tool material. $\bar{A}$ is the area factor, which is a function of the aspect ratio of the surface area represented by m/l. The value of $\bar{A}$ can be found according to the aspect ratio m/l in the following equation.

$$\frac{m}{l} = \frac{d}{2 * a_{i1}} \tag{6.14}$$

where, d is the width of chip and a_{i1} is the chip contact length in the cutting direction.

The initial chip temperature is

$$T_0{}' = \overline{T_{s-chip1}} \tag{6.15}$$

Due to the cutting temperature on the chip and tool should be equal, the resultant cutting temperature can be expressed as:

$$\overline{T_{s-chip2}} = \overline{T_{s-tool1}}$$
$$R_2 = \frac{1 + \frac{T_0 - \overline{T_{s-chip1}}}{q_2 * i_4}}{1 + \frac{i_3}{i_4}} \tag{6.16}$$

The dimensionless velocity parameter L_2 is defined as below:

$$L_2 = \frac{V_c * \frac{a_{i1}}{2}}{2 * K_2} \tag{6.17}$$

where, K_2 is the thermal diffusivity of the chip at the final temperature.

The heat flows from the interface per unit time per unit area q_2 can be expressed as below:

$$q_2 = \frac{F_c * V_c}{J * d * a_{i1}} \tag{6.18}$$

The value of R_2 is modified and calculated from the following equation:

$$R_2 = \frac{q_2 * \left(a_{i1} * \frac{\bar{A}}{k'}\right) - \overline{T_{s-chip1}} + T_0}{q_2 * \left(a_{i1} * \frac{\bar{A}}{k'}\right) + \frac{0.754 * q_2 * \frac{a_{i1}}{2}}{k * \sqrt{L_2}}} \tag{6.19}$$

Therefore, the chip and tool temperature at the secondary shear zone can be expressed as below:

$$\begin{aligned}
&\overline{T_{s-chip2}} \\
&= \frac{0.754 * \frac{\frac{F_c * V_c}{J * d * a_{i1}} * \left(a_{i1} * \frac{\bar{A}}{k'}\right) - \overline{T_{s-chip1}} + T_0}{\frac{F_c * V_c}{J * d * a_{i1}} * \left(a_{i1} * \frac{\bar{A}}{k'}\right) + \frac{0.754 * \frac{F_c * V_c}{J * d * a_{i1}} * \frac{a_{i1}}{2}}{k * \sqrt{L_2}}} * \frac{F_c * V_c}{J * d * a_{i1}} * \frac{a_{i1}}{2}}{k * \sqrt{L_2}} \\
&+ \overline{T_{s-chip1}} \\
&\overline{T_{s-tool1}} \\
&= \frac{(1 - \frac{\frac{F_c * V_c}{J * d * a_{i1}} * \left(a_{i1} * \frac{\bar{A}}{k'}\right) - \overline{T_{s-chip1}} + T_0}{\frac{F_c * V_c}{J * d * a_{i1}} * \left(a_{i1} * \frac{\bar{A}}{k'}\right) + \frac{0.754 * \frac{F_c * V_c}{J * d * a_{i1}} * \frac{a_{i1}}{2}}{k * \sqrt{L_2}}}) * \frac{F_c * V_c}{J * d * a_{i1}} * a_{i1}}{k'} \\
&* \bar{A} + T_0
\end{aligned} \tag{6.20}$$

(3) Friction heat in the tertiary shear zone

The friction between tool flank face and the remained workpiece surface is observed as another heat source in precision machining of MMCs. The heat source in this friction area can be observed as the elliptical shape heat source with uniform heat flux distribution. The cutting temperature generated in this cutting zone can be illustrated by the following equation [248]:

$$\Delta T_{f(3)} = \frac{2 * q_3 * a_{i1}}{k_1 * \sqrt{\pi * (E * S_e + P_{e1})}} \tag{6.21}$$

(4) Friction heat in material separate zones

The heat source in these two friction areas can be observed as the elliptical shape heat source with uniform heat flux distribution. Thus, the temperature rise in these areas and the total cutting temperature on these two contact surfaces can be calculated with the following equations respectively [248].

$$\Delta T_{f(4a)} = \frac{2 * q_4 * a_{i2}}{k_2 * \sqrt{\pi * (E * S_e + P_{e2})}}$$
$$\Delta T_{f(4b)} = \frac{2 * q_5 * a_{i3}}{k_3 * \sqrt{\pi * (E * S_e + P_{e3})}} \tag{6.22}$$

where, $q4$ and $q5$ are the heat flux densities, which are the heat rate supply per unit area. a_{i2} is the contact length between chip and tool rake surface and a_{i3} is the contact length between the tool flank surface and workpiece. $k2$ and $k3$ are the thermal conductivity of the workpiece materials. Due to the material removal processed are from the same workpiece, the thermal conductivity in these two equations can be expressed as $k2 = k3 = k$. E is the constant. P_{e2} and P_{e3} are the Peclet number of the workpiece material. The Peclet number is further illustrated as below.

Peclet number or Peclet criterion, as a similarity number to characterise the influence of the regime in metal cutting with respective to the machining workpiece material, is used to better understand on the thermal energy in hard machining process. The Peclet number is used to represent the critical process variables in terms of machining process parameters. In MMCs precision machining process, due to the cutting edge radius cannot be ignored, the Peclet number is used particularly for illustrating the parameters in tool-workpiece sliding and chip formation process as shown in the following equations:

$$P_{e1} = \frac{v_1 * t_1}{w_w}$$
$$P_{e2} = \frac{v_2 * t_2}{w_w} \tag{6.23}$$

where, v_1 and v_2 are the velocities of the moving sources in these two processes, w_w is the thermal diffusivity of the workpiece material. w_w can be calculated from the following equation:

$$w_w = \frac{k_w}{(C_p\rho)_w} \tag{6.24}$$

where, k_w is the thermal conductivity of the workpiece material, $(C_p\rho)_w$ is the volume specific heat of the workpiece material.

$$\Delta T_{f-tool2} = \frac{2 * q * (a_{i1} + a_{i2} + a_{i3})}{k * \sqrt{\pi * (E * S_e + P_e)}} \tag{6.25}$$

Due to the deformation heat in the precision machining process is much low than other heat, the heat generated in deformation zone can be observed as $\Delta T_{f(5)} = 0$.

Thus, the temperature of the cutting tool can be expressed as below:

$$T_{tool} = \Delta T_{f-tool2} + \overline{T_{s-tool1}} \tag{6.26}$$

6.1.2 Multiphysics based finite element analysis of cutting temperature

Accrding to the consideration from Loewen and Shaw that chip and workpiece material were seen as two separated bodies, the cutting energy is not totally contained in these equations. In addition, the MMCs precision machining process is much more complex than the conventional metal cutting that the friction between tool-workpiece couple and the chip generation performs significant differences. Thus, the cutting temperature is then predicted through the aspects of total heat source by introducing multiphysics based FE modelling and analysis.

The thermal-mechanical-tribological coupled multiphysics method is applied in the simulation of heat partition. As the MMCs material properties and the material removal process are strongly depended on the temperature, the change of material properties will in turn affect the heat generation and temperature distribution. In addition, the physics are fully coupled together and affect each other; the simulation process is therefore becoming much more complicate.

In MMCs precision machining process, the most dissipated energy due to material deformation and tool-chip interfacial friction is assumed to convert into thermal energy

as a heat source. The chip formation and chip sliding on the tool rake face results in the increase of cutting temperature, and governs the tool wear and tool failure. In this multiphysics based FE analysis, the inelastic energy dissipation due to plastic deformation gives rise to a heat rate per unit volume that can be expressed as [236]:

$$r^{pl} = \eta_m \sigma \varepsilon^{pl} \tag{6.27}$$

where, r^{pl} is the heat rate per unit volume, η_m is the fraction of dissipated mechanical energy converted to heat, σ is the equivalent stress, and ε^{pl} is the rate of plastic straining. As a fraction of heat flow away along the chips, the rest is dissipated into cutting tool and remained workpiece.

The frictional heat at tool-chip interface can be observed as another heat source. Thus, the heat rate per unit area released at the tool-chip interface can be expressed as [236]:

$$r_f = \eta_f \tau_c \dot{\gamma} \tag{6.28}$$

where, r_f is heat rate per unit area in friction area, η_f is the fraction of the friction energy convert into heat, τ_c is the frictional stress, and $\dot{\gamma}$ is the slip rate.

The density of heat flux at tool-chip interface r_t can be illustrated as a function of heat generation in friction area r_f, heat flux results from the chip deformation at friction region r_c and fraction of heat energy convert into chip β and can be given by:

$$r_t = r_c - \beta r_f \tag{6.29}$$

Fraction of heat energy convert into chip β, which is used to demonstrate the heat rate conducted into the cutting tool according to the heat absorption co-efficient of cutting tool material, is given as:

$$\beta = \frac{E_c}{E_c + E_t} \tag{6.30}$$

where, E_c and E_t are the heat energy conducted on the chip and cutting tool respectively. These can be expressed as:

$$\begin{aligned} E_c &= \sqrt{K_c \rho_c C_{pc}} \\ E_t &= \sqrt{K_t \rho_t C_{pt}} \end{aligned} \tag{6.31}$$

where, K_c and K_t are conductivities of chip and tool surfaces respectively, C_{pc} and C_{pt} are heat capacities of chip and tool contact surfaces respectively. In this machining process, part of the heat will lose to the environment owing to convection and radiation, and the ambient temperature is assumed to stay constant.

The simulation set-up is illustrated in Chapter 4 in details. The target material is SiC/Al MMCs and SiC particles with 5 μm grain size are embedded into the aluminium matrix. The cutting tools applied are straight flute PCD end mill and PCD inserts with zero rake angle. The simulations are carried out at varied cutting speed and DOC for investigating the heat generation and temperature distribution which is determined by heat flux conducted from the too-workpiece interaction.

6.1.3 Simulation results and discussion

Figure 6-2 and Figure 6-3 show the cutting temperature distribution at varied DOC and cutting speed respectively in the simulations of MMCs machining. When machining on the matrix material, the simulation results indicate that the highest temperature on the workpiece material is normally along the round cutting edge rather than the area that largest plastic deformation occurs. In term of the cutting tool, the highest temperature occurs around the round cutting edge while close to the material separation point. This attributes to the heat source results from both material plastic deformation and tool/workpiece interfacial friction. When machining on the brittle particles, the highest temperature can be observed at the tool-particle interaction point where particle fracture occurs as shown in Figure 6-4. The resultant temperature is much higher than that in machining on matrix material.

It also can be found that the maximum cutting temperature at the same cutting length increase when increase the depth of cut. This is due to more material deformation occurs at larger DOC and more heat are generated. In addition, the maximum cutting temperature always increases along with the cutting speed increase. This is due to the strain rate in primary and secondary deformation zones as well as friction force increase at higher cutting speed.

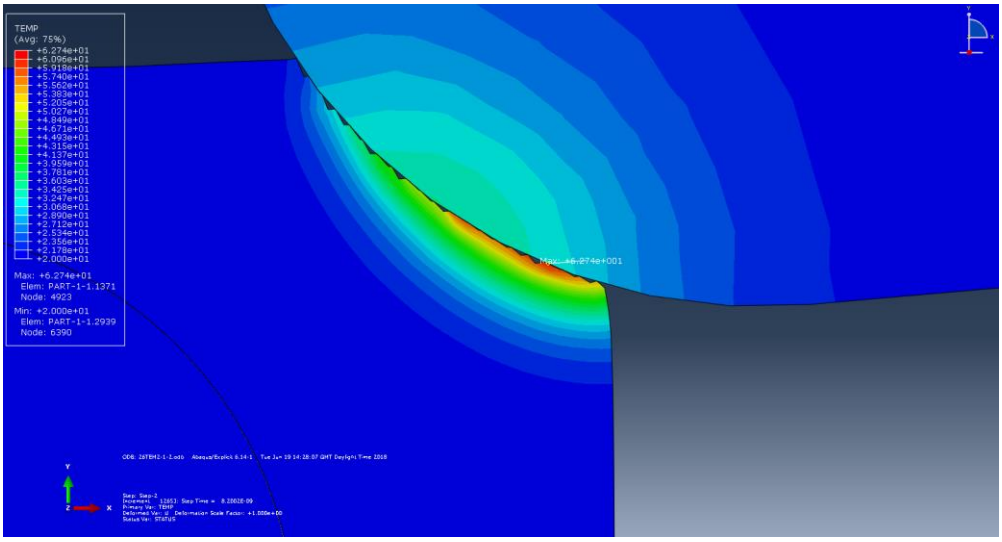

(a) DOC: 1.5 μm

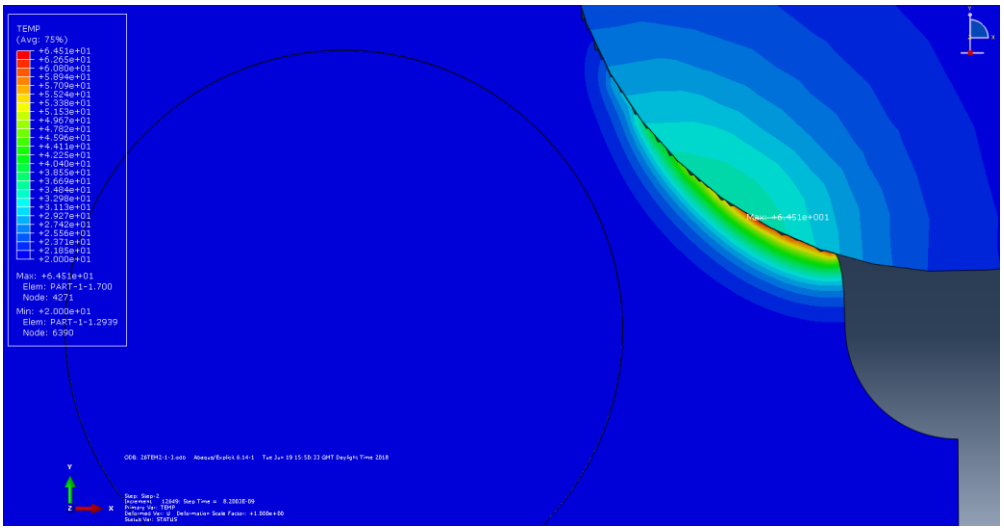

(b) DOC: 3 μm

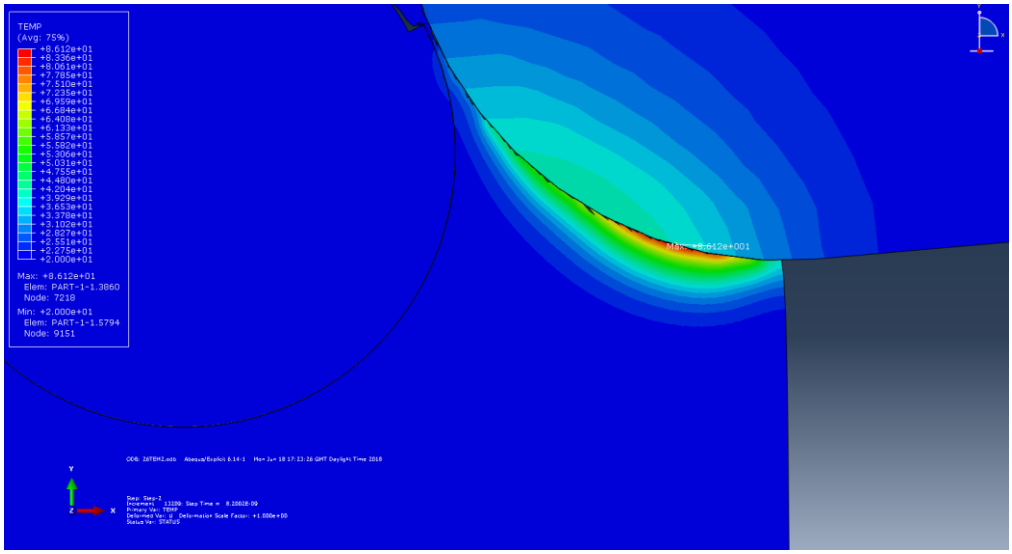

(c) DOC: 4.5 μm

Figure 6-2 Cutting temperature under varied depth of cut

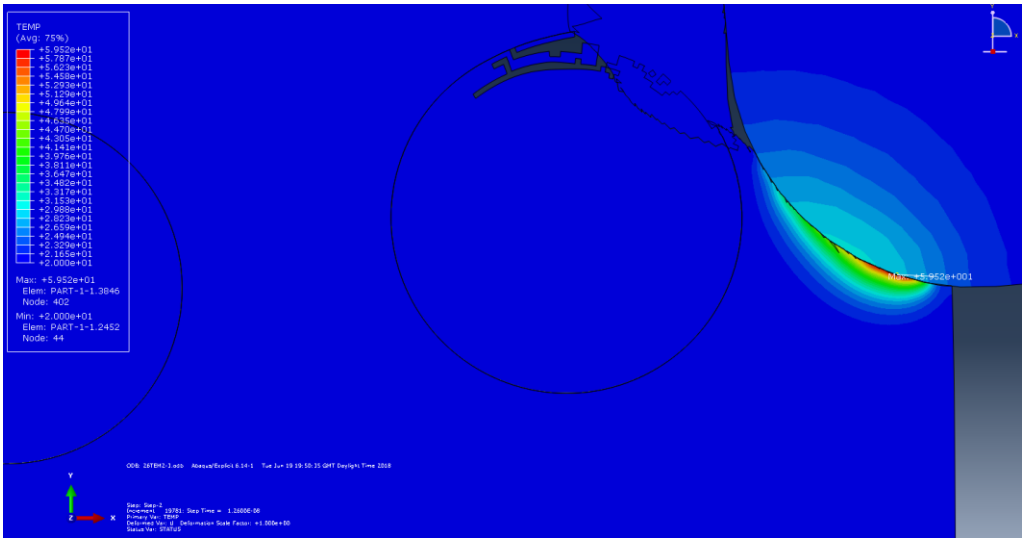

(a) Cutting speed: 94.2 m/min

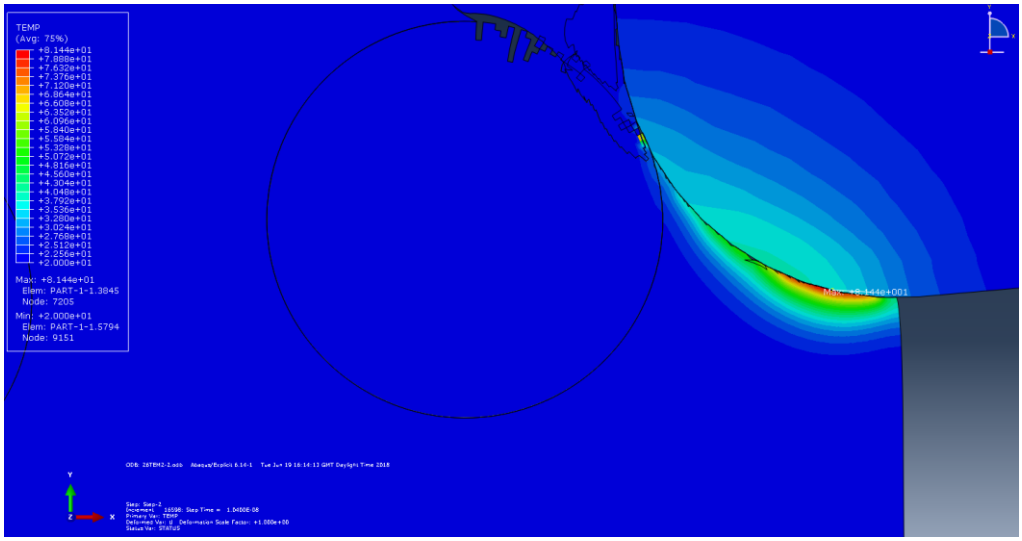

(b) Cutting speed: 125.7 m/min

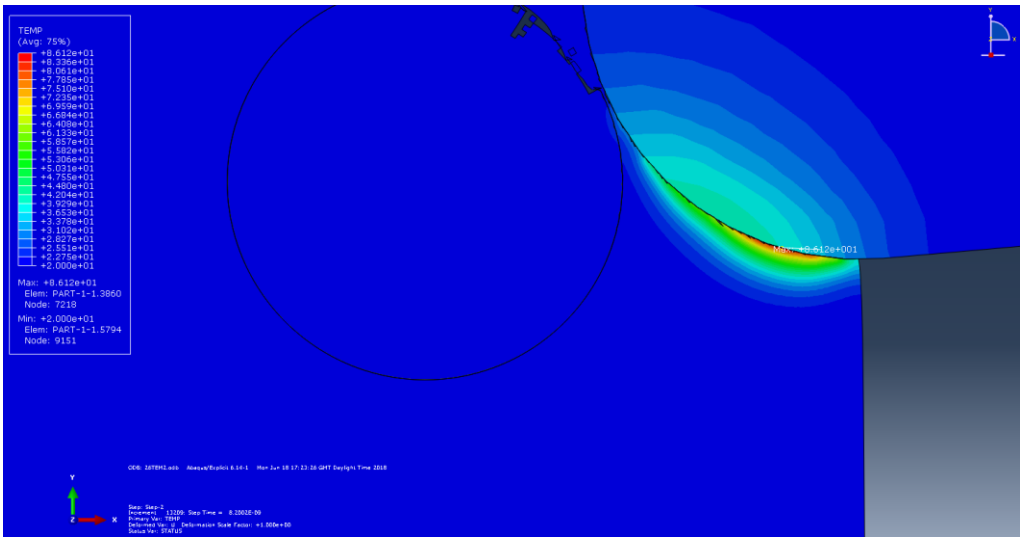

(c) Cutting speed: 157.0 m/min

Figure 6-3 Cutting temperature under varied cutting speed

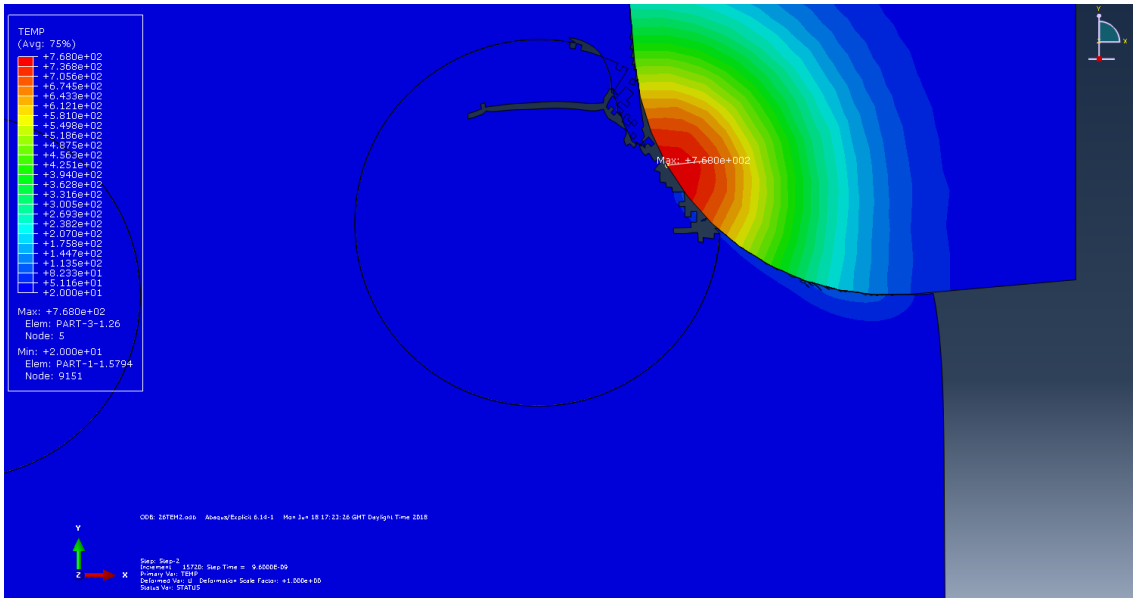

Figure 6-4 Cutting temperature at tool-particle interface

6.2 Tool wear mechanism and characterisation

Tool wear is an of great importance aspect especially in precision machining due to the slight change on tool conditions will significantly affect the machining process and deteriorate the quality of machined parts. In MMCs precision machining, the tool wear is normally rapid due to the existence of hard particles and specific microstructure of workpiece. The excessive tool wear results in the poor surface integrity with higher surface roughness, more surface defects and further lead to the poor functional performance of machined components. The resultant tool wear also increases the cutting force and cutting temperature. These will in turn lead to extensive tool wear and badly affect the resultant cutting performance. Therefore, an in-depth understanding on the tool wear mechanism in MMCs precision machining is critical. In this chapter, the tool wear mechanism and characterisation are firstly investigated. Afterwards, the tool wear magnitude is then quantified based on the feasible measurement techniques and instruments. Modified tool wear rate model is proposed to better present wear conditions. The tool wear analysis and wear rate model are also evaluated and validated via experiments.

6.2.1 Tool wear mechanism

The literature review on the tool wear types indicates that abrasive and adhesive wear are the major tool wear in MMCs machining. In addition, edge chipping also frequently occurs. In order to investigate the tool wear mechanism in MMCs precision machining,

new tools and wear tools are measured and photographed by using high precision metrology measurement instruments. The tool integrity especially for the geometry, cutting edge profile and surface morphology of new tools and wear tools in the experiments are shown in Figure 6-5 and Figure 6-6 respectively.

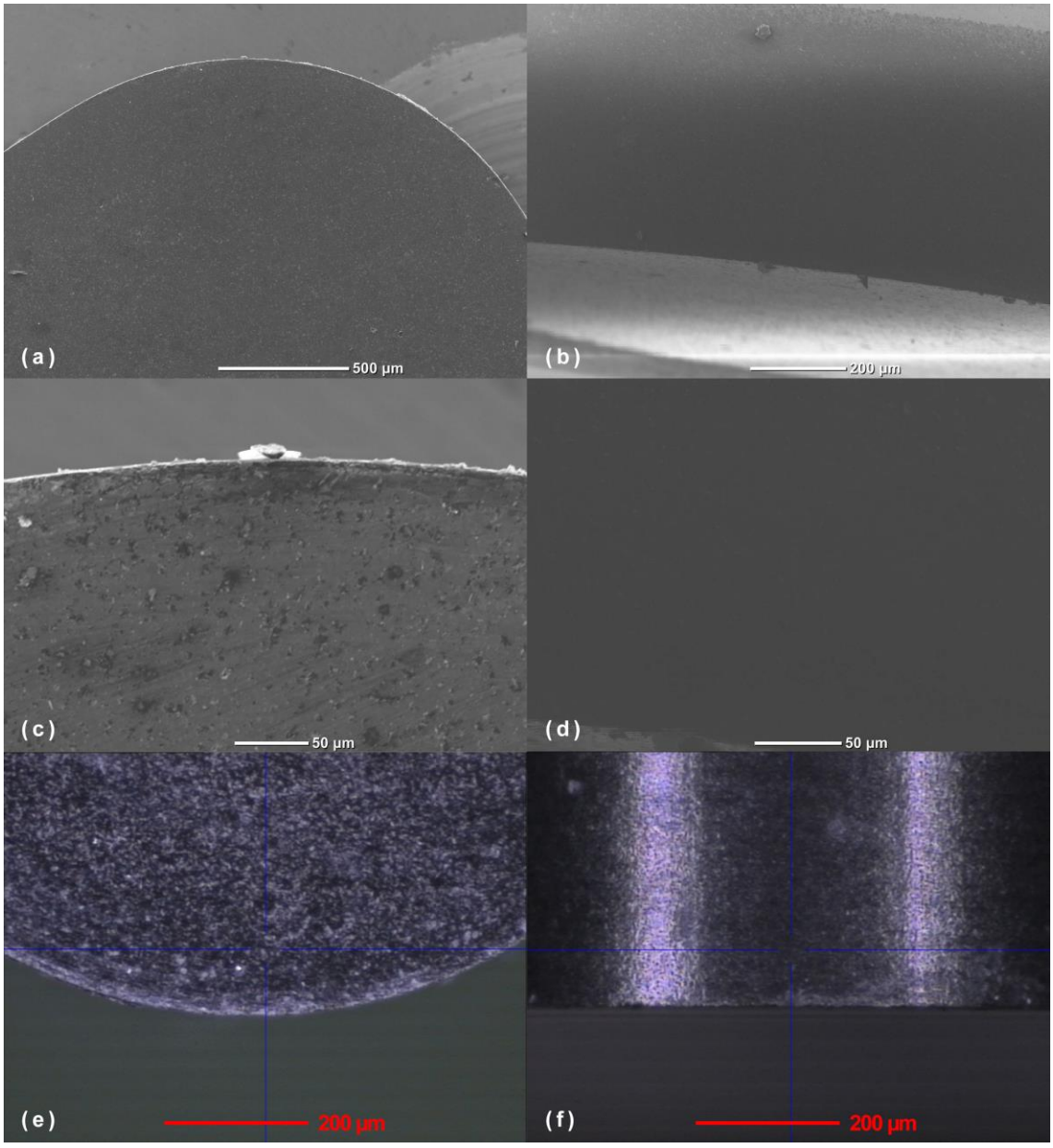

(a) PCD inserts

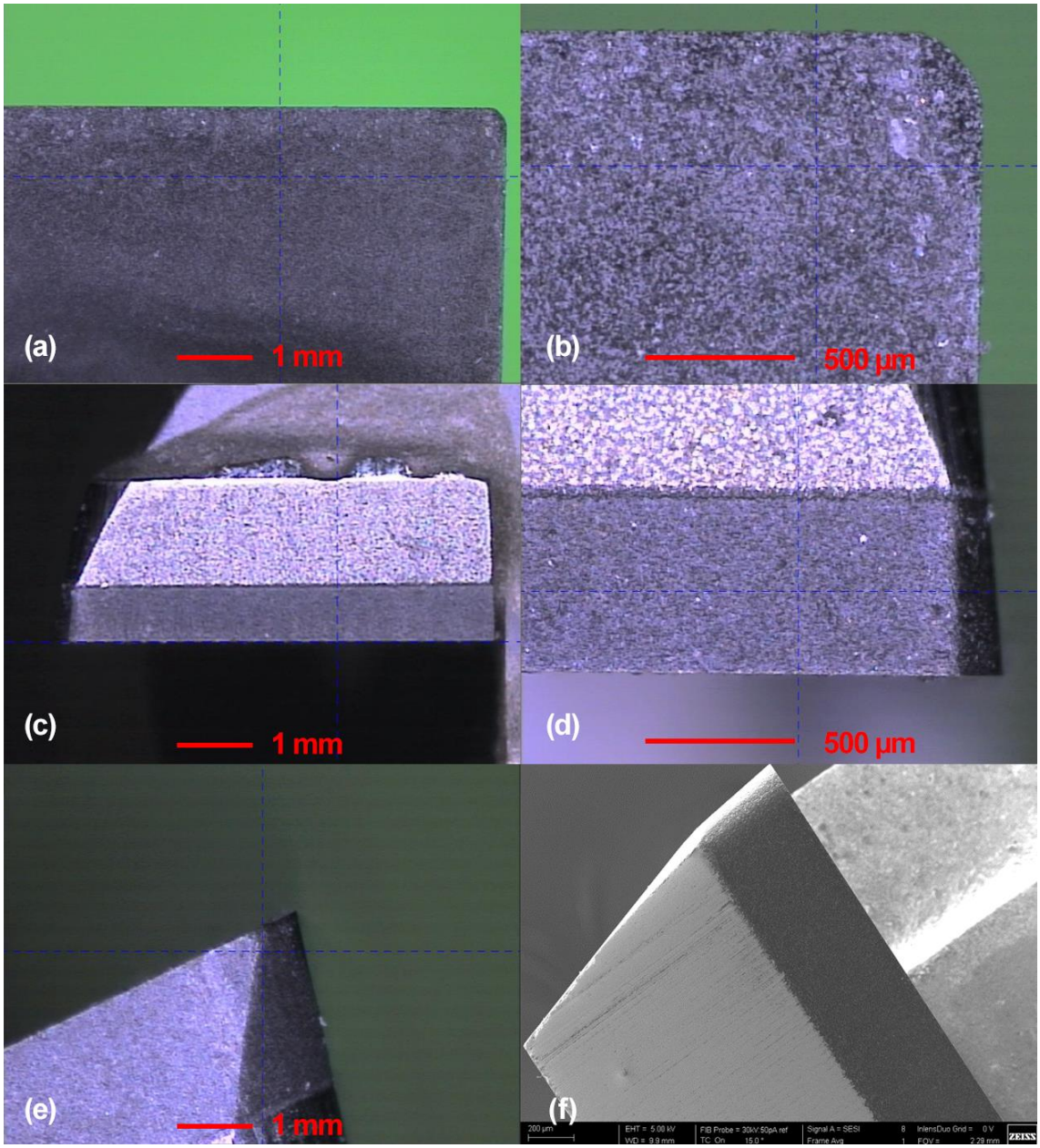

(b) PCD end mills

Figure 6-5 New tools before MMCs precision machining

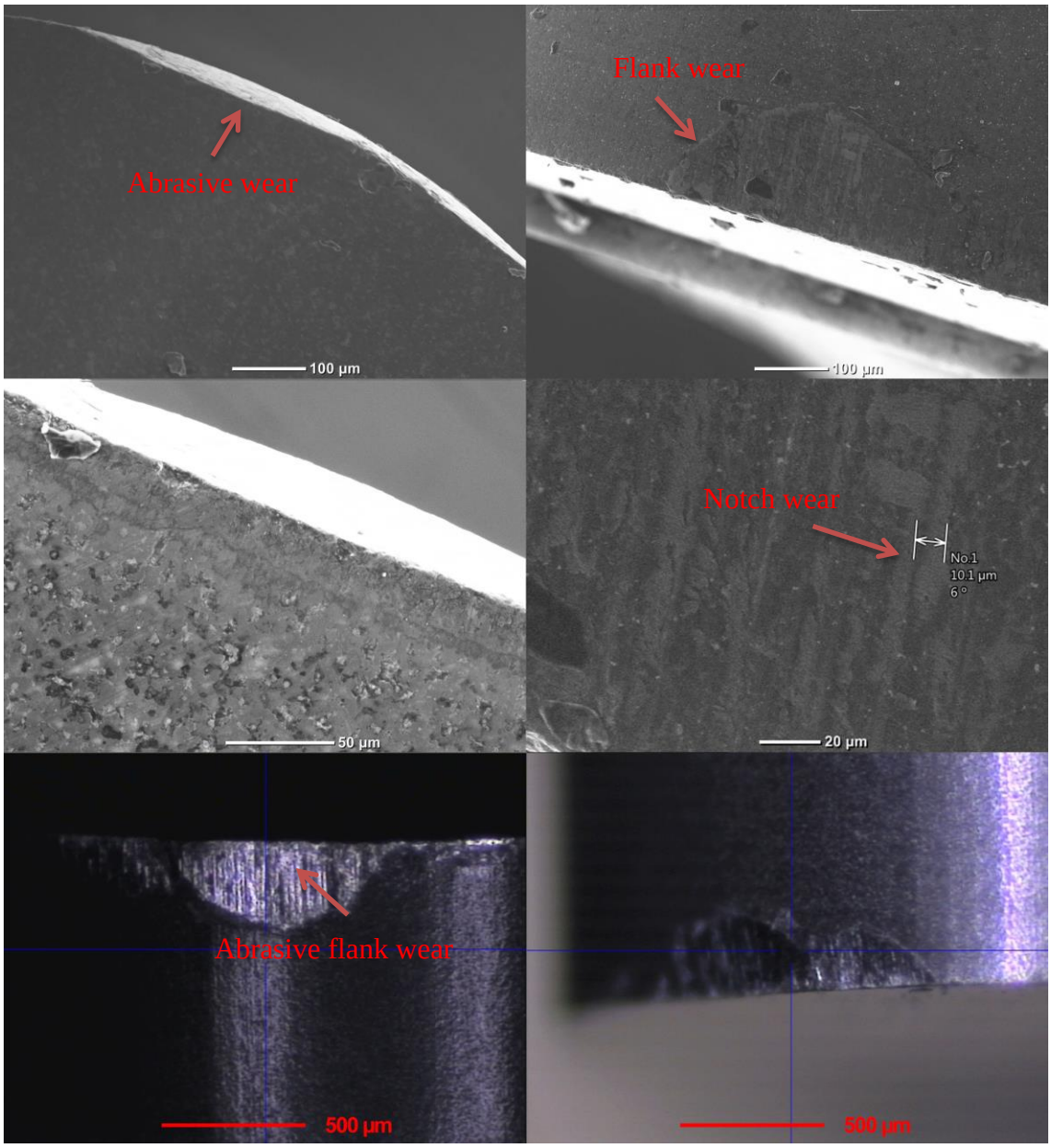

(a) PCD inserts

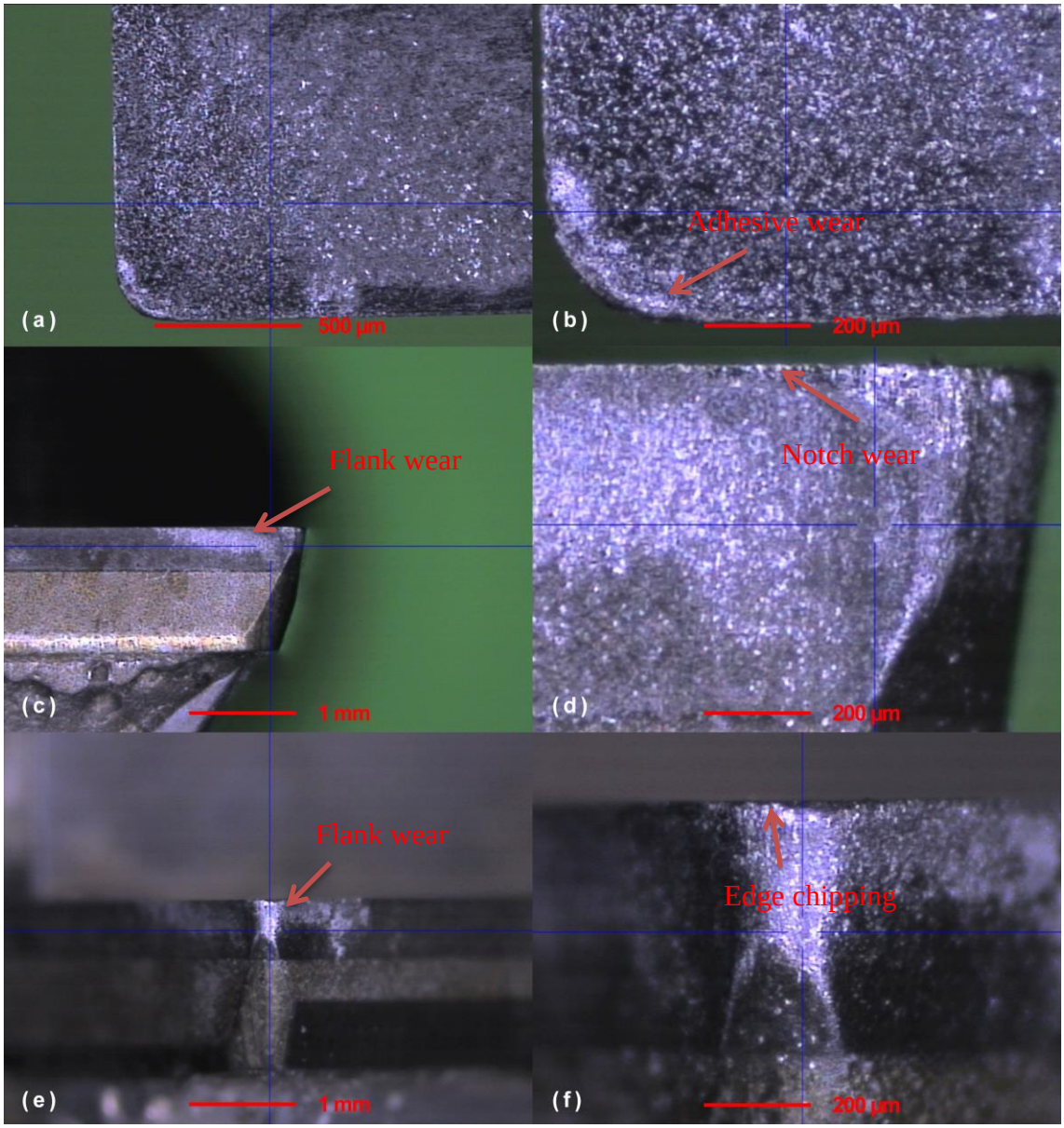

(b) PCD end mills

Figure 6-6 Wear tools after MMCs precision machining

From the measurement results of PCD inserts, it can be found that abrasion tool wear is the most significant tool wear especially on the flank face in MMCs precision machining due to the existence of extremely hard particles in the workpiece. Abrasion wear patterns with parallel grooves generated in the direction of the chip flow can be observed as the primary wear on the flank face. This may be caused by embedded particles dislodged from workpiece and dug into the tool surface. Adhesion wear under various cutting conditions is not significant in these experiments due to the abrasive wear is dominated. Only a few matrix materials can be seen adhesive on the rake face of cutting tool. On the other hand, edge chipping and grooving start to appear and can be

found mainly on the cutting edge towards feed rate direction due to the continued impact of hard particles. In addition, notch wear can be observed on the flank face. This tool wear is resulted from the undulating ridges that have the similar size with cutting feed rate on the machined surface. In addition, it normally occurs at lower cutting speed.

In term of PCD end mill, abrasion tool wear is also the most dominate tool wear on the flank face particularly on the tool nose area in MMCs micro milling process. The abrasion wear at the exterior side of tool diameter is much more significant and quicker than the inner side. Adhesion wear with build-up-edge is also significant on the tool rake face. Edge chipping along the whole cutting edge gradually occurs. Figure 6-8 shows the measured cutting edge radius before and after MMCs machining. Edge rounded can be found both on cutting edge and tool nose as the edge radius increase from 3.4122 μm to 3.4634 μm after a few cutting cycles.

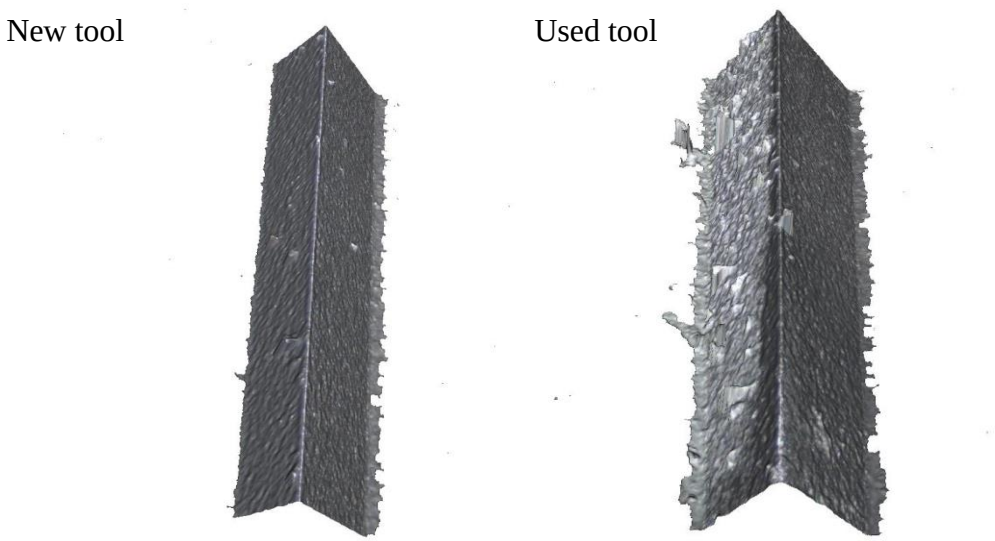

Figure 6-7 PCD end mill surface morphology of new and used tools

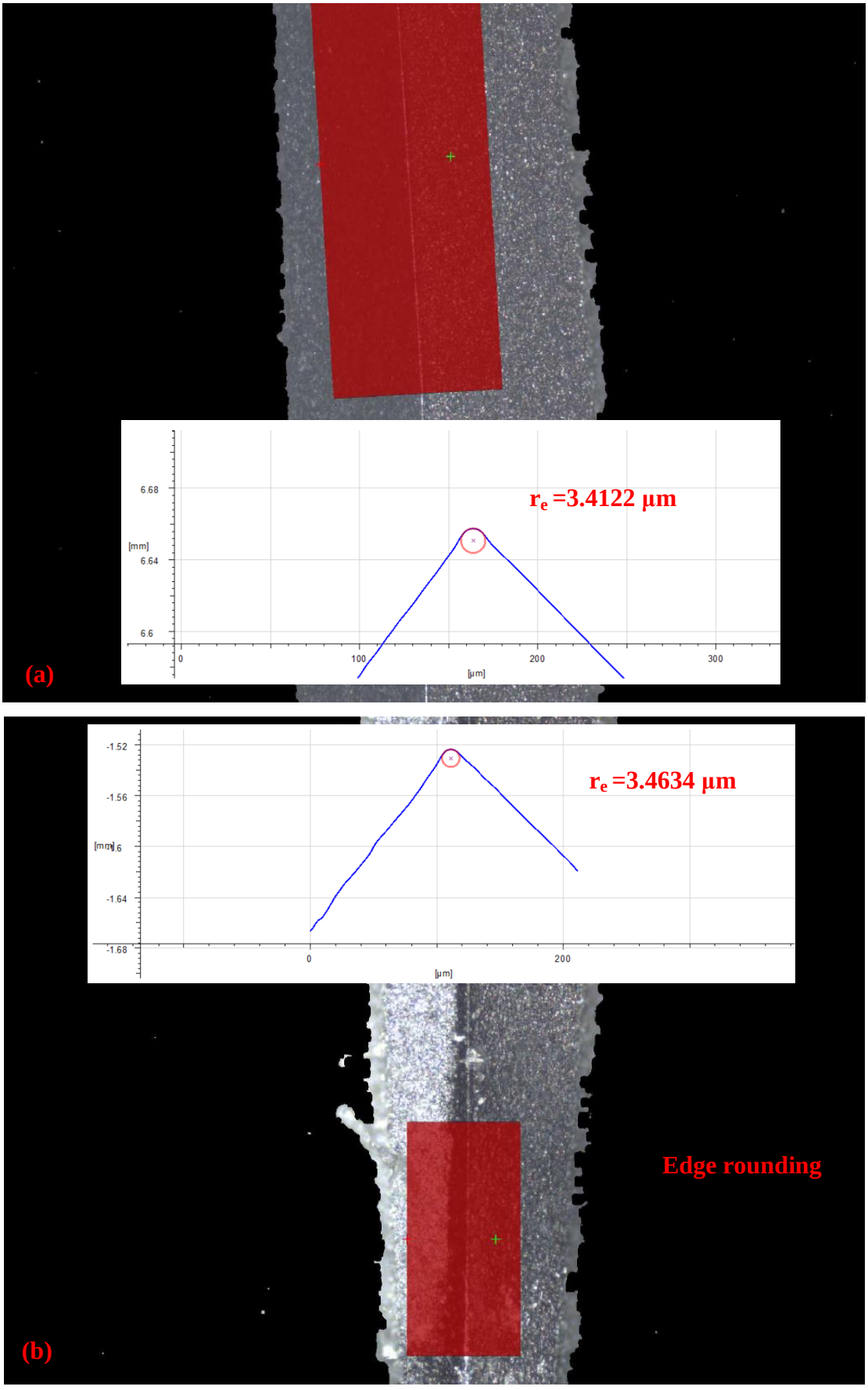

Figure 6-8 Edge radius of PCD tool (a) New tool (b) Used tool

6.2.2 Multiphysics coupling on tool wear in MMCs precision machining

A theoretical tool wear model is proposed according to the multiphysics based modelling and analysis, and also modified tool wear rate model. Based on the simulation law in Chapter 4, the basic Johnson-Cook constitutive model is employed to estimate the von mises flow stress. Considering the size effect, fully coupled thermo-mechanical-tribological multiphysics model is introduced to demonstrate the cutting shear stress.

Due to tool wear significantly affect the resultant surface roughness, better surface integrity with lower surface roughness is presume at minimum tool wear conditions. Thus, tool wear is the obvious factor to form the relationship between cutting parameters and surface roughness in precision machining processes. The tool wear model presented by tool wear rate can be expressed as [196]:

$$\frac{dW}{dt} = c_1 \sigma v e^{-c_2/T} \tag{6.32}$$

where, c_1 and c_2 are the constants achieved from experimental analysis in this equation. W is total tool wear height. Thus, the tool wear rate model can be modified by combining the Johnson-Cook shear stress model σ as below:

$$W_t = c_1 v e^{-c_2/T}[A + B(\varepsilon^{pl})^n]\left(1 + Cln\frac{\dot{\varepsilon}}{\dot{\varepsilon}_0}\right)\left[1 - \left(\frac{T - T_0}{T_m - T_0}\right)^m\right] \tag{6.33}$$

The FE based simulations and analysis are performed under the following cutting parameters respectively: spindle speed of 3,000/6,000/9,000/12,000/15,000/18,000 RPM and feed rate of 2/3/4/5/6/7 μm/tooth. The simulation results are obtained with the distribution of various cutting parameters as shown in Figure 6-9. From the simulation results, it can be significantly observed that tool wear rate gradually increase with the increase of cutting speed. The tool wear rate then significantly rise to a high value after a short stable at relative lower cutting speed. In term of feed rate, tool wear rate keep increasing due to the significant increase of cutting force at larger feed rate. The tool wear rate states the similar results at different cutting speed and feed rate. However, the tool-workpiece contact time is much longer at lower feed rate which results in the total tool wear dramatically increases. Thus, the optimal cutting parameters for precision machining of MMCs should be obtained by considering the total tool wear, material removal rate and resultant surface roughness. According to the MMCs machinability

assessment, the cutting parameter with 9,000RPM spindle speed and 5 μm /tooth feed rate are selected as the optimal parameters in this micro milling process.

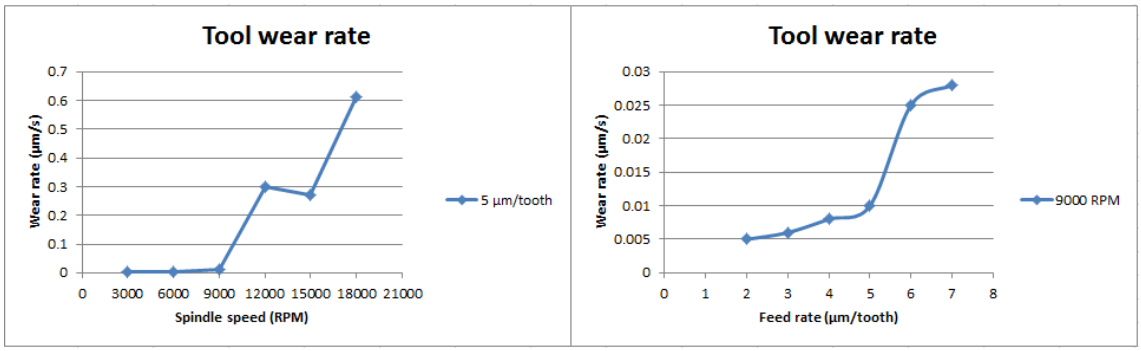

Figure 6-9 Tool wear vs spindle speed and feed rate in MMCs micro milling

6.2.3 Tool wear measurement and analysis

In order to evaluate the tool wear in MMCs precision machining process, wear height as an effective method to analyse the tool wear condition were measured. In addition, as flank wear is universally taken as the criterion of tool life characterisation, flank wear at the bottom face of cutting tool were measured as well. Figure 6-10 shows the method of measuring tool wear height and total flank wear length respectively.

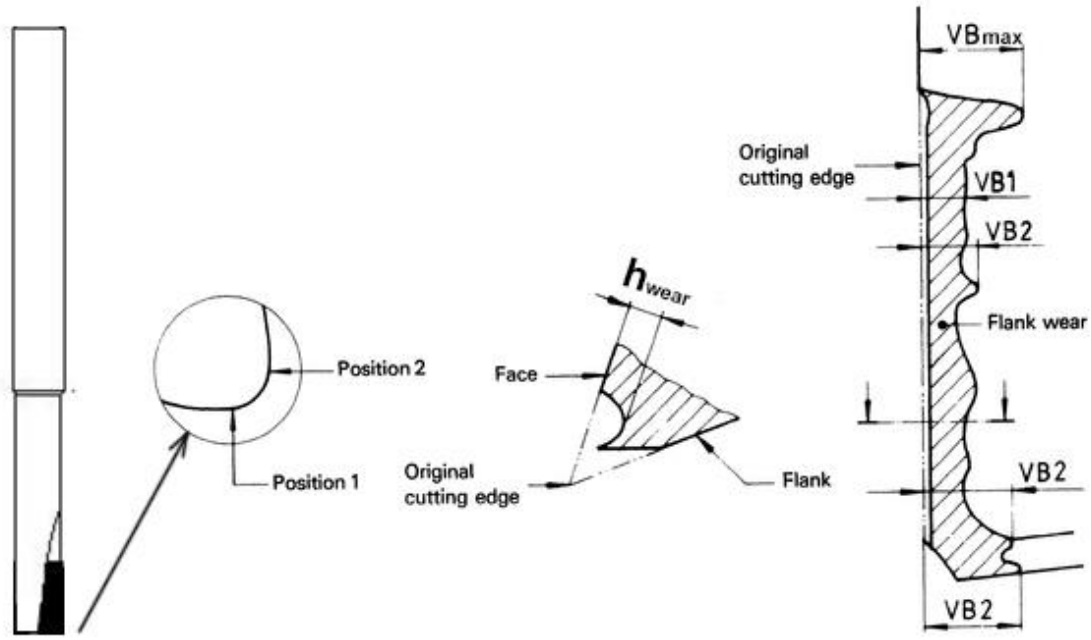

Figure 6-10 Method of measuring wear height and flank wear length

The magnitudes of wear height for PCD insert and PCD end mill are measured by using the online method via laser system and offline method via TESA 200 optical

microscope respectively. The tool flank wear magnitudes for both tools are measured and analyse by using TESA 200 optical microscope. The measured tool wear magnitudes are shown in Table 6-1. After 50 mins continued machining using optimal cutting parameters with 9,000 RPM spindle speed and 5 μm /tooth feed rate, the milling tool wear height and wear length are measured as 28.2 μm and 170 μm respectively. According to the tool wear rate model, the predicted total tool wear height under the same machining process is around 30 μm. This shows a reasonable agreement with the experimental results. The experimental based investigation and analysis on the cutting tool wear and resultant machined surface quality in MMCs micro drilling process is also conducted and shown in Appendix 2.

Table 6-1 PCD tool wear and wear rate in MMCs micro milling process

Tool	PCD
Time (s)	3000
Wear height (μm)	28.2
Wear length (μm)	170
Wear rate (height) (μm/s)	0.0094
Wear rate (length) (μm/s)	0.057

6.3 Concluding remarks

In this chapter, the cutting temperature distribution and cutting tool wear in MMCs precision machining have been investigated through multiphysics coupled thermal-mechanical-tribological simulation and experimental analysis. The findings in this chapter can be summarised as below.

In MMCs precision machining, the heat are generated and dissipated at five different areas around tool-workpiece interface. Estimation of cutting temperature distribution is determined by applying the heat source which contains uniform heat flux distribution. A modified cutting temperature model is proposed by introducing the temperature rise theory to have a better understanding on the heat flows in tool-chip-workpiece system. Heat generated at the shear plane will flow into the workpiece and chip; heat generated by the chip formation will partly transfer to the tool-chip interaction point and the rest will transfer to the chip and tool body; friction heat generated at the tertiary shear zone

will partly transfer to the workpiece and tool body and the rest will transfer into the ambient environment; heat generated by friction between the tool and workpiece material at the tool-chip interface and tool-remain surface interface; heat generated by material deformation will totally convert into heat source in the workpiece. Results from multiphysics simulation and analysis indicate that maximum cutting temperature increases at each cutting position when increase either depth of cut or cutting speed.

In MMCs precision machining, tool wear mechanisms are extensively identified. The abrasive wear on the flank face and edge chipping are performed as the dominated tool wear. Adhesive wear, build-up-edge, notch wear and edge rounded also can be observed on the worn tools. The tool wear in MMCs precision machining is presented by combining the coupled thermal-mechanical-tribological cutting stress and modified wear rate model together. The experimental evaluation on the tool wear and tool life characterisation is conducted by measuring wear height and flank wear length of cutting tool respectively. The simulation and experimental results imply that the selection of optimal cutting parameters is critical and effective for MMCs machinability assessment.

Chapter 7 Machinability assessment in precision machining of MMCs

7.1 Machinability assessment framework

With increasing industrial demands for functional MMCs, machinability of MMCs have become bottleneck issues and thus drawn extensive attention in various research aspects. Machinability is normally assessed by means of various machining characterisation factors including a combination of cutting forces, surface roughness, tool wear, burr formation and power consumption. A better machinability is determined as the machining process with small chip loads, good surface finish, minimum tool wear, free burrs and low cutting energy. Accordingly, the determination of MMCs precision machining characteristics, especially on the cutting force, machined surface roughness, material removal rate, and the tool wear and tool life aspects, is essential for further machinability assessment. In addition, the high precision engineering applications are heavily dependent on the machining accuracy, surface quality, production efficiency and cost-effective. Although various non-traditional processes have been attempted on machining MMCs to even produce parts with intricate shape and profiles [35], the processes are normally inefficient and often limited. Thus, the conventional machining process is still indispensable during finish machining [36]. Never the less, precision machining of MMCs is observed as a scientific challenge, due to their hard-to-machine property and often the poor surface finish. Substantial researches have been undertaken on the machining process optimisation and machinability assessment. However, the high surface roughness and deterioration and large defects of the machined surface significantly affect the functional performance of engineering components. This is currently becoming one of the major reasons limiting the widespread application of MMCs in precision engineering industries. In addition, machinability of particulate MMCs is less understood as being progressed so far.

In this chapter, a systematic research is carried out to experimentally investigate the machining behaviour and machinability of particle reinforced MMCs. The well-designed precision machining trials on MMCs workpiece by using polycrystalline diamond tools are performed to investigate the effects of workpiece materials, cutting tools and cutting parameters, particularly for the cutting speed, depth of cut and feed

rate, on the machined surface roughness, surface morphology and further machinability. Moreover, contribution percentage of these variables are analysed accompanying with adjusting process parameters so as to achieve better surface quality.

7.2 Surface generation

7.2.1 Tool-workpiece system dynamics

In previous mechanistic models, the tooling system and workpiece system are assumed as rigid. However, both of these systems perform as the spring-damper system under all cutting conditions in real cutting process. The vibration and deviation of tool and workpiece have significant influence on the fluctuation of real tool trajectory, workpiece position and tool-workpiece interaction. This results in the change on the cutting force magnitude, cutting temperature and tool wear rate. On the other hand, the vibration significantly affects the surface generation and surface performance. Figure 7-1 schematically shows the tooling spring-damper system and workpiece spring-damper system.

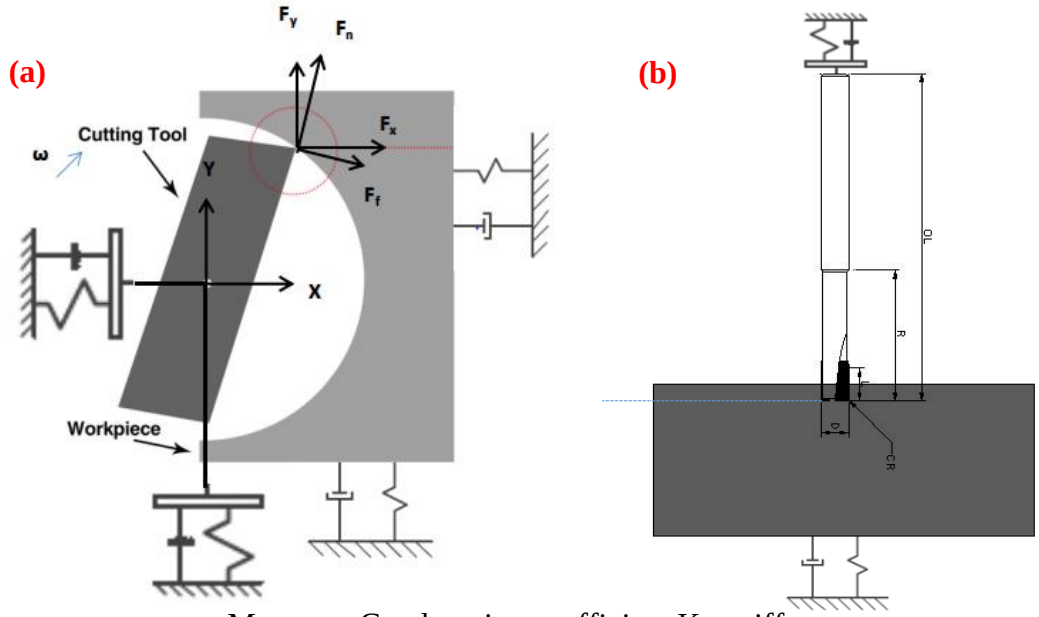

M---mass C---damping coefficient K---stiffness

Figure 7-1 Tooling spring-damper system and workpiece spring-damper system (a) X direction and Y direction (b) Z direction

7.2.2 Surface generation analysis

The last section implies that the real surface generation is not only affected by the initial conditions, including the cutting tool conditions, workpiece properties and cutting

parameters, but also significantly influenced by the tool-workpiece oriented spring-damper system. Thus, by taking these contributory factors into account, the surface generation in MMCs precision machining can be better predicted according to the modified models shown in previous chapters. The simulation process of surface generation is developed and shown in Figure7-2.

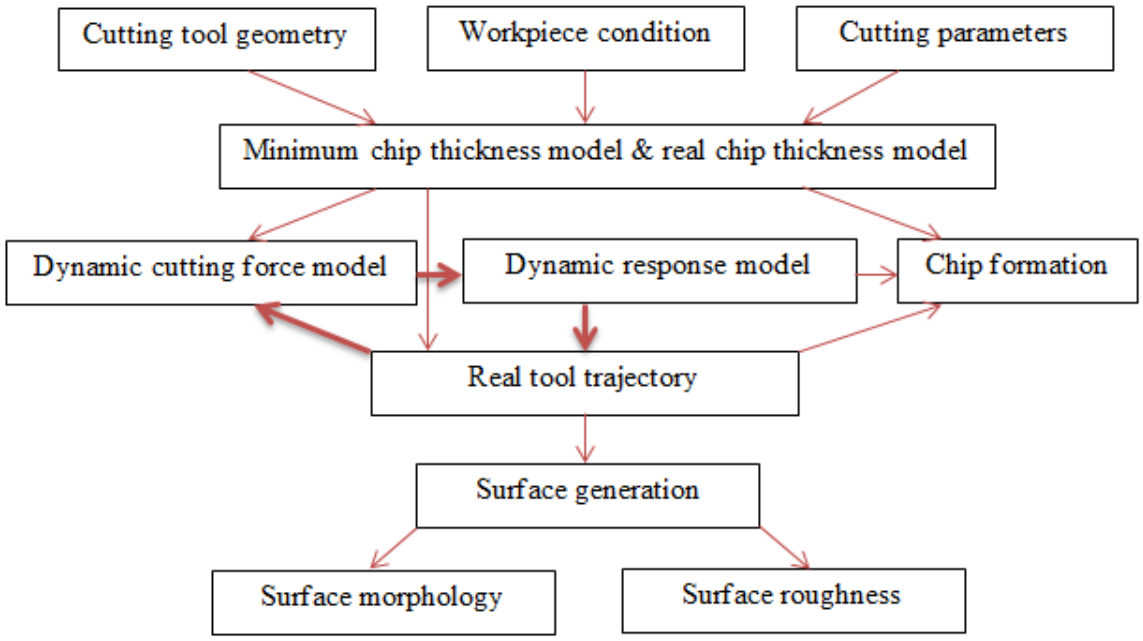

Figure 7-2 Surface generation simulation process

In this simulation process, cutting tool geometry, workpiece condition and cutting parameters are considered as the initial factors that determine the surface generation of final products. As the in-process factor, dynamic response in machining process is conducted as the most critical aspect that affects the real tool trajectory and further influence the surface generation especially in material shearing process. In addition, the close loop shown in Figure 7-2 indicates that the dynamic response will result in the fluctuation of the tool path accompanied with the continued change of cutting force. This will in turn enhance the cutting dynamic error and affect the surface performance. In addition, the cutting edge radius and reinforced particle size are observed have significant effects on the material elastic recovery and minimum chip thickness. This will also contribute to the real tool trajectory and affect the machined surface topography and surface generation directly.

According to the interrelationship between the machining input and output as shown in Figure 7-2, it can be observed that machining dynamic response is closely linked to the

dynamic cutting force. Thus, the machined surface generation can be predicted by analysing the relations between dynamic response of displacement and real cutting force generated on both cutting tool and workpiece in three directions. The interrelationship is commonly characterised by introducing the transfer functions. A force-displacement test by using Kistler impact hammer 9722A500 and capacitive sensor 5810, as shown in Figure 7-3, is applied to obtain the frequency response function (FRF) represented by transfer function of cutting tool and workpiece in each cutting direction.

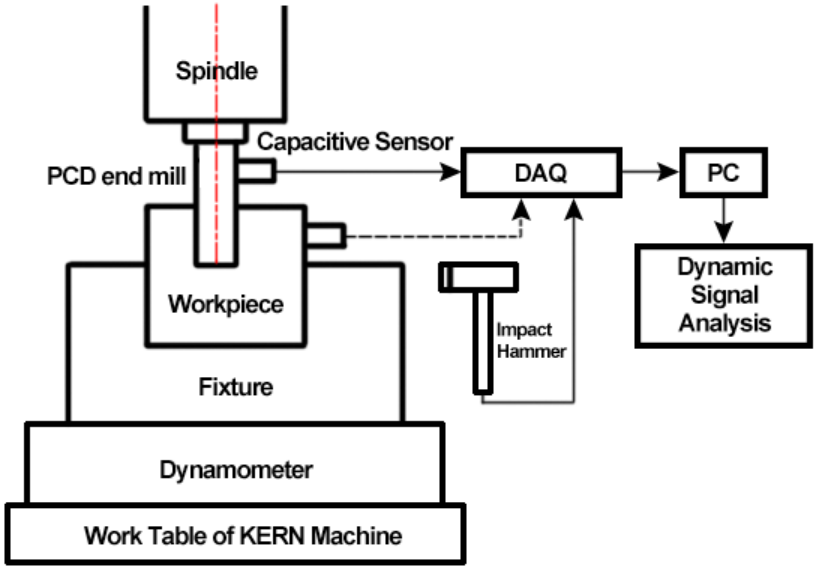

Figure 7-3 Transfer function identification for tool and workpiece in X and Y directions

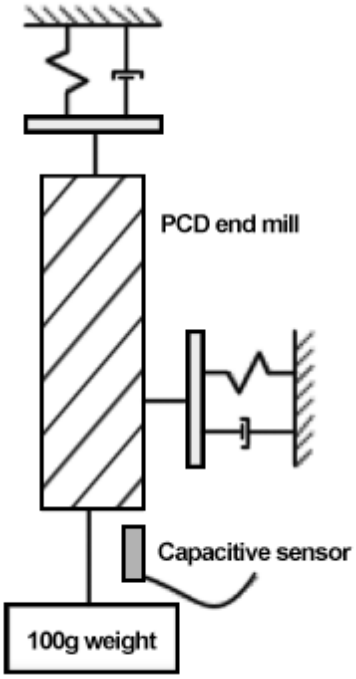

Figure 7-4 Transfer function identification for cutting tool in Z direction

The experimental identification of transfer functions for cutting tool in Laplace form are shown as below:

$$\frac{X_x(s)}{F_x(s)} = \frac{1}{M_x s^2 + C_x s + K_x}$$
$$\frac{X_y(s)}{F_y(s)} = \frac{1}{M_y s^2 + C_y s + K_y} \quad (7.1)$$
$$\frac{X_z(s)}{F_z(s)} = \frac{1}{M_z s^2 + C_z s + K_z}$$

where, $X_{x,y,z}$ and $F_{x,y,z}$ are the dynamic response of displacement and static cutting force for cutting tool respectively; $M_{x,y,z}$, $C_{x,y,z}$ and $K_{x,y,z}$ are the mass, damping coefficient and stiffness in three directions respectively. Due to the high rigid and low resistance to impact of cutting tool in Z direction, the transfer function cannot be obtained from this method. Thus, a step signal implemented by the sudden drop of a 100g weight to approximately simulate 1N force signal is applied instead. This method is shown in Figure 7-4. According to the force-displacement test from hammer-capacitive sensor system, the system input and output in each direction are shown in Figure 7-5.

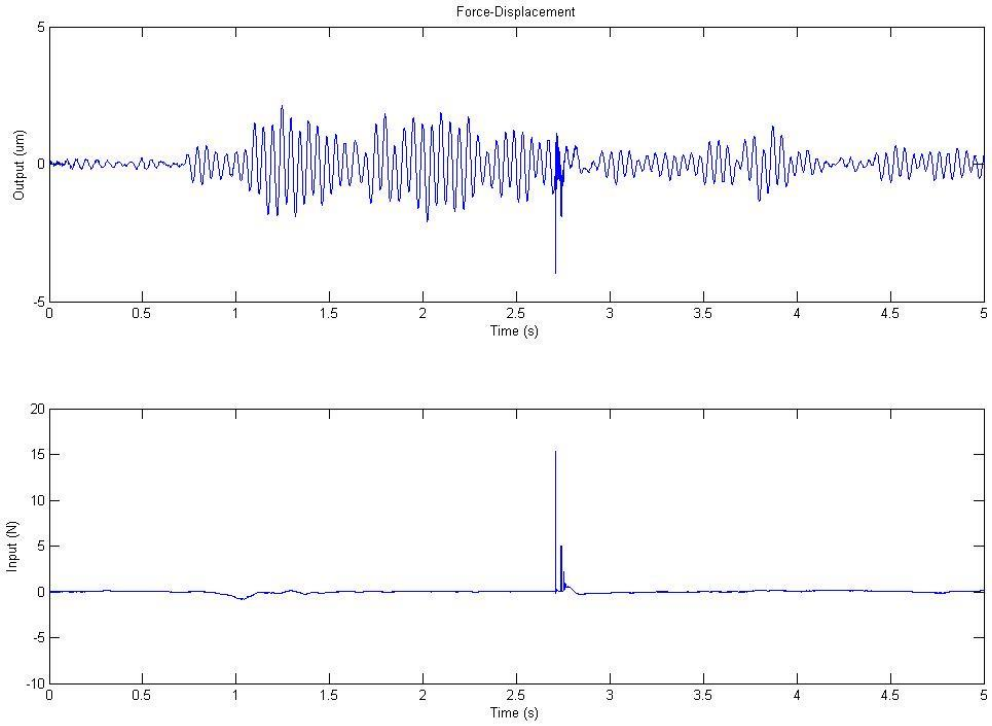

(a) Input and output signals in X direction

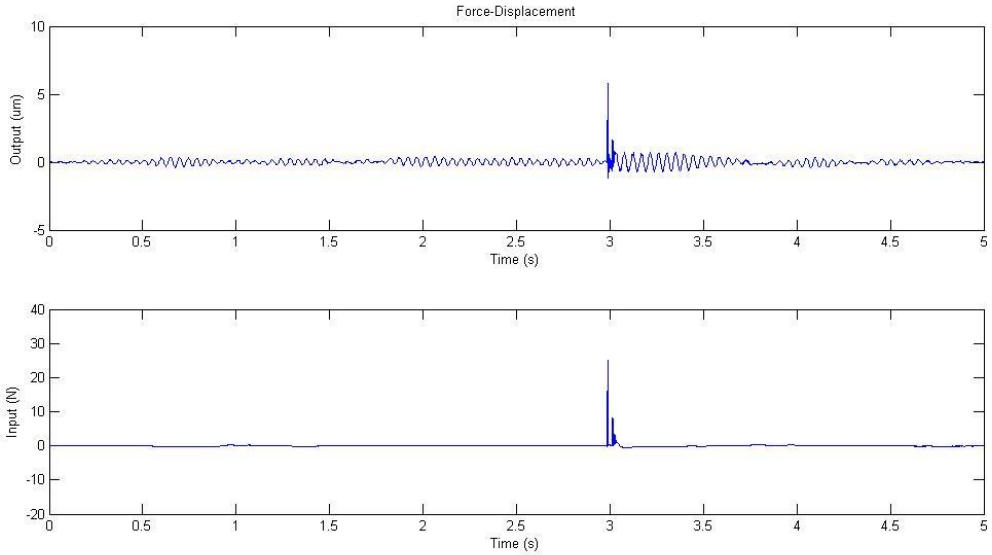

(b) Input and output signals in Y direction

Figure 7-5 Input and output signals for cutting tool in each direction

The dynamic response characteristics of cutting tool is shown in Figure 7-5 and the transfer function of dynamic response can be then expressed as:

$$\frac{X_x(s)}{F_x(s)} = \frac{1}{2.93e^4 s^2 + 2.47e^{-2} s + 31.80}$$
$$\frac{X_y(s)}{F_y(s)} = \frac{1}{1.78e^4 s^2 + 2.71s + 20.07} \quad (7.2)$$

The experimental transfer functions for workpiece in Laplace form are shown as below:

$$\frac{x_x(s)}{F_x(s)} = \frac{1}{m_x s^2 + c_x s + k_x}$$
$$\frac{x_y(s)}{F_y(s)} = \frac{1}{m_y s^2 + c_y s + k_y} \quad (7.3)$$
$$\frac{x_z(s)}{F_z(s)} = \frac{1}{m_z s^2 + c_z s + k_z}$$

where, $x_{x,y,z}$ and $F_{x,y,z}$ are the dynamic response of displacement and static cutting force for workpiece respectively; $m_{x,y,z}$, $c_{x,y,z}$ and $k_{x,y,z}$ are the mass, damping coefficient and stiffness in three directions respectively.

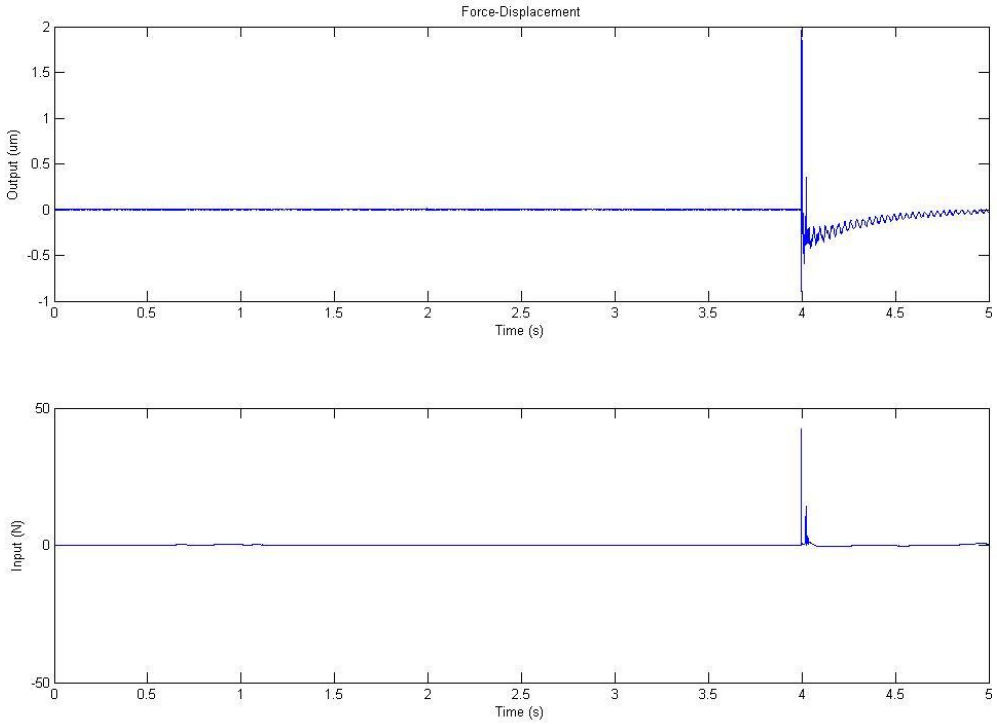

(a) Input and output signals in X direction

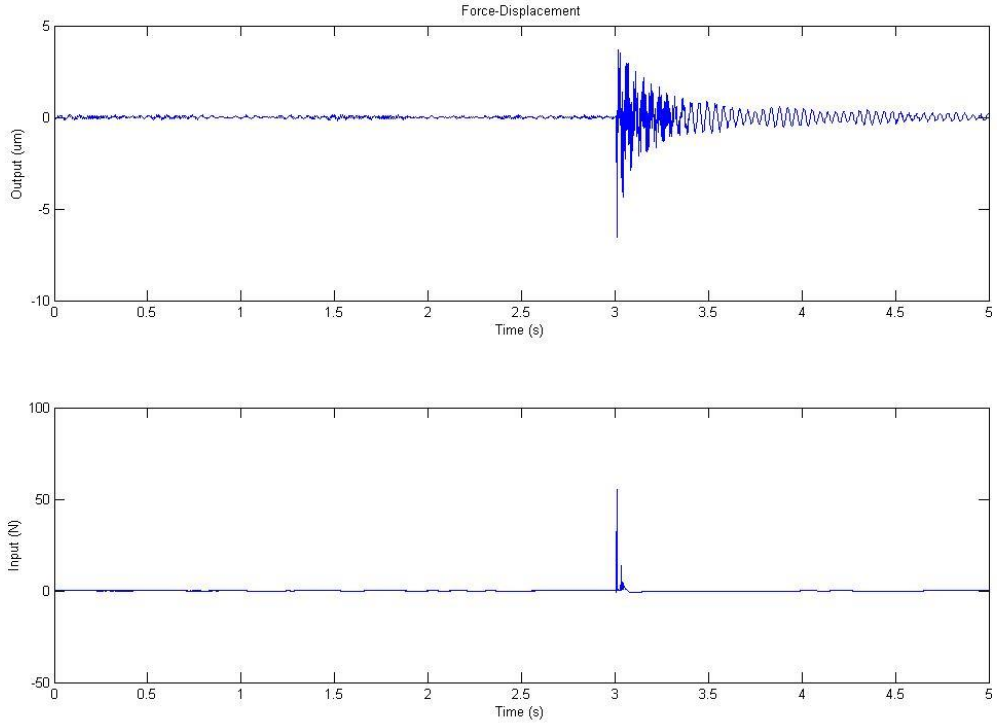

(b) Input and output signals in Y direction

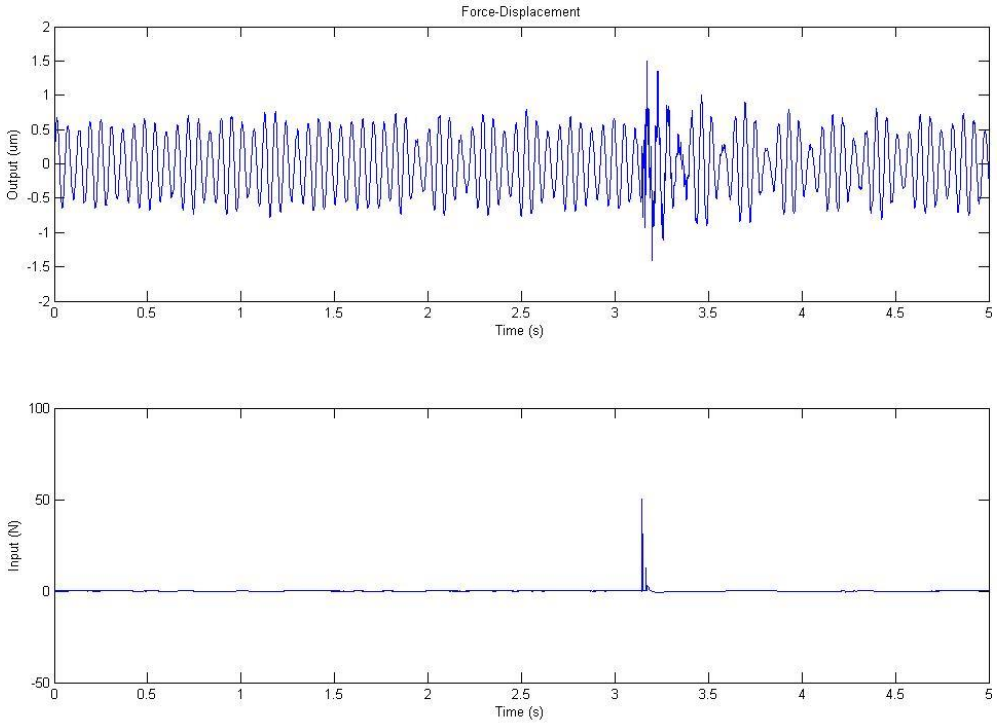

(c) Input and output signals in Z direction

Figure 7-6 Input and output signals for workpiece in each direction

According to the force-displacement test from hammer-capacitive sensor system, the dynamic response character of workpiece is shown in Figure 7-6 and the transfer function of dynamic response can be then expressed as:

$$\begin{aligned} \frac{x_x(s)}{F_x(s)} &= \frac{1}{1.24e^5 s^2 + 4.41e^3 s + 6.83e^{-2}} \\ \frac{x_y(s)}{F_y(s)} &= \frac{1}{8.03e^3 s^2 + 3.89s + 10.66} \\ \frac{x_z(s)}{F_z(s)} &= \frac{1}{4.45e^5 s^2 + 3.40s + 3.22e^2} \end{aligned} \tag{7.4}$$

Therefore, the dynamic displacement of cutting tool and workpiece at each time increment can be obtained according to the calculated dynamic cutting force at each time point and the above mentioned transfer function in each direction. The actual chip formation and real tool trajectory can be further predicted through total displacement by means of the sum of cutting tool displacement and workpiece displacement. As a result, the machined surface topography and surface generation can be predicted in a high precision level.

7.3 Process optimisation strategies

In order enhance the engineering applications of particulate MMCs in high precision level, its machinability assessment is critical and precision machining characteristics need to be optimised in various aspects including surface roughness, surface morphology, tool wear and cutting force etc. The objective of this part is to experimentally investigate the machining behaviour of various particulate MMCs under varied cutting parameters by using different tools. The comparison of related cutting performance and tool performance are undertaken in order to identify the respective machinability under different cutting conditions.

7.3.1 Optimisation on cutting parameters

According to the literature review, cutting parameters are the most crucial factor for machinability assessment. In order to determine the material characteristic of particulate MMCs and their machinability under different cutting parameters and further optimised these independent variables through experiments, three levels of milling speed, feed rate and axial depth of cut are employed.

7.3.1.1 Surface roughness

For MMCs micro milling process, the experimental set-up has been introduced in Chapter 5 in details and experimental results of machined surface roughness is analysed in this section. The orthogonal array of cutting parameters and the machined surface roughness under different settings of input factors are shown in Table 7-1.

Table 7-1 Orthogonal array of cutting parameters and the machined surface roughness

Experimental number	Spindle speed (rpm)	Cutting speed (m/min)	Feed rate (μm/rev)	Axial depth of cut (μm)	Surface roughness (nm)	S/N ratio
1	3,000	94.248	5	70	69	-36.7770
2	3,000	94.248	5	150	64	-36.1236
3	3,000	94.248	5	250	52	-34.3201
4	3,000	94.248	10	70	46	-33.2552
5	3,000	94.248	10	150	28	-28.9432
6	3,000	94.248	10	250	33	-30.3703

7	3,000	94.248	20	70	75	-37.5012
8	3,000	94.248	20	150	51	-34.1514
9	3,000	94.248	20	250	60	-35.5630
10	6,000	188.496	5	70	35	-30.8814
11	6,000	188.496	5	150	34	-30.6296
12	6,000	188.496	5	250	45	-33.0643
13	6,000	188.496	10	70	28	-28.9432
14	6,000	188.496	10	150	20	-26.0206
15	6,000	188.496	10	250	44	-32.8691
16	6,000	188.496	20	70	50	-33.9794
17	6,000	188.496	20	150	35	-30.8814
18	6,000	188.496	20	250	50	-33.9794
19	9,000	282.743	5	70	33	-30.3703
20	9,000	282.743	5	150	32	-30.1030
21	9,000	282.743	5	250	68	-36.6502
22	9,000	282.743	10	70	72	-37.1466
23	9,000	282.743	10	150	25	-27.9588
24	9,000	282.743	10	250	43	-32.6694
25	9,000	282.743	20	70	113	-41.0616
26	9,000	282.743	20	150	71	-37.0252
27	9,000	282.743	20	250	78	-37.8419
Workpiece material: Al/5 μmB_4C/50p; Radial depth of cut: 3 mm						

The arithmetic surface roughness values (Ra) of micro-milled bottom surface are shown in Figure 7-7. Figure 7-7(a) presents the surface roughness as a function of cutting speed at various feed rate and axial depth of cut. It can be observed that surface roughness decreases gradually with the rise of cutting speed; with continue increasing the cutting speed, surface roughness slightly increases in most cases. This is due to the material strain rate increases with the increase of cutting speed. When machining with higher cutting speed, the higher strain rate results in the matrix material can be removed with less deformation occurs on the machined surface and generating a surface with smaller roughness [246]. In addition, the cracks generated on the particles have less time to transfer or further process into larger cavities due to the reduced tool-particle

interaction time. As a result, particles are cut through with few defects at higher cutting speed. However, the higher cutting speed results in the increase of cutting temperature, which will lead to rapid tool wear and reduce the machined surface quality [77]. Thus, a better surface performance can be obtained when increasing the cutting speed properly.

Figure 7-7(b) illustrates the surface roughness as a function of feed rate at various cutting speed and axial depth of cut. The experimental results indicate that the tendency is towards smaller roughness value with the increases of feed rate when feed rate is smaller than 10 μm/rev. However, when the feed rate is larger than 10 μm/rev, the roughness value increases with the increase of feed rate and the tendency rate is similar to that feed rate is smaller than 10 μm/rev. Due to the milling tool has two flutes, the feed rate of each tooth is 2.5 μm/tooth, 5 μm/tooth and 10 μm/tooth respectively in three levels. Thus, better surface quality can be obtained when the feed rate is equal or close to the particle size, which is 5 μm. This is due to the surface has been pre-machined in each cutting path; when the feed rate is equal to the particle grain size, most of the particles will be totally removed or perfectly cutting through along the cutting line rather than badly fractured or even pulled out. In addition, the amount of plastic deformation will be increased along with the continue increase of feed rate and this will finally facilitate the formation of large cracks on the reminded matrix material and pits on the matrix-particle bonding areas.

Figure 7-7(c) demonstrates the surface roughness Ra as a function of axial depth of cut at various cutting speed and feed rate. The experimental results present that surface roughness decreases with the increase of DOC when DOC is smaller than 150 μm; while, the roughness value increases when the DOC is over 150 μm. This can be attributed to the chatter stability of cutting tool is low and cutting process vibrations is high during the milling operation. Damping, as the main factor in MMCs micro milling due to the existing of high volume particles, is able to stable end milling operations by raising the critical axial depth of cut and the damping is more effective at higher DOC [17, 249]. While, due to the cutting force increases with the continue increase of DOC, the cutting process vibrations increase and significantly reduce the surface quality. However, in most cases, the influence of DOC on surface roughness is much smaller compare to cutting speed and feed rate, a proper larger DOC will contribute to the efficiency in micro machining process.

According to the experimental results, cutting speed of 188.496 m/min, feed rate of 10 μm/rev and axial depth of cut of 150 μm are visualised as the optimal cutting conditions to obtain the best surface quality with surface roughness Ra< 20 nm in MMCs micro milling processes.

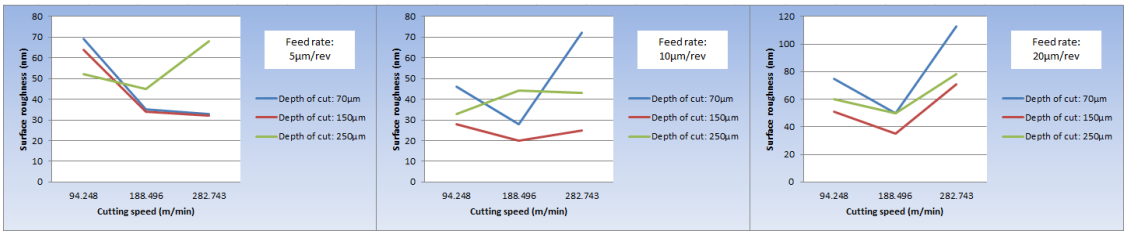

(a) Surface roughness vs Cutting speed

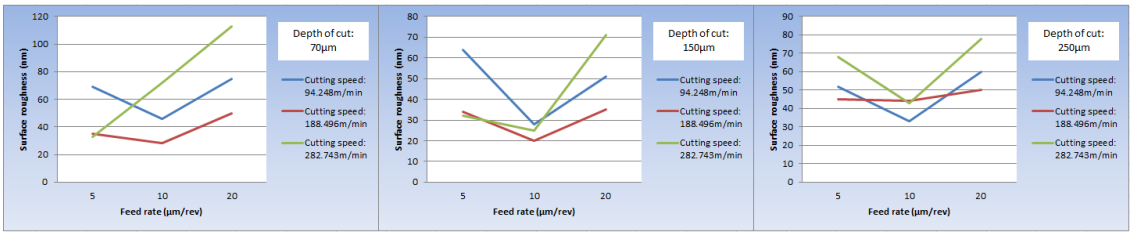

(b) Surface roughness vs Feed rate

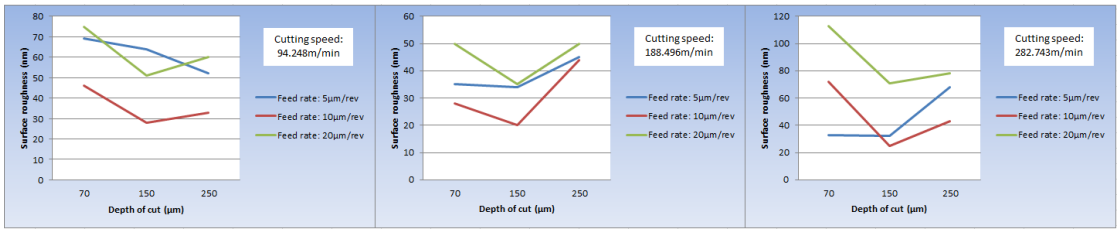

(c) Surface roughness vs Depth of cut

Figure 7-7 Surface roughness obtained under various cutting parameters

(1) Analysis of means

The effects of cutting parameters on surface roughness values are further evaluated through Taguchi method. The S/N ratios, which are known as the signal-to-noise ratios, are shown in Table 7-1. As the aim of this research is to make the machined surface roughness response as small as possible, “smaller the better” characteristic is applied to predict the S/N ratio against each level of initial parameters and can be expressed by:

$$\frac{S}{N_{smaller}} = -10\log_{10}[\frac{1}{n}\sum_{i=1}^{n} Y_i^2] \quad (7.5)$$

where, Y_i is the experimental value of surface roughness in the i^{th} test and n is the number of replications.

The variations of response due to the change of cutting parameters are shown in Table 7-2 and Table 7-3 below. These tables illustrate that feed rate has the most influence on the surface roughness, followed by cutting speed and the effect of depth of cut is minimal. This will be further validated through analysis of variance (ANOVA).

Table 7-2 Response for surface roughness

Level	v	f	a_p
1	53.11111	48	57.88889
2	37.88889	37.66667	40
3	59.44444	64.77778	49
Delta	21.55556	27.11111	17.88889
Rank	2	1	3

Table 7-3 Response for S/N ratios

Level	v	f	a_p
1	-34.1117	-33.2133	-34.4351
2	-31.2498	-30.9085	-31.3152
3	-34.5363	-35.776	-34.1475
Delta	3.2865	4.867579	3.119901
Rank	2	1	3

The response parameters are presented by the S/N ratio and the main effects are plotted from the mean value of Ra and S/N ratio. Figure 7-8(a) and Figure 7-8(b) below indicate that increase the level of these three cutting parameters, significant response can be observed on surface roughness and S/N ratios. According to the Taguchi method, the lower surface roughness due to the smaller-the-better characteristic and higher S/N ratio, which means the signal level is much higher than the noise level and further lead to an optimal machined surface, are applied. As a result, a level of factor with the lowest

mean value of Ra and the highest mean value of S/N ratio is observed as the optimal cutting parameter. Thus, the optimal cutting conditions in this MMCs micro milling process i.e. cutting speed of 188.496 m/min, feed rate of 10 µm/rev and axial depth of cut of 150 µm are adopted to obtain the lowest surface roughness. This shows a good agreement with the presented analytical results of machined surface roughness.

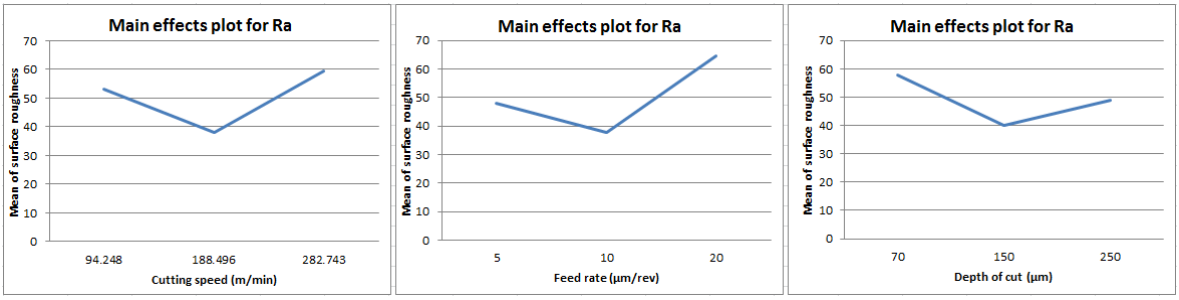

(a) Main effects plot for the surface roughness

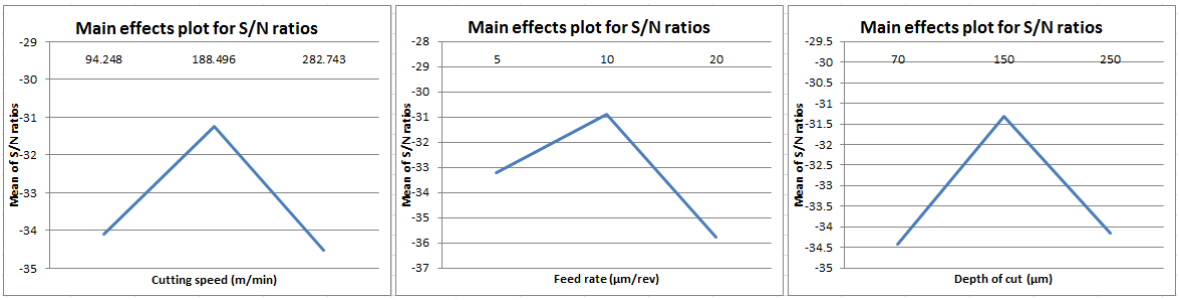

(b) Main effects plot for the S/N ratio

Figure 7-8 Main effects plotted from the mean value of Ra and S/N ratio

(2) Analysis of variance

Figure 7-8(a) and Figure 7-8(b) imply that these three cutting parameters have similar effects on the surface roughness; however, their contributions on the machined surface are contrast and can be achieved through ANOVA. ANOVA, as a confirmation test used with the identified optimum levels of all the parameters, is conducted in Matlab. This method is applied to identify the factors significance on response and influence of each factor on the resultant surface roughness. The approach is carried out for a confidence level of 95%, which means the factors with a P-value less than 0.05 are considered to have significant influence on resultant surface roughness. In addition, the contribution percentages of these cutting parameters are presented to find the most effective factor.

Table 7-4 ANOVA values for different factors

Analysis of Variance						
Source	Sum Sq.	d.f.	Mean Sq.	F-ratio	P-value	Contribution
v	2209.4	2	1104.7	8.12	0.0119	19.2%
f	3369.9	2	1684.93	12.38	0.0036	29.3%
a_p	1518.3	2	759.15	5.58	0.0304	13.2%
v*f	1816.1	4	454.04	3.34	0.0691	15.8%
v* a_p	776.4	4	194.09	1.43	0.3094	6.7%
f* a_p	736.6	4	184.15	1.35	0.3309	6.4%
Error	1088.7	8	136.09			9.4%
Total	11515.4	26				100%
(Indicates statistically full significant factors at 95% confidence level)						

According to the statistical results shown in Table 7-4, cutting speed, feed rate and axial depth of cut are observed to have a P-value less than 0.05. This indicates cutting speed, feed rate and axial depth of cut have significant contribution to the machined surface performance. Based on the specific value, feed rate has the highest influence on machined surface roughness, followed by cutting speed, interaction of cutting speed and feed rate, and axial depth of cut. Whereas the effects of interaction of these factors, particular for axial depth of cut, on surface roughness are minimal.

For MMCs precision turning process, the experimental setup has been introduced in Chapter 4 and experimental results of machined surface roughness is also analysed in this part. The orthogonal array of cutting parameters and the machined surface roughness under different settings of input factors are shown in Table 7-5.

Table 7-5 Orthogonal array of cutting parameters and resultant surface roughness

Experimental number	Cutting speed (m/min)	Feed rate (μm/rev)	Depth of cut (μm)	Surface roughness (nm)	S/N ratio
1	157.0	30	4	132	-42.4115
2	157.0	30	2.5	102	-40.1720

3	157.0	30	1	105	-40.4238
4	157.0	20	4	126	-42.0074
5	157.0	20	2.5	99	-39.9127
6	157.0	20	1	90	-39.0849
7	157.0	10	4	90	-39.0849
8	157.0	10	2.5	71	-37.0252
9	157.0	10	1	86	-38.6900
10	125.7	30	4	136	-42.6708
11	125.7	30	2.5	134	-42.5421
12	125.7	30	1	106	-40.5061
13	125.7	20	4	135	-42.6067
14	125.7	20	2.5	109	-40.7485
15	125.7	20	1	113	-41.0616
16	125.7	10	4	97	-39.7354
17	125.7	10	2.5	90	-39.0849
18	125.7	10	1	99	-39.9127
19	94.2	30	4	148	-43.4052
20	94.2	30	2.5	135	-42.6067
21	94.2	30	1	136	-42.6708
22	94.2	20	4	132	-42.4115
23	94.2	20	2.5	117	-41.3637
24	94.2	20	1	136	-42.6708
25	94.2	10	4	113	-41.0616
26	94.2	10	2.5	99	-39.9127
27	94.2	10	1	129	-42.2118

The machined surface roughness against cutting parameters has been illustrated in Chapter 4. Therefore, only their in-depth relationship is analysed in this section.

(1) Analysis of means

The influence of cutting parameters on surface roughness values in MMCs precision turning are evaluated through Taguchi method as well. The S/N ratios are shown in

Table 7-5. As the aim is to optimise the material machinability via reducing the machined surface roughness response as small as possible, "smaller the better" characteristic is applied to predict the S/N ratio against each level of initial parameters.

The variations of response due to the change of cutting parameters are shown in Table 7-6 and Table 7-7 below. These tables show the similar results to those in micro milling that feed rate has the most influence on the surface roughness, followed by cutting speed and the effect of depth of cut is minimal. This will be further validated through ANOVA.

Table 7-6 Response for surface roughness

Level	v	f	a_p
1	100.1111	126	123.2222
2	113.2222	117.4444	106.2222
3	127.2222	97.11111	111.1111
Delta	27.11111	28.88889	17
Rank	2	1	3

Table 7-7 Response for S/N ratios

Level	v	f	a_p
1	-39.868	-41.9343	-41.7105
2	-40.9854	-41.3186	-40.3743
3	-42.035	-39.6354	-40.8036
Delta	2.166946	2.298878	1.336274
Rank	2	1	3

The response parameters are presented by the S/N ratio and the main effects are plotted from the mean value of Ra and S/N ratio. The results shown in Figure 7-9(a) and Figure 7-9(b) demonstrate that significant response can be observed on surface roughness and S/N ratios when changing the level of these three cutting parameters. In addition, the lower surface roughness occurs due to the smaller-the-better characteristic and higher S/N ratio, which means the level of signal is much higher than the noise level and

further lead to an optimal machined surface. Therefore, the optimal cutting parameter is the one that presents a level of factor with the lowest mean value of Ra and the highest mean value of S/N ratio is observed. In this MMCs precision turning process, the optimal cutting conditions i.e. cutting speed of 157.0 m/min, feed rate of 10 µm/rev and depth of cut of 2.5 µm are found with resultant lowest surface roughness. This shows a good agreement with the presented analytical results of machined surface roughness.

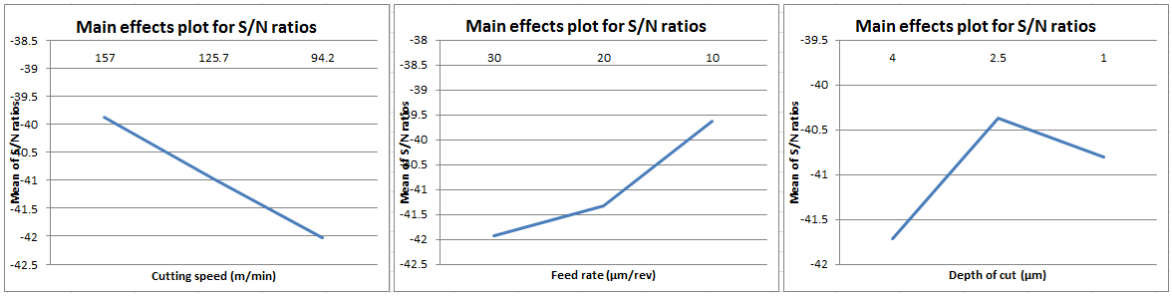

(a) Main effects plot for the surface roughness

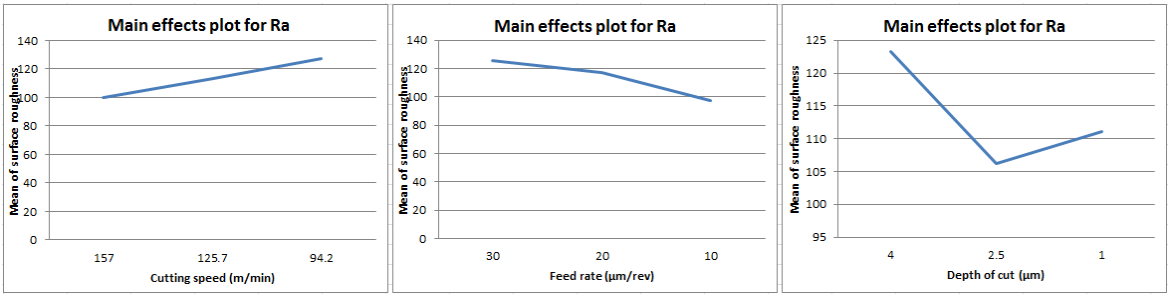

(b) Main effects plot for the S/N ratio

Figure 7-9 Main effects plotted from the mean value of Ra and S/N ratio

(2) Analysis of variance

The contributions of these three cutting parameters on the machined surface are contrast and can be achieved through ANOVA. This method is applied to identify the factors significance on response and influence of each factor on the resultant surface roughness. The approach is carried out for a confidence level of 95%, which means the factors with a P-value less than 0.05 are considered to have significant influence on resultant surface roughness.

Table 7-8 ANOVA values for different factors

Analysis of Variance						
Source	Sum Sq.	d.f.	Mean Sq.	F-ratio	P-value	Contribution
v	3308.7	2	1654.37	42.38	0.0001	31.4%
f	3963.6	2	1981.81	50.77	0.0001	37.6%
a_p	1378.7	2	689.37	17.66	0.0012	13.1%
v*f	74.4	4	18.59	0.48	0.7529	0.7%
v* a_p	690.6	4	172.65	4.42	0.0353	6.5%
f* a_p	822.4	4	205.59	5.27	0.0224	7.8%
Error	312.3	8	39.04			2.9%
Total	10550.7	26				100%
(Indicates statistically full significant factors at 95% confidence level)						

According to the statistical results shown in Table 7-8, cutting speed, feed rate, axial depth of cut and their combinations are observed to have a P-value less than 0.05, which means cutting speed, feed rate and axial depth of cut have significant effects on the machined surface. Based on the P-value and contribution percentage, feed rate has the highest influence on machined surface roughness, followed by cutting speed, depth of cut and interaction of these three parameters. Whereas the effects of interaction of cutting speed and feed rate on surface roughness are minimal.

7.3.1.2 Surface morphology

The surface roughness chart indicates that surface quality deteriorates dramatically due to the distinct microstructure of MMCs. As Ra cannot exactly depict the characteristics of machined surface, the surface profile and surface defects are further measured by 3D profiler and SEM.

Figure 7-10 shows the machined surface morphology. As can be observed from the images, the feed marks are noticeable which means most of particles are perfectly cut through rather than badly fractured or pulled out. Significant burrs can be seen on the machined surface particular along the tool paths shown in Figure 7-10(b) and Figure 7-10(d). Small pits are visible on the machined surface and the size of these pits is approximately 5 μm as shown in Figure 7-10(a) and Figure 7-10(c). This may formed

due to the particles pulled out from Al matrix. The similar results can be significantly observed from the results of precision turning experiment shown in Figure 7-11.

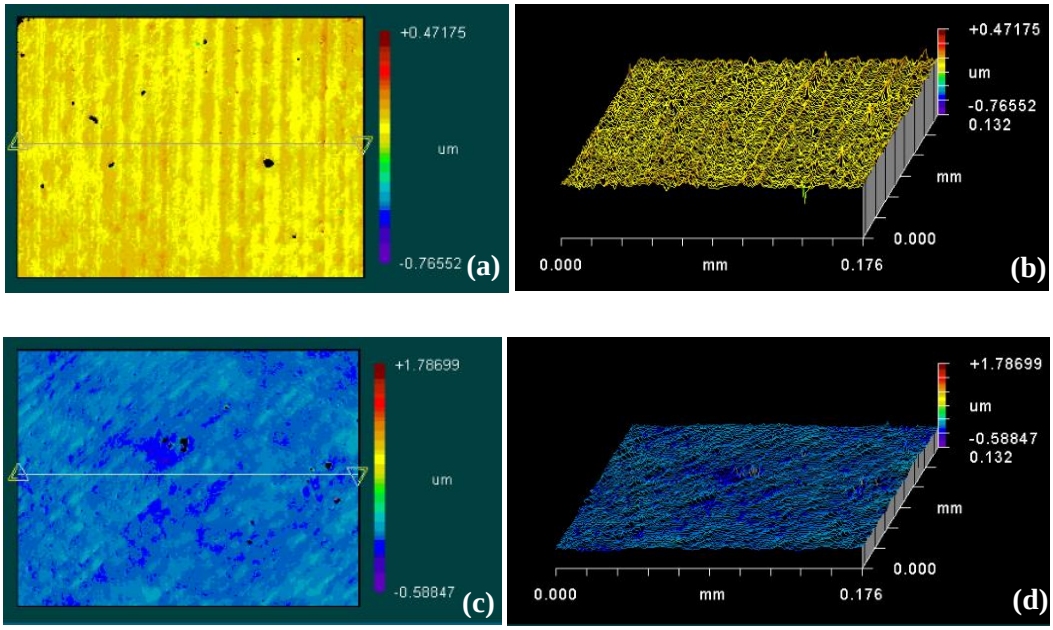

Figure 7-10 Surface morphology of the machined B_4C/Al MMCs workpiece in micro milling process

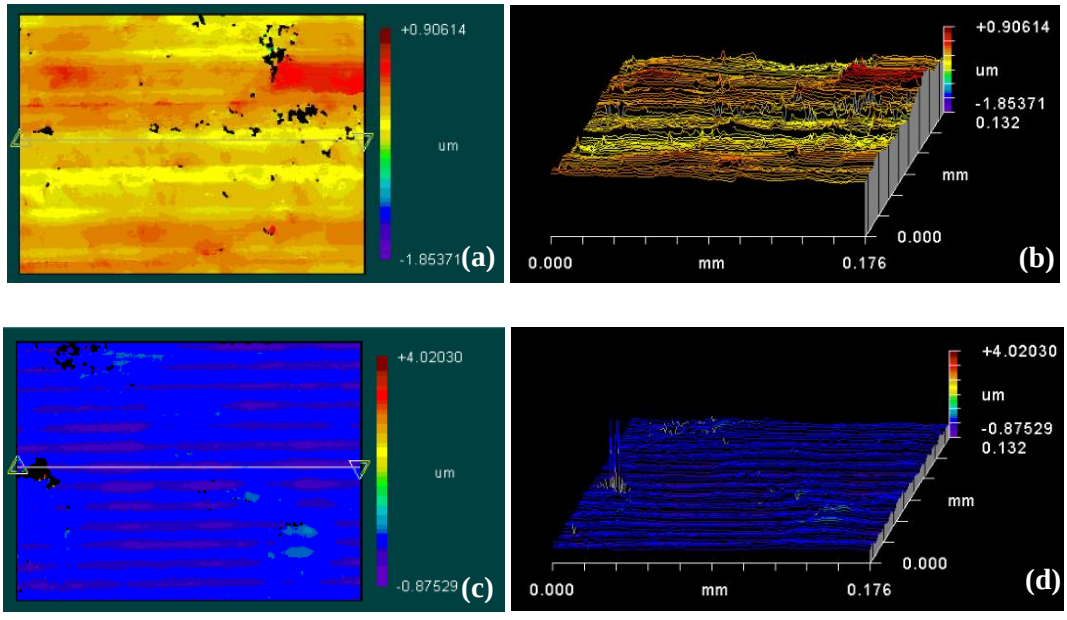

Figure 7-11 Surface morphology of the machined B_4C/Al MMCs workpiece in precision turning process

Figures 7-12(a) and Figure 7-12(b) demonstrate the microstructures and surface profiles of the un-machined and machined surfaces respectively through SEM images. From the

images, it is found that the reinforced B_4C particles can be distinguished from the Al matrix by different colour scale. It can be observed that particles are fractured into small pieces while Al matrix still bonded to the particles and machined surface quality enhanced. This implies that the plastically deformed aluminium fills the gaps of small particles which formed during machining. In addition, the cracks and pits formed on the fractured particles are also covered by the deformed aluminium. Thus, the machined surface areas are smoother.

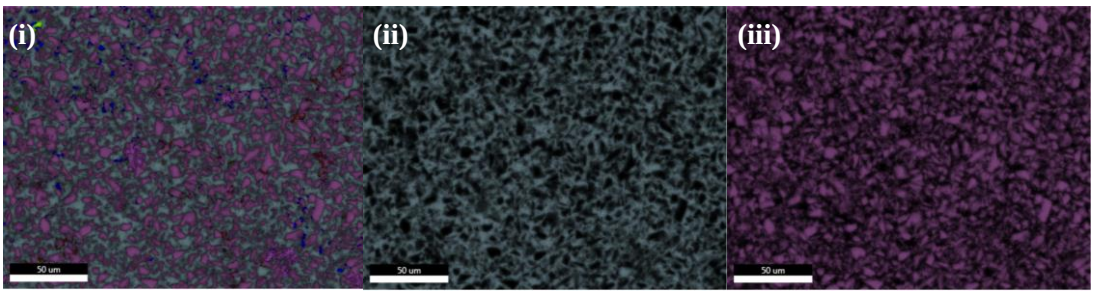

(a) SEM images of the un-machined surface: (i) B_4C/Al, (ii) Al matrix, (iii) B_4C particles

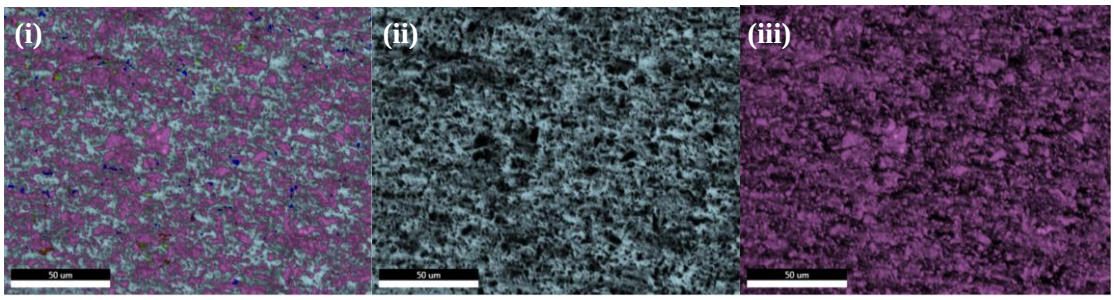

(b) SEM images of the machined surface: (i) B_4C/Al, (ii) Al matrix, (iii) B_4C particles

Figure 7-12 SEM images of the un-machined and machined surfaces

(a) Surface morphology of un-machined MMCs

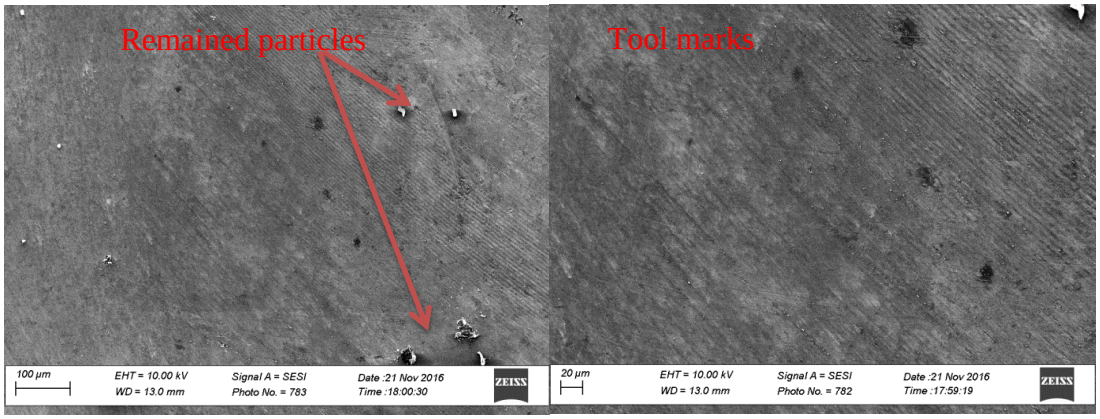

(b) Surface morphology of machined MMCs

Figure 7-13 Surface morphology of un-machined and machined MMCs

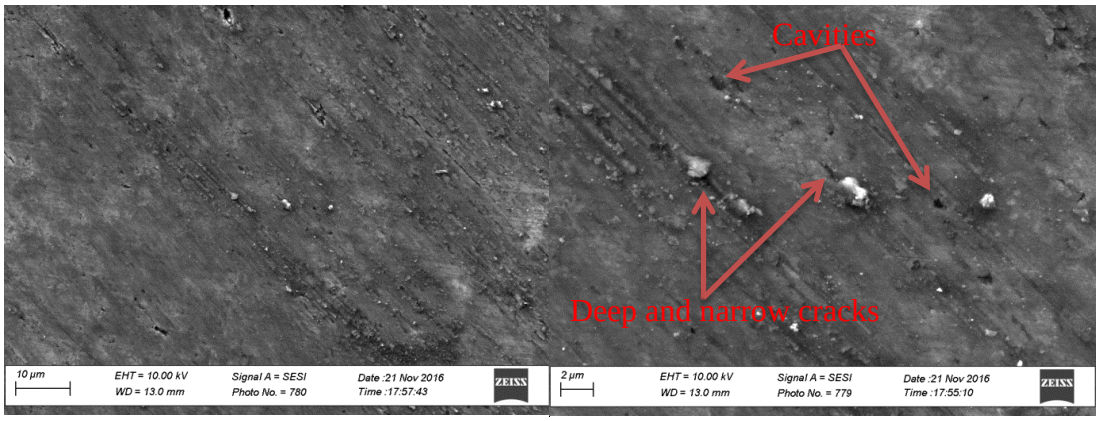

Figure 7-14 Surface morphology of machined MMCs

The surface topography and surface profile are further measured by SEM. Figure 7-13 shows that the tool path is still significant on the machined surface even the surface roughness is quite small while still relative larger than homogeneous material. The machined surface performs a good surface profile as shown in Figure 7-14, while some typical surface defects still can be found. Large cavities occur due to the particles are pulled out together with surrounding matrix material or debonding. Larger particles with deep and narrow crack surrounded can be observed on the machined surface due to the debonded particles between the tool and workpiece are pressed into the machined surface or the machining process experience elastic/plastic deformation on matrix material that results in the particles dislocated. Most areas of machined surface are quite smooth with few defects which mean the particles located at these areas are perfectly cut through or the plastically deformed aluminium fills the gaps of particle fracture

defects and matrix-particle interfacial defects and further enhance the final surface quality and integrity.

7.3.2 Optimisation on cutting tools

The precision turning experimental trials are conducted by using PCD tools with different nose angles and also natural diamond tools with relative sharp cutting edge. Under the same experimental conditions, the machining characteristics of B_4C/Al MMCs by using different tools can be concluded as below. The machinability derived from the cutting trials is assessed based on the evaluation indicators including machined surface integrity, tool integrity and cutting force variation.

(1) Tool geometry

In order to find the influence of cutting tool geometry on the machinability of MMCs, three PCD inserts with zero rake angle while different nose radius as shown in Figure 7-15 are performed in the experimental trials. The comparison of machining characteristics is illustrated as below. The machined surface roughness and cutting force by using these three tools under same cutting conditions and cutting parameters are shown in Table 7-9.

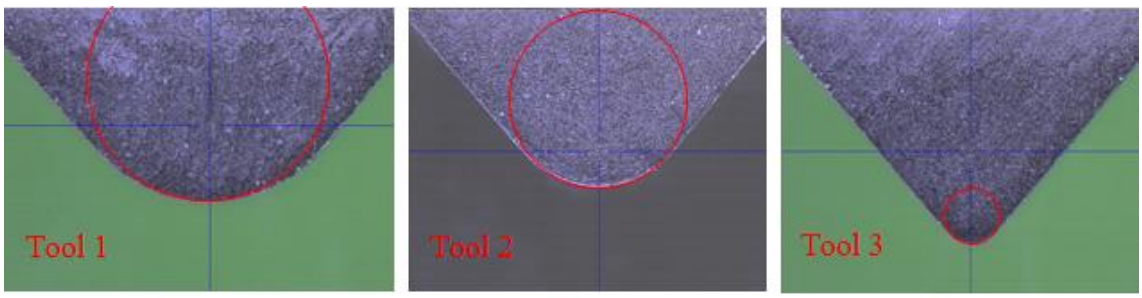

Figure 7-15 PCD inserts in MMCs precision turning process

Table 7-9 Surface roughness and cutting force in MMCs precision turning by using different tools

No.	Cutting tool	Feed rate (μm/rev)	Depth of cut (μm)	Cutting speed (m/min)	Cutting force (N)			Surface roughness (nm)
					Feed force	Normal force	Cutting force	
1	Tool 1	10	2.5	157.0	9.499	4.509	10.515	70
2	Tool 2	10	2.5	157.0	9.934	5.333	11.275	71
3	Tool 3	10	2.5	157.0	12.030	6.350	13.603	75
4	Tool 1	10	4	94.2	21.830	11.870	24.848	109
5	Tool 2	10	4	94.2	22.030	11.820	25.001	113
6	Tool 3	10	4	94.2	23.760	13.410	27.036	115

The experimental results of machined surface roughness indicate that cutting tool nose radius has effects on the machined surface quality. Surface roughness increase with the decrease of tool nose radius under entire cutting conditions and cutting parameters. The tool wear did not state significant differences for these three tools due to the extremely short cutting time. However, the tool wear can be observed and predicted from the machined surface roughness and cutting force. The roughness value of outer side machined surfaces, which is the starting point of cutting process and cutting tool wear is observed as zero, are almost the same in each cutting cycle; while for the surface roughness at the centre of machined workpiece shown in Table 7-9, the best surface quality only can be find when using PCD tools with larger tool nose radius. In addition, the force components in both feed and normal directions together with total force magnitudes shown in Table 7-9 indicate that the smallest cutting force occurs at larger nose radius. This contributes to the reduction of tool wear rate. As a result, tool with larger nose radius and zero rake angles is seen as the optimal cutting tool for obtaining better cutting performance including smaller surface roughness, lower tool wear rate and smaller cutting force.

(2) Tool material

The cutting tool property is another critical factor that affects the machinability of MMCs. In this part, PCD insert and natural diamond insert both with zero rake angle and same nose radius are conducted to evaluate the workpiece machinability. Figure 7-

16 shows the tools used in these experiments. Table 7-10 demonstrates the machined surface roughness by using these two tools respectively.

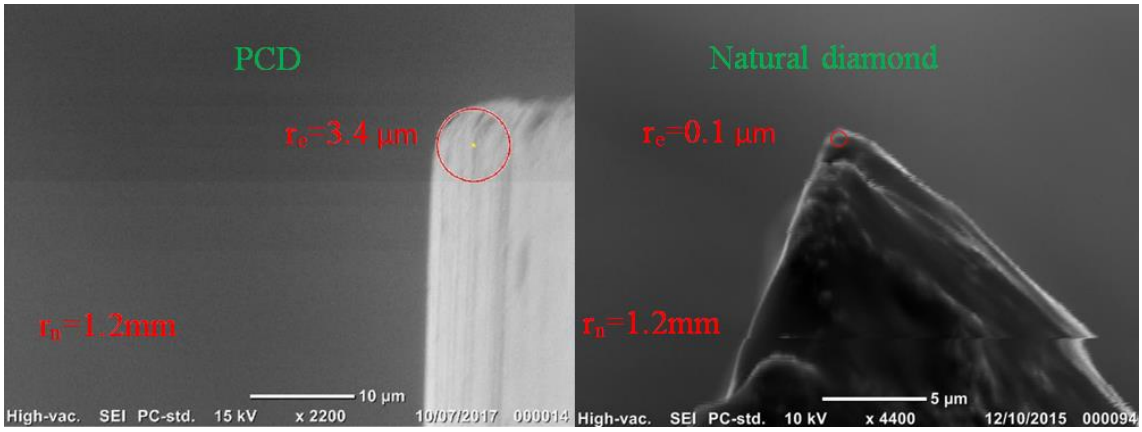

Figure 7-16 Cutting tools used in MMCs precision turning process

Table 7-10 Machined surface roughness by using PCD and natural diamond tools

Experiment No.	Cutting tool	Feed rate (μm/rev)	Depth of cut (μm)	Cutting speed (m/min)	Surface roughness (nm)
1	PCD	10	2.5	157.0	71
2	Diamond	10	2.5	157.0	124
3	PCD	10	4	157.0	90
4	Diamond	10	4	157.0	153
5	PCD	10	2.5	94.2	113
6	Diamond	10	2.5	94.2	173

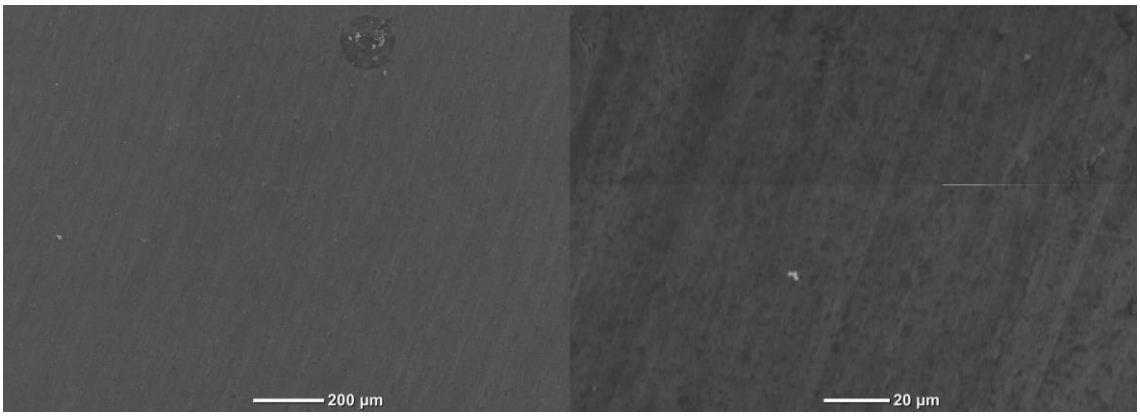

(a) Machined surface morphology by using PCD tools

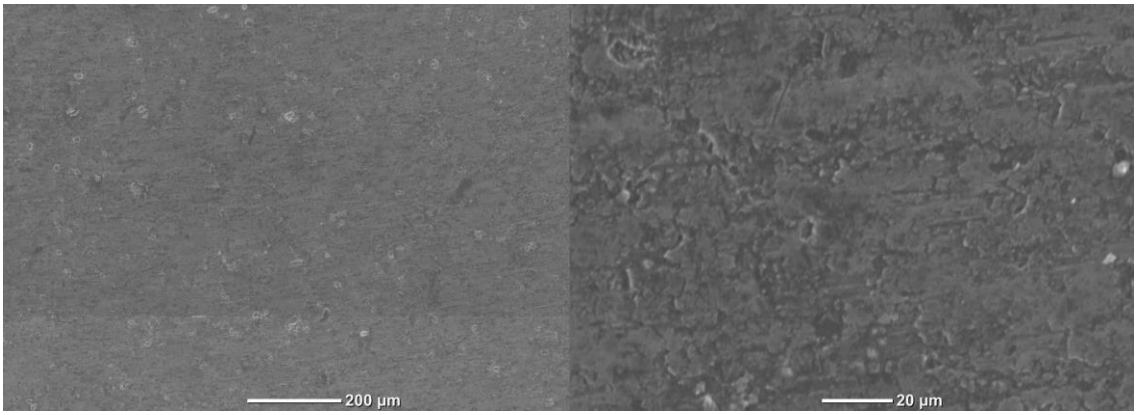

(b) Machined surface morphology by using natural diamond tools

Figure 7-17 Machined surface morphology by using two different tools

In term of the machine surface roughness, the roughness value shown in Table 7-10 implies that machined surface has much smaller roughness by using PCD tool than natural diamond tool. In addition, both of these two tools exhibit characteristic abrasive wear patterns. However, the tool wear rate especially on the wear height of natural diamond tool is excessive in a single cut as shown in Table 7-12, while the wear on PCD tool is insignificant under same cutting conditions. The actual tool wear presenting by the wear height and flank wear length is shown in Figure 7-20 and Figure 7-21. For the cutting force in MMCs precision turning process, Table 7-11 and Figure 7-18 show the cutting force magnitude in MMCs precision turning by using PCD tool and natural diamond tool respectively. The cutting force magnitude by using natural diamond tool is almost 10 times smaller than using PCD tool; however, the force increment in this cutting process is significant and much larger than that of PCD tool. This is due to the rapid tool wear of natural diamond tool when machining particulate MMCs. On the other hand, due to the low thermal stability of natural diamond, MMCs machining with high temperature generation will lead to its carbonized (ie, graphitized) at 700-800 ° C, and further acceleration of the tool wear rate. As a result, dramatically decrease in tool life and poor surface finish of machined parts occurs. Even the chip load is extremely small when using natural diamond tool due to the relative small edge radius, the rapid tool wear and poor surface integrity of machined parts make it unreliable in MMCs precision machining.

Table 7-11 Cutting force value by using PCD and natural diamond tools

No.	Cutting tool	Cutting force (N)		
		F_c	F_t	F_{total}
1	PCD	9.934	5.333	11.275
2	Diamond	1.502	0.530	1.593
3	PCD	12.740	7.806	14.941
4	Diamond	2.602	0.999	2.787
5	PCD	9.942	5.621	11.421
6	Diamond	1.656	0.548	1.744

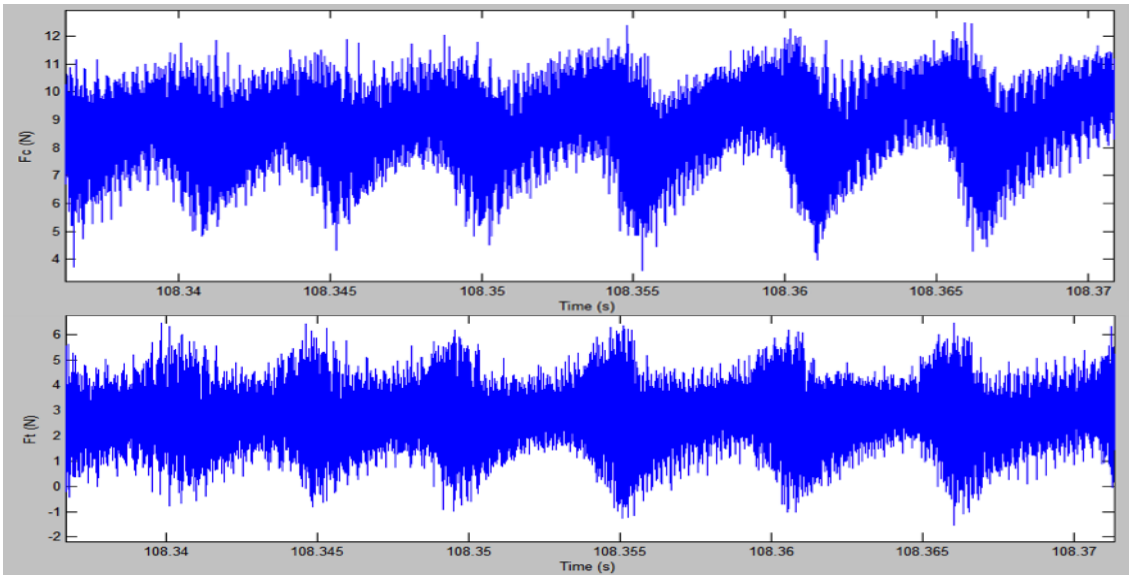

(a) Cutting force signal by using PCD tool

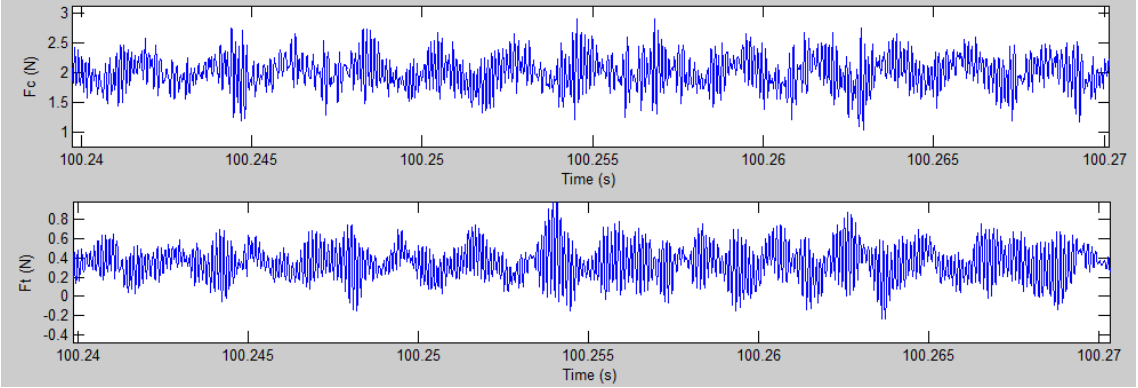

(b) Cutting force signal by using natural diamond tool

Figure 7-18 Cutting force in MMCs precision turning by using PCD tool and natural diamond tool under same cutting parameters

Table 7-12 Tool wear and wear rate by using PCD and natural diamond tools

Tool	PCD	Natural diamond
Time (s)	3000	150
Wear height (μm)	28.2	4.1
Wear length (μm)	170	12.1
Wear rate (height) (μm/s)	0.0094	0.027
Wear rate (length) (μm/s)	0.057	0.081

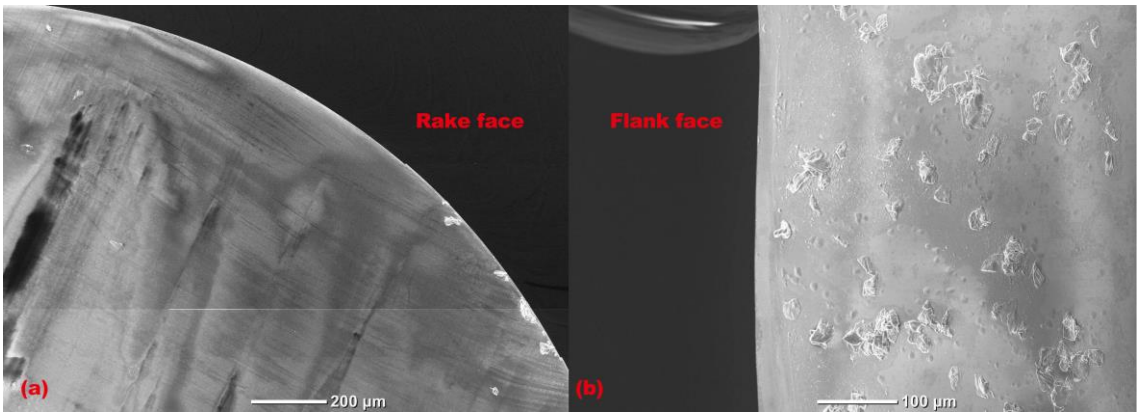

Figure 7-19 Surface morphology of new natural diamond tools

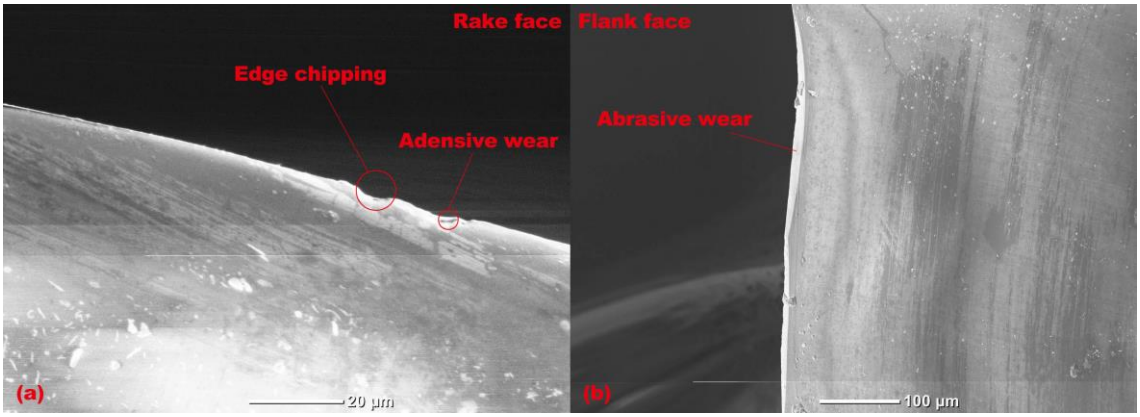

Figure 7-20 Cutting tool wear by using natural diamond tools

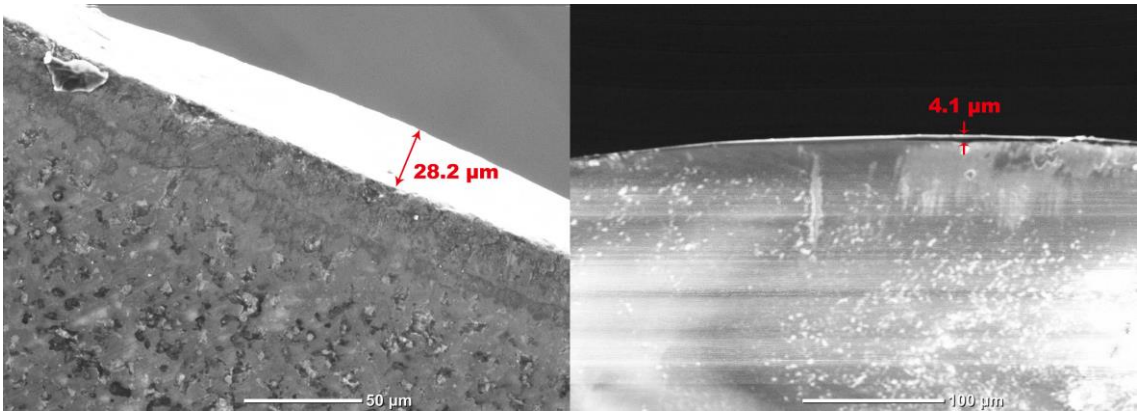

(a) Wear height

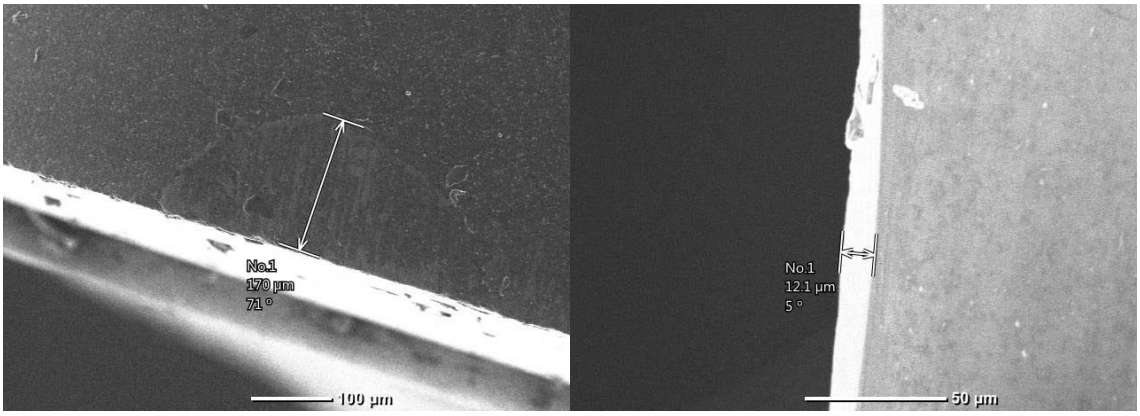

(b) Flank wear length

Figure 7-21 Cutting tool wear by using PCD and natural diamond tools

7.3.3 Optimisation on workpiece microstructures

The micro milling experiments are further conducted on three different MMCs materials including 45% SiC/Al MMCs with 5 µm particle size, 60% SiC/Al MMCs with 90 µm particle size and 50% B_4C/Al MMCs with 5 µm particle size. The machining process variables and cutting conditions are set as the same. The experimental results on machining characteristics are recorded and analysed by using the same methods as shown in section 7.1. The distinct machining characteristics for these three materials are summarised in the following Tables. The machined surface roughness of B_4C/Al MMCs has been illustrated in Table 7-1 in the previous section.

Table 7-13 Machined surface roughness of SiC/Al MMCs under varied cutting parameters

Experimental number	Spindle speed (rpm)	Cutting speed (m/min)	Feed rate (μm/rev)	Axial depth of cut (μm)	Surface roughness (nm)
1	6,000	188.496	10	150	60
2	6,000	188.496	20	150	95
Workpiece material: Al/5 μm SiC/45p; Radial depth of cut: 3 mm					
3	6,000	188.496	5	150	118
4	6,000	188.496	10	150	105
Workpiece material: Al/90 μm SiC/60p; Radial depth of cut: 3 mm					

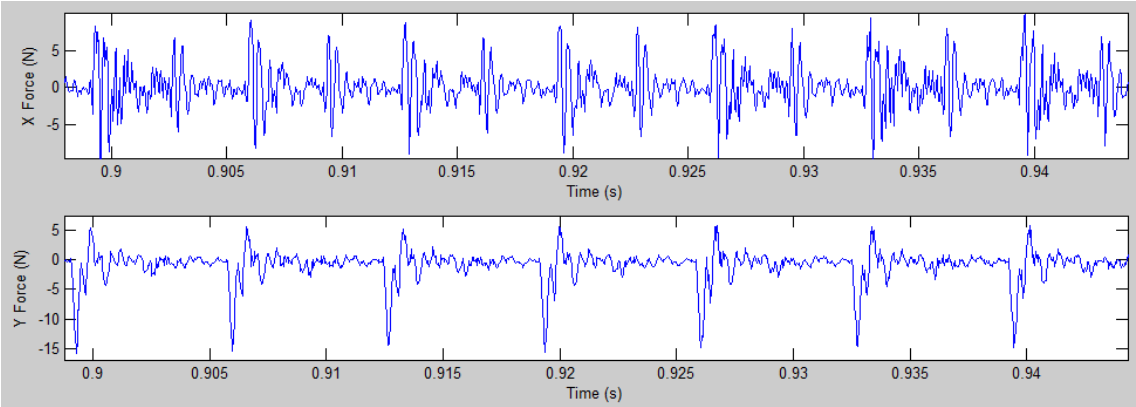

(a) Cutting force for 45% SiC/Al MMCs with 5 μm particle size

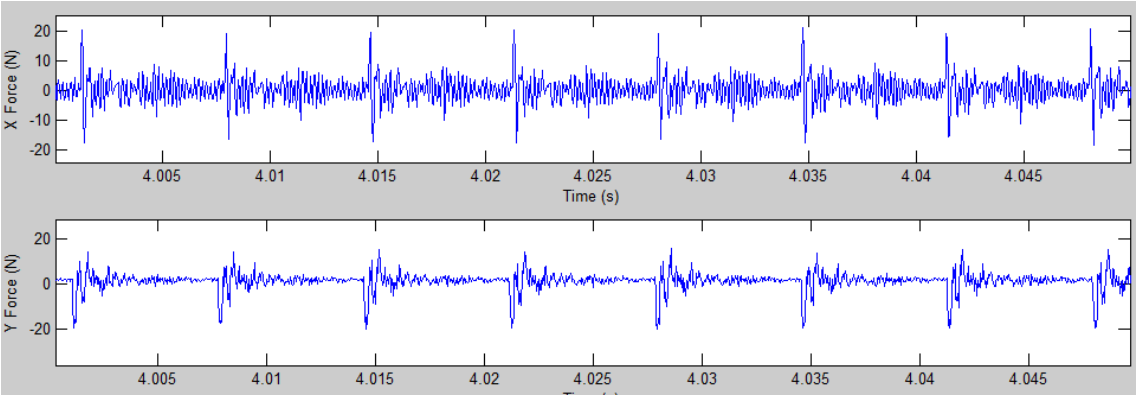

(b) Cutting force for 60% SiC/Al MMCs with 90 μm particle size

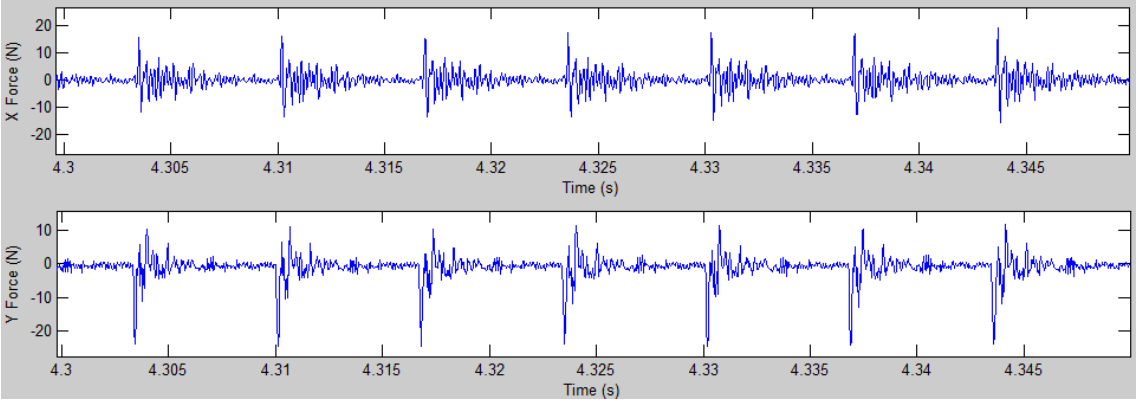

(c) Cutting force for 50% B_4C/Al MMCs with 5 μm particle size

Figure 7-22 Cutting force for three different materials under same cutting condition

From the experimental results, it can be observed the surface roughness of B_4C/Al is smaller than that of SiC/Al shown in Table 7-13 at each set of cutting parameters and cutting conditions when the material composition is similar. This is due to the bonding of B_4C/Al is stronger as revealed by the good mechanical properties [250]. With stronger bonding, particles are mostly cut through rather than debonding which leave larger defects on the machined surface and lead to poor machining quality. In term of SiC/Al MMCs with different grain size of particles, the SiC/Al MMCs with 90 μm particle size performs a surface roughness of 105 nm and 118 nm while the roughness value is 60 nm and 70 nm respectively for SiC/Al MMCs with 5 μm particle size under same cutting parameters. This indicates that the smaller the particle grain size is, the smaller the surface roughness will be obtained. From the force signals shown in Figure 7-22, it can be found that 45% SiC/Al MMCs with 5 μm particle size has smallest cutting force with less variation which means the progressive tool wear is smaller than machining on other materials. In addition, better surface quality can be obtained for MMCs with lower particle volume fraction due to the reduced cutting force and decreased tool wear with fewer defects generated on the machined surface. The detailed machined surface characteristics are shown in Figure 7-23. The cutting force on B_4C/Al MMCs is the highest due to its relative higher hardness. However, the better surface profiles with less defects including cracks, voids and cavities, smaller surface variation and smaller surface roughness can be observed on the machined surface of B_4C/Al MMCs with small particles and low volume fraction, while the larger surface roughness with significant surface defects occurs when machining on 60% SiC/Al with 90 μm grain size. Thus, the better machinability is observed on the MMCs with smaller particle

size and lower volume with normal distribution, and better surface finish performed on MMCs with B_4C reinforcements rather than SiC reinforcements.

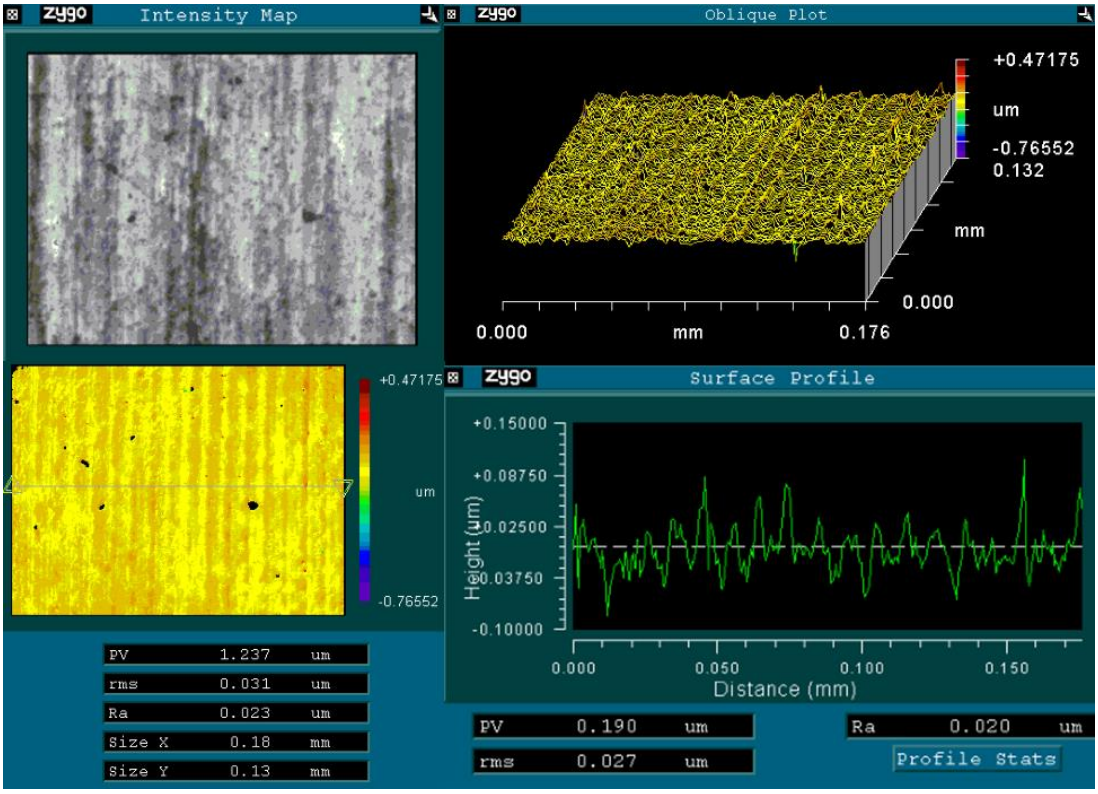

(a) Machined surface characteristics of 5 µm B_4C/Al MMCs

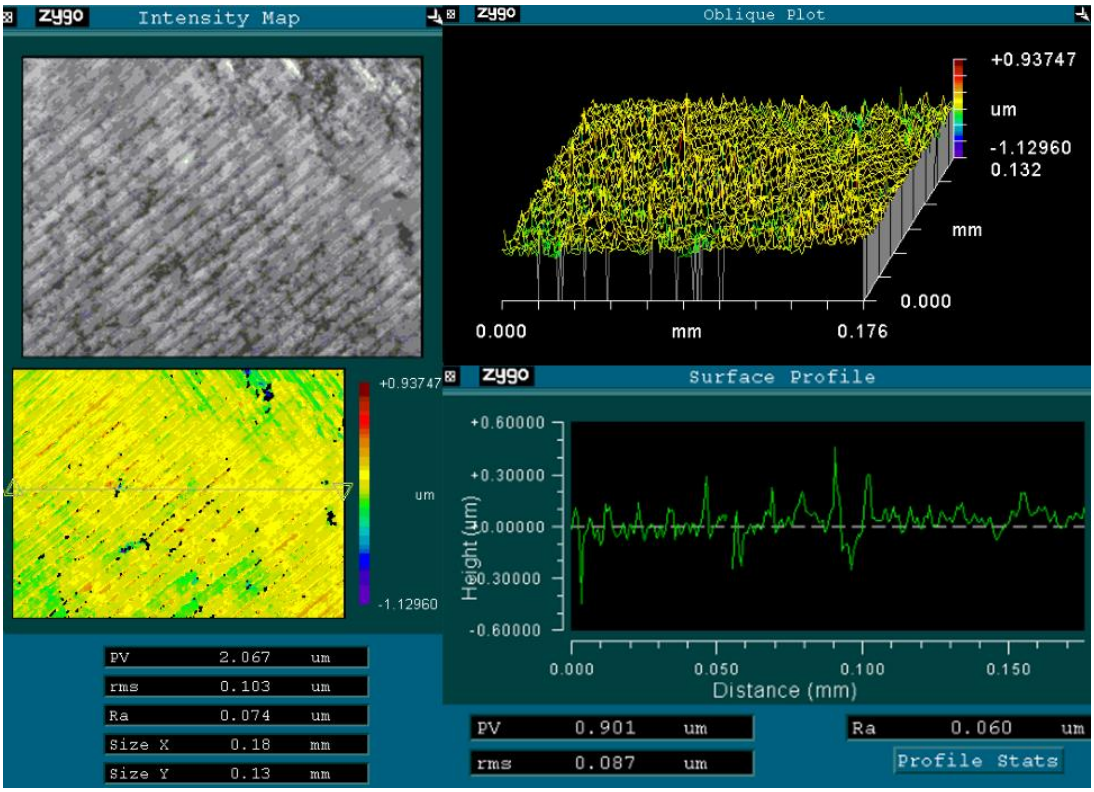

(b) Machined surface characteristics of 5 µm SiC/Al MMCs

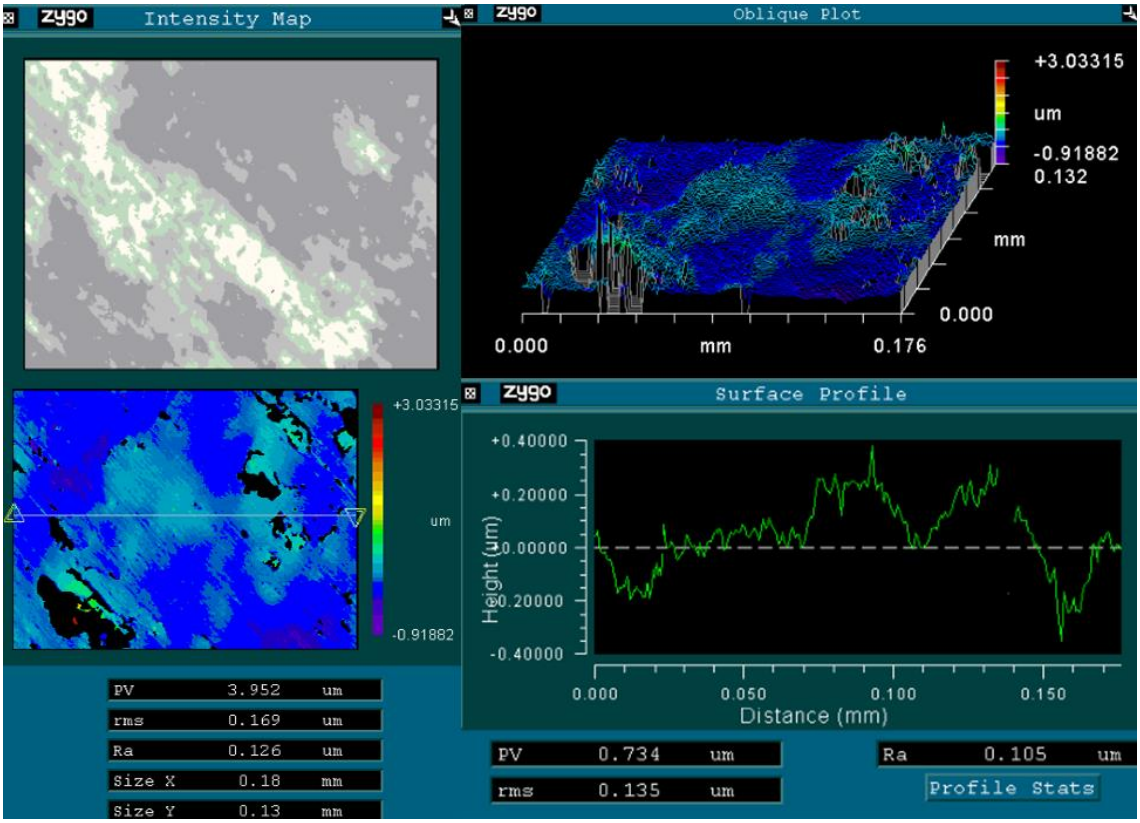

(c) Machined surface characteristics of 90 µm SiC/Al MMCs

Figure 7-23 Machined surface characteristics of three different materials under the cutting parameters: cutting speed: 188.496 m/min, feed rate: 10 µm/rev, DOC: 150 µm

7.4 Concluding remarks

This chapter presents the machinability assessment of three different metal matrix composite materials in precision turning and micro milling processes. An experimental study on the cutting performance of MMCs and the machining process optimisation are conducted under varied cutting parameters, cutting tool conditions and workpiece material properties. The following conclusions can be drawn from the experimental results and analysis:

1. A series of high precision milling experiments on Al/5µmB_4C/50p MMCs by using PCD end mills are performed to investigate the surface generation and the material machinability can be achieved against the process variables. The optimal cutting parameters, i.e. cutting speed of 188.496 m/min, feed rate of 10 µm/rev and axial depth of cut of 150 µm, are identified towards lower surface roughness and better surface morphology. Analysis of means (ANOM) results reveal that these three cutting parameters have similar effects on the surface roughness and

the optimal cutting conditions via roughness analysis are confirmed by ANOM. Analysis of variance (ANOVA) results indicate that contribution percentages of these parameters on the machined surface are contrast. Feed rate, as the dominate factor, has the highest influence on the responses, followed by cutting speed and depth of cut. Interaction of these factors has the minimal effects on the machined surface roughness.

2. Precision turning experiments on Al/5μmB_4C/50p MMCs are also carried out to investigate the surface generation. The optimal cutting conditions i.e. cutting speed of 157.0 m/min, feed rate of 10 μm/rev and axial depth of cut of 2.5 μm are found with lowest resultant surface roughness. The experimental results also show the similar results to those in micro milling process that feed rate has the highest influence on machined surface roughness, followed by cutting speed, depth of cut and interaction of these three parameters. Whereas the effects of interaction of cutting speed and feed rate on surface roughness are minimal.
3. For the surface morphology, feed marks, burrs and pits are noticeable in MMCs precision machining. Some of the reinforced particles are pulled out during the machining, while most are perfectly cut through. Plastically deformed aluminium fills the gaps and covers the cracks and pits generated on the fractured particles, which helps result in a smoother surface with smaller surface roughness and better surface quality to some extent.
4. The further material machinability assessment and process optimisation results indicate that tool with larger nose radius and zero rake angles is observed as the optimal cutting tool for obtaining better cutting performance including smaller surface roughness, lower tool wear rate and smaller cutting force. In addition, PCD tool has better tool performance and cutting performance than natural diamond tool in MMCs precision machining process. Even the chip load is extremely small when using natural diamond tool, the rapid tool wear and poor surface integrity make it unreliable. Moreover, the better surface profiles with less defects and smaller surface roughness can be seen on the machined surface of B_4C/Al MMCs with small particles and low volume fraction. This is due to the bonding between Al matrix and B_4C particles are strongest as revealed by the good mechanical properties. The better cutting performance under higher cutting force occurs due to most particles under strong bonding condition are perfectly cut through rather than badly fractured, debonding or dislocation.

Chapter 8 Conclusions and recommendations for future work

8.1 Conclusions

In this research, the cutting mechanics of particulate metal matrix composites, material machinability and machining process optimisation are extensively investigated through multiscale multiphysics based integrated approach. A scientific understanding on MMCs precision machining process is obtained from the aspects of MMCs chip formation mechanism, dynamic cutting force modelling, multiphysics coupled thermal-mechanical-tribological tool wear analysis and machinability assessment. The distinctive conclusions for this research work can be drawn from the following aspects.

(1) Multiscale multiphysics based approach to investigate the MMCs precision machining process is proposed. The integrated approach demonstrates the interrelationship of key process factors and provides an in-depth understanding of MMCs precision machining process especially for its cutting mechanics, cutting performance, machinability assessment and process optimisation.

(2) The minimum chip thickness in MMCs precision machining has been identified through multiscale based mathematical analysis and experimental evaluation and validation on precision turning machine. The perfectly matched outcomes show that minimum chip thickness value is significantly influenced by the cutting edge radius and reinforced particle grain size together.

(3) Multiphysics based FE simulation and analysis is further conducted under varied cutting conditions and cutting parameters. The simulation outcomes show that the material removal mechanism and machined surface profile are strongly affect by the tool-workpiece interaction including tool/matrix material pair, tool/particle pair and tool/ bonding interface pair. The best surface quality can be observed in the scenario of depth of cut is equal to the particle radius along with proper lower feed rate and higher cutting speed.

(4) The chips are found as powder form with extremely small chip length from the FE simulation and analysis. This is evaluated and validated via well-designed precision turning trials. Discontinued short curled chips due to combined fracture/rupture/crumbling process can be identified in each cutting cycle.

(5) The chip morphology analysis shows that the inner surface of chip performs ribbon form topography due to the material shearing and outer surface exhibits a relative smooth morphology with small texture along the cutting direction due to the rake face texture of PCD tool and tool-chip interfacial friction. In addition, a significant variation ranging from prominent saw-tooth profile to light waviness is commonly featured on the chip outer surface with the orientation vertical to the cutting direction that attributes to the existence of reinforced particles and their location along the cutting line. The chip formation has slightly difference under different cutting parameters.

(6) The dynamic cutting force model has been proposed. By considering the cutting tool runout, instantaneous chip thickness, real tool trajectory and etc., the detailed MMCs milling force variation including the matrix material shearing force and particle fracture force are demonstrated appropriately. Simulation results indicate that feed rate, radial depth of cut, axial depth of cut and also the particle size and volume fraction have significantly effects on the predicted cutting force variation. Experimental evaluation and validation are carried out by compensating the measured forces via hammer-dynamometer test determined transfer function. The force model has a good agreement with the actual force value from experiments. The modified force model is further applied to improve the resultant surface form accuracy and also reduce the surface roughness by choosing the optimal process variables in MMCs precision machining process.

(7) The heat generation and cutting temperature are represented by the heat sources in five different cutting areas. The cutting temperature partition in MMCs precision machining is investigated by means of multiphysics coupled thermal-mechanical-tribologial modelling and simulation. Simulation results show that the highest temperature on the workpiece material is normally along the round cutting edge rather than the area that largest plastic deformation occurs. In term of the cutting tool, the highest temperature occurs around the round cutting edge while close to the material separation point. When machining on the brittle particles, the highest temperature can be observed at the tool-particle interaction point where particle fracture occurs. The resultant temperature is much higher than that in machining on matrix material.

(8) The tool wear type and characteristics have been investigated via experimental trials. The tool wear rate model is proposed by taking the cutting stress and cutting

temperature obtained from multiphysics based simulation into consideration. The outcomes indicate the tool wear model is reasonable to apply for the prediction of cutting tool wear.

(9) The machined surface generation and machinability assessment of particulate MMCs are investigated covering the aspects of machined surface roughness, cutting force, tool wear, tool life and machining efficiency. Cutting parameters, cutting tool conditions and workpiece material conditions are found as the most critical factors that have significant effects on the tool performance and cutting performance. The machinability of particulate MMCs can be improved through process optimisation by taking account of these factors.

Major contributions to the knowledge spanned out from this research can be as follows:

(1) A multiscale multiphysics based approach to modelling and analysis of MMCs precision machining is formulated, which is particularly helping address the intrinsic relationships among the micro geometry of the cutting tool, process variables, particles size and density, tool-workpiece interfacial multiphysics phenomena in the cutting.

(2) The dynamic cutting force model is developed by considering the multiscale aspects of tool-workpiece interface in the dynamic process and also the tool runout, instantaneous chip thickness and real tool trajectory in micro milling. This improved force model can be further applied to predict the cutting force variations in precision turning and micro milling of MMCs.

(3) The holistic experimental study is conducted in light of the research approach above to investigate the surface generation and surface roughness in MMCs precision machining, and the corresponding process optimisation.

8.2 Recommendations for future work

The recommendations for future work can be summarised in the following aspects:

(1) In this research, the simulation set-up has not taken all the bonding conditions into consideration. For mechanical bonded particle-matrix interface, the set-up with only tied together is enough due to the fabrication method of MMCs. However, for MMCs with chemical bonding methods, the simulation set-up is worth investigating in the following research.

(2) The dynamic cutting force model still need to be improved due to the current multiscale model did not take cutting temperature and tool wear into account. The change of material properties at different cutting temperature and change of tool geometries under continue tool wear condition may obviously affect the cutting force behaviour and magnitude.

(3) Cutting temperature partition model has not been verified due to the cutting heat areas cannot be divided in real cutting condition and also the limitation of experimental environment. The experimental validation process and improvement are required.

(4) Tool wear characterisation especially for the wear status throughout its lifespan is still less understood and need to be further analysed from frequency analysis and wavelet analysis.

References

[1] Matthews, F. L. and Rawlings R. D. (1999) *Composite Materials: Engineering and Science*. UK, Woodhead Publishing Limited.

[2] Scherm, F., Völkl, R., Smaalen, S., Mondal, S., Plamondon, P., L'Espérance, G., Bechmann, F. and Glatzel, U. (2009) Microstructural characterization of interpenetrating light weight metal matrix composites. *Materials Science and Engineering: A*. 518(1-2), 118-123.

[3] Ramnath, B. V., Elanchezhian, C., Annamalai, R. M., Aravind, S., Atreya, T. S. A., Vignesh, V. and Subramanian, C. (2014) Aluminium metal matrix composites - a review. *Reviews on Advanced Materials Science*. 38, 55-60.

[4] Dabade, U. A. and Jadhav, M. R. (2016) Experimental study of surface integrity of Al/SiC particulate metal–matrix composites in hot machining. *Procedia CIRP*. 41, 914-919.

[5] Shorowordi, K. M., Laoui, T., Haseeb, A. S. M. A., Celis, J. P., and Froyen, L. (2003) Microstructure and interface characteristics of B_4C, SiC and Al_2O_3 reinforced Al matrix composites: a comparative study. *Journal of Materials Processing Technology*. 142(3), 738-743.

[6] Sahoo, A. K., Pradhan, S. and Rout, A. K. (2013) Development and machinability assessment in turning Al/SiCp-metal matrix composite with multilayer coated carbide insert using Taguchi and statistical techniques. *Archives of Civil and Mechanical Engineering*. 13(1), 27-35.

[7] Krishna, M. V. and Xavior, A. M. (2014) An Investigation on the mechanical properties of hybrid metal matrix composites. *Procedia Engineering*. 97, 918-924.

[8] Xavior, A. M. and Kumar, J. P. A. (2017) Machinability of hybrid metal matrix composite - a review. *Procedia Engineering*. 174, 1110-1118.

[9] Si, C., Tang, X., Zhang, X., Wang, J. and Wu, W. (2017) Microstructure and mechanical properties of particle reinforced metal matrix composites prepared by gas-solid two-phase atomization and deposition technology. *Materials Letters*. 201, 78-81.

[10] Seeman, M., Ganesan, G., Karthikeyan, R. and Velayudham, A. (2010) Study on tool wear and surface roughness in machining of particulate aluminum metal matrix composite-response surface methodology approach. *Int J Adv Manuf Technol*. 48, 613-624.

[11] Ramanujam, R., Muthukrishnan, N. and Raju, R. (2011) Optimization of cutting parameters for turning Al-SiC(10p) MMC using ANOVA and grey relational analysis. *Int J Precis Eng Manuf*. 12, 651-656.

[12] Andrewes, C. J. E., Feng, H-Y., Lau, W. M. (2000) Machining of an aluminum/SiC composite using diamond inserts. *J Mater Process Technol*. 102, 25-29.

[13] Ding, X., Liew, W. Y. H., Liu, X. (2005) Evaluation of machining performance of MMC with PCBN and PCD tools. *Wear*. 259, 1225-1234.

[14] Pramanik, A., Zhang, L. C. and Arsecularatne, J. A. (2008) Machining of metal matrix composites: Effect of ceramic particles on residual stress, surface roughness and chip formation. *International Journal of Machine Tools & Manufacture*. 48, 1613-1625.

[15] Ehmann, K. F., Bourell, D., Culpepper, M. L., Hodgson, T. J., Kurfess, T. R., Madou, M., Rajurkar, K. and Devor, R. E. (2005) *International assessment of research and development in micro-manufacturing*. WORLD TECHNOLOGY EVALUATION CENTER INC BALTIMORE MD.

[16] Nikhilesh, C. and Krishan, K. C. (2013) *Metal Matrix Composites*. Springer-Verlag New York.

[17] Cheng, K. and Huo, D. H. (2013) *Micro Cutting: Fundamentals and Applications*. Chichester, John Wiley & Sons.

[18] http://www.machinedesign.com/materials/future-metal-matrix-composites. (Accessed on 18 May 2018)

[19] https://www.designnews.com/electronics-test/metal-ceramic-matrix-composites-beat-heat/106075980443686/page/1/0. (Accessed on 18 May 2018)

[20] https://materion.com/products/composites-compounds-ceramics/metal-matrix-composites/supremex. (Accessed on 18 May 2018)

[21] Rawal, S. (2001) Metal-matrix composites for space applications. *JOM Journal of the Minerals, Metals and Materials Society*. 53(4), 14-17.

[22] Liu, J. (2012) *Experimental Study and Modeling of Mechanical Micro-Machining of Particle Reinforced Heterogeneous Materials*. Ph.D. Dissertation, University of Central Florida, Orlando, FL.

[23] Kainer, K. U. (2006) *Metal Matrix Composites -- Custom-made Materials for Automotive and Aerospace Engineering*. Wiley-VCH Verlag GmbH & Co. KGaA.

[24] Teti, R. (2002) Machining of composite materials. *CIRP Annals*. 51(2), 611–634.

[25] Tomac, N., Tannessen, K., and Rasch, F. O. (1992) Machinability of particulate aluminium matrix composites. *CIRP Annals*. 41(1), 55-58.

[26] Balazinski, M., Songmene, V., and Kishawy, H. A. (2012) Analyzing the machinability of metal matrix composites. *Machining Technology for Composite Materials*. A volume in Woodhead Publishing Series in Composites Science and Engineering, 394-411.

[27] Liu, J., Li, J., and Xu, C. (2014) Interaction of the cutting tools and the ceramic-reinforced metal matrix composites during micro-machining: A review. *CIRP Journal of Manufacturing Science and Technology*. 7(2), 55-70.

[28] Kannan, S., Kishawy, H. A. and Balazinski, M. (2004) An energy based analytical force model for orthogonal cutting of metal matrix composites. *Annals of the CIRP*. 53(1), 91-94.

[29] Ghandehariun, A., Hussein, H. M. and Kishawy, H. A. (2016) Machining metal matrix composites: novel analytical force model. *Int J Adv Manuf Technol*. 83, 233–241.

[30] Pramanik, A., Zhang, L. C. and Arsecularatne, J. A. (2006) Prediction of cutting forces in machining of metal matrix composites. *International Journal of Machine Tools & Manufacture*. 46, 1795-1803.

[31] Jiao, F. (2015) *Investigation on micro-cutting mechanics with application to micro-milling*. Ph.D. Dissertation, Brunel University London, UK.

[32] Ghosh, N., Ravi, Y. B., Patra, A., Mukhopadhyay, S., Paul, S., Mohanty, A. R. and Chattopadhyay, A. B. (2007) Estimation of tool wear during CNC milling using neural network-based sensor fusion. *Mechanical Systems and Signal Processing*. 21(1), 466-479.

[33] Zhou, J. H., Pang, C. K., Zhong, Z. W., and Lewis, F. L. (2011) Tool wear monitoring using acoustic emissions by dominant-feature identification. *Instrumentation and Measurement*. 60(2), 547-559.

[34] Stephenson, D. A. and Agapiou, J. S. (2016) *Metal Cutting Theory and Practice*. CRC Press.

[35] Pramanik, A. (2014) Developments in the non-traditional machining of particle reinforced metal matrix composites. *International Journal of Machine Tools and Manufacture*. 86, 44-61.

[36] Nicholls, C. J., Boswell, B., Davies, I. J. and Islam, M. N. (2017) Review of machining metal matrix composites. *The International Journal of Advanced Manufacturing Technology*. 90, 2429-2441.

[37] Kaczmar, J. W., Pietrzak, K. and Wlosinski, W. (2000) The production and application of metal matrix composite materials. *Journal of Materials Processing Technology*. 106, 58-67.

[38] Kandpal, B. C., Kumar, J. and Singh, H. (2014) Production technologies of metal matrix composite: A review. *International Journal of Research in Mechanical Engineering & Technology*. 4(2), 27-32.

[39] Bains, P. S., Sidhu, S. S. and Payal, H. S. (2016) Fabrication and machining of metal matrix composites: A review. *Materials and Manufacturing Processes*. 31(5), 553-573.

[40] Bodukuri, A. K., Eswaraiah, K., Rajendar, K. and Sampath, V. (2016) Fabrication of Al–SiC–B4C metal matrix composite by powder metallurgy technique and evaluating mechanical properties. *Perspectives in Science*. 8, 428-431.

[41] Schwartz, M. M. (1997) *Composite Materials, Volume II: Processing Fabrication and Applications*, Prentice Hall PTR.

[42] Willis, T. C., White, J., Jordan, R. M. and Hughes, I. R. (1987) *In Third lnt. Solidification Processing Conference, University of Sheffield*. London. pp. 21-24.

[43] Miller, W. S., Lenssen, L. A. and Humphreys, F. J. (1989) The strength, toughness and fracture behaviour in aluminium-lithium based metal matrix composites. *In Aluminium-Lithium V, ed. by Starke, Jr. B.A.; Sanders, Jr. T.H.; MCEP Ltd.* Birmingham. pp. 931-941.

[44] Harrigan, J. W. C. (1998) Commercial processing of metal matrix composites. *Materials Science and Engineering: A.* 244 (1), 75-79.

[45] Sahu, P. S. and Banchhor, R. (2016) Fabrication methods used to prepare Al metal matrix composites- A review. *International Research Journal of Engineering and Technology*. 3(10), 123-132.

[46] Ullbrand, J. M., Co´rdoba, J. M., Tamayo-Ariztondo, J., Elizalde, M. R., Nygren, M., Molina-Aldareguia, J. M. and Ode´n, M. (2010) Thermomechanical properties of copper–carbon nanofibre composites prepared by spark plasma sintering and hot pressing. *Composites Science and Technology*. 70 (16), 2263-2268.

[47] Rosso, M. (2006) Ceramic and metal matrix composites: Routes and properties. *Journal of Materials Processing Technology*. 175 (1), 364-375.

[48] Zadra, M. and Girardini, L. (2014) High-performance, low-cost titanium metal matrix composites. *Materials Science and Engineering: A.* 608, 155-163.

[49] William, C. and Harrigan, J. (1998) Commercial processing of metal matrix composites. *Materials Science and Engineering: A*. 244(1), 75-79.

[50] Kainer, K. U. (2006) *Metal Matrix Composites -- Custom-made Materials for Automotive and Aerospace Engineering*. Wiley-VCH Verlag GmbH & Co. KGaA.

[51] Rana, R. S., Purohit, R. and Das, S. (2012) Review of recent studies in Al matrix composites. *International Journal of Scientific & Engineering Research*. 3(6), 1-15.

[52] Sidhu, S. S., Batish, A. and Kumar, S. (2013) Fabrication and electrical discharge machining of metal–matrix composites: A review. *Journal of Reinforced Plastics and Composites*. 32 (17), 1310-1320.

[53] Callister, W. D. (2001) *Fundamentals of Materials Science and Engineering*. Wiley: New York.

[54] Congress, U. S. (1998) *Advanced materials by design, Chapter 4*. Washington, Office of Technology Assessment, DC: U.S. Government Printing Office.

[55] Liang, Y. and Dutta, S. P. (2001) Application trend in advanced ceramic technologies. *Technovation*. 21, 61-65.

[56] Heath, P. J. (2001) Developments in applications of PCD tooling. *J. Mater. Process. Technol*. 116, 31-38.

[57] Arsecularatne, J. A., Zhang, L. and Montross C. (2004) *MMC work materials for machining tests and tool wear/life*. Research Report, School of AMME, The University of Sydney.

[58] Tomac, N., Tannessen, K. and Rasch, F. O. (1992) Machinability of particulate aluminium matrix composites. *Annals of CIRP*. 41(1), 55-58.

[59] Lin, J. T., Bhattacharyya, D. and Lane, C. (1995) Machinability of a silicon carbide reinforced aluminium metal matrix. *Wear*. 181-183, 883-888.

[60] Muthukrishnan N., Murugan M. and Prahlada R. K. (2008) Machinability issues in turning Al–SiC (10 p) metal matrix composites. Int. *J. Adv. Manuf. Technol*. 39, 211-218.

[61] Muthukrishnan, N. and PauloDavim, J. (2009) Optimization of machining parameters of Al/SiC-MMC with ANOVA and ANN analysis. *Journal of Materials Processing Technology*. 209(1), 225-232.

[62] Grzesik, W. (2008) Machinability of engineering materials. In: Grzesik W (ed) *Advanced machining processes of metallic materials*. Amsterdam, Elsevier.

[63] Lin, J. T., Bhattacharyya, D. and Ferguson, W. G. (1998) Chip formation in the machining of SiC-particle reinforced aluminium-matrix. *Composites Science and Technology*. 58, 285-291.

[64] Lucca, D. A., Seo, Y. W. and Komanduri, R. (1993) Effect of tool edge geometry on energy dissipation in ultraprecision machining. *CIRP Annals - Manufacturing Technology*. 42(1), 83-86.

[65] Bissacco, G., Hansen, H. N. and De Chiffre, L. (2006) Size effects on surface generation in micro milling of hardened tool steel. *CIRP Annals - Manufacturing Technology*. 55(1), 593-596.

[66] Lai, X., Li, H., Li, C., Lin, Z. and Ni, J. (2008) Modeling and analysis of micro scale milling considering size effect, micro cutter edge radius and minimum chip thickness. *International Journal of Machine Tools and Manufacture*. 48(1), 1-14.

[67] Aramcharoen, A. and Mativenga, P. T. (2009) Size effect and tool geometry in micromilling of tool steel. *Precision Engineering*. 33(4), 402-407.

[68] Oliveira, F. B., Rodrigues, A. R., Coelho, R. T. and Souza, A. F. (2015) Size effect and minimum chip thickness in micromilling. *International journal of machine tools and manufacture*. 89, 39-54.

[69] Shaw, M. C. (2003) The size effect in metal cutting. *Sadhana*. 28(5), 875-896.

[70] Dinesh, D., Swaminathan, S., Chandrasekar, S. and Farris, T. N. (2001) An intrinsic size effect in machining due to the strain gradient. In: *Proceedings of ASME International Mechanical Engineering Congress and Exposition.* New York, USA. pp. 1-8.

[71] Weber, M., Hochrainer, T., Gumbsch, P., Autenrieth, H., Delonnoy, L. Schulze, V. Löhe, D. Kotschenreuther J. and Fleischer J. (2007) Investigation of size-effects in machining with geometrically defined cutting edges. *Machining Science and Technology*. 11(4), 447-473.

[72] Kopalinsky, E. M. and Oxley, P. L. B. (1984) Size effects in metal removal processes. In: *Proceedings of the third conference on mechanical properties at high rates of strain*. Institute of Physics Conference Series. 70, 389-396.

[73] Larssen B. J. and Oxley, P. L. B. (1972) Effect of strain-rate sensivity in scale phenomena in chip formation. In: *Proceedings of the 13th MTDR Conference*. pp. 209-216.

[74] Denkena, B., Becker, J. C. and Jivishov, V. (2003) Scaling effects on chip formation and forces in hard tuning. In: Vollertsen, F. and Ju¨ptner, W. (eds.) *Process Scaling.* BIAS Verlag, Strahltechnik. 24, 113-119.

[75] Mian, A. J., Driver, N. and Mativenga, P. T. (2011) Identification of factors that dominate size effect in micro-machining. *International Journal of Machine Tools and Manufacture*. 51(5), 383-394.

[76] Liu, J., Li, J., Ji, Y. and Xu, C. (2011) Investigation on the effect of SiC nanoparticles on cutting forces for micro-milling magnesium matrix composites. *Proceedings of ASME International Manufacturing Science and Engineering Conference (MSEC2011)*. 2, 525-536.

[77] Teng, X., Huo, D., Wong, E., Meenashisundaram G. and Gupta, M. (2016) Micro-machinability of nanoparticle-reinforced Mg-based MMCs: an experimental investigation. *Int J Adv Manuf Technol.* 87, 2165-2178.

[78] Kim, C. J., Bono, M. and Ni, J. (2002) Experimental analysis of chip formation in micro-milling. *Transactions of NAMRI/SME*. 30,1-8.

[79] Vogler, M. P., Liu, X., Kapoor, S. G., Devor, R. E. and Ehmann, K. F. (2002) Development of meso-scale machine tool (mmt) systems. *Technical Paper - Society of Manufacturing Engineers*. 181, 1-9.

[80] Vogler, M. P., DeVor, R. E. and Kapoor, S. G. (2003) Microstructure-level force prediction model for micro-milling of multi-phase materials. *Journal of Manufacturing Science and Engineering.* 125(2), 202-209.

[81] Kim, C. J., Mayor, J. R. and Ni, J. (2004) A static model of chip formation in microscale milling. *Journal of Manufacturing Science and Engineering.* 126(4), 710-718.

[82] Chae, J., Park, S. S. and Freiheit, T. (2006) Investigation of micro-cutting operations. *Int. J. Machine Tools and Manufacture*. 45, 313-332.

[83] Pramanik, A., Zhang, L. C. and Arsecularatne, J. A. (2008) Deformation mechanisms of MMCs under indentation. *Compos. Sci. Technol*. 68, 1304-1312.

[84] Jawahir, I. S. and van Luttervelt, C. A. (1993) Recent developments in chip control research and applications. *Annals of CIRP*. 42(2), 659-693.

[85] Dikshit, A., Samuel, J., DeVor, R. E. and Kapoor, S. G. (2008) Microstructure-level machining simulation of carbon nanotube reinforced polymer composites — part I: model development and validation. *Journal of Manufacturing Science and Engineering*. 130(3), 031114-031118.

[86] Dikshit, A., Samuel, J., DeVor, R. E. and Kapoor, S. G. (2008) Microstructure-level machining simulation of carbon nanotube reinforced polymer composites — part II: model interpretation and application. *Journal of Manufacturing Science and Engineering*. 130(3): 031115-031118.

[87] Davis, B., Dabrow, D., Ju, L., Li, A., Xu, C. and Huang, Y. (2017) Study of chip morphology and chip formation mechanism during machining of magnesium-based metal matrix composites. *Journal of Manufacturing Science and Engineering.* 139, 1-10.

[88] Monaghan, J. M. (1994) The use of a quick stop test to study the chip formation of SiC/Al metal matrix composite material and its matrix alloy. *Process. Adv. Mater*. 9, 170-179.

[89] Joshi, S. S., Ramakrishnan, N. and Ramakrishnan, P. (1999) Analysis of chip breaking during orthogonal machining of Al/SiCp composites. *Journal of Materials Processing Technology*. 88, 90-96.

[90] Joshi, S. S., Ramakrishnan, N. and Ramakrishnan, P. (2001) Micro-structural analysis of chip formation during orthogonal machining of Al/SiCp composites. *Journal of Engineering Materials and Technology*. 123, 315-321.

[91] Karthikeyan, R., Ganesan, G., Nagarazan, R. S. and Pai, B. C. (2001) Acriticalstudyon machining of Al/SiC composites. *Materials and Manufacturing Processes*. 16(1), 47-60.

[92] El-Gallaba, M. and Skladb, M. (1998) Machining of Al/SiC particulate metal matrix composites: Part II: Workpiece surface integrity. *Journal of Materials Processing Technology*. 83(1-3), 277-285.

[93] Dabade, U. A. and Joshi, S. S. (2009) Analysis of chip formation mechanism in machining of Al/SiCp metal matrix composites. *Journal of Materials Processing Technology*. 209, 4704-4710.

[94] Monaghan, J. and Brazil, D. (1998) Modelling the flow processes of a particle reinforced metal matrix composite during machining. *Compos Part A: Appl Sci Manuf.* 29, 87-99.

[95] Zhu, Y. and Kishawy, H. A. (2005) Influence of alumina particles on the mechanics of machining metal matrix composites. *International Journal of Machine Tools and Manufacture*. 45(4-5): 389-398.

[96] Pramanik, A., Zhang, L. C. and Arsecularatne, J. A. (2007) An FEM investigation into the behavior of metal matrix composites: Tool–particle interaction during orthogonal cutting. *International Journal of Machine Tools & Manufacture*. 47, 1497-1506.

[97] Zhou, L., Huang, S. T., Wang, D., et al. (2011) Finite element and experimental studies of the cutting process of SiCp/Al composites with PCD tools. *Int J Adv Manuf Technol*. 52, 619-626.

[98] Fathipour, M., Zoghipour, P., Tarighi, J. and Yousefi, R. (2012) Investigation of reinforced Sic particles percentage on machining force of metal matrix composite. *Mod Appl*. 6, 9-20.

[99] Wang, T., Xie, L. and Wang, X. (2015) Simulation study on defect formation mechanism of the machined surface in milling of high volume fraction SiCp/Al composite. *Int J Adv Manuf Technol.* 79, 1185-1194.

[100] Dandekar, C. R. and Shin, Y. C. (2012) Modeling of machining of composite materials: A review. *International Journal of Machine Tools & Manufacture.* 57, 102-121.

[101] Monaghnan, J. and Brazil, D. (1997) Modeling the sub-surface damage associated with the machining of a particle reinforced MMC. *Computational Materials Science.* 9, 99-107.

[102] Liu, J., Cheng, K., Ding, H., Chen, S. and Zhao, L. (2017) Simulation study of the influence of cutting speed and tool–particle interaction location on surface formation mechanism in micromachining SiCp/Al composites. *Proc IMechE Part C: J Mechanical Engineering Science*. 0(0) 1-13.

[103] Dandekar, C. R. and Shin, Y. C. (2009) Multi-step 3D finite element modeling of subsurface damage in machining particulate reinforced metal matrix composites. *Composites, PartA: Applied Science and Manufacturing*. 40(8), 1231-1239.

[104] Umer, U., Ashfaq, M., Qudeiri, J. A., Hussein, H. M. A., Danish, S. N. and Al-Ahmari, A. R. (2015) Modeling machining of particle-reinforced aluminum-based metal matrix composites using cohesive zone elements. *Int J Adv Manuf Technol.* 78,1171-1179.

[105] Ghandehariun, A., Kishawy, H. A., Umer, U. and Hussein, H. M. (2016) Analysis of tool-particle interactions during cutting process of metal matrix composites. *Int J Adv Manuf Technol*. 82,143-152.

[106] Ghandehariun, A., Kishawy, H. A., Umer, U., et al. (2016) On tool-workpiece interactions during machining metal matrix composites: investigation of the effect of cutting speed. *Int J Adv Manuf Technol*.84, 2423-2435.

[107] Kan, Y., Liu, Z. G., Zhang, S. H., et al. (2014) Microstructure-based numerical simulation of the tensile behavior of SiCp/Al composites. *J Mater Eng Perform*. 23, 1069-1076.

[108] Kannan, S., Kishawy, H. A. and Deiab, I. (2009) Cutting forces and TEM analysis of the generated surface during machining metal matrix composites. *Journal of Materials Processing Technology*. 209(5), 2260-2269.

[109] Davim, J. P. (2012) Diamond tool performance in machiningmetal–matrix composites. *J Mater Process Technol*. 128, 100-105.

[110] Kannan, S., Kishawy, H. A. and Balazinski, M. (2004) An energy based analytical force model for orthogonal cutting of metal matrix composites. *Annals of the CIRP*. 53 (1), 91-94.

[111] Ghandehariun, A., Hussein, H. M. and Kishawy, H. A. (2016) Machining metal matrix composites: novel analytical force model. *Int J Adv Manuf Technol*. 83, 233-241.

[112] Altintas, Y. (2012) *Manufacturing Automation: Metal Cutting Mechanics, Machine Tool Vibrations, and CNC Design*. Cambridge University Press.

[113] Cheng, K. (2001) Chapter 4 Abrasive Micromachining and Microgrinding. In: McGeough, J. (ed) *Micro Machining of Engineering Materials*. CRC Press.

[114] Liu, J., Li, J. and Xu, C (2014) Interaction of the cutting tools and the ceramic-reinforced metal matrix composites during micro-machining: A review. *CIRP Journal of Manufacturing Science and Technology*. 7, 55-70.

[115] Pramanik, A., Zhang, L. C. and Arsecularatne, J. A. (2006) Prediction of cutting forces in machining of metal matrix composites. *International Journal of Machine Tools and Manufacture*. 46, 1795-1803.

[116] Dabade, U., Dapkekar, D., Joshi, S. S. (2009) Modeling of chip-tool interface friction to predict cutting forces in machining of Al/SiCp composites. *International Journal of Machine Tools and Manufacture*. 49, 690-700.

[117] Sikder, S. and Kishawy, H. A. (2012) Analytical model for force prediction when machining metal matrix composite. *International Journal of Mechanical Sciences.* 59, 95-103.

[118] Niu, Z., Jiao, F. and Cheng, K. (2018) An innovative investigation on chip formation mechanisms in micro-milling using natural diamond and tungsten carbide tools. *Journal of Manufacturing Processes.* 31(1), 382-394.

[119] Vogler, M. P., DeVor, R. E. and Kapoor, S. G. (2003) Microstructure-level force prediction model for micro-milling of multi-phase materials. *Journal of Manufacturing Science and Engineering*. 125(2), 202-209.

[120] Vogler, M. P., Kapoor, S. G. and DeVor, R. E. (2004) On the modeling and analysis of machining performance in micro-endmilling, part II: Cutting force prediction. *Journal of Manufacturing Science and Engineering*. 126(4), 695-705.

[121] El-Gallab, M. and Sklad, M. (2000) Machining of Al/SiC particulate metal matrix composites—part III:comprehensive tool wear models. *Journal of Materials Processing Technology*. 101, 10-20.

[122] Reddy, P. R. and Sriramakrishna, A. A. (2002) Analysis of orthogonal cutting of aluminum-based composites. *Defence Science Journal*. 52(4), 375-382.

[123] Chou, Y. K. and Liu, J. (2005) CVD diamond tool performance in metal matrix composite machining. *Surface and Coatings Technology*. 200, 1872-1878.

[124] Liu, J. and Chou, Y. K. (2007) Cutting tool temperature analysis in heat-pipe assisted composite machining. *Transactions of the ASME, Journal of Manufacturing Science and Engineering*. 129, 902-910.

[125] Aurich, J. C., Zimmermann, M., Schindler, S. and Steinmann, P. (2016) Effect of the cutting condition and the reinforcement phase on the thermal load of the workpiece when dry turning aluminum metal matrix composites. *Int J Adv Manuf Technol*. 82, 1317-1334.

[126] Nicholls, C. J., Boswell, B., Davies, I. J. and Islam, M. N. (2017) Review of machining metal matrix composites. *Int J Adv Manuf Technol.* 90, 2429-2441.

[127] Songmene, V and Balazinski, M. (1999) Machinability of graphiticmetal matrix composites as a function of reinforcing particles. *CIRP Ann Manuf Technol.* 48(1), 77-80.

[128] Cronjäger, L. and Meister, D. (1992) Machining of fibre and particlereinforced aluminium. *CIRP Ann Manuf Technol* 41(1), 63-66.

[129] Narahari, P., Pai, B. C. and Pillai, R. M. (1999) Some aspects of machining cast Al-SiCp composites with conventional high speed steel and tungsten carbide tools. *J Mater Eng Perform*. 8(5), 538-542.

[130] Cronjager, L. and Meister, D. (1992) Machining of fiber and particle-reinforced aluminum. *Annals of the CIRP*. 41, 63-66.

[131] Manna, A. and Bhattacharyya, B. (2005) Influence of machining parameters on the machinability of particulate reinforced Al/SiC-MMC. *International Journal of Advances in Manufacturing Technology*. 25, 850-856.

[132] Muthukrishnan, N., Murugan, M. and Rao, K. P. (2008) An investigation on the machinability of Al-SiC metal matrix composites using PCD inserts. *International Journal of Advances in Manufacturing Technology*. 38, 447-454.

[133] Barnes, S and Pashby, I. R. (1995) Machining of aluminium based metal matrix composites. *Appl Compos Mater.* 2, 31-42.

[134] Durante, S., Rutelli, G. and Rabezzana, F. (1997) Aluminum-based MMC machining with diamond-coated cutting tools. *Surf Coat Technol.* 94-95, 632-640.

[135] Tomac, N. and Tonnessen, K. (1992) Machinability of particulate aluminium matrix composites. *CIRP Ann Manuf Technol.* 41(1), 55-58.

[136] Davim, J. P. (2010) *Machining of Composite Materials*. John Wiley & Sons, New York.

[137] Kannan, S. and Kishawy, H. A. (2008) Tribological aspects of machining aluminium metal matrix composites. *Journal of Materials Processing Technology*. 198, 399-406.

[138] Hung, N. P., Venkatesh, V. C. and Loh, N. L. (1998) Cutting tools for metal matrix composites. *Key Engineering Materials*. 138-140, 289-325.

[139] Weinert, K. and Biermann, D. (1993) Turning of fiber and particle reinforced aluminium. *Proceedings of the international conference on machining of advanced materials*. Gaithersburg, Maryland. pp. 437-453.

[140] Ding, X., Liew, W. Y. H. and Liu, X. D. (2005) Evaluation of machining performance of MMC with PCBN and PCD tools. *Wear*. 259, 1225-1234.

[141] Looney, L.A., Monaghan, J.M., O'Reilly, P., et al. (1992) The turning of an Al/SiC metal-matrix composite. *J Mater Process Tech*. 33(4), 453-468.

[142] Hung, N. P., Boey, F. Y. C., Khor, K. A., Phua, Y. S. and Lee, H. F. (1996) Machinability of aluminum alloys reinforced with silicon carbide particulates. *J Mater Process Technol.* 56(1-4), 966-977.

[143] Ciftci, I., Turker, M. and Seker, U. (2004) CBN cutting tool wear during machining of particulate reinforced MMCs. *Wear*. 257(9-10), 1041-1046.

[144] Durante, S., Rutelli, G. and Rabezzana, F. (1997) Aluminum-based MMC machining with diamond-coated cutting tools. *Surf Coat Technol*. 94-95, 632-640.

[145] Andrewes, C. J. E., Feng, H. Y. and Lau, W. M. (2000) Machining of an aluminum/SiC composite using diamond inserts. *J Mater Process Technol*. 102(1-3), 25-29.

[146] Cheng, K. (2008) *Machining Dynamics: Fundamentals, Applications and Practices*. London, Springer.

[147] Davim, J. P. (2002) Diamond tool performance in machining metal–matrix composites. *J Mater Process Technol*. 128(1-3), 100-105.

[148] El-Gallab, M. and Sklad, M. (1998) Machining of Al/SiC particulatemetal–matrix composites, Part I: Tool performance. *J MaterProcess Technol*.83, 151-158.

[149] Hooper, R. M., Henshall, J. L. and Klopfer, A. (1999) The wear of polycrystalline diamond tools used in the cutting of metal matrix composites. *Int J Refract Metals Hard Mater*. 17, 103-109.

[150] Chambers, A. R. (1996) The machinability of light alloy MMCs. *Composites A*. 27A, 143-147.

[151] Schwartz, M. M. (1997) *Composite materials: processing, fabrication, and applications*. Englewood Cliffs, NJ: Prentice-Hall.

[152] Hung, N. P., Loh, N. L. and Venketesh, V. C. (2002) Machining of metal matrix composites. *S. Jahanmir, M. Ramulu (Eds.), Machining of Ceramics and Composites, Marcel Dekker Inc*. 289-325

[153] Garay-Reyes, C. G., González-Rodelas, L., Cuadros-Lugo, E., Martínez-Franco, E., Aguilar-Santillan, J., Estrada-Guel, I., Maldonado-Orozco M. C. and Martínez-Sánchez, R. (2017) Evaluation of hardness and precipitation in Zn-modified Al2024 alloy after plastic deformation and heat treatments. *Journal of Alloys and Compounds*. 705, 1-8.

[154] Gururaja, S., Ramulu, M. and Pedersen, W. (2013) Machining of MMCs: A review. *Machining Science and Technology*. 17(1), 41-73.

[155] Hocheng, H. (2012) *Machining Technology for Composite Materials*. Woodhead Publishing, Cambridge, UK.

[156] Hung, N. P., Boey, F. Y. C., Khor, K. A., Ho, C. A. and Lee, H. F. (1995) Machinability of cast and powder-formed aluminum alloys reinforced with SiC particles. *J Mater Process Technol.* 48(1-4), 291-297.

[157] Arsecularatne, J. A., Zhang, L. C. and Montross, C. (2006) Wear and tool life of tungsten carbide, PCBN and PCD cutting tools. *International Journal of Machine Tools & Manufacture*. 46, 482-491.

[158] Manna, A. and Bhattacharayya, B. (2003) A study on machinability of Al/SiC-MMC. *J Mater Process Technol.*140, 711-716.

[159] Parka, K. H. and Kwon, P. Y. (2011) Flank wear of multi-layer coated tool. *Wear*. 270, 771-780.

[160] Antonio, C. A. C. and Davim, J. P. (2002) Optimum cutting conditions in turning of particulate metal matrix composites based on experimental and a generic search model. *Composites A.* 33, 213-219.

[161] Lin, J. T., Bhattacharyya, D. and Lane, C. (1995) Case study-machinability of a silicon carbide reinforced aluminium metal matrix composite. *Wear*. 181-183, 883-888.

[162] Jaspers, S. P. F. C. and Dautzenberg, J. H. (2002) Material behaviour in metal cutting: strains, strain rates and temperatures in chip formation. *J Mater Process Technol*. 121, 123-135.

[163] Lin, C. B., Hung, Y. W., Liu, W. C. and Kang, S. W. (2001) Machining and fluidity of 356Al/SiC(p) composites. *J Mater Process Technol*. 110, 152-159.

[164] Weinert, K. and Konig. W. (1993) A consideration of tool wear mechanism when machining metal matrix composites (MMC). *Annals of the ClRP*. 42(1), 95-98.

[165] El-Gallab, M. and Sklad, M. (1998) Machining of Al/SiC particulate metalmatrix composites. Part II: Workpiece surface integrity. *J. Mater. Process. Technol*. 83, 277-285.

[166] Chambers, A. R. (1996) The machinability of light alloy MMCs. *Composites A*. 27A, 143-147.

[167] Ciftci, I., Turker, M. and Seker, U. (2004) Evaluation of tool wear when machining SiCp-reinforced Al-2014 alloy matrix composites. *Mater Des.* 25, 251-255.

[168] Sahoo, A. K., Pradhan, S. and Rout, A. K. (2013) Development and machinability assessment in turning Al/SiCp-metal matrix composite with multi-layer coated carbide insert using Taguchi and statistical techniques. *Arch Civil Mech Eng*. 13, 27-35.

[169] Sahin, Y., Kok, M. and Celik, H. (2002) Tool wear and surface roughness of Al2O3 particle-reinforced aluminium alloy composites. *J Mater Process Tech*. 128(1-3), 280-291.

[170] Weinert, K. (1993) A consideration of tool wear mechanism when machining metal matrix composite (MMC). *Ann. CIRP*. 42, 95-98.

[171] Dimla, E. and Dimla, Snr. (2000) Sensor signals for tool-wear monitoring in metal cutting operations—a review of methods. *International Journal of Machine Tools & Manufacture*. 40, 1073-1098.

[172] Ghani, J. A., Rizal, M., Rizal, M. Z., Ghazal, M. J and Haron, C. H. C. (2011) Monitoring online cutting tool wear using low-cost technique and User-friendly GUI. *Wear*. 271, 2619-2624.

[173] Shahabi, H. H. and Ratnam. M. M. (2016) Simulation and measurement of surface roughness via grey scale image of tool in finish turning. *Precision Engineering.* 43, 146-153.

[174] Waydande, P., Ambhore, N. and Chinchanikar, S. (2016) A review on tool wear monitoring system. *Journal of Mechanical Engineering and Automation*. 6(5A), 49-53.

[175] Choi, D., Kwon, W. T. and Chu, C. N. (1999) Real-time monitoring of tool fracture in turning using sensor fusion. *International Journal of Advanced Manufacturing Technology*. 15(5), 305-310.

[176] Jemielniak, K. and Otman, O. (1998) Tool failure detection based on analysis of accoustic emission signals. *Journal of Material Processing Technology*. 76, 192-197.

[177] Ko¨nig, W., Kutzner, K. and Schehl, U. (1992) Tool monitoring of small drills with acoustic emission. *International Journal of Machine Tools and Manufacture*. 32(4), 487-493.

[178] Sarwar, M., Li, J., Penlington, R. and Ahmed, W. (1996) Development of thermal imaging systems for metal cutting applications. *Proceedings Advanced Manufacturing Processes Systems and Technologies Conference*. Bradford, UK. pp.361-369.

[179] Lin, J. (1995) Inverse estimation of the tool-work interface temperature in end milling. *International Journal of Machine Tools and Manufacture*. 35(5), 751-760.

[180] Stephenson, D. A. and Ali, A. (1990) Tool temperatures in interrupted metal cutting. *Winter Annual Meeting of the ASME*. 43, 261-281.

[181] Tansel, I., Trujillo, M., Nedbouyan, A., Velez, C., Bao, W., Arkan, T. T. and Tansel, B. (1998) Micro-end-milling—III. Wear estimation and tool breakage detection using acoustic emission signals. *International Journal of Machine Tools and Manufacture*. 38(12), 1449-1466.

[182] Jemielniak, K. and Otman, O. (1998) Tool failure detection based on analysis of accoustic emission signals. *Journal of Material Processing Technology*. 76, 192-197.

[183] Kakade, S., Vijayaraghavan, L. and Krishnamurthy, R. (1994) In-process tool wear and chip-form monitoring in face milling operation using acoustic emission. *Journal of Material Processing Technology*. 44, 207-214.

[184] Chow, J. G. and Wright, P. K. (1988) On-line estimation of tool/chip interface temperatures for a turning operation. *ASME Trans. Journal of Engineering for Industry*. 110, 56-64.

[185] Kitagawa, T., Maekawa, K., Shirakashi, T. and Usui, E. (1988) Analytical prediction of flank wear of carbide tools in turning plain carbon steels (Part 1), Bull. *Japan Soc. Precision Engineering*. 22(4), 263-269.

[186] Radulescu, R. and Kapoor, S. G. (1994) An analytical model for prediction of tool temperature fields during continuous and interrupted cutting. *ASME Trans. Journal of Engineering for Industry*. 116(2), 135-143.

[187] Raman, S., Shaikh, A. and Cohen, P. H. (1992) A mathematical model for tool temperature sensing. *ASME Computational Methods in Materials Processing*. 61, 181-193.

[188] El-Wardany, T. I., Gao, D. and Elbestawi, M. A. (1996) Tool condition monitoring in drilling using vibration signature analysis. *International Journal of Machine Tools and Manufacture*. 36(6), 687-711.

[189] Yao, Y., Fang, X. D. and Arndt, G. (1991) On-line estimation of groove wear in the minor cutting edge for finish machining. *Annals of the CIRP*. 40(1), 41-44.

[190] Rotberg, J., Braun, S. and Lenz, E. (1987) Mechanical signature analysis in interrupted cutting. *Annals of the CIRP*. 36(1), 249-252.

[191] Du, R., Zhang, B., Hungerford, W. and Pryor, T. (1993) Tool condition monitoring and compensation in finish turning using optical sensor. *ASME Symposium Mechatronics.* 63, 245-251.

[192] Noori-Khajavi, A. and Komanduri, R. (1995) Frequency and time domain analyses of sensor signals in drilling—I. Correlation with drill wear. *International Journal of Machine Tools and Manufacture*. 35(6), 775-793.

[193] Constantinides, N. and Bennett, S. (1987) An investigation of methods for on-line estimation of tool wear. *International Journal of Machine Tools and Manufacture*. 27 (2), 225-237.

[194] Ghosh, N., Ravi, Y. B., Patra, A., Mukhopadhyay, S., Paul, S., Mohanty, A. R. and Chattopadhyay, A. B. (2007) Estimation of tool wear during CNC milling using neural network-based sensor fusion. *Mechanical Systems and Signal Processing*. 21(1), 466-479.

[195] Zhu, K., Mei, T. and Ye, D. (2015) Online condition monitoring in micromilling: A force waveform shape analysis approach. *IEEE Transactions on Industrial Electronics*. 62(6), 3806-3813.

[196] Zhou, L., Peng, F. Y., Yan, R., Yao, P. F., Yang, C. C. and Li, B. (2015) Analytical modeling and experimental validation of micro end-milling cutting forces

considering edge radius and material strengthening effects. *International Journal of Machine Tools & Manufacture*. 97, 29-41.

[197] Malekian, M., Park, S. S. and Jun, M. B. G. (2009) Tool wear monitoring of micro-milling operations. *Journal of Materials Processing Technology*. 209(10), 4903-4914.

[198] Muthukrishnan, N. and Davim, J. P. (2009) Optimization of machining parameters of Al/SiC-MMC with ANOVA and ANN analysis. *Journal of materials processing technology*. 209, 225-232.

[199] Li, X. and Seah, W. K. H. (2001) Tool wear acceleration in relation to workpiece reinforcement percentage in cutting of metal matrix composites. *Wear*. 347, 161-171.

[200] Dabade, U. A. and Jadhav, M. R. (2016) Experimental study of surface integrity of Al/SiC particulate metal–matrix composites in hot machining, *Procedia CIRP*. 41, 914-919.

[201] Bian, R., He, N., Li, L., Zhan, Z. B., Wu, Q., Shi, Z. Y. (2014) Precision milling of high volume fraction SiCp/Al composites with monocrystalline diamond end mill. *The International Journal of Advanced Manufacturing Technology*.71, 411-419.

[202] Wang, T., Xie, L. J., Wang, X. B., Jiao, L., Shen, J. W., Xu, H. and Nie, F. M. (2013) Surface integrity of high speed milling of Al/SiC/65p aluminum matrix composites. *Procedia CIRP*. 8, 475-480.

[203] Karabulut, Ş. (2015) Optimization of surface roughness and cutting force during AA7039/Al2O3 metal matrix composites milling using neural networks and Taguchi method. *Measurement.* 66, 139-149.

[204] Palanikumar, K. and Karthikeyan, R. (2007) Assessment of factors influencing surface roughness on the machining of Al/SiC particulate composites. *Materials and Design*. 28, 1584-1591.

[205] Kumar, R. and Chauhan, S. (2015) Study on surface roughness measurement for turning of Al 7075/10/SiCp and Al 7075 hybrid composites by using response surface methodology (RSM) and artificial neural networking (ANN). *Measurement*. 65, 166-180.

[206] Tomac, N, Tannessen, K. and Rasch, F. O. (1992) Machinability of particulate aluminium matrix composites. *CIRP Annals*. 41(1), 55-58.

[207] Rao, P., Bhagyashekar, C. R. and Narendraviswanath, M. S. (2014) Effect of machining parameters on the surface roughness while turning particulate composites. *Procedia Engineering.* 97, 421-431.

[208] Karabulut, Ş., Karakoç, H. and Çıtak, R. (2016) Influence of B4C particle reinforcement on mechanical and machining properties of Al6061/B4C composites. *Composites Part B: Engineering.* 101, 87-98.

[209] Kannan, S. and Kishawy, H. (2008) Tribological aspects of machining aluminium metal matrix composites. *Journal of Materials Processing Technology*. 198(1-3), 399-406.

[210] Kilickap, E., Cakir, O., Aksoy, M. and Inan, A. (2005) Study of tool wear and surface roughness in machining of homogenised SiC-p reinforced aluminum metal matrix composite. *Journal of Materials Processing Technology*. 164-165, 862-867.

[211] Sahoo, A. K. and Pradhan, S. (2013) Modeling and optimization of Al/SiCp MMC machining using Taguchi approach. *Measurement*. 46, 3064-3072.

[212] Manna, A. and Bhattacharayya, B. (2003) A study on machinability of Al/SiC-MMC. *Journal of Materials Processing Technology*. 140(1-3), 711-716.

[213] Karakas, M. S., Acır, A., Ubeyli, M., et al. (2006) Effect of cutting speed on tool performance in milling of B4Cp reinforced aluminum metal matrix composites. *J Mater Process Tech*. 178(1-3), 241-246.

[214] Seeman, M., Ganesan, G., Karthikeyan R, et al. (2010) Study on tool wear and surface roughness in machining of particulate aluminum metal matrix composite-response surface methodology approach. *Int J Adv Manuf Tech*. 48(5-8), 613-624.

[215] Karthikeyan, R., Ganesan, G., Nagarazan, R. S., et al. (2001) A critical study on machining of Al/SiC composites. *Mater Manuf Process.* 16(1), 47-60.

[216] Seeman, M., Ganesan, G. and Karthikeyan, R. (2010) Study on tool wear and surface roughness in machining of particulate aluminum metal matrix composite-response surface methodology approach. *International Journal of Advances in Manufacturing Technology*. 48, 613-624.

[217] Ozben, T., Kilickap, E. and Cakir, O. (2008) Investigation of mechanical and machinability properties of SiC particle reinforced Al-MMC. *Journal of Materials Processing Technology*. 198, 220-225.

[218] Gururaja, S., Ramulu, M. and Pedersen, W. (2013) Machining of MMCs: A review. *Machining Science and Technology*. 17(1), 41-73.

[219] Sekhar, R. and Singh, T. P. (2015) Mechanisms in turning of metal matrix composites: a review. *J MATER RES TECHNOL*. 4(2), 197-207.

[220] Hakami, F., Pramanik, A. and Basak, A. K. (2017) Tool wear and surface quality of metal matrix composites due to machining: A review. *Proc IMechE Part B: J Engineering Manufacture.* 231(5), 739-752.

[221] Dabade, U. A., Sonawane, H. A. and Joshi, S. S. (2010) Cutting forces and surface roughness in machining Al/SiCp composites of varying composition. *Mach Sci Technol*. 14(2), 258-279.

[222] Li, X. and Seah, W. K. H. (2001) Tool wear acceleration in relation to workpiece reinforcement percentage in cutting of metal matrix composites. *Wear*. 247(2), 161-171.

[223] Quan, Y. and Zhou, Z. (2000) Tool wear and its mechanism for cutting SiC particle-reinforced aluminium matrix composites. *J Mater Process Tech.* 100(1), 194-199.

[224] Kanta, D. D, Mishra, P. C., Singh, S., et al. (2015) Tool wear in turning ceramic reinforced aluminum matrix composites – a review. *J Compos Mater*. 49, 2949-2961.

[225] Kannan, S., Kishawy, H. A. and Balazinski, M. (2006) Flank wear progression during machining metal matrix composites. *Journal of Manufacturing Science and Engineering*. 128, 787-791.

[226] Cheung C. F., Chan K. C., To S., et al. (2002) Effect of reinforcement in ultra-precision machining of Al6061/SiC metal matrix composites. *Scripta Mater.* 47(2), 77-82.

[227] Ozben, T., Kilickap, E. and Cakır, O. (2008) Investigation of mechanical and machinability properties of SiC particle reinforced Al-MMC. *J Mater Process Tech.* 198(1–3), 220-225.

[228] Venkatesan, K., Ramanujam, R., Joel, J., et al. (2014) Study of cutting force and surface roughness in machining of Al alloy hybrid composite and optimized using response surface methodology. *Proced Eng.* 97, 677-686.

[229] Pendse D. M. and Joshi S. S. (2004) Modeling and optimization of machining process in discontinuously reinforced aluminium matrix composites. *Mach Sci Technol.* 8(1), 85-102.

[230] Basheer A. C., Dabade U. A., Joshi S. S., et al. (2008) Modeling of surface roughness in precision machining of metal matrix composites using ANN. *J Mater Process Tech.* 197(1-3), 439-444.

[231] Tosun, G. and Muratoglu, M. (2004) The drilling of Al/SiCp metal–matrix composites. Part II: workpiece surface integrity. *Compos Sci Technol.* 64(10–11), 1413-1418.

[232] Fathipour, M., Hamedi, M., and Yousefi, R. (2013) Numerical and experimental analysis of machining of Al (20 vol% SiC) composite by the use of ABAQUS software. *Materials Science and Engineering*. 44(1), 14-20.

[233] Kumar, R., and Chauhan, S. (2015) Study on surface roughness measurement for turning of Al 7075/10/SiCp and Al 7075 hybrid composites by using response surface methodology (RSM) and artificial neural networking (ANN). *Measurement*. 65, 166-180.

[234] Johnson, G. R. and Cook, W. H. (1983) A constitutive model and data for metals subjected to large strains, high strain rates and high temperatures. *Proceedings of the 7th International Symposium on Ballistics 1983, The Netherlands*. pp. 541-547.

[235] Zhang, H., Ramesh, K., and Chin, E. (2005) Effects of interfacial debonding on the rate-dependent response of metal matrix composites. *Acta Materialia*. 53(17), 4687-4700.

[236] Hibbitt, Kaarlsson and Sorensen (2001) *ABAQUS/Explicit user's manual*. Hibbitt, Karlsson and Sorensen Incorporated.

[237] Zorev, N. N. (1963) Interrelationship between shear processes occurring along tool face and on shear plane in metal cutting. *Proceedings of the International Research in Production Engineering Conference*, ASME, New York. pp. 42-49.

[238] Niu, Z. and Cheng, K. (2016) Multiscale multiphysics-based modeling and analysis on the tool wear in micro drilling. *Journal of Multiscale Modelling.* 7(1), 1-22.

[239] Abdullah, A. B. Chia, L. Y. and Samad, Z. (2008) The effect of feed rate and cutting speed to surface roughness. *Asian Journal of Scientific Research.* 1, 12-21.

[240] Jiang, J., Sheng, F. and Ren, F. (1998) Modelling of two-body abrasive wear under multiple contact conditions. *Wear*. 217, 35-45.

[241] Venkatachalam, S. and Liang, S. Y. (2007) Effects of ploughing forces and friction coefficient in microscale machining. *J. Manuf. Sci. Eng.* 129, 274-280.

[242] Colwell, L. V. (1954) Predicting the angle of chip flow for single-point cutting tool. *Trans. ASME*. 76, 199-204.

[243] Pramanik, A., Zhang, L. C. and Arsecularatne, J. A. (2008) Machining of metal matrix composites: effect of ceramic particles on residual stress, surface roughness and chip formation. *Int. J. Mach. Tools Manuf.* 48, 1613-1625.

[244] Kishawy, H. A., Kannan and S., Balazinski, M. (2004) An energy based analytical force model for orthogonal cutting of metal matrix composites. *CIRP Ann. Manuf. Technol.* 53, 91-94.

[245] Niu, Z., Jiao, F. and Cheng, K. (2018) Investigation on innovative dynamic cutting force modelling in micro milling and its experimental validation. *Nanomanufacturing & Metrology*. 1, 82-95.

[246] Wang, T., Xie, L. J., Wang, X. B., Jiao, L., Shen, J. W., Xu, H. and Nie, F. M. (2013) Surface integrity of high speed milling of Al/SiC/65p aluminum matrix composites. *Procedia CIRP*. 8, 475-480.

[247] Shaw M. C. (1984) *Metal cutting principles*. Oxford, Oxford University Press.

[248] Luo, X. (2004) *High Precision Surfaces Generation: Modelling, Simulation and Machining Verification.* Ph.D. Dissertation, Leeds Metropolitan University, UK.

[249] Ahmed, G. M S., Reddy, P. R. and Seetharamaiah, N. (2012) Experimental evaluation of critical axial depth of cut with magneto rheological damping in end milling process. *International Journal of Scientific and Research Publications*. 2(8), 1-11.

[250] Senthilvelan, T. Gopalakannan, S., Vishnuvarthan S. and Keerthivaran, K. (2012) Fabrication and characterization of SiC, Al_2O_3 and B_4C reinforced Al-Zn-Mg-Cu alloy (AA 7075) metal matrix composites: A study. *Advanced Materials Research*. 622-623, 1295-1299.

Appendice

Appendix 1 List of Publications Arising from this Research

(1) Z. Niu and K. Cheng, Multiscale Multiphysics-Based Modeling and Analysis on the Tool Wear in Micro Drilling, Journal of Multiscale Modelling, Vol. 7, No. 1, 2016, pp.1-22 .

(2) K. Cheng, Z. Niu, C. Wang, R. Rakowski and R. Bateman, Smart Cutting Tools and Smart Machining: Development Approaches, and Their Implementation and Application Perspectives, Chinese Journal of Mechanical Engineering, Vol. 30, No. 5, 2017, pp. 1162-1176.

(3) Z. Niu, F. Jiao and K. Cheng, An Innovative Investigation on Chip Formation Mechanisms in Micro-milling Using Natural Diamond and Tungsten Carbide Tools, Journal of Manufacturing Processes, Vol. 31, 2018, pp. 382-394.

(4) Z. Niu, F. Jiao and K. Cheng, Investigation on Innovative Dynamic Cutting Force Modelling in Micro Milling and Its Experimental Validation, Nanomanufacturing & Metrology, Vol. 1, 2018, pp. 82-95.

(5) Z. Niu and K. Cheng, An Experimental Investigation on Surface Generation in Ultraprecision Machining of Particle Reinforced Metal Matrix Composites, International Journal of Advanced Manufacturing Technology, 2018. (Accepted)

(6) Z. Niu and K. Cheng, A Multiphysics Oriented Investigation on Tool Wear in Micro Drilling Metal Matrix Composites, CAPE 23 Conference, Edinburgh, UK, 2015.

(7) Z. Niu and K. Cheng, Multiphysics Based Modelling and Analysis of Micro Milling Metal Matrix Composites (MMCs) Against the Effects of Key Process Variables, euspen's 16th International Conference, Nottingham, UK, 2016.

(8) Z. Niu and K. Cheng, Investigation on the Material Removal and Surface Roughness in Ultraprecision Machining of Al/B_4C/50p Metal Matrix Composites, Journal of Manufacturing Science and Engineering, 2018. (Submitted)

(9) Z. Niu and K. Cheng, Improved Dynamic Cutting Force Model in Micro Milling Metal Matrix Composites Part I: Theoretical Model and Simulation, International Journal of Advanced Manufacturing Technology, 2018. (Submitted)

(10) Z. Niu and K. Cheng, Improved Dynamic Cutting Force Model in Micro Milling Metal Matrix Composites Part II: Experimental Validation and Prediction, International Journal of Advanced Manufacturing Technology, 2018. (Submitted)

Appendix 2 Tool Wear in Micro Drilling of PMMC

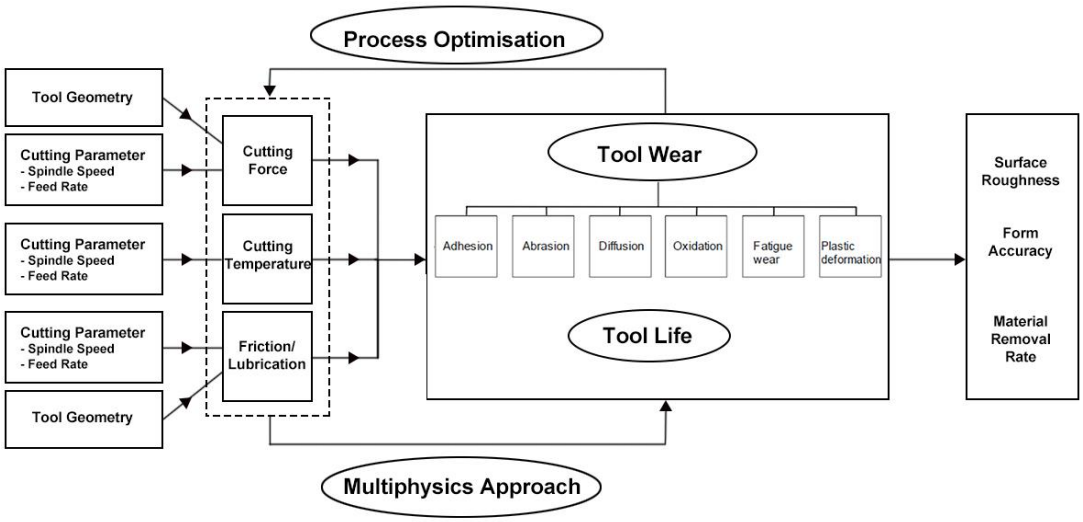

Figure 1 Multiphysics based approach to analyse the tool wear in MMCs micro drilling

As illustrated in Figure 1, tool wear is significantly affected by cutting force, cutting temperature and friction due to the interaction between tool and workpiece. There is an intrinsic relationship among these three cutting physics. Friction force and cutting force especially for thrust force are significantly affected by cutting tool geometry and cutting parameters. The actual cutting force is also affected by chip formation process. On the other hand, cutting speed and feed rate in micro drilling processes determine the resultant drilling temperature. In addition, the resultant heat between tool, chip and workpiece at deformation and friction zone result in the cutting temperature gradually increased. Moreover, the resultant tool wear, in turn, increases the cutting force, cutting temperature and friction during continuous cutting processes. This vicious circle prompts us to find out the interrelationship between the process variables and cutting tool wear in order to enhance the tool performance and cutting performance. Therefore, an investigation on the thermo-mechanical-tribological properties of micro-drills and workpiece is of great important to have a better understanding on the MMCs micro cutting mechanics. In addition, multiphysics based analysis and experimental evaluation and validation are critical to select the optimal cutting parameters in MMCs micro drilling process.

The test material in this micro drilling experiment is aluminium metal matrix composite material reinforced by silicon carbide particles with 17.8% volume fraction. The external dimension of MMCs workpiece is 50*50*2 mm. Table 1 illustrates the microstructure of this metal matrix composite workpiece and its chemical composition that measured by SEM respectively. The grain size of silicon carbide particles is normally ranged from 2 μm to 40 μm and the average grain size of SiC in this workpiece is around 25 μm. The chemical composition and mechanical properties of Al/SiC MMC workpiece are shown in Table 1. Tungsten carbide

drills with identical diameter of 0.5 mm are used in these micro drilling experiments. Table 2 shows the specifications of the micro drills.

Table 1 Chemical composition and mechanical properties of the MMC workpiece

Al (%)	SiC (%)	Cu (%)	Mg (%)	Mn (%)
Balanced	17.8	3.3	1.2	0.4

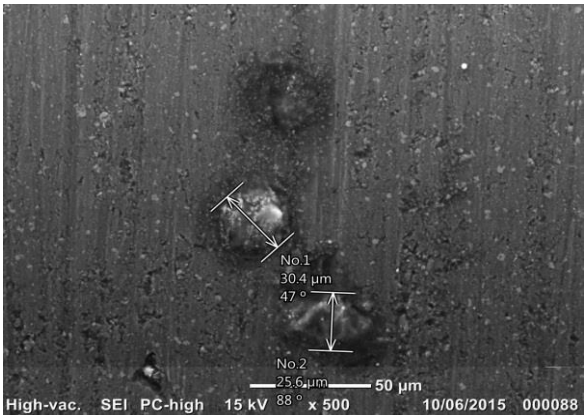

(a) Silicon carbide particles' sizes

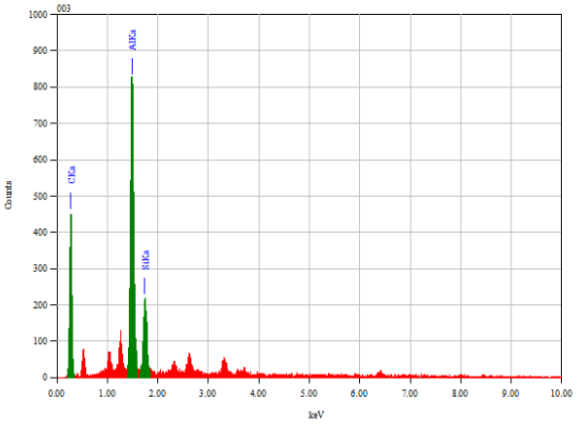

(b) Elemental composition (Si, C, Al %)

Density (g/cm3)	Tensile modulus (GPa)	Tensile strength (MPa)	Yield strength (MPa)	Poisson's ratio (1)	Thermal conductivity (W/(m*K))	Thermal expansion (1/K)	Heat capacity (J/(kg *K))
2.85	100	610	400	0.32	247	23e-6	897

Table 2 Micro drilling tool specifications

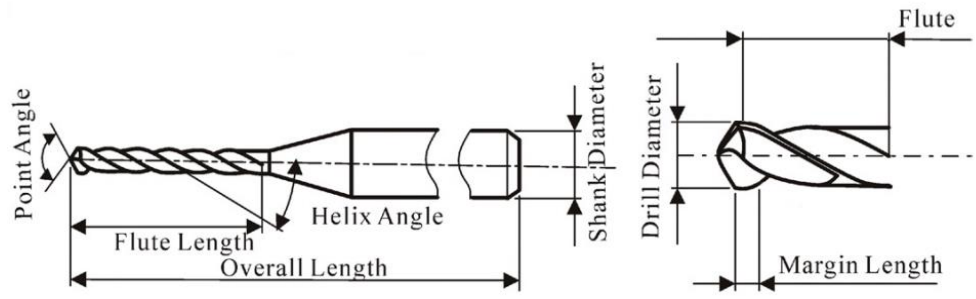

Drill type	Surface condition	Drill diameter	Flute length	Overall length	Shank diameter	Point angle	Helix angle
Twist drill	UT coat	0.5mm	7.5mm	38mm	3mm	130^{o}	30^{o}

Micro drilling experimental set-up

The schematic of the micro drilling experimental set-up is shown in Figure 2. The MMC micro drilling experiments were conducted on the KERN CNC machine. The data acquisition system consists of a Kistler 9256C dynamometer connected to PC with A/D card and LabView programming for acquisition of drilling thrust force data. Tool wear and surface profile were analysed by imaging and further measured with JCM-6000 Benchtop SEM and TESA Visio 200 GL.

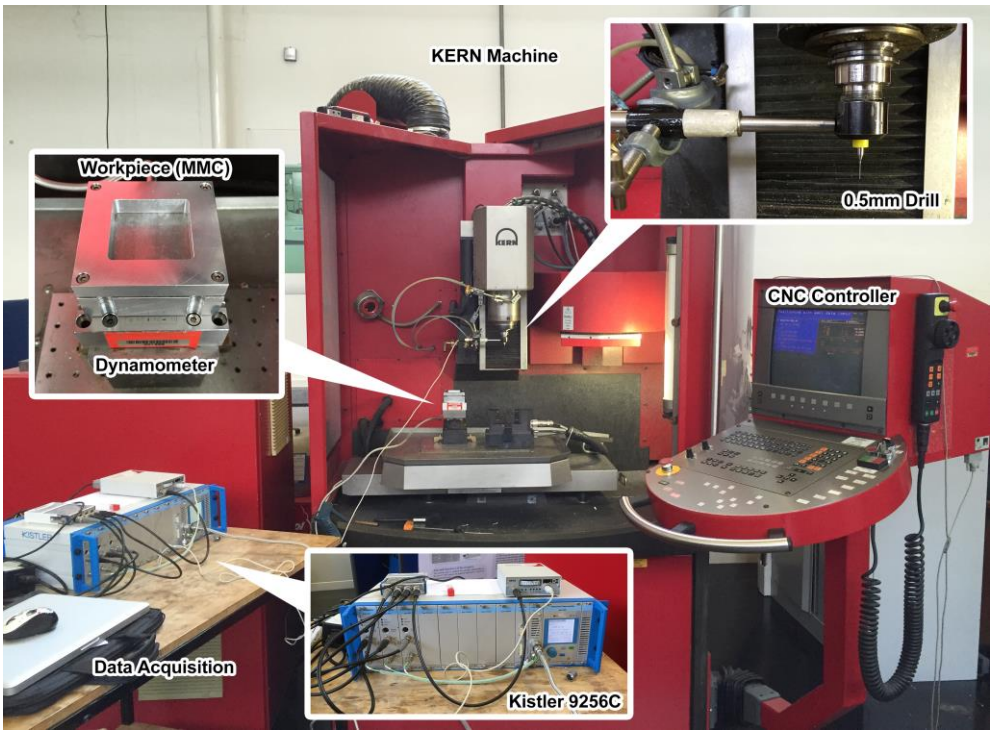

Figure 2 Micro drilling experimental set-up

Micro drilling experimental trials and procedures

In the micro drilling experiments, Taguchi's method, as a powerful tool, was applied to identity the optimal drilling parameters. In these experiments, spindle speed and feed rate were the process parameters that significantly affected the tool wear in micro drilling processes. Thus, during these experiments, only one of them was varied while another was hold constant in order to observe the effects of input parameter. For a comparison study, the different combinations of these parameters were investigated. Due to the SiC particles were easily debonded and flushed away which leave the voids and pits on the machined surface when using the coolant, all of these micro drilling experiments were conducted under dry cutting conditions. Table 3 below shows the micro drilling conditions and orthogonal array of input parameters.

Table 3 Orthogonal array of micro drilling parameters and cutting conditions

Environmental temperature: 20°C Relative humidity: 50% Cutting condition: Dry			
Experiment No.	Spindle speed (rpm)	Cutting speed (m/min)	Feed rate (mm/min)
1	6,000	9.425	12
2	6,000	9.425	24
3	6,000	9.425	36
4	9,000	14.137	12
5	9,000	14.137	24
6	9,000	14.137	36
7	12,000	18.850	12
8	12,000	18.850	24
9	12,000	18.850	36

Results, analysis and discussion

(1) Micro drilling force analysis

Micro drilling thrust force against the micro-drills into the MMC workpiece material was recorded during the entire micro drilling processes. In order to better characterise the generation between the cutting force and process parameters, drilling thrust force in various spindle speed and feed rate that measured by dynamometer respectively were showed in Figure 3. Figure 3 illustrates drilling thrust force performance in a complete circle. It can be found that thrust force increased as more holes drilled in each cutting parameter. This occurred due to the significant increase of tool wear on micro-drills.

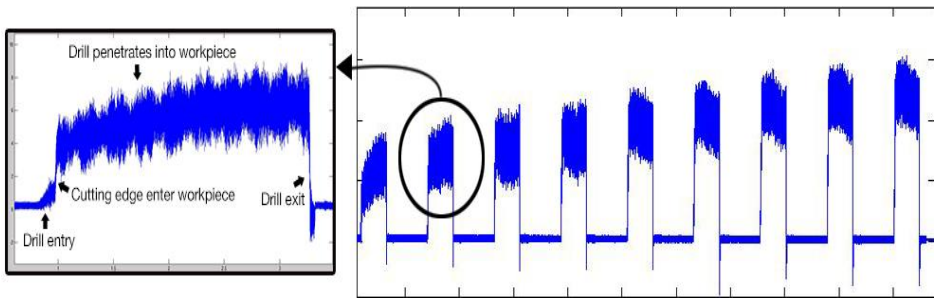

Figure 3 Micro drilling thrust forces in one circle

Figure 4 shows thrust force in one rotation of micro drills. Due to the inhomogeneity of MMC, the suddenly increase of cutting force occurred when the cutting edge touches the SiC particles and against this hard-to-machined material as shown in Figure 4. In this cutting processes, the shear deformation of Al matrix occurs when the micro drill cutting through the workpiece. When the tool tip meets the SiC particle, the stress concentration increases while the SiC still

not fracture. With the continuing increase of cutting force, the SiC particle reaches its limit strength and break into chips together with the Al matrix. Then the cutting force suddenly decrease and keep cutting through Al matrix.

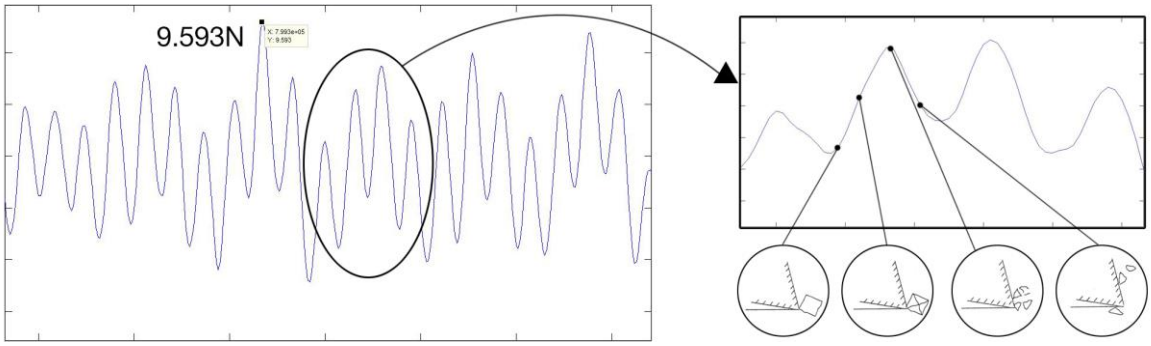

Figure 4 Micro drilling thrust force specification

Figure 5 shows the comparison of thrust force in various process parameters. It can be observed that for a given spindle speed, the drilling thrust force increases with the increase of feed rate and the ratio of force increased became higher. In addition, with the continually increase of feed rate, the rapid micro-drills breakage occurred after drilling only a few holes. In addition, for a given feed rate, the drilling thrust force had a slight decrease and then gradually increased with the increase of spindle speed. In addition, considering the simulation results and experimental results together, the micro drilling thrust force versus spindle speed and feed rate are completed matched. Thus, it can be concluded that feed rate and spindle speed are the main factor that affect the micro drilling thrust force.

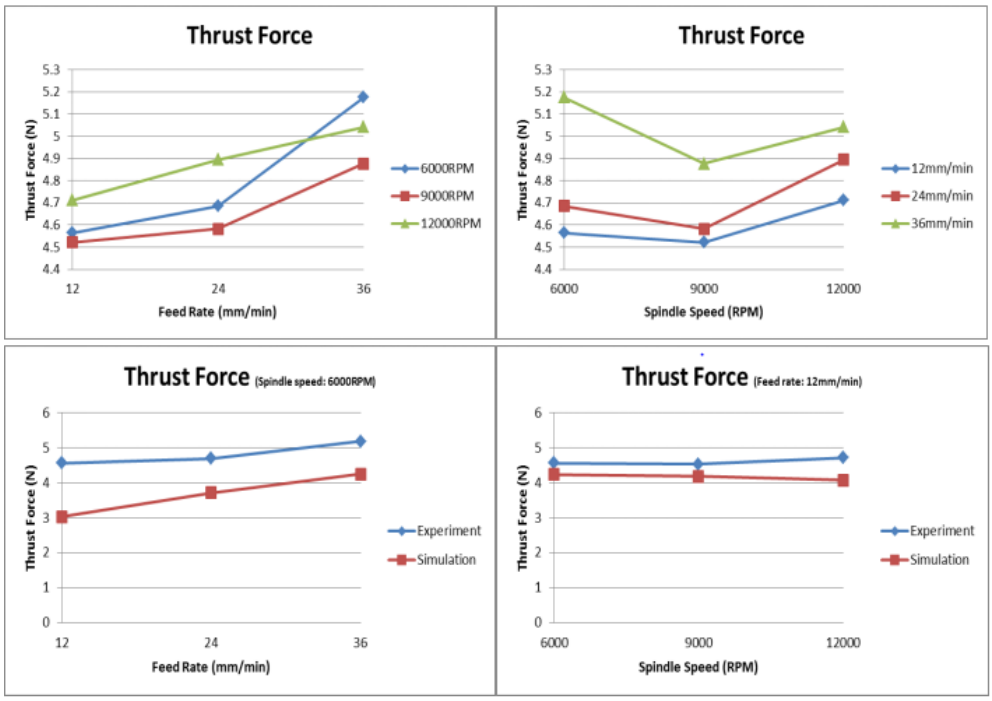

Figure 5 Micro drilling thrust forces against feed rate and spindle speed

(2) Micro drilling tool wear mechanism and characterisation

In MMC micro drilling processes, tool wear can be significantly observed. These tool wear are mainly attributed to the interaction between the micro drills and workpiece. Due to the specific hardness of SiC particles, the tool surface were rubbed by these particles above, below or on the cutting line when micro drills cutting through the workpiece surface. Figure 6 below shows the wear characterization of the micro-drills. From the experimental results it can be observed that adhesion, abrasion, diffusion, fatigue and plastic deformation are the typical wear significantly occurred on micro-drills. Abrasive wear, as the main wear on micro-drills, occurred on flank, rake face and also chisel edge. The reinforced SiC particles with pretty high hardness continue rubbing on the micro-drills and lead to the extremely high abrasive wear. In addition, cutting chips are difficult to be removed from the cutting area due to the dry drilling condition. Thus, cutting chips, that rubbed and damaged the tool surface, significantly increase the speed of tool wear. It can be observed that abrasive wear with the form of grooves mainly existed in at the outer corner of micro-drills cutting edge. This occurs due to the contact length is the largest in this area. Thus, the edge rounding can be observed on micro-drills. In term of other tool wear, adhesive wear mainly occurs on the tool tip and helical flute. Build-up edge (BUE) easily occurs on the helix flute and cutting edge due to the adhesive property of Al. Margin wear, as another tool wear, gradually appeared on micro-drills with the increased number of holes drilled.

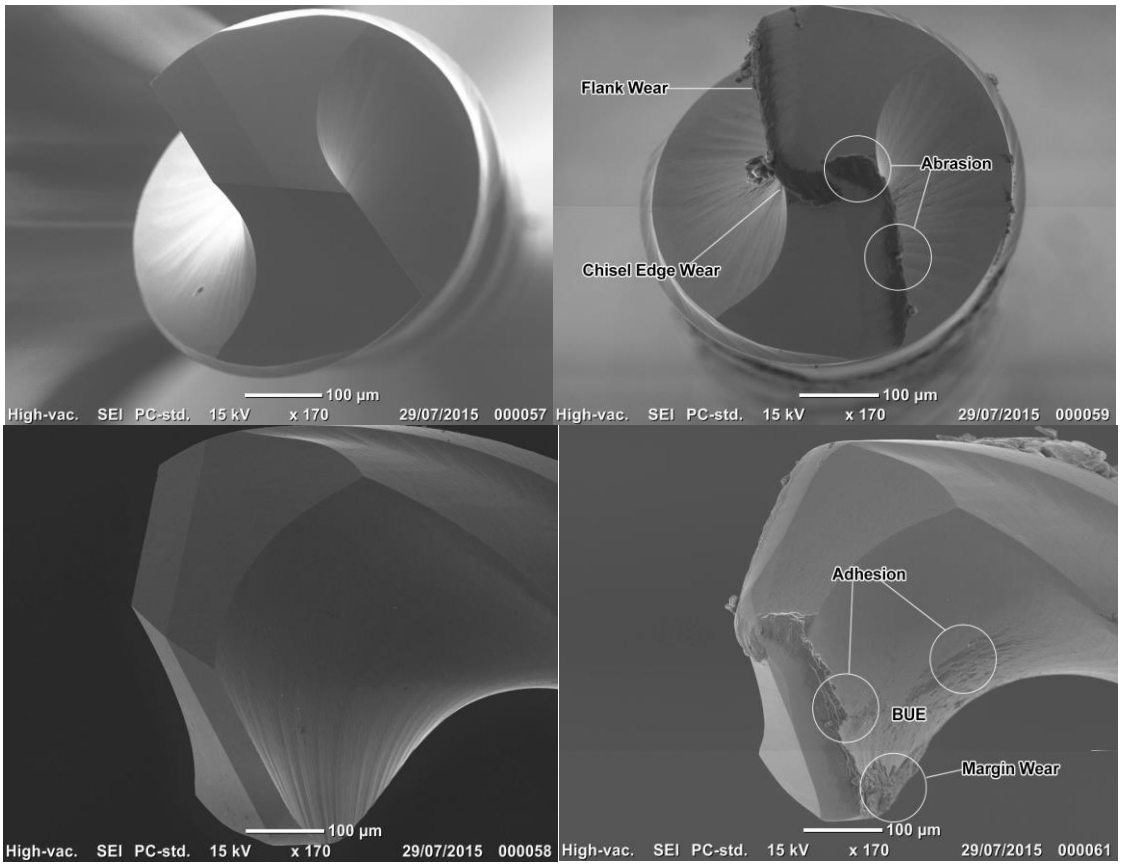

Figure 6 Tool wear characterisation in micro drilling MMCs

(3) Tool wear analysis against the process parameters

Wear characterisation of micro drills in various cutting parameters were measured afterwards by using SEM respectively. The SEM images showed the effects of each factor on the wear of micro-drills. Table 4 illustrates the effects of feed rate and spindle speed on the tool wear in different levels. Wear height, as an effective method to analyse the tool wear, were measured. Figure 7 shows the method of measuring average wear height and maximum wear height. According to the comparison of tool wear as shown in Figure 8, it can be found that tool wear was extremely obvious with process parameters varied when micro drilling on MMC materials. The wear degree on micro drills increased with the increase of feed rate. This attributed to the build-up-edge (BUE). In micro drilling, BUE generally formed in high feed rate conditions and raised the friction coefficient and cutting force. In addition, the adhesive property of Al matrix led to the BUE easily occurred. Thus, the higher feed rate resulted in the large BUE, chip removal rate reduced and eventually accelerated the tool wear. On the other hand, the resultant higher friction coefficient and cutting force led to the increase of friction between micro drills and workpiece. Thus, the flank wear rate significantly increased. In term of spindle speed, cutting temperature increased with the increase of spindle speed and the diffusion wear rate would be raised. From the experimental results, it was found that the wear rate of micro-drills decreases with the increase of the spindle speed. This can be illustrated that the abrasive wear was dominant at lower cutting speed. In addition, abrasive wear have a much higher impact on the resultant tool wear than the high temperature oriented diffusion wear achieved in the higher spindle speed conditions. At the point of view of these process parameters, feed rate and spindle had significantly effects on the tool wear in micro drilling MMC. Feed rate was much more dominant than spindle speed. A lower feed rate and higher spindle speed (12 mm/min in feed rate and 12,000 RPM in spindle speed) were observed as the optimal process parameters to minimise tool wear and extend tool life appropriately in micro drilling MMCs.

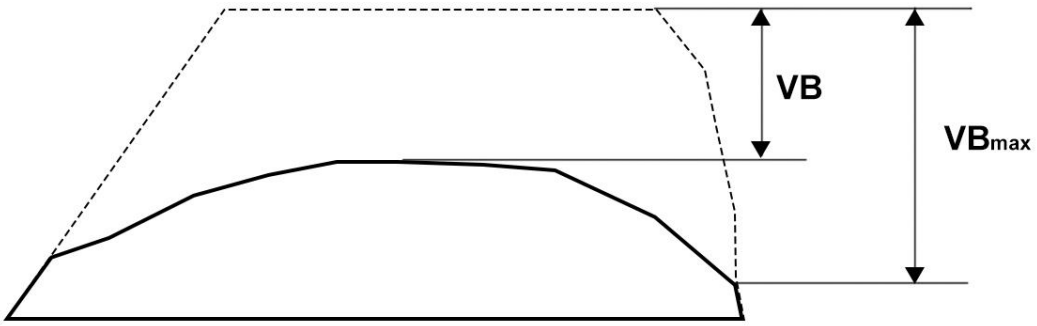

Figure 7 Method of measuring the micro drilling tool wear

Table 4 Wear of micro-drills with respect to spindle speed and feed rate by using SEM

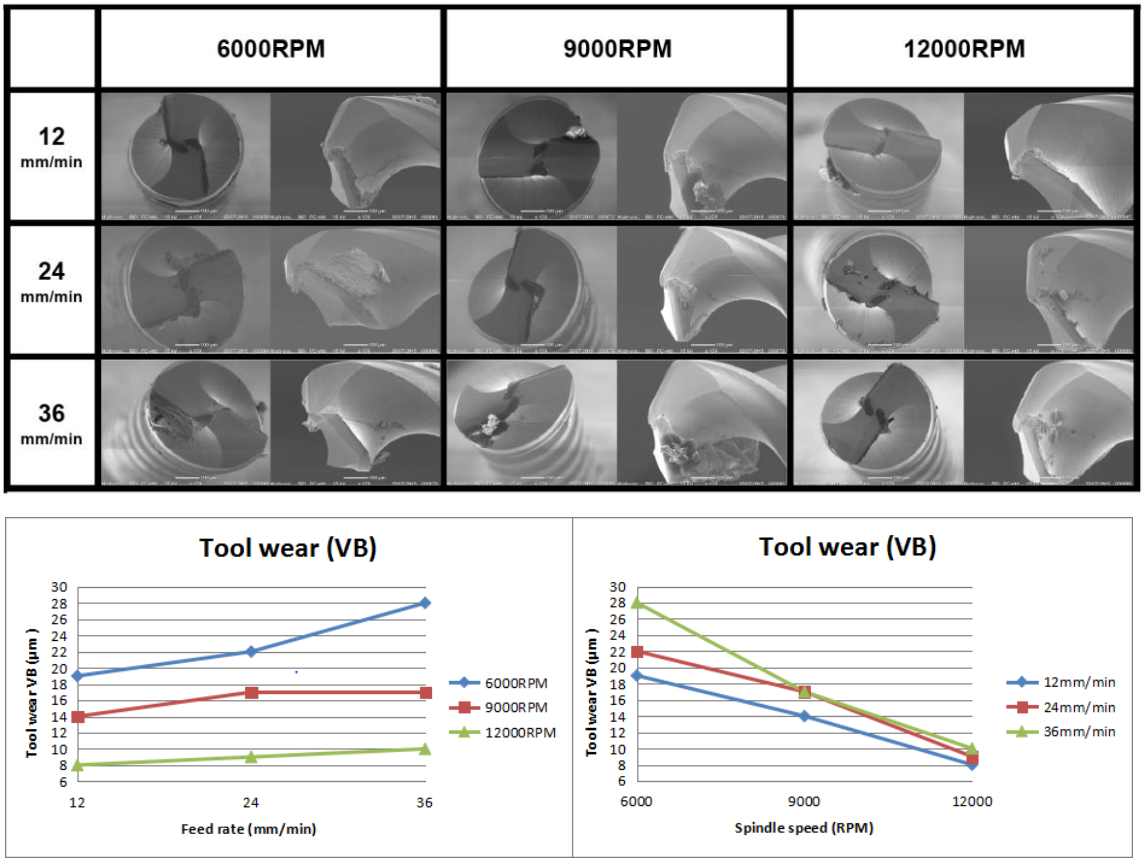

Figure 8 Variation of tool wear with respect to drilling feed rate and spindle speed

Conclusions

In this part, a multiphysics based investigation is presented on micro drilling metal matrix composites (MMCs). The simulation results on the drilling tool wear and thrust force are validated with well-designed micro drilling experiments. The detailed conclusions can be drawn as follows:

(1) Micro drilling tooling performance especially for the tool wear was significantly affected by the fully coupled cutting force, cutting temperature and friction between the micro drills and workpiece. The intrinsic relationships of these three factors can be established based on the drilling tool geometry and process parameters.

(2) Abrasive wear, as the most obvious wear in micro drilling processes, mainly occurs on the flank face, chisel edge and rake face of micro-drills. The SiC particles with high hardness rubbing the tool surface in drilling MMC lead to the excessive abrasive wear. Adhesion, BUE, diffusion, fatigue and plastic deformation also occur on micro-drills during the micro drilling processes.

(3) The cutting spindle speed and feed rate are considered as the main factors that affect the tool wear and tool life in micro drilling processes. Wear rate of micro drills decreases with the decrease of feed rate and increase of spindle speed. In addition, feed rate is more

dominate to the tool wear than spindle speed. Drilling with appropriate lower feed rate and higher spindle speed can significantly reduce the tool wear and extend tool life.

(4) Micro drilling thrust force, as the collective simulation and experimental results, is affected by process parameters as well. The drilling thrust force increases with the increase of drilling feed rate. With the continuous increase of the feed rate, micro-drills breakage occurs. In addition, the increase of the drilling spindle speed results in the slightly change of drilling thrust force. The influence of spindle speed on thrust force is insignificant compare to feed rate.

Appendix 3 Technical Specifications of Kistler 9256C2 MiniDyn

Force

KISTLER
measure, analyze, innovate.

MiniDyn

Type 9256C...

Multicomponent Dynamometer up to 250 N

Multicomponent dynamometer for measuring the three orthogonal components of a force. Its very low threshold allows measuring extremely small forces.

- For cutting force measurements in ultra precise machining
- Small design
- High sensitivity and natural frequency
- Small temperature error
- Top plate made of titanium

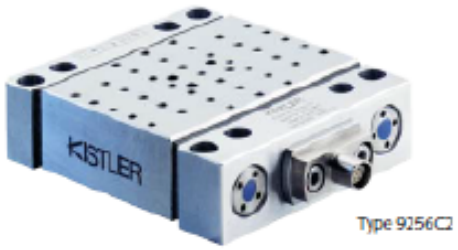

Type 9256C2

Description

The dynamometer consists of four 3-component force sensors mounted under high preload between the cover plate and the two lateral base plates.

A low temperature error is obtained by this special mounting of the sensors. Each force sensor contains three crystal rings, of which one is sensitive to pressure in the y-direction and the two others to shear in the x- and z-directions. The forces are measured practically without displacement.

The outputs of the four mounted force sensors are fed to the 7-pole flanged socket. There are also multicomponent force-moment measurements possible.

The four sensors are fitted so that they are ground-isolated. This largely eliminates ground loop problems.

The dynamometer is corrosion-resistant and protected against penetration by splashing water or cutting fluid. The dynamometer including connecting cable Type 1696A5 or Type 1697A5 meets the degree of protection IP67.

Examples of Application

- Cutting force measurement in precision machining such as:
  - cutting wafers
  - grinding hard-disk read heads
  - diamond turning
  - high speed machining
  - micromachining
- Ultra-high precision machining of brittle hard materials
- Multicomponent force measurement of small forces
- Force measurement in confined spaces

Technical Data

Measuring range	F_x, F_y, F_z	N	–250 ... 250
Type 9256C1	M_x, M_z	N·m	–8 ... 8
Type 9256C2	M_x, M_z	N·m	–11 ... 11
Calibrated measuring range			
100 %	F_x, F_y, F_z	N	0 ... 250
10 %	F_x, F_y, F_z	N	0 ... 25
Overload	F_x, F_y, F_z	N	–300/300
Threshold		N	<0,002
Sensitivity	F_x, F_z	pC/N	≈–26
	F_y	pC/N	≈–13
Linearity, all ranges		%FSO	≤±0,4
Hysteresis, all ranges		%FSO	≤0,5
Crosstalk		%	≤±2
Rigidity	c_x, c_z	N/µm	>250
	c_y	N/µm	>300
Natural frequency (mounted on rigid base)			
Type 9256C1	f_n (x)	kHz	≈5,1
	f_n (y)	kHz	≈5,5
	f_n (z)	kHz	≈5,6
Type 9256C2	f_n (x)	kHz	≈4,0
	f_n (y)	kHz	≈4,8
	f_n (z)	kHz	≈4,6
Operating temperature range		°C	0 ... 70
Insulation resistance		Ω	$>10^{13}$
Ground isolation		Ω	$>10^{8}$
Degree of protection EN60529 (with connecting cable Type 1696A5/1697A5)			IP67
Weight			
Dynamometer	Type 9256C1/C2	kg	0,75/0,87
Top plate	Type 9256C1/C2	kg	0,24/0,36
Clamping area			
Type 9256C1		mm	39x80
Type 9256C2		mm	55x80

Appendix 4 Technical Specifications of Impact Hammer 9722A500

Technical Data

Type	Units	9722A500	9722A2000
Force Range	lbf	0 ... 100	0 ... 500
Maximum Force	lbf	500	2500
Sensitivity nom.	mV/lbf	50	10
Resonant Frequency	kHz	27	27
Frequency Range with steel impact tip (-10 dB)	Hz	8200	9300
Time Constant nom	s	500	500
Rigidity	lbf/µin	4.8	4.8
Temperature Range Operating	°F	-5 ... 160	-5 ... 160
Output:			
Voltage F.S.	V	±5	±5
Bias nom.	VDC	11	11
Impedance	Ω	<100	<100
Source:			
Voltage	V	20 ... 30	20 ... 30
Constant current	mA	2 ... 20	2 ... 20
Hammer head dimensions:			
Diameter	in	0.69	0.69
Length	in	2.4	2.4
Weight	gram	100	100
Length of handle	in	7.4	7.4
Connector	type	BNC neg.	BNC neg.

1 N = 0.2248lb, 1 g = 9.80665 m/s2, 1 inch = 25.4 mm, 1 gram = 0.03527 oz

Accessories Included	Type
• impact tip, steel	9902A
• impact tip, steel with Delrin cap	9904A
• impact tip, soft PVC	9906
• impact tip, rubber hard (green)	9908
• impact tip, rubber medium (red)	9910
• impact tip, rubber soft (gray)	9912
• adapter for rubber impact tips	9928
• extender mass (50 grams)	9922
• impact tip wrench	1370
• Plastic carrying case	

Ordering Key

Measuring Range — 9722A ☐

100 lbf (500 N)	500
500 lbf (2000 N)	2000

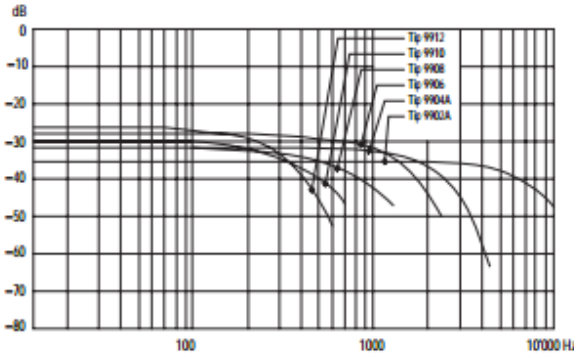

Appendix 5 Experimental Trials Results: Minimum Chip Thickness

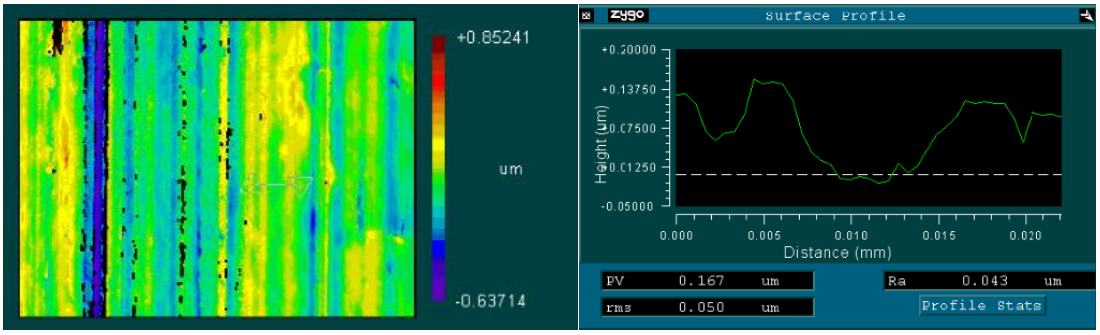

(a) DOC: 0.2 µm

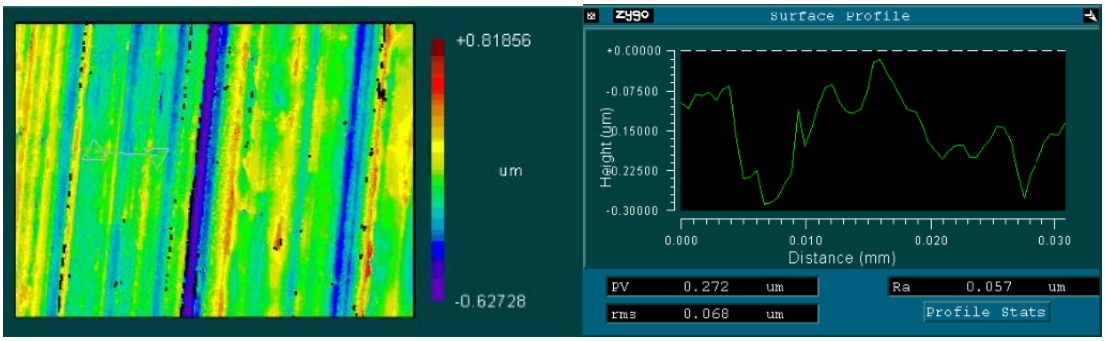

(b) DOC: 0.3 µm

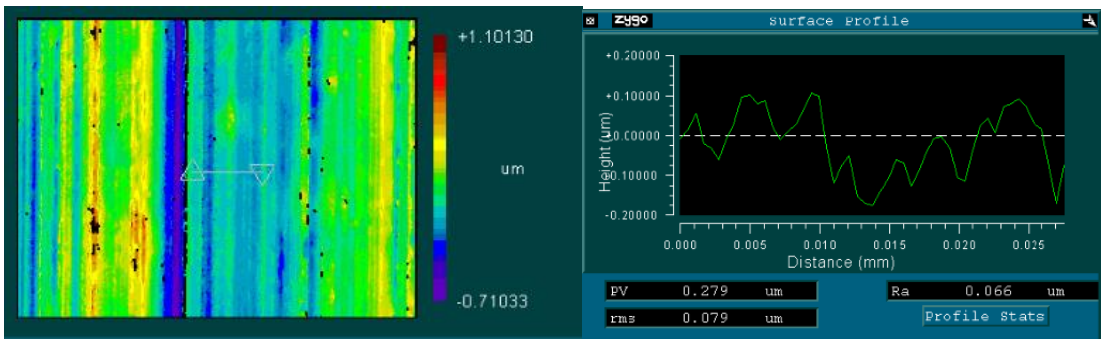

(c) DOC: 0.4 µm

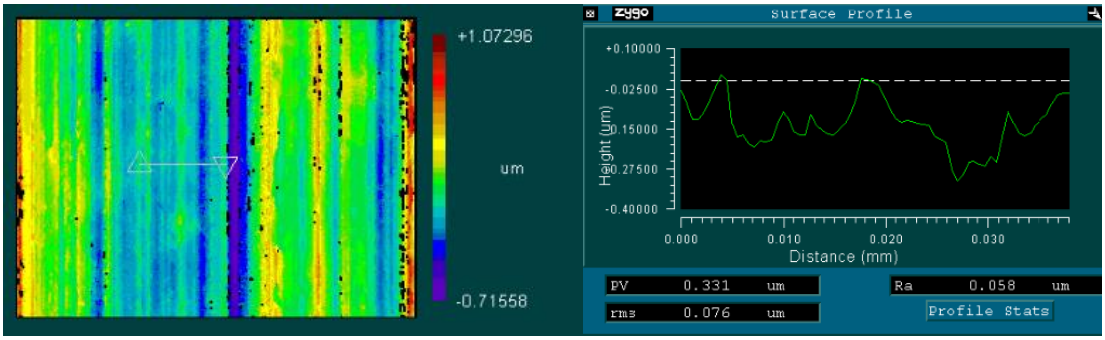

(d) DOC: 0.5 µm

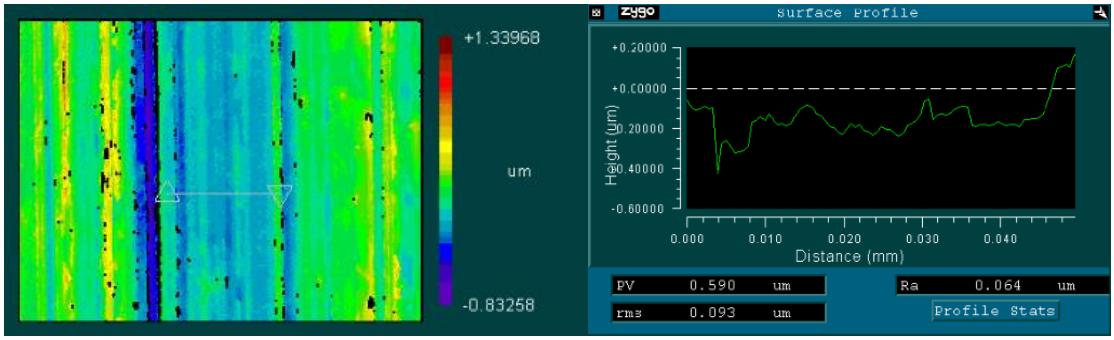

(e) DOC: 0.6 µm

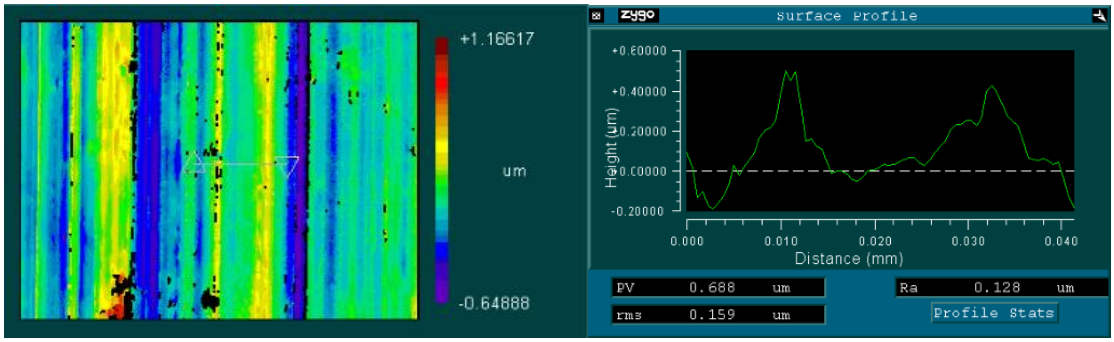

(f) DOC: 0.7 µm

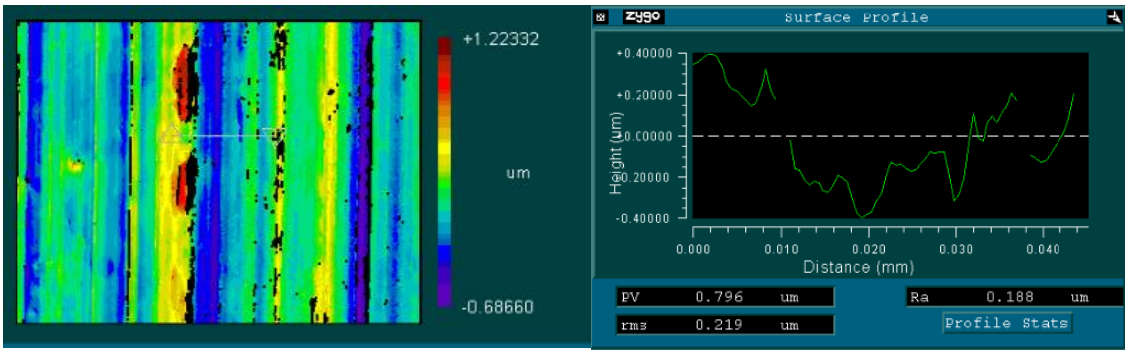

(g) DOC: 0.8 µm

Figure 1 Machined surface roughness at various depth of cut

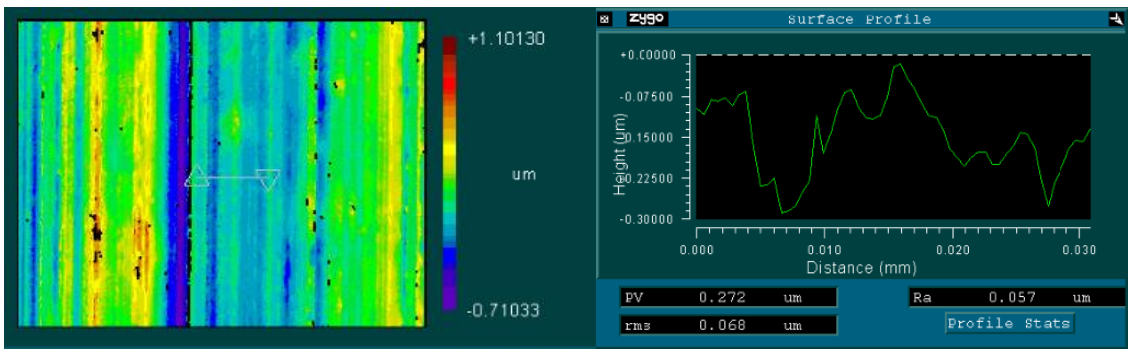

(a) Cutting speed: 157.0 m/min

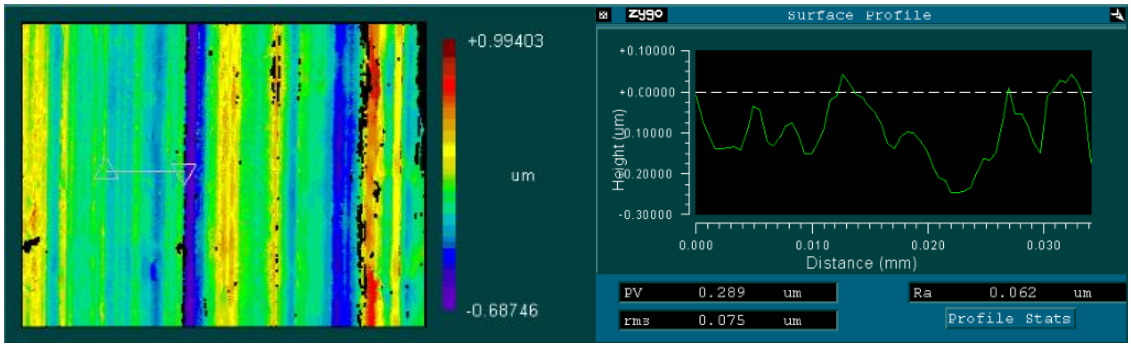

(b) Cutting speed: 125.7 m/min

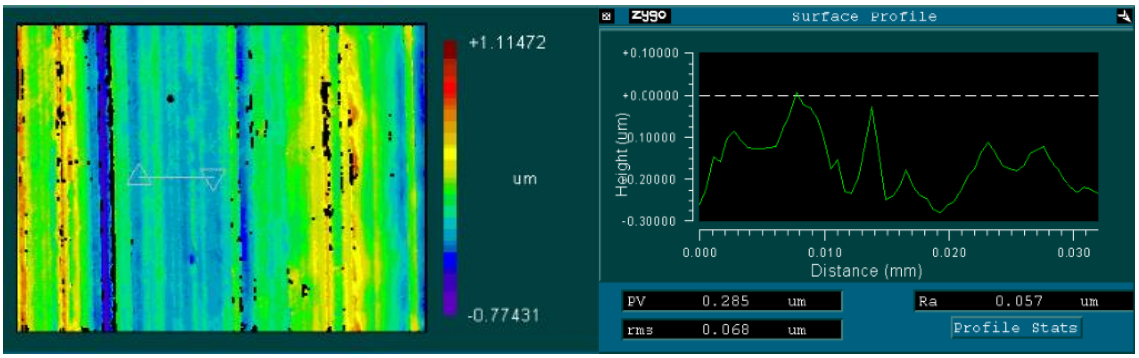

(c) Cutting speed: 94.2 m/min

Figure 2 Machined surface roughness at varied cutting speed when DOC is 0.4 μm

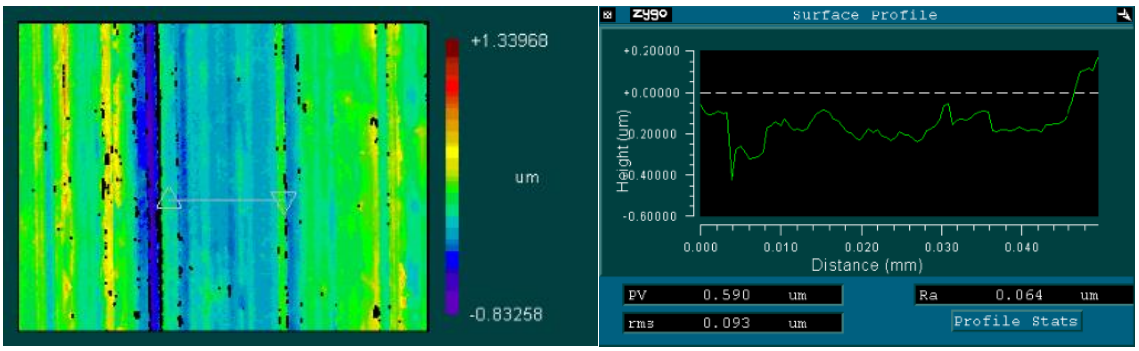

(a) Cutting speed: 157.0 m/min

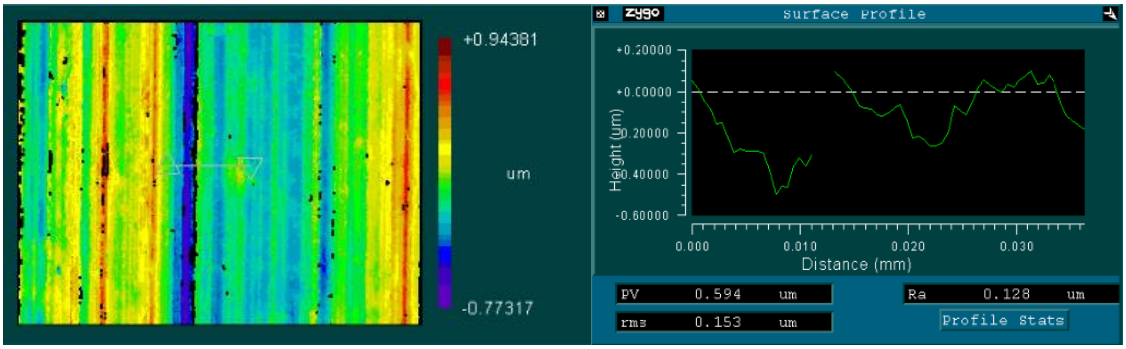

(b) Cutting speed: 125.7 m/min

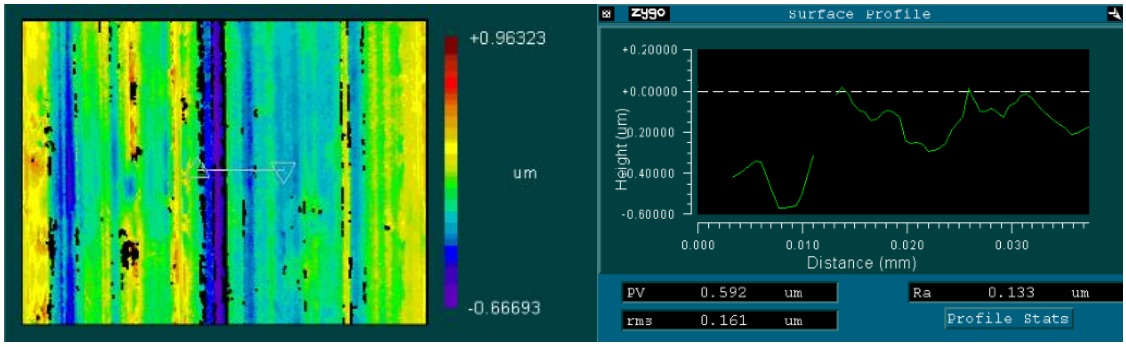

(c) Cutting speed: 94.2 m/min

Figure 3 Machined surface roughness at varied cutting speed when DOC is 0.6 µm

Appendix 6 Part of Programs for Dynamic Cutting Force Modelling

```
x1 =[a1 a2 a3 a4 a5 a6];
y1 =[b1 b2 b3 b4 b5 b6];
ellipse_t = fit_ellipse(x1,y1);
t=linspace(0, 2*pi,10000); %rotation angle
phi=linspace(0, 2*pi,10000); %rotation angle
a=ellipse_t.a;
b=ellipse_t.b;
x0=ellipse_t.X0;
y0=ellipse_t.Y0;
X=a*cos(t+pi/2)-x0;
Y=b*sin(t+pi/2)-y0;
Z=sqrt(X.^2+Y.^2);
d=0.25; %depth of cut
f=0.010; %feed rate
beta=0.4845; %friction angle
alpha=0; %rake angle
rn=0.2; %nose radius
re=0.002; %edge radius
f1=0.1;
p=0.75; %per of SiC
rs=0.0025; % radius of SiC
K=3.3;%particle fracture toughness
miu=K/(sqrt(2*rs*0.001)); %particle fractur stress
Theta=acot((rn+f/2)/d); %tool approach angle
A=d/sin(Theta); %actural DOC (mm)
c=f*sin(Theta); %actural feed rate (mm/r)
c1=f*sin(Theta); %actural feed rate (mm/r)
ts=1500; %shear strength of MMC (Mpa)
tm=283; %shear strength of Al (Mpa)
Phi=atan(rct*cos(alpha)/(1-rct*sin(alpha))); %shear angle (deg)
```

```
H=re*(1+sin(alpha)); % Hight of ploughing zoon
sigma=asin(H/(2*rs+2*re));
l=rn*(Theta+asin(f/(2*rn)))+((d-rn*(1-cos(Theta)))/sin(Theta));
L=2*rs/(l*p);
Ft=(tm*A*c.*sin(phi)).*((0<=phi)&(phi<theta1))+(ts*A*c.*sin(phi)*cos(beta-
alpha)/(sin(Phi)*cos(Phi+beta-
alpha))+tm*l*re*tan(pi/4+alpha/2)+miu*rs*l*p*pi/2*sin(1600*phi)).*((theta1<=phi)&(
phi<=pi/4))+0*((pi/4<phi)&(phi<=pi))+(tm*A*c.*sin(phi)).*((pi<phi)&(phi<pi+theta1)
)+(ts*A*c1.*sin(phi)*cos(beta-alpha)/(sin(Phi)*cos(Phi+beta-alpha))-
tm*l*re*tan(pi/4+alpha/2)-
miu*rs*l*p*pi/2*sin(1600*phi)).*((pi+theta1<=phi)&(phi<=5*pi/4))+0*((5*pi/4<phi)
&(phi<=2*pi));
Fc=(tm*A*c.*sin(phi)).*((0<=phi)&(phi<theta1))+(ts*A*c.*sin(phi)*sin(beta-
alpha)/(sin(Phi)*cos(Phi+beta-
alpha))+tm*l*re*tan(pi/4+alpha/2)*(1+pi/2)*sin(Theta)+miu*rs*l*p*pi/2*sin(1600*phi
)*tan(sigma)*sin(Theta)).*((theta1<=phi)&(phi<=pi/4))+0*((pi/4<phi)&(phi<=pi))+(tm
*A*c.*sin(phi)).*((pi<phi)&(phi<pi+theta1))+(ts*A*c1.*sin(phi)*sin(beta-
alpha)/(sin(Phi)*cos(Phi+beta-alpha))-tm*l*re*tan(pi/4+alpha/2)*(1+pi/2)*sin(Theta)-
miu*rs*l*p*pi/2*sin(1600*phi)*tan(sigma)*sin(Theta)).*((pi+theta1<=phi)&(phi<5*pi/
4))+0*((5*pi/4<phi)&(phi<=2*pi));
Fa=tm*A*re*tan(pi/4+alpha/2)*(1+pi/2)*cos(Theta)+miu*rs*l*p*pi/2*sin(1600*phi)*t
an(sigma)*cos(Theta)+tm*2.8*re*tan(pi/4+alpha/2)*(1+pi/2);
Fx=(Ft.*cos(phi)+Fc.*sin(phi));
Fy=(-Ft.*sin(phi)+Fc.*cos(phi));
Fz=Fa;
plot(phi,Ft,(phi+2*pi),Ft,'Color',[0 0 1]);
plot(phi,Fc,(phi+2*pi),Fc,'Color',[0 1 1]);
plot(phi,Fa,(phi+2*pi),Fa,'Color',[1 1 1]);
plot(phi,Fx,(phi+2*pi),Fx,'Color',[1 0 1]);
plot(phi,Fy,(phi+2*pi),Fy,'Color',[1 0 0]);
plot(phi,Fz,(phi+2*pi),Fz,'Color',[0 1 0]);
```

Appendix 7 Part of Programs for Measuring Tool Edge Radius

```
% this program calculates the approximate cutting edge radius by selecting points that consists of the edge circle based on least-square algorithm and draws the fitted circle and its center.
clc
clear all
[FileName,PathName] = uigetfile('*.jpg','Select the Image');
IM=imread(FileName);
I=rgb2gray(IM);
imshow(I);
% Get size of image.
m = size(I,1);
n = size(I,2);
% Get center point of image for initial positioning.
midy = ceil(m/2);
midx = ceil(n/2);
% get resolution every pixel represents
r=find(I(:,midx)==255,1);
s=find(I(r+3,:)==255,1,'first');
e=find(I(r+3,:)<=10,1,'first');
l=e-s+1; % pixels of the scale bar
prompt = {'Enter bar length:','Enter zoom factor:'};
IN=inputdlg(prompt);
bl=str2num(IN{1}); %bar length in um
d=bl/l;
% zoom in on tool tip
zoom(str2num(IN{2}))
% select points that consists of cutting edge circle
[x, y]=getpts(gcf);

% solve for parameters a, b, and c in the least-squares sense by
```

```
% using the backslash operator
abc = [x y ones(length(x),1)] \ -(x.^2+y.^2);
a = abc(1); b = abc(2); c = abc(3);

% calculate the location of the center and the radius
xc = -a/2;
yc = -b/2;
radius  =  sqrt((xc^2+yc^2)-c);
% display circle
viscircles([xc yc],radius);
% display calculated center
hold on;
plot(xc,yc,'yx','LineWidth',2);
Ra=radius*d;
title(['The estimated radius is ',num2str(Ra),' microns'],'FontSize',16,'Color','b');
```

Appendix 8 Part of Programs for Measuring Chip Dimensions

```
% this program calculates the approximate cutting chip dimensions
clc
clear all
[FileName,PathName] = uigetfile('*.jpg','Select the Image');
IM=imread(FileName);
I=rgb2gray(IM);
figure
imshow(I);
% % Get size of image.
% m = size(I,1);
% n = size(I,2);
% % Get center point of image for initial positioning.
% midy = ceil(m/2);
% midx = ceil(n/2);
% % get resolution every pixel represents
% r=find(I(:,midx)==255,1);
% s=find(I(r+3,:)==255,1,'first');
% e=find(I(r+3,s:end)<=250,1,'first');
% % l=e-s+1; % pixels of the scale bar
% l=e;
prompt = {'Enter bar length:','Enter zoom factor:'};
IN=inputdlg(prompt);
bl=str2num(IN{1}); %bar length in um
% d=bl/l;
% zoom in on tool tip
zoom(str2num(IN{2}))
% measure bar length
[xb, yb]=getpts(gcf);
re=bl/(xb(2)-xb(1));
% measure chip length
```

```
[xc, yc]=getpts(gcf);
num=length(xc);
for i=1:num-1
   Ds(i)=sqrt((xc(i)-xc(i+1))^2+(yc(i)-yc(i+1))^2)*re;
end
```